
Semiconducting Block and Brush Copolymers via CuAAC Click Chemistry

DISSERTATION

zur Erlangung des akademischen Grades
Doktor der Naturwissenschaften (Dr. rer. nat.)
im Promotionsprogramm Polymer Science
der Bayreuther Graduiertenschule für Mathematik und Naturwissenschaften
an der Universität Bayreuth

vorgelegt von
Christian David Heinrich

geboren in Kiel

Bayreuth, 2018

Die vorliegende Arbeit wurde in der Zeit von September 2012 bis August 2017 in der Arbeitsgruppe Angewandte Funktionspolymere am Lehrstuhl Makromolekulare Chemie I der Universität Bayreuth unter Betreuung von Herrn Prof. Dr. Mukundan Thelakkat angefertigt.

Vollständiger Abdruck der von der Graduiertenschule für Mathematik und Naturwissenschaften (BayNAT) der Universität Bayreuth genehmigten Dissertation zur Erlangung des akademischen Grades eines Doktors der Naturwissenschaften (Dr. rer. nat.).

Dissertation eingereicht am:	09.08.2017
Zulassung durch das Leitungsgremium:	20.09.2017
Datum des wissenschaftlichen Kolloquiums:	07.02.2018

Amtierender Direktor der Graduiertenschule:	Prof. Dr. Dirk Schüler
---	------------------------

Prüfungsausschuss:

Prof. Dr. Mukundan Thelakkat	(Erstgutachter)
Prof. Dr. Andreas Greiner	(Zweitgutachter)
Prof. Dr. Markus Retsch	(Vorsitz)
Prof. Dr. Carlo Unverzagt	

It's not magic, it's science !

Bill Nye, The Science Guy

Table of Contents

	Summary / Zusammenfassung	1
1	Introduction	7
2	Objective of the Thesis	43
3	Overview of the Thesis	45
	Individual Contributions to Joint Publications	55
4	Impact of Molecular Dynamics on Structure Formation of Donor-Acceptor Block Copolymers	57
5	Poly(-3-hexylthiophene) Bottlebrush Copolymers with Tailored Side-Chain Lengths and High Charge Carrier Mobilities	87
6	Densely Grafted Liquid Crystalline Copper Phthalocyanine Side Chain Polymer: Synthesis and Characterization	121
7	Monolayer Brushes for Highly Efficient Polymeric SAMFETs	149
8	Appendix: Nanoscale Morphology From Donor-Acceptor Block Copolymers: Formation and Functions	171
	List of Publications	215
	Acknowledgements	217
	Erklärung	219

Summary

This thesis addresses the tailor-made synthesis of novel semiconducting materials via a combination of controlled polymerization techniques such as KCTP, RAFT etc. and azide-alkyne“click”-chemistry. In particular, we were interested in the study of influence of polymer architecture on the structure formation and thus the electrical properties of the novel materials. This concept of combination of different synthetic approaches benefits from its modularity and makes it possible to synthesize highly defined and comparable polymers. Consequently, the influence on the material properties can be identified by only changing one parameter for example the side-chain length.

For the first part of this thesis, donor-acceptor diblock copolymers, P3HT-*b*-PPBI with poly(3-hexylthiophene) (P3HT) as donor block and a perylene bisimide sidechain polymer (PPBI) as acceptor block, were synthesized by a novel approach and characterized regarding their structure formation. P3HT was synthesized in a first step and is subsequently functionalized with a RAFT-agent to get a macroinitiator. Using this , in a sequential polymerization, poly(propargyloxystyrene) was synthesized as a second block. In a last step the second block was decorated with two differently substituted perylene bisimides (PBI). This can be achieved by the copper-catalyzed azide-alkyne cycloaddition (CuAAC) in a quantitative fashion. Therefore, two highly comparable diblock copolymers with different PBI sidechains were obtained. We showed that both polymers are microphase-separated with a cylindrical microstructure. The influences of the different PBIs were investigated in detail by temperature dependent XRD measurements, DSC, TEM and AFM.

For the second part of the thesis, bottlebrushes of high molecular weight P3HT grafted-to a polystyrene backbone were synthesized as novel semiconducting materials

and the design principles for such materials were investigated and compared to linear P3HTs. These densely grafted brush copolymers, with semiconducting sidechain polymer segments, may be very interesting for organic electronics because new unique material properties arise from the brush architecture. The grafting-to method, that is the grafting of sidechains to a backbone polymer by polymer analogous reaction, makes it possible to synthesize defined polymers with far higher molecular weights reaching about $144000 \text{ g mol}^{-1}$. The high molecular weight alone increases the stability of thin films of such polymers against delamination. As a perspective, these Bottlebrushes can also be one part of diblock copolymers. Improved microphase separation and changes in orientation are to be expected and may render a possible way towards preferentially vertically aligned donor-acceptor block copolymers in future works. For the first time, we report the influence of the P3HT sidechain lengths on the electrical properties of P3HT bottlebrushes. The grafting-to approach utilizing the copper-catalyzed azide-alkyne cycloaddition (CuAAC) proved to be highly reliable in terms of the grafting density, even for the sidechains with the highest molecular weight. The modularity made sure that only the sidechain length was changed within the series of four bottlebrushes. We identified the sidechain length as the crucial parameter for the performance of the bottlebrushes, measured in terms of the charge carrier mobility of organic field effect transistors (OFETs). The best material exhibits an equally high charge carrier mobility in comparison to its linear counterpart combined with a superior film stability at elevated temperatures.

Our grafting strategy can be successfully applied for the synthesis of diblock and brush copolymers. In the third part of this thesis, I describe how the same grafting-to strategy is applied for the synthesis of a novel donor polymer (PCuPc). For this, a polystyrene backbone (polypropargyloxystyrene) was decorated with a copper phthalocyanine (CuPc) derivative with three oligo ethylene swallow-tail solubilizing units. The hydrophilic nature of the resulting PCuPC makes the polymer a potential candidate for bio-electronics. We synthesized a polymer with a high molecular weight ($M_n = 88000 \text{ g mol}^{-1}$), a narrow distribution $\text{Đ} = 1.20$ and a high solubility in solvents such as acetone, ethyl acetate and THF. A MALDI-ToF spectrum with a resolution of the

repeating unit was obtained regardless of the high mass of the polymers. This was an important indicator for quantitative and, therefore, dense grafting. The obtained material was characterized as liquid crystalline by XRD and exhibits a very high melting temperature, well beyond 300 °C. Measurements of the space charge limited current (SCLC) in diode configuration revealed a bulk hole-mobility of $5.3 \cdot 10^{-6} \text{ cm}^2 \text{ V}^{-1} \text{ s}^{-1}$.

In the fourth chapter of the thesis, we show that the grafting-to concept can be extended beyond sidechain and brush copolymers towards the modification of surfaces with semiconducting materials to get self-assembled monolayers of semiconductor polymers. We demonstrate the versatility of the CuAAC for surface grafting of electronically active materials. After functionalizing a substrate with an azido silane, P3HT can be coupled to the surface with high grafting density. Surface grafted brushes with high molecular weight P3HT were fabricated. We are the first to use P3HT with a very high molecular weight of about 11400 g mol^{-1} to get dense surface grafted systems. The successful grafting was verified by AFM and UV-Vis spectroscopy. The ultra-thin P3HT brush film ($< 4 \text{ nm}$ thick) was characterized by measuring the charge carrier mobility in SAMFETs. The measured charge carrier mobility of $1.6 \cdot 10^{-3} \text{ cm}^2 \text{ V s}^{-1}$ is the highest reported value for a polymeric SAMFET and is very high for such a thin film SAMFET and exceeds the value of previously reported P3HT brushes by nearly two orders of magnitude.

Zusammenfassung

Diese Arbeit beschäftigt sich mit der maßgeschneiderten Synthese von neuartigen halbleitenden Materialien, die durch die Kombination von kontrollierten Polymerisationstechniken und „Click“-Chemie hergestellt werden. Im Besonderen interessierte uns der Einfluss der Polymerarchitektur auf die Strukturbildung und folglich auf die elektronischen Eigenschaften. Dieses Konzept, dass verschiedene synthetische Ansätze verbindet, zeichnet sich durch seine Modularität aus, die es ermöglicht definierte Polymere mit hoher Vergleichbarkeit zu synthetisieren. Daher kann der Einfluss auf die Materialeigenschaften bei Änderung eines Parameters, wie beispielsweise die Länge der Polymerseitenketten, untersucht werden.

Für den ersten Teil dieser Arbeit wurden Donor-Akzeptor Diblockcopolymere P3HT-*b*-PPBI, mit Poly(3-hexylthiophen) (P3HT) als Donorblock und einem Perylenbisimid Seitenkettenpolymer (PPBI) als Akzeptorblock, mittels einer neuartigen Strategie synthetisiert und hinsichtlich ihrer Strukturbildung charakterisiert. Als Erstes wurde P3HT synthetisiert und im Anschluss mit einem RAFT-Agens funktionalisiert. Von diesem Makroinitiator wurde Polypropargyloxy-styrol als zweiter Block polymerisiert. Im letzten Schritt wurden unterschiedliche Perylenbisimid (PBI) als Seitenketten an den zweiten Block angebracht. Dies ist mithilfe der 1,3-Dipolaren Cycloaddition von Aziden mit Alkinen quantitativ möglich. Wir konnten daher zwei Diblockcopolymere mit unterschiedlichen PBI-Seitenketten erhalten. Beide Polymere sind mikrophasen-separiert und bilden eine zylindrische Struktur aus. Der Einfluss der PBIs auf die Strukturbildung wurde im Detail mittels temperaturabhängiger Röntgenmessungen, DSC, TEM und AFM untersucht.

Im zweiten Teil der Arbeit beschreibe ich wie Bürstenpolymere von an ein Polystyrolrückgrat gepfropften, hochmolekularem P3HT synthetisiert werden. Diese neuartigen, halbleitenden Materialien wurden untersucht und mit linearem P3HT verglichen. Derartige Bürstenpolymere mit halbleitenden Seitenketten-polymeren können für die organische Elektronik äußerst interessant sein, da die Architektur die Eigenschaften dieser Materialien entscheidend beeinflusst. In derartigen Pfropfco-

polymeren, bei denen die Seitenketten durch eine polymeranaloge Reaktion mit dem Rückgrat verknüpft wurden, können deutlich höhere Molekulargewichte bis etwa $144000 \text{ g mol}^{-1}$ erreicht werden. Dies allein wirkt sich positiv auf die Stabilität dünner Filme dieser Materialien aus. Außerdem können Bürstenpolymere einen Teil eines Diblockcopolymer bilden und dadurch Einfluss auf die Mikrophasenseparation nehmen. Besonders die Möglichkeit die Orientierung zu beeinflussen könnte es in zukünftigen Arbeiten erlauben Donor-Akzeptor Blockcopolymer zu synthetisieren, die im dünnen Film eine hauptsächlich vertikal orientierte Mikrophasenstruktur ausbilden. Als Erste haben wir den Einfluss der P3HT Seitenkettenlängen auf die elektrischen Eigenschaften der P3HT Bürstenpolymere untersucht. Das *grafting-to* Konzept mittels CuAAC erwies sich als sehr zuverlässig. Dies zeigte sich durch die durchgehend hohen Pfropfdichten, die auch für die längsten P3HT Seitenketten erreicht werden konnten. Die Modularität dieses Konzeptes ermöglichte dabei die Synthese einer Reihe von vier Bürstenpolymeren, welche sich nur hinsichtlich der Länge ihrer P3HT Seitenketten unterscheiden. Es zeigte sich außerdem, dass die Seitenkettenlänge die Eigenschaften des Materials, beispielsweise die Ladungsträgermobilität, entscheidend beeinflusst. Die Ladungsträgermobilität wurde in organischen Feldeffekttransistoren (OFET) gemessen wobei das beste Bürstenmaterial mit linearem P3HT vergleichbare Ladungsträgermobilitäten erzielt bei überlegener thermischer Stabilität im dünnen Film.

In den ersten beiden Kapiteln wird gezeigt, dass unsere Synthesestrategie sowohl für die Synthese von Diblockcopolymeren als auch Bürstenpolymeren erfolgreich angewendet werden kann. Im dritten Teil dieser Arbeit wird eine ähnliche Synthesestrategie verwendet um ein neuartiges Donorpolymer (PCuPc) herzustellen. In diesem Fall wurde ein Kupferphthalocyanin Derivat (CuPc) mit löslichkeitsvermittelnden Oligoethylenseitenketten mit einem Polystyrolrückgrat (Propargyloxystyrol) verknüpft. Die hydrophile Natur von PCuPC macht dieses Polymer interessant für Anwendungen in der Bioelektronik. Ein Polymer mit einem hohen Molekulargewicht ($M_n = 88000 \text{ g mol}^{-1}$), Verteilung $\bar{D} = 1,20$ und hoher Löslichkeit in Lösungsmitteln wie Aceton, Essigester oder THF wurde synthetisiert. Trotz des hohen

Molekulargewichts konnte ein MALDI-ToF Spektrum, in welchem die Wiederholeinheit des Polymers aufgelöst ist, aufgenommen werden. Weitere Untersuchungen mittels Röntgenbeugung zeigten, dass das Material flüssigkristalline Eigenschaften besitzt und erst jenseits von 300 °C schmilzt. Durch die Messung des raumladungsbegrenzten Stroms (SCLC) in Dioden-Konfiguration konnte eine Ladungsträgermobilität von $5,3 \cdot 10^{-6} \text{ cm}^2 \text{ V}^{-1} \text{ s}^{-1}$ bestimmt werden.

Im vierten Kapitel zeigen wir, dass das *grafting-to* Konzept nicht auf Seitenketten- und Bürstenpolymere beschränkt ist sondern auch angewendet werden kann um Oberflächen zu modifizieren. Damit können selbstassemblierte Monolagen von halbleitenden Polymeren realisiert werden. Wir weisen die Vielseitigkeit der CuAAC nach indem wir ein elektronisch aktives Material chemisch auf einer Oberfläche anbringen. Zuerst wird ein Substrat mit einem Azidosilan funktionalisiert worauf P3HT mit Alkin-Endgruppe mit dem Substrat bei hoher Pfropfdichte chemisch verknüpft werden kann. Derartige, mit auf einem Substrat geankerte, Bürsten wurden von hochmolekularem P3HT hergestellt. Dabei haben wir als Erste P3HT mit einem sehr hohen Molekulargewicht von 11400 g mol^{-1} verwendet um hohe Pfropfdichten zu erreichen. Die erfolgreiche Reaktion konnte mittels AFM und UV-Vis Spektroskopie nachgewiesen werden. Die ultradünnen P3HT-Bürsten ($< 4 \text{ nm}$) wurden direkt in organischen Feldeffekttransistoren SAMFET eingesetzt, wobei eine Ladungsträgermobilität von $1,6 \cdot 10^{-3} \text{ cm}^2 \text{ V s}^{-1}$ gemessen wurde. Dieser Wert ist dabei der höchste, der bisher für Polymer-Bürsten gemessen wurde und ist zwei Größenordnungen größer als bisher publizierte Mobilitätswerte für P3HT-Bürsten.

Introduction

1 Semiconducting Polymers

1.1 Controlled Synthesis of Semiconducting Polymers

The term controlled polymerization refers to several types of chain-growth polymerizations where the probability of termination reactions is reduced. In the case of reactions where the termination is almost absent, they are called living polymerization. The term controlled polymerization is most commonly associated with the controlled radical polymerization (CRP)¹ techniques but also describes a number of controlled metal catalyzed polycondensation reactions, most prominently the Kumada catalyst transfer polymerization (KCTP).² The growth of a polymer chain is either started by an initiator (CRP) or by a metal catalyst and each of these starting species starts a single polymer chain in an ideal case. The ratio of the initiator/catalyst to monomer is directly proportional to the achievable degree of polymerization. The degree of polymerization increases linearly with the monomer conversion, due to the chain growth mechanism. The polymerization may only be considered as controlled, if the molecular mass of the polymer is directly proportional to the conversion, as well as the initiator/catalyst concentration and the molecular weight distribution is narrow. This allows the control of molecular weight and any desired molecular weight can be exactly synthesized. Additionally, the active end groups allow the precise functionalization of end groups or synthesis of block copolymers. A (pseudo) 1st-order kinetic, on the other hand, is not a necessity for a controlled polymerization. Additionally, it has to be noted that controlled polymerizations are not necessarily living. The term living refers to the total absence of termination and transfer reactions and can be strictly speaking only be applied to the anionic polymerization.³

Kumada Catalyst Transfer Polymerization (KCTP)

The controlled synthesis of conjugated polymers is challenging and only a few examples, most prominently the polymerization of poly(3-hexylthiophene) (P3HT) or other electron-rich derivatives by KCTP, have been reported.⁴ Polymers with defined molecular mass and narrow distribution can be used to study effects of the influence of the molecular mass on the material's properties. More complex systems such as well-defined microphase-separated donor-acceptor block copolymers (D-A BCPs) can also only be realized if the synthesis of each block can be controlled.⁵ The Kumada coupling reaction can be applied to control the polymerization of aryl monomers thereby giving access to well defined conjugated polymers. This KCTP method has been applied to synthesis of polythiophenes, polyfluorenes and phenylene-/pyrrole-based polymers.⁴ P3HT is not only the most studied conjugated polymer, but is also the most prominent representative of polymers synthesized via KTCP. The synthesis of polythiophenes was optimized over the course of time. In the beginning only irregular polythiophenes⁶ could be synthesized. The development of Ni-catalyzed synthesis routes made it possible to obtain regioregular P3HT.^{7,8} Mc Cullough *et al.* and Yokozawa *et al.* independently showed that P3HT can be polymerized in a controlled manner (**Fig. 1**).⁹⁻¹² The active monomer species **2a** can be prepared either from 2-bromo-3-hexyl-5-iodothiophene **1** or 2,5-dibromo-3-hexylthiophene **3**. In case of **3**, during Grignard metathesis, a second sterically hindered and therefore inactive species **2b** is formed. The followings steps are identical for both routes. The Ni-catalyst is added and the inserted dimer **4** is formed, which then reacts to form the initiating species **5** via reductive elimination followed by intermolecular oxidative addition,. The nature of this first coupling step is the reason that at least one regiodeflect is generated in every polymer chain. From here on the polymerization proceeds in a chain-growth fashion, in which the monomers are solely coupled head-to-tail, until the monomer is consumed or the polymerization is quenched. The polymer chains are active even after the monomer is consumed if no quenchers are added. This living character can be used to synthesize BCPs and other complex polymers with different architectures. Studying the reactions during the polymerization in detail has helped to optimize the synthetic procedure of P3HT. LiCl can be used as an additive to decrease the time of the consumption of t-BuMgCl as it is

important to have a complete formation of the active monomer.¹⁴ With LiCl as additive, the second sterically disfavored monomer species **2b** is also incorporated which increases the molecular weight. One could expect, that this would lead to the formation of irregular polymers but Wu *et al.* found that the incorporation of the second monomer reduces the regioregularity only minimally.¹⁵ The sterically disfavored monomer species **2b** is still less reactive and is only built into the polymer chain after the majority of the monomer **2a** is consumed. Consequently, only one additional tail-to tail coupling defect is typically introduced to each chain. It is also possible to control the end-groups¹³ and to influence the final product by the choice of the quenching agent.¹⁶ End capping, thereby stopping the polymerization, with a functional Grignard reagent is a straightforward and elegant way to obtain different functional end-groups.¹⁷ Surprisingly, this method does not only lead to the formation of monocapped products as expected. A random walk of the catalyst along the polymer chain is the reason for formation of dicapped products unless the catalyst is bound

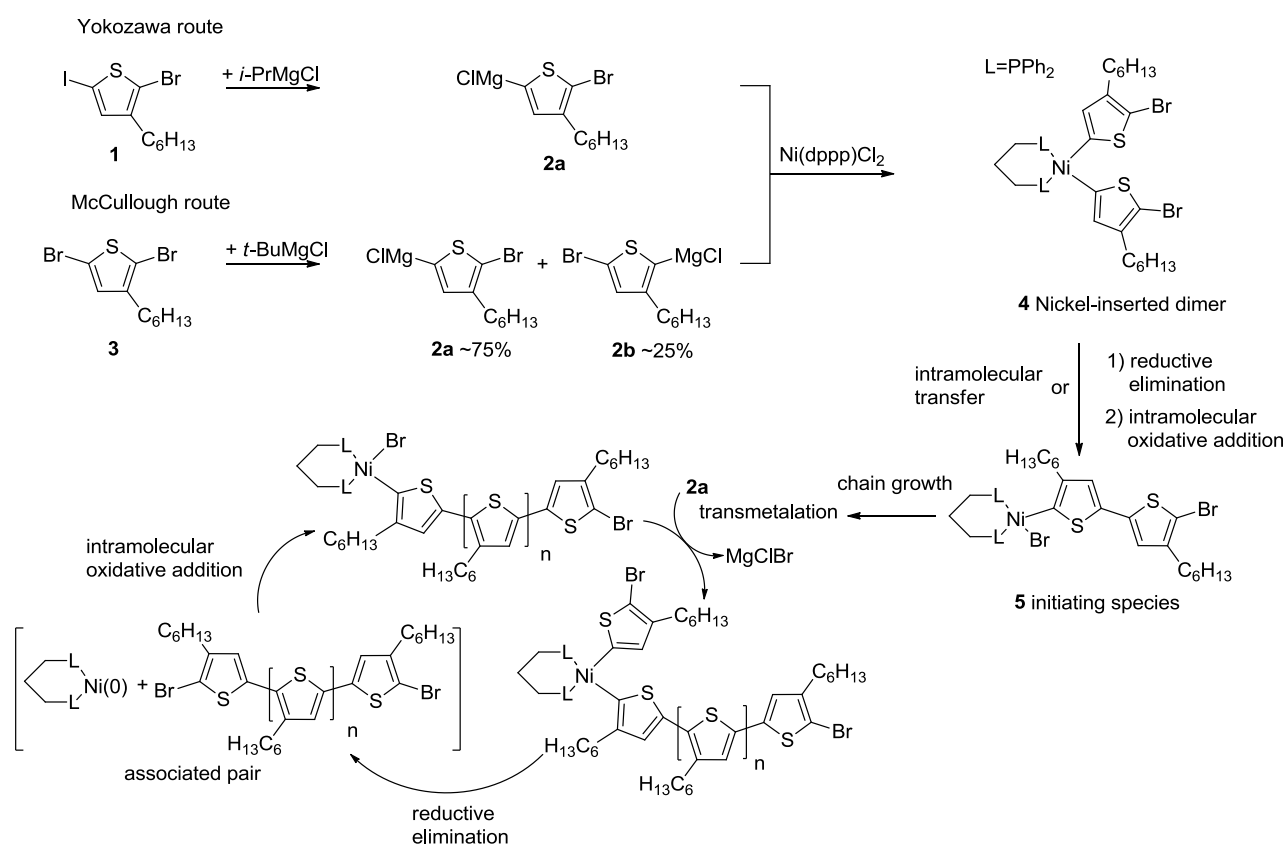


Fig. 1 The polymerization of the active Grignard monomer **2a** is characterized by a chain growth mechanism. The active Grignard monomer **2a** can be obtained from the 2-bromo-3-hexyl-5-iodothiophene (**1**, Yokozawa route) or 2,5-dibromo-3-hexylthiophene (**3**, McCullough route). Adapted from Lohwasser *et al.*¹³

by a stable π -complex like in the case of alkynes.¹⁸ The mobility of the catalyst along the polymer chain also effects the polymerization itself. The chain can indeed grow in both directions. At the end of the polymerization the initial regiodeflect from the initiating species **5** will not be at chain end but anywhere in the chain. Even though the catalyst is mobile along the chain, it does not exist in a free dissociated state. This is most important for the control of the polymerization which can only be maintained if every catalyst molecule starts exactly one chain and sticks on to that chain.

Nitroxide Mediated Radical Polymerization (NMRP)

The nitroxide-mediated radical polymerization (NMRP)^{19,20} is the oldest of the three major techniques of CRP, the other two being atom transfer radical polymerization (ATRP)^{21,22} and reversible addition-fragmentation chain transfer (RAFT)^{23,24} polymerization. In 1985 it was discovered that radical polymerizations can be controlled by decreasing the concentration of the active growing polymer radicals with the help of alkoxyamines.²⁵ NMRP makes it possible to control the radical polymerization of standard monomers like, e.g., styrene in order to produce well-defined polymers. The identification of suitable alkoxyamines, which provides both the initiating and the persistent radical, was important for the implementation of NMRP. In 1999 Hawker *et al.* reported a universal alkoxyamine system which greatly increased the set of monomers that could be polymerized via NMRP in a controlled way.²⁶ The newly introduced system is applicable for the NMRP of styrenes, acrylates, acrylonitriles and other functional vinyl monomers. The mechanism of NMRP relies on the equilibrium between an active species and a dormant species. Initially, the alkoxyamine decomposes thermally into a reactive radical and a not self-terminating persistent radical (**Fig. 2**). The persistent radical effect is the source of control of NMRP.²⁷ At the beginning, the concentration of active radicals and the persistent one is equal. The concentration of the active radicals is reduced due to self-termination whereas the persistent radicals' concentration stays constant. This drives the equilibrium towards the dormant species and the reduction of the overall radical concentration makes it possible to control the polymerization. For a high degree of control it is important to reach the equilibrium fast.²⁸ The addition of excess persistent radical can increase the control of the polymerization while at the same time the reaction speed is further decreased.^{29,30}

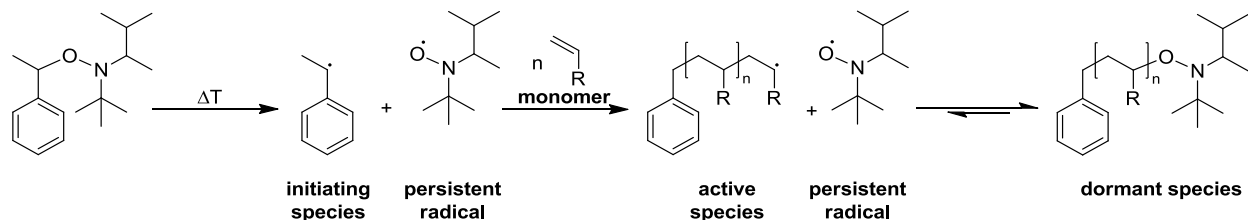


Fig. 2 Mechanism of NMRP. The initiating radical and the persistent radical are formed after thermal decomposition of the alkoxyamine. The initiating species starts the polymerization of the monomer. The control of the reaction is governed by the equilibrium between the active species and the dormant species.

The persistent radical effect predicts a decreasing radical concentration during the course of the reaction. This drastically slows down the reaction and a 2/3-order kinetic is expected.^{28,31,32} This also poses a problem for reaching high conversions. To increase the reaction rate high temperatures above 100 °C are generally applied, temperatures at which monomers such as styrene already exhibit a significant amount of thermal initiation.³³

Reversible Addition-Fragmentation Chain Transfer Polymerization (RAFT)

Aside from NMRP and ATRP which both rely on the persistent radical effect, a third major controlled polymerization technique with a fundamentally different mechanism was developed. The RAFT polymerization is a versatile tool for the synthesis of defined polymers due to its wide ranging applicability for many different monomers and a high tolerance to many different functional groups.^{23,34} Thang *et al.* were the first to report polymerizations controlled by different dithioesters.³⁵ The chain transfer agent (CTA) reversibly terminates the propagating chains and provides control over the polymerization. Many different CTAs have been developed including dithiobenzoates, dithioesters, trithio-carbonates, dithiocarbamates and xanthates.^{23,36,37} All CTAs (**Fig. 3**) generally have a reactive C=S double bond, the so-called Z-group and an R-group. The Z-group can be modified to optimize the addition and fragmentation rates and the R-group is the radical leaving group which has to be able to reinitiate the polymerization. The RAFT process differs from NMRP in the need of an external radical initiator. Azobis(isobutyronitrile) (AIBN), for example, is commonly used as thermal initiator. The initiating radical reacts with the monomer and forms the propagating radical P_n^\bullet which will eventually react with the CTA. The intermediate radical will then fragment either releasing P_n^\bullet or the radical R^\bullet which will start a new polymer chain.

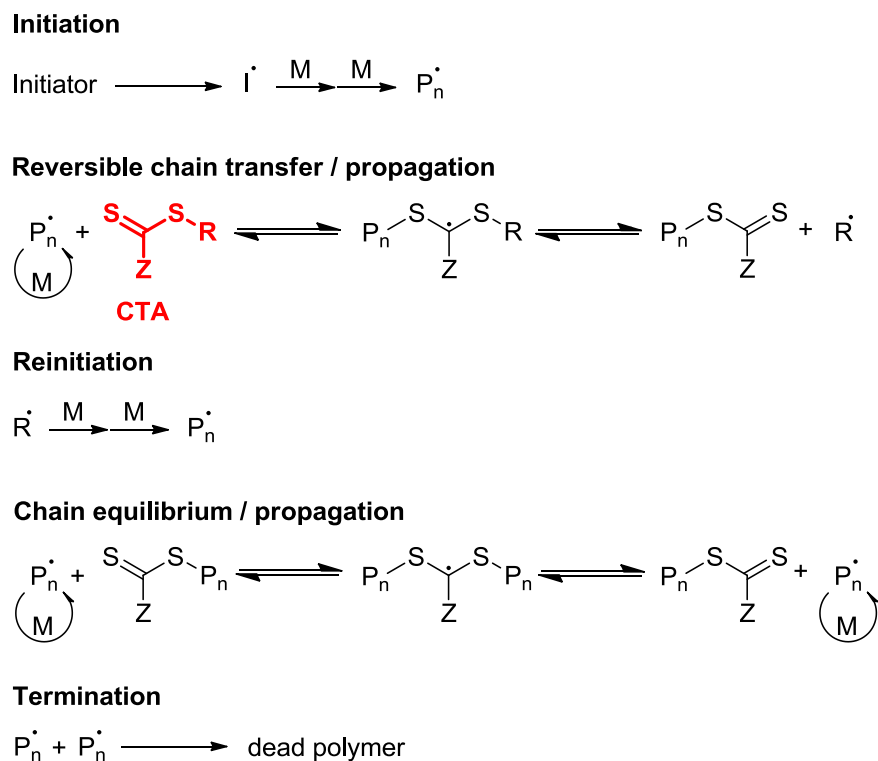


Fig. 3 Mechanism of RAFT. The chain transfer agent (CTA) is highlighted in red (Adapted from Ref. 23).

The equilibrium between the propagating chains and the intermediate radical species reduces the overall concentration of reactive radicals and the probability of termination reactions. It is crucial for good control that this equilibrium is reached rapidly. First order kinetics can be observed as the concentration is constant during the course of the polymerization. In the ideal case each polymer chain carries the R-group on the one side and a thiocarbonyl end group on the other side after the reaction is stopped. This allows post-polymerization reactions if R-groups with functional groups were used. This also makes it possible to combine RAFT with "click" chemistry by introducing functionalities such as azides or alkynes for the Cu(I) catalyzed azide/alkyne cycloaddition.³⁸ Such a RAFT agent which can be used for the polymerization of styrene derivatives was published by Gondi *et al.*³⁹ The thiocarbonyl group on the other hand can reinitiate the polymerization to form multiblock polymers. It was shown that the end group fidelity in α - and ω -position is strongly dependent on the amount of used initiator.⁴⁰ The amount of chains that are started by an initiator radical instead of the R-Group is higher, if the concentration of the initiator is increased thus decreasing the number of functionalized chains. A similar effect can be

observed in the ω -position, which influences the livingness of the polymerization and consequently the ability to reinitiate the polymerization. All initiator derived chains will eventually terminate. The livingness is therefore also higher if a lower amount of initiator is used.⁴¹⁻⁴³

1.2 Copper-Catalyzed Azide-Alkyne Cycloaddition

In order to modify polymer end groups, introduce side chains or couple two polymers in a post polymerization step highly efficient reactions are necessary. The reactions that are summarized by the term “click” chemistry in 2001 by Sharpless *et al.* are highly suitable for this task.⁴⁴ The stimulus for the success of this definition was the development of the copper-catalyzed azide-alkyne cycloaddition (CuAAC).^{45,46} The thermal cycloaddition of azides alkynes had been known since 1963 when it was described by Huisgen.^{47,48} The development of the CuAAC greatly broadened the applicability of the reaction. Both the azide- and alkyne-functionality are fairly inert in the absence of a catalyst, but the reaction is very fast and quantitative, even at room temperature, in presence of a Cu(I) catalyst and can be conducted in a wide variety of solvents including water.

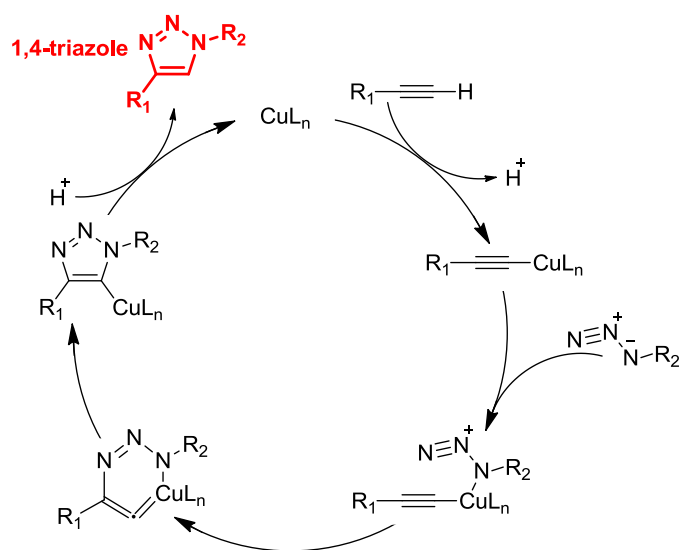


Fig. 4 Mechanism of the copper-catalyzed azide-alkyne of organic azides and terminal alkynes generating the 1,4-regioisomer of the disubstituted triazoles compound. Adapted from Fokin *et al.*⁴⁵

The proposed catalytic cycle is depicted in **Fig. 4**. In the first step the copper(I) acetylide is formed. Subsequently the organic azide is activated by a coordinating to copper followed by the formation of the C-N bond which leads to a strained metallacycle. The strained cycle rearranges to form the copper triazolide which in the last step releases 1,4-isomer of the triazole compound and sets the catalyst free to start the next cycle.⁴⁵

1.3 Donor Acceptor Block Copolymers

Donor-acceptor block copolymers (D-A BCPs) consist of two different semi conducting blocks. One is the electron rich donor polymer, transporting the holes, whereas in the other, the acceptor block with a high electron affinity, the electrons are transported. BCPs are generally known for their ability to form a thermodynamically stable morphology with dimensions of tens of nanometers depending on the block lengths. This phenomenon is called microphase separation and it has been theoretically described by Bates *et al.* for amorphous coil-coil BCPs with two immiscible blocks.^{49,50} The segregation of the two blocks is described by the Flory-Huggins interaction parameter χ and the degree of polymerization N .⁵¹⁻⁵³ Below a certain segregation strength ($\chi N < 10$) microphase separation is not

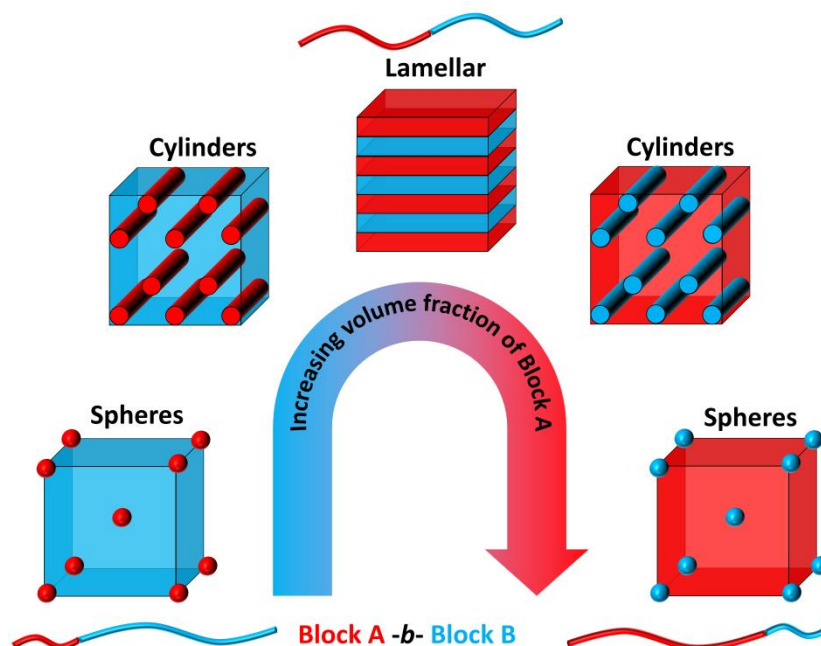
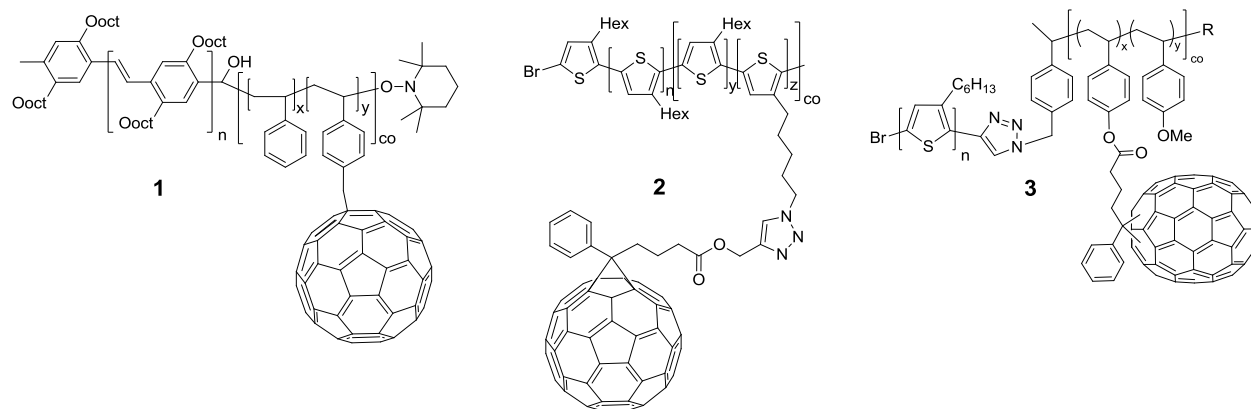


Fig. 5. Most commonly observed equilibrium morphologies observed in microphase-separated coil-coil BCPs. Depending on the volume fraction of the block either a spherical, cylindrical or lamellar morphology with either Block A or Block B as matrix can be observed. (Adapted from Ref. 54)

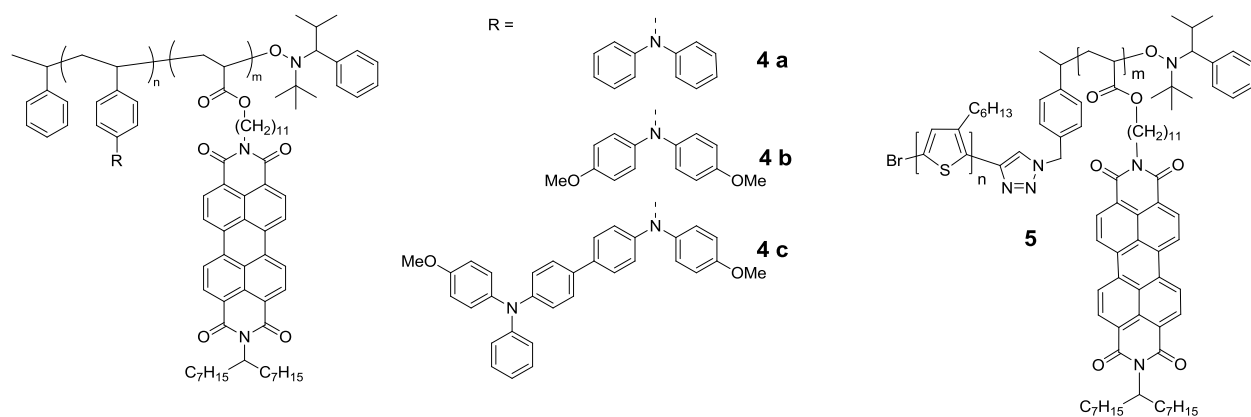
observed. For $\chi N > 10$ the blocks will demix and form an ordered morphology due to the constraints imposed by the connection of the polymers which prevents macrophase separation. For diblock copolymers a few defined morphologies are expected in relation to the volume fraction composition of the polymers (**Fig. 5**). Spherical, cylindrical or lamellar morphologies are the most commonly observed morphologies in addition to the gyroid morphology present between cylindrical and lamellar structures. Conjugated semiconducting polymers often have a stiffer backbone (rod-like) and have a tendency to crystallize due to π - π interactions between the aromatic moieties.⁵⁵ Diblock copolymers with a conjugated block, therefore, add a greater complexity to the system.⁵⁶ Apart from the segregation strength χN and the copolymer's composition the Maier-Saupe parameter μN may be necessary to describe the microphase separation in such a system.⁵⁷ If at least one of the blocks is crystalline several different scenarios for crystallization influenced phase separation can be distinguished.⁵⁵ Depending on the segregation strength the BCP will be either microphase-separated or disordered in the melt. For the first case the crystallization of a block can destroy the ordered structure; this is called break out crystallization. When the force to crystallize is weaker than the tendency to form a microphase-separated domain, the crystallization will occur within the confinement of the nano domains. This is called confined crystallization and it was reported for a D-A copolymer by our group, proving the possibility of ordered microphase separation in such systems.⁵⁸ In the case of a disordered melt, the crystallization of one block can induce the microphase separation.

D-A copolymers are interesting materials for organic photovoltaics. The formation of ordered and thermodynamically stable morphologies on the nano scale was proposed to provide maximum D-A interface, domain sizes in the range of exciton diffusion length and excellent charge transport pathways for both holes and electrons and these materials can work as compatibilizers to stabilize a D-A blend of a bulk heterojunction solar cell.^{54,59,60} This concept has a number of challenges as well.⁶¹ Firstly, new controlled synthesis routes had to be developed as ordered microphase separation is only observed in defined copolymers with narrow mass distribution. Secondly, the orientation of the morphology in thin films has to be controlled in order to provide charge transport pathways perpendicular to the substrate, a task which is still unsolved.

a) Side-chain fullerene grafted donor-acceptor copolymers



b) Side-chain perylene bisimide grafted donor-acceptor copolymers



c) All-conjugated donor-acceptor copolymers

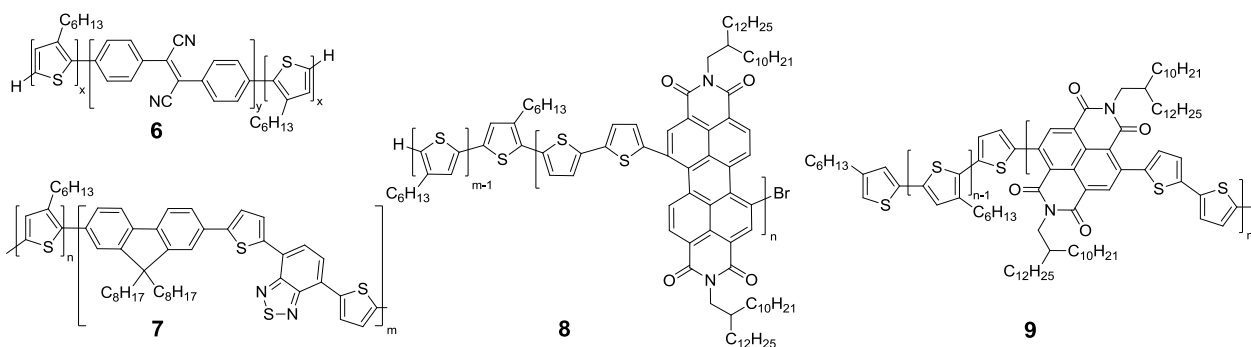


Fig. 6 Overview on donor-acceptor block copolymers with some examples: Chemical structures of side chain D-A BCPs with fullerene (a)^{70,77,78} and perylene bisimide (b)^{67,58} as acceptor. Chemical structures of all-conjugated polymers (c).^{85,86,93,94}

A brief selection of recent reports on D-A polymers will be given in following section, divided into three classes (see **Fig. 6**). A more comprehensive survey of the research can be found in a number of reviews on the topic.⁶²⁻⁶⁵ Several of the earliest studies focused on copolymers with fullerene side chains as acceptor units. A number of publications reporting studies on defined copolymers with perylene bisimide acceptors can also be found after the seminal work of Lindner and Sommer *et al.*^{66,67} Recently, some reports focused on all-conjugated D-A copolymers have appeared.

Fullerene grafted D-A copolymers comprised of a poly(p-phenylene vinylene) (PPV) block and polystyrene grafted with fullerene such as **1** were synthesized in the group of G. Hadziioannou.⁶⁸⁻⁷² In 2006 Fréchet *et al.* made a BCP by polymerizing a fullerene-derivatized norbornene and a P3HT norbornenyl macromonomer via ROMP.⁷³ Advances in the synthesis of P3HT led to several reports on BCPs with P3HT as donor block.^{74,75} Hashimoto *et al.* synthesized BCPs where the fullerene was grafted to the hexyl side chain of P3HT achieving an efficiency of 2.46 % in a single layer device of **2**.^{76,77} Recently, Hufnagel *et al.* synthesized fullerene-grafted D-A BCPs with C₆₀ and C₇₀-units.⁷⁸⁻⁸⁰ The composition, grafting density and molecular weights were changed in order to systematically investigate the influence of polymer design on structure formation and charge transport.

The second class of D-A polymers to be mentioned here have perylene bisimide (PBI) as acceptor. This strategy of using a controlled polymerization of a PBI containing acrylate was developed in our group by Lindner and Sommer *et al.*^{66,67} A number of coil-coil polymers comprised of different triphenylamine based donor blocks and a perylene bisimide acrylate acceptor block were obtained (**4 a-c**).⁶⁷ Functional vinyl monomers carrying the donor and the acceptor were synthesized and polymerized sequentially. Due to the better opto-electronical properties, the donor was changed to P3HT.⁸¹⁻⁸³ By a macroinitiator route starting from P3TH, Lohwasser *et al.* synthesized **5** with high molecular weight and narrow distribution.⁵⁸ They could show for the first time that microphase separation into ordered lamellar or cylindrical morphologies is possible in D-A polymers with a crystalline P3HT block.

Other acceptor polymers have been implemented aside from perylene bisimides or fullerenes. Several recent reviews^{61,62,84} can be found on this topic and a few examples will

be highlighted here. Scherf *et al.* reported one of the first fully conjugated D-A copolymers with a P3HT donor block and several different acceptor polymers (**6**), usually combining polycondensation and KCTP. One major drawback of this approach is that the final product is a mixture of block copolymer and homopolymers and the block obtained by polycondensation is ill-defined.⁸⁵ In a two-step synthesis triblock copolymers were generated under Yamamoto conditions. Poly(3-hexylthiophene)-*block*-poly-((9,9-dioctylfluorene)-2,7-diyl-*alt*-[4,7-bis-(thiophen-5-yl)-2,1,3 benzothiadiazole]-2',2''-diyl) (P3HT-*b*-PFTBT)(**7**) has been reported by several groups⁸⁶⁻⁸⁸ and solar cells with this copolymer exhibited the best performance yet for a single component all-polymer solar cell.⁸⁹ A recent study also examined the influence of hydrophilic side chains on the structure formation in a similar polymer.⁹⁰ Hawker *et al.* synthesized poly(3-hexylthiophene)-*block*-poly(diketopyrrolopyrrole-terthiophene) (P3HT-*b*-DPPT-T) and studied the influence of the copolymer's structure in solution on the observed micro structure in the dried state. They could show that solvents can influence the nanoscale structure in thin films.^{91,92} The copolymer P3HT-*b*-PBIT (**8**) with a main chain perylene bisimide block was synthesized by Shifan Wang *et al.* via Stille coupling.⁹³ In all-polymer solar cells with a simple active layer they achieved a power conversion efficiency of 1.0 %. P3HT-*b*-PNDIT2 (**9**) with P3HT as donor material and an alternating donor-acceptor naphthalenediimide bithiophene copolymer, poly{[N,N'-bis(2-octyldodecyl) naphthalene-1,4,5,8-bis(dicarboximide)-2,6-diyl]-*alt*-5,5'-(2,2'-bithiophene)} (PNDIT2) as acceptor material were synthesized by Yamamoto⁹⁴ and Stille^{95,96} coupling. In the group of M. Sommer P3HT-*b*-PNDIT2 was synthesized via direct C-H arylation condensation which is the first time a fully conjugated diblock copolymer was realized by this method.⁹⁷ In the field of acceptor blocks, a strategy to obtain well-defined blocks with controlled molecular weight and high end group fidelity is still elusive. But first reports from Kiriy *et al.* (using Zn intermediates) and Seferos *et al.* (using new Ni-catalysts) have been published.^{98,99} Further optimization if reaction control can finally result in well-defined donor-acceptor block copolymers with narrow dispersity.

Even if the scientific challenges of synthesis of well-defined D-A block copolymers are solved, a necessary and reliable vertical alignment of microdomains in microphase

separated block copolymer thin film remains as the holy grail of the research topic of block copolymers for solar cell applications.

1.4. Bottlebrush Copolymers

Bottlebrush copolymers are comb polymers consisting of backbones which have one or more side chains at every repeating unit.^{100,101} The densely packed side chains force the backbone into an extended chain through steric repulsion. This leads to a stiffening of the backbone and, therefore, an increased persistence length. Unique material properties that arise due to the architecture are higher polymer chain-mobilities compared to linear polymers and the absence of chain entanglements. Bottlebrushes may be especially interesting for organic photovoltaics (OPV). One of the major unsolved challenges for all-polymer solar cells with an ordered morphology, as proposed by our group,⁵⁹ is the vertical alignment of the nanostructure.⁶¹ S. W. Hong *et al.* showed that a vertical alignment might be the thermodynamically stable in brush diblock copolymers.¹⁰² In thin films of linear BCPs a parallel orientation of the morphology is usually observed due to the preferential wetting of the substrate by one of the blocks (see **Fig. 7**). In thin films of brush copolymers a parallel alignment of the rigid backbone is favored which leads to a vertical orientation of the side chain nano domains. There are also other beneficial properties of brush copolymers than merely the orientation in thin films. Generally, much higher molecular

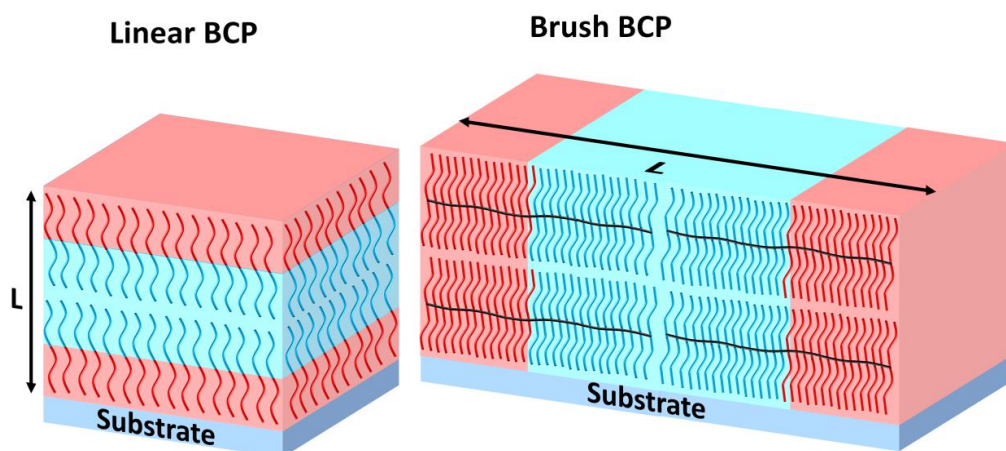


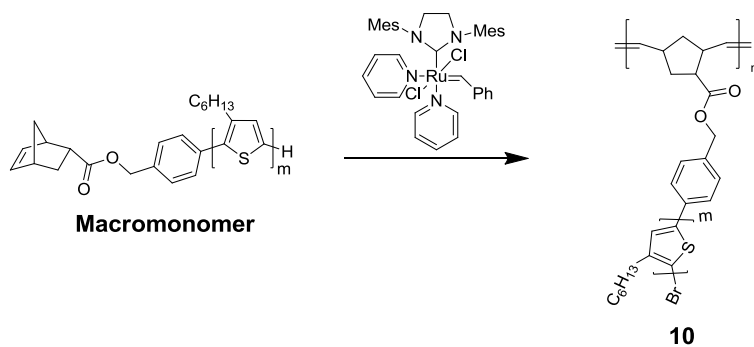
Fig. 7 Schematic of the parallel orientated lamellar microstructure in thin film of a linear BCP (left) in contrast to a perpendicular morphology in a thin film of a brush BCP (right). (Adapted from Ref. 102)

weights leading to better thermal stability of thin films can be obtained in brush copolymers than in linear polymers. Particularly the controlled polymerization of semiconductor polymers is limited to a relatively low degree of polymerization mainly due to solubility issues. Secondly, the domain size L of the microphase-separated structures depends on the degree of polymerization (or molecular weight) of the linear block (**Fig. 7**) whereas in brush BCPs the domain size can be tuned by the degree of polymerization of the extended backbone.¹⁰³ In particular, very large domains are accessible which cannot be realized in linear BCPs.

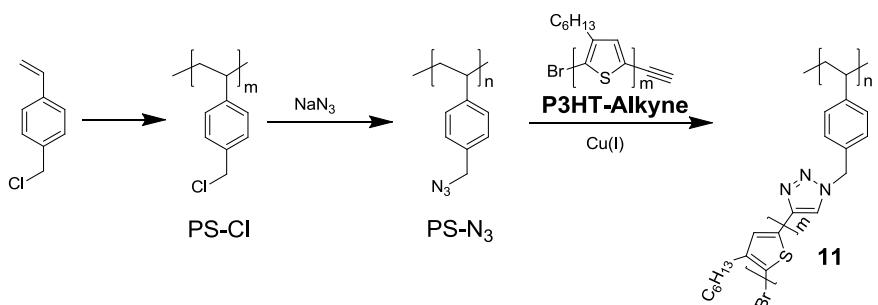
There are only very few examples of brush copolymers with P3HT as semiconducting side chains (**Fig. 8**). Synthetically these systems are available either by a grafting-through or grafting-to processes. Norbornenyl macromonomer of P3HT are synthesized to polymerizes poly(norbornene)-*g*-P3HT bottlebrushes **10** via grafting-through. Method S. Ahn *et al.* polymerized brushes with short side chains and observed the formation of irreversible aggregates in these systems.¹⁰⁴ In another report, the side chain length was varied and the bottlebrushes were tested in solar cells.¹⁰⁵ Bottlebrushes with short P3HT are also accessible by a modular grafting-to approach. Poly(chloromethylstyrene) can be quantitatively converted to poly(azidomethylstyrene) and grafted with P3HT alkyne via CuAAC to obtain the bottlebrushes (PS-*g*-P3HT) (**11**) with a styrenic backbone.¹⁰⁶

The first report of a P3HT grafted brush (**12**) by K. Sivula *et al.* also proved that D-A copolymer brushes can be realized via a sequential grafting-through polymerization.⁷³ This year, new random bottlebrushes incorporating P3HT and polylactide (PLA) side chains with a statistical distribution along a polynorbornene backbone were reported (**13**).¹⁰⁷ For bottlebrush copolymers with symmetric compositions, ordered lamellar structures were observed. The latest report on fully conjugated D-A copolymers is a grafted P3HT brush with a poly[[9-(1-octylnonyl)-9H-carbazole-2,7-diyl]-2,5-thiophenediyl-2,1,3-benzothiadiazole 4,7-diyl-2,5-thiophenediyl] backbone as acceptor polymer **14** (PCDTBT-*g*-P3HT).¹⁰⁸ Their synthetic approach allowed for an independent control over the grafting length, the grafting density and the backbone length. Additionally, the P3HT used in this study is a higher than previously reported which is important due to the optimum of the electronic properties for P3HT near a molecular weight of 12000 g mol⁻¹.

a) Grafting-through: PNB-g-P3HT



b) Grafting-to: PS-g-P3HT



c) Copolymer brushes

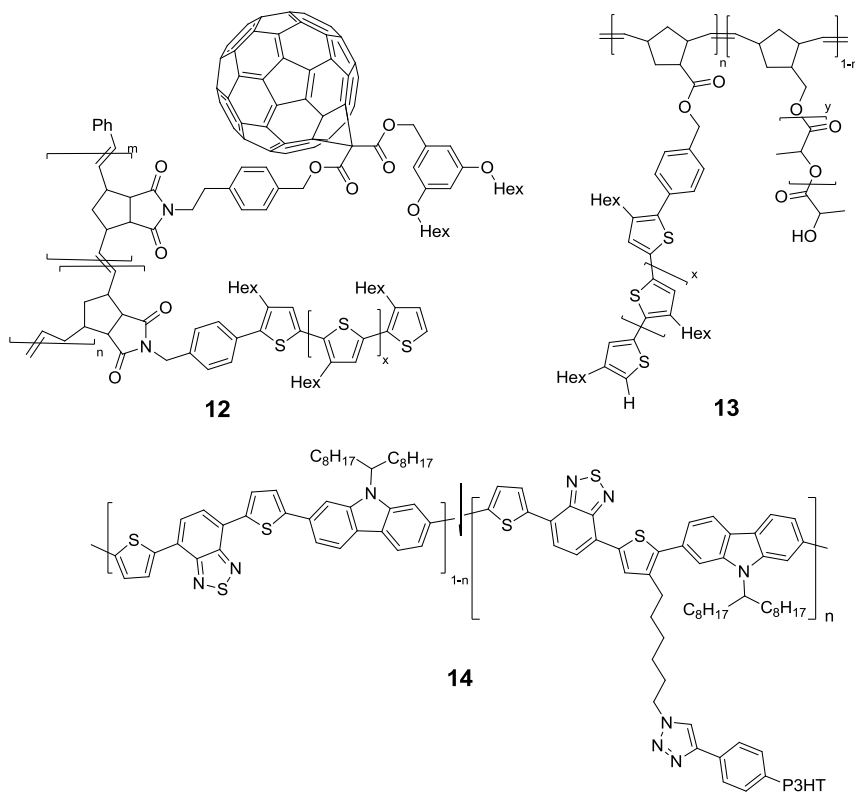


Fig.8 Scheme of the synthesis of P3HT bottlebrushes via a grafting-through (a)^{104,105} and grafting-to (b)¹⁰⁶ method. c) Chemical structures of copolymers brushes containing P3HT.^{73,107,108}

1.5. Surface Grafted Brushes

Polymers that are tethered to a substrate or the surface of particles are often generally referred to by the term polymer brush. A brief introduction to the characteristics of this system is given in the following section and the recommendation to follow a more narrow definition of the term bottlebrush will be explained.¹⁰⁹

The first studies on polymer brushes in the 1950s focused on grafting polymers to colloidal particles.¹¹⁰⁻¹¹⁵ The fundamentals of the theory of polymer brushes were later published by Alexander¹¹⁶ and de Gennes.^{117,118} While the early work focused on the physisorption¹¹⁹⁻¹²¹ of polymers on a surface, end-chain grafted polymers with covalent attachment became increasingly interesting due to the higher stability of the films. Such layers are synthetically accessible either by grafting-from or grafting-to techniques. For the grafting-from method an initiator must be coupled to the surface and the polymer chain grows directly from the surface. Brushes with high density are accessible but the characterization of the formed polymers is not trivial. Brushes synthesized by different living and controlled techniques, were reported including P3HT brushes via surface initiated KCTP.¹²²⁻¹²⁴ Also, preformed polymers, which can be accurately characterized, can be bound covalently to the surface by the grafting-to method.¹²⁵ The main challenge for this second method is the realization of a high density of the polymer at the surface. The achievable grafting-density for the grafting-to approach is governed by the reaction time, the polymer's concentration and the molecular weight of the polymer.¹⁰⁹

The properties of such polymers tethered to a substrate are highly dependent on the density of polymer chains on the surface. At low grafting densities, the distance between two tethered polymers is higher than the gyration radius R_g of the polymer chains. This regime is usually called mushroom regime. When the density (σ) increases the distance between the polymer chains will eventually be smaller than their size (**Fig. 9**). At this point the chain will overlap and a continuous film will form (transition to the brush regime). At even higher densities the polymer chains are forced into a chain extended conformation. This high stretching of the chains is the defining parameter of the true brush regime. W. J. Brittain and S. Minko,¹⁰⁹ therefore, recommend to use the term polymer brush only for such densely grafted layers.

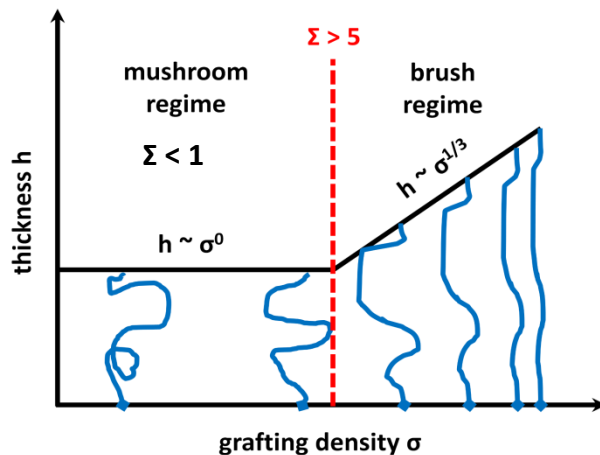


Fig. 9 Dependence of the thickness of tethered polymer films on the grafting density. For low densities the thickness is constant (mushroom regime), whereas the stretching of the polymer chains leads to an increased thickness for higher grafting densities (brush regime). The brush regime can be observed if the reduced tethered density Σ is higher than 5. (Adapted from Ref. 109 and 126)

The aforementioned regimes and their behavior were described theoretically and experimentally. Wu *et al.*¹²⁶ synthesized surface anchored polyacrylamides with a density gradient and were able to observe the crossover between mushroom and brush regime by determining the thickness of the wet film. In the mushroom regime the thickness is independent of the low grafting density. Whereas in the brush regime the thickness h increases with the density σ according to:^{126,127}

$$h \sim \sigma^{1/3} \quad (1)$$

In order to determine the regime of a grafted polymer film, the reduced tethered density Σ can be used. This parameter indicates the number of polymer chains which are in an area that would otherwise be occupied by one non-interacting polymer chain in the respective solvent and at the specific temperature. It is defined as:

$$\Sigma = \sigma \pi R_g^2 \quad (2)$$

where R_g is the gyration radius of the polymer chains. The grafting density can be determined depending on the brush thickness h and the molecular weight M_n of the polymer:

$$\sigma = \frac{h \rho N_A}{M_n} \quad (3)$$

(N_A = Avogadro's number; ρ = bulk density of the polymer)

There are several reports on the transition from mushroom to brush regime and films of tethered polymers chains can thus be divided into three regimes. For $\Sigma < 1$ the films are in the mushroom regime, characterized by separated non-interacting chains on the surface. Between $1 < \Sigma < 5$ the transition to the brush-regime is observed. Above $\Sigma > 5$ the “true” brush regime can be observed.

In organic electronics self-assembled monolayer layers (SAMs) are used to functionalize surfaces,¹²⁴ e.g. in organic photovoltaics (OPV) they function as charge extraction layers for holes or electrons.^{129,130} Chemical bound interlayers which are stable towards solution based processing may be beneficial in terms of performance and processing of the device.¹³⁰ Additionally, several SAM based organic field effect conductors (SAMFETs) have been reported with small molecules.¹³¹⁻¹³³ P-type SAMFETs based on oligothiophene derivatives with charge carrier mobilities up to $2.0 \cdot 10^{-2} \text{ cm}^2 \text{ V}^{-1} \text{ s}^{-1}$ have been described.^{132,133} The best n-type SAMFETs, based on perylene bisimides (PBIs) were reported by Ringk *et al.* with a mobility of $1.5 \cdot 10^{-3} \text{ cm}^2 \text{ V}^{-1} \text{ s}^{-1}$.¹³⁴

The synthesis of different surface tethered films of semiconducting polymers such as poly(triphenylamine),¹³⁵ poly(fluorine)¹³⁶, P3HT¹²⁴ or poly(p-phenylene)¹³⁷ has been reported. P3HT brushes on nano particles^{138,139} or on a substrate^{140,141} can be synthesized by the grafting-from approach via surface initiated KCTP. Polymer brushes of P3HT by the grafting-to approach were also realized on oxidic substrates,^{142,143} gold nanoparticles¹⁴⁴ or graphene oxide sheets.¹⁴⁵ P3HT brushes were grafted on an indium-tin oxide (ITO) electrode as interlayer by N. Doubina *et al.*¹⁴⁶ and J. Alonzo *et al.*¹⁴⁷ used such a brush as anode buffer layer in organic solar cells. Recently it was reported that the thermal conductance of poly(3-methylthiophene) brushes is 6 times better than spin-cast films of the same materials.¹⁴⁸ There are still only few examples where the electrical properties in semiconducting polymer brushes has been studied. The only report on SAMFETs of P3HT brushes revealed a very low charge carrier mobility of $5 \cdot 10^{-5} \text{ cm}^2 \text{ V}^{-1} \text{ s}^{-1}$.¹⁴²

2 Characterization Methods

2.1 Polymer Characterization Methods

Molecular Weight Determination

The properties of polymers are governed by their molecular weight and distribution. Characterizing polymers in order to determine these parameters is therefore quintessential for gaining insights into the material properties. The most important relative method for this is size exclusion chromatography (SEC).¹⁴⁹ Similar to other chromatographic methods the analyte, i.e., the polymer sample is eluted by a solvent over a solid-state column. SEC is conducted in a regime where no enthalpy interactions between the analyte and the column take place and the sample is only separated by the difference in hydrodynamic radius of the polymer coil in solution. Smaller coils are held back in the porous column material while the biggest chains elute first (**Fig. 10 a**). After the column the fractions can be detected by concentration dependent (refractive index, UV-Vis) and molecular mass sensitive detectors (light scattering). Setups with multiple detectors provide even more information simultaneously, e.g., absorption measurements at different wavelengths can give additional information about the sample's chemistry.¹⁵⁰ SEC is a standard method for polymer

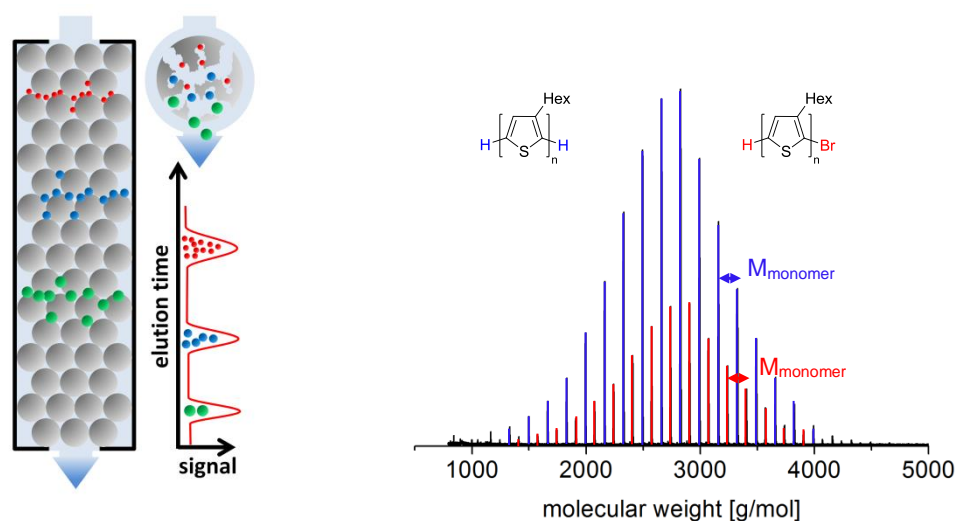


Fig. 10 Principles of size exclusion chromatography (SEC) (left). Bigger molecules have the smallest elution time while smaller molecules are held back in the porous column and are eluted later. The graph on the right shows a MALDI-ToF spectrum of P3HT. Two peak series can be observed and assigned to polymer chains with different end groups.

characterization but more complex systems like BCPs or branched polymers have to be characterized with care. The elution time relies on the hydrodynamic radius of the polymer in the specific solvent under the assumption that the polymer does not interact with the column materials or eluent and the molecular weights are calibrated with a particular calibration material. This makes SEC a relative method and no absolute molecular weights can be accurately determined by this method^{151,152} The molecular weight calibration is done by measuring the elution time of a series of well-defined polymers with known molecular weights. Polymer standards are only available for a small number of polymers such as polystyrene or polymethylmethacrylate. Thus even the relative molecular weight of novel polymers determined with SEC and some calibration polymer should be interpreted with care. The solution aggregation of the polymer and attractive or repulsive interactions between the polymer and the column or eluent may also impede the analysis.¹⁴⁹ If possible a second method besides SEC should be employed. Matrix assisted desorption laser spectroscopy (MALDI) with time of flight (ToF) detector is a complementary measurement technique. MALDI-ToF allows non-destructive mass spectrometry of polymers and absolute molecular weights can be determined.¹⁵⁴ For low molecular weights, it is also possible to obtain spectra with a resolution of repeating units and the polymer's end groups can be exactly determined (**Fig. 10 b**). As a downside this technique is restricted to polymers with rather low molecular weight or only for those which fly as charged species in a field and reach the detector and which have very narrow distribution. The measurement conditions also have to be optimized for every unknown polymer. Additionally, polymers with labile end groups of complex architectures are difficult to measure.¹⁵⁵

Kinetics and Conversion of Polymerization Reactions

Several methods for controlling polymerizations have been mentioned before. In order to obtain defined materials it is important to determine whether the polymerization was conducted in a controlled fashion. The most important feature of controlled polymerizations is the possibility to make polymers with predefined molecular weights. For a successful polymerization, the molecular weight can be predicted from the conversion and the ratio of the catalyst, initiator or transfer agent to the monomer. The molecular weight and the conversion must be monitored during the polymerization in order to

determine the controlled fashion of the reaction. By NMR-spectroscopy the conversion can be monitored and monomer ratios in case of copolymerizations can be monitored. In some cases it is even possible to determine the degree of polymerization by end group analysis. Other techniques like IR-spectroscopy, which can be used for *insitu* monitoring, or gas chromatography can also be used to determine the conversion. SEC can be used to determine the molecular weight evolution by analyzing samples at different time intervals and kinetics of polymerization can be studied. The shape of the molecular weight distribution in SEC can be indicative of side-reactions. A broad distribution is the result of bad control and low- or high-molecular weight shoulders have their origin in unwanted transfer and termination reactions. For polymerizations with macroinitiators SEC is a reliable technique that can discern between the growth of a second block and the formation of homopolymers. After the conversion and the molecular weight are determined a linear relationship between both parameters must be observed with a slope which is proportional to ratio of the catalyst, initiator or transfer agent to the monomer, otherwise side reactions occurred and the control was lost.³

Complex polymer structures can be obtained by polymer analogous reactions of functionalized polymers. Here, the reactions of end and side groups have to be monitored. For small molecules IR-spectroscopy in combination with NMR can be easily applied for this task. This combination can also be used to quantify the grafting of small molecule side chains to a polymer backbone.¹⁵⁶ End groups on the other hand can be more difficult to characterize quantitatively due to the high dilution. MALDI-ToF can be used to identify end groups more accurately by the appearance of different peak series. The assessment of click conjugations of polymers and the formation of block/brush copolymers is often not straightforward. SEC can provide important information but is often misinterpreted. After the conjugation of two polymers a new copolymer should be obtained. In SEC a new distribution at lower elution values can be observed and also unreacted fractions of the precursor polymers. Low/high molecular weight shoulders or multimodal distributions are signs of an incomplete reaction or unwanted side reactions. This is only true if both polymers have truly narrow distributions. Barner-Kowollik showed that the quantitative

conjugation of polymers with broad distributions can lead to products with bimodal distributions.¹⁵⁷

2.2 X-ray Diffraction

Structure and structure formation has great influence on the electronic properties of organic semiconductors and the performance of devices made from these materials.^{158,159} A very versatile and reliable characterization technique for polymers is X-ray scattering.¹⁶⁰ In contrast to microscopy techniques, which only give information about a small area at a surface (atomic force microscopy - AFM) or thin cut of a material (transmission electron microscopy - TEM), X-ray scattering can measure average bulk properties over a larger volume.

X-rays interact with the electrons in a material. The excited electrons start to oscillate and scatter X-rays. If this scattering of X-rays occurs at multiple positions in an ordered lattice, the scattered wave will form constructive and destructive interferences depending on the distance of the lattice planes d , which results in distinct diffraction patterns. The Bragg equation¹⁶¹ gives the condition for constructive interference (**Fig. 11 a**):

$$n\lambda = 2d\sin\theta \quad (4)$$

where $\lambda = 0.154 \text{ nm}^{-1}$ ($\text{CuK}\alpha$ radiation) is the wave length of the X-ray and θ is the angle of incidence.

Depending on the incidence angle of the X-rays θ , different size ranges can be analyzed. In the wide-angle X-ray scattering range (WAXS) sizes smaller than 5 nm can be analyzed (**Fig. 11 b**). Therefore, the crystalline lattice and crystal sizes and π - π distances can be analyzed.¹⁶² Temperature-dependent measurements in this region allow the observation of phase transitions between crystalline phases, meso-phases and amorphous melts. At smaller angles (SAXS), structures with a size of up to 100 nm can be measured. This is especially useful to detect microphase separation in BCPs and the lamellar long period in crystallites¹⁶³

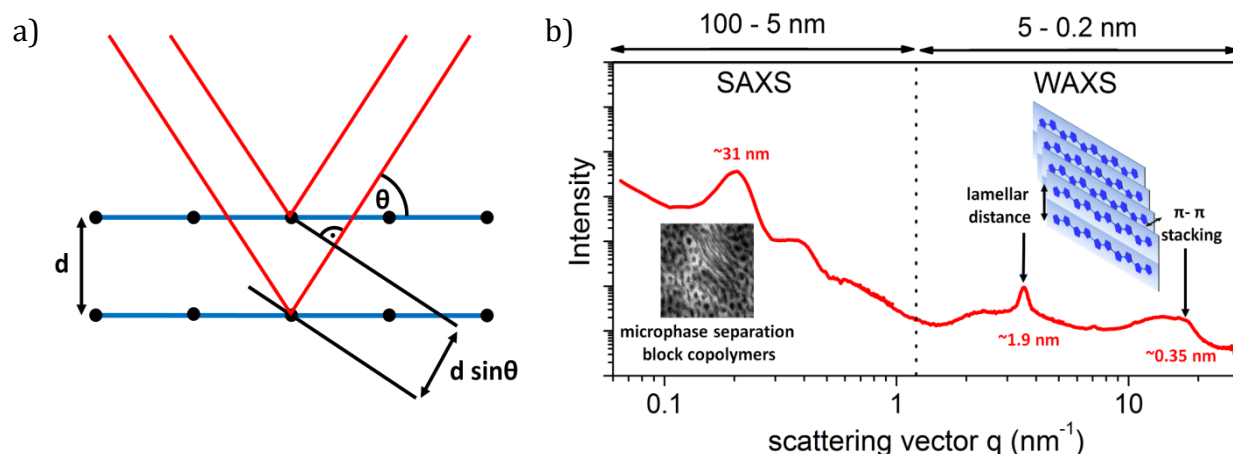


Fig. 11 a) Scheme of the diffraction of X-rays at a lattice. b) Accessible length scale in SAXS and WAXS. The X-ray scattering of a microphase-separated diblock copolymer with a crystalline block is shown. In the SAXS region the microphase-separated domain can be observed. In the WAXS region the lamellar distance ($a \sim 1.9 \text{ nm}$) and the π - π -stacking of the crystalline block are visible.

The characterization of thin films is possible by grazing incidence X-ray scattering at small (GISAXS) as well as wide angles (GIWAXS) and allows for the characterization of inner morphology of the film.¹⁶⁴ By GISAXS/GIWAXS it is possible to measure the orientation of the nanostructure and crystals within the film. This information is crucial for understanding the performance of these polymers in organic electronics. The crystal orientation, for example, has a profound influence on the charge carrier transport in a device due to the high anisotropy of the charge carrier mobility in polymeric semiconductors.¹⁶⁵ GISAXS/GIWAXS has become an important method to understand the material properties of organic semiconductors in thin films.^{166,167} Only the necessity of a strong X-ray source such as a synchrotron due to the small measured volume and the low scattering contrast of organic materials prevents even wider application.¹⁶⁶

2.3 Charge Transport in Organic Semiconductors

The performance of devices incorporating organic semiconductors, such as organic photovoltaics (OPV), organic light emitting diodes (OLEDs) or organic field-effect transistors (OFETs), is coupled mainly to the efficiency of the charge transport. Organic semiconductors are disordered materials and, therefore, relatively low charge carrier mobilities are obtained in comparison to inorganic semiconductors.¹⁶⁸ Several techniques are available for measuring this property. Two of them, space-charge limited current (SCLC) measurements and organic field-effect transistors (OFETs), were used in this thesis. Both methods will be discussed briefly.

After the generation of charge carriers, either electrons or holes, their movement is either driven by an electric field F or a gradient of the charge concentration. The charge carrier mobility μ is the motion of the charge carriers and is defined as the charge's effective drift velocity v per unit electric field:¹⁶⁹

$$\mu = vF^{-1} \quad (5)$$

The drift velocity is often not proportional to the electric field leading to a field dependence of the mobility μ . By Ohm's law the current j is given by the materials conductivity σ_c and the electrical field as $j = \sigma_c F$. The current can also be described by $j = env = en\mu F$ (n is the number of charge carriers and e is the elementary charge) and we can therefore, relate the mobility and conductivity by:

$$\sigma_c = en\mu \quad (6)$$

Organic semiconductors are predominantly disordered materials (amorphous glasses, or semi-crystalline materials). In contrast to inorganic semiconductors, where band-transport can be observed¹⁶⁹, the transport in organic semiconductors is usually described by disorder-controlled transport or hopping transport. The disorder in form of chemical or structural defects is the reason for localized states in the organic semiconductor and the transport of charges can only occur by a non-coherent transfer of electrons. This hopping process is thermally activated and the mobility μ becomes depended on the temperature T and the electrical field F . Additionally, in each method, the charge carrier concentration varies and the charge density influences the charge carrier mobility.¹⁷⁰ Therefore, the mobility values determined by two different methods can vary orders of magnitude.

Additional parameters that influence the measured charge carrier mobility are the preferential orientation of the polymer chains depending on molecular weight, processing conditions and nature of substrate.

Space-Charge Limited Current Measurements

The charge carrier mobility of organic semiconductors can be obtained by measuring the space-charge limited current (SCLC) in a diode configuration (**Fig. 12**).^{171,172} In this setup the material is sandwiched between specially selected electrodes, one of which allows only the injection of one kind of charges (holes or electrons) and the other allows the extraction of the same charges. In other words, the current flowing through the sample should not be injection limited. Charges are injected from an electrode into the semiconductor and the current-voltage characteristics are measured. Single carrier devices are usually fabricated in order to measure either the charge transport of holes or electrons. In hole-only devices the charges are injected and transported through the semiconductor's HOMO while in electron-only devices the charge transport takes place in the LUMO. Typical device configurations can be glass/ITO/PEDOT:PSS/semiconductor/Au for hole only devices and glass/ITO/ZnO/semiconductor/Ca/Al for electron only devices.

The choice of the electrodes is crucial for the characterization of the semiconductor's mobility. For electrodes that can inject more charges than the semiconductor can transport, called ohmic electrodes, the measured current is limited by the material's space-charge and, therefore, the bulk mobility of the semiconductor. The dependence of the space-charge limited current J_{SCL} on the charge carrier mobility, in the absence of traps, is described by the Mott-Gurney equation:¹⁷³

$$J_{SCL} = \frac{9}{8} \epsilon_0 \epsilon_r \mu \frac{V^2}{L^3} \quad (7)$$

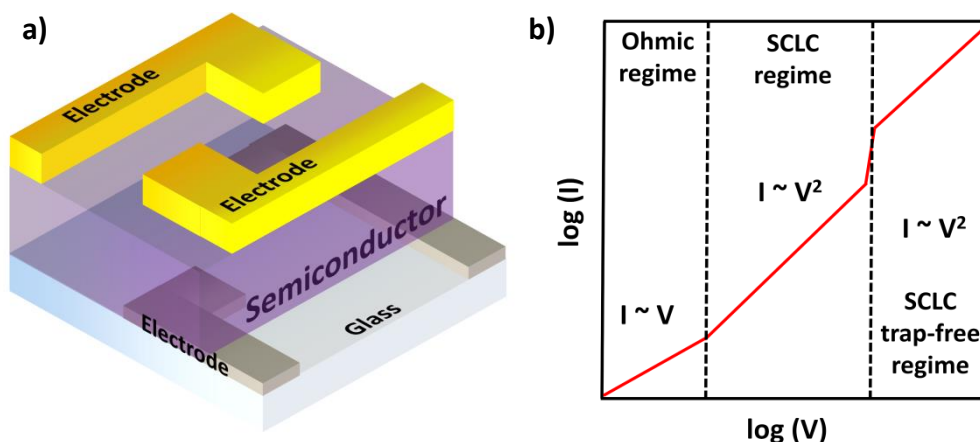


Fig. 12 a) Sketch of two simplified SCLC devices on a substrate. b) a typical theoretical SCLC curve can be plotted in which both linear regime and SCLC regime can be seen

where μ is the charge carrier mobility, ϵ_0 the vacuum permittivity, ϵ_r the relative permittivity of the material, V the applied voltage and L the film thickness of the semiconductor. The material's bulk mobility can only be determined if the SCLC regime is verified. This means that both a dependency of $J_{\text{SCL}} \sim V^2$ and $J_{\text{SCL}} \sim L^{-3}$ have to be observed. Deviations from these power laws can indicate an injection limited current, by a poor choice of the electrodes or the presence of traps. The obtained measurements have to be analyzed with care as the mobility cannot be accurately determined in these cases.

If true SCLC behavior is observed, the values obtained by SCLC measurements in a diode configuration are the bulk mobilities of the organic semiconductors. In the diode configuration, the charge carrier transport is also measured perpendicular to the substrate i.e. the electrodes and realistic values of the charge transport can be obtained for devices with similar configuration such as OPVs.

Organic Field-Effect Transistors

The charge carrier mobility of an organic semiconductor can also be measured in organic field-effect transistors (OFETs).¹⁷⁴⁻¹⁷⁷ The obtained values by this method are not the bulk property of the material as in the case of the charge carrier mobility values obtained by the SCLC-method. In OFETs the charge transport is generally probed in a few nanometer thin layer at the interface of the dielectric and the semiconductor. The choice of the dielectric as well as the OFET configuration and the morphology of the semiconductor

at the interface have great influence on the obtained values.^{169,178} Additionally, the charge carrier concentration in an OFET is much higher than in a diode (SCLC) and therefore, the OFET mobility values are always higher than the respective bulk values.

Organic field-effect transistors consist of three electrodes, a dielectric and, in case of OFETs, an organic semiconductor. Different transistor configurations are possible. In the following the so called bottom-contact, bottom-gate configuration will be discussed (**Fig. 13**). This configuration has the advantage that only the semiconductor has to be deposited on otherwise premanufactured devices. The transistor current flows between two gold electrodes, the source and the drain electrode. The semiconductor is also separated by a dielectric, such as SiO₂, from the third electrode, called gate electrode (e.g n-doped Si). To prevent charge traps at the SiO₂ surface, silanes are often used to passivate the interface.¹⁷⁹

The operating principle of an OFET is as follows.¹⁷⁸ If a voltage is applied at the gate electrode, a layer of positive or negative charges accumulates at the semiconductor-dielectric interface, depending on the sign of the gate voltage. This accumulation layers form the channel for the charge transport. The gate voltage V_g has to overcome a certain threshold voltage (V_{th}) to provide a layer of charges that can move freely. If a potential is applied at the drain electrode (V_d) at a constant V_g above the threshold, the charges move between the source- and drain-electrode and a drain current I_d is measured. If V_d is increased the current I_d will also increase linearly with V_d according to Ohm's law (linear

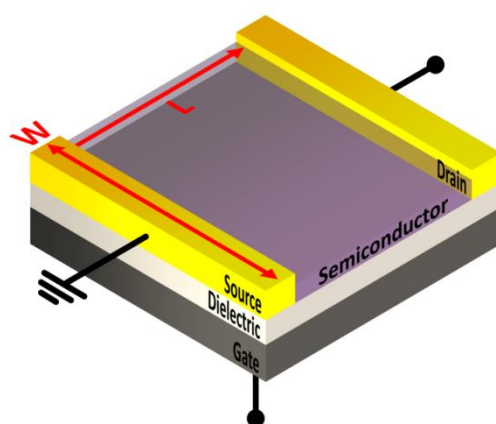


Fig. 13 Scheme of an organic field-effect transistor (OFET) in bottom-contact, bottom-gate configuration. W is the channel width and L is the channel length.

regime). The accumulation layer at the interface is depleted until the channel is pinched off at the drain electrode (pinch-off point). The depletion region will expand for even higher drain voltages but the current I_d saturates as the potential drop between the pinch-off point and the source electrode is approximately constant (saturation regime) (**Fig. 14 a**).¹⁷⁸ This sweep of V_d at a constant gate voltage V_g is called the output-characteristic of the transistor and it is usually conducted at several different gate voltages. The charge carrier mobility of the semiconductor can be obtained by measuring the drain current I_d in dependence of the gate voltage at a fixed potential at the drain electrode V_d (transfer characteristic).

For a gate voltage sweep the drain current I_d at a fixed drain voltage V_d is described by:

$$I_{d,sat} = \frac{W}{L} \mu C_i \left[(V_g - V_{th}) V_d - \frac{1}{2} V_d^2 \right] \quad (8)$$

where W is the channel width, L is the channel length and C_i the capacitance of the dielectric. The mobility values are usually obtained from the saturation regime and the equation then changes to:

$$I_{d,sat} = \frac{1}{2} \frac{W}{L} \mu_{sat} C_i (V_g - V_{th})^2 \quad (9)$$

The saturation mobility μ_{sat} can be calculated by:

$$\mu_{sat} = \left(\frac{\delta \sqrt{I_d}}{\delta V_g} \right)^2 \frac{2L}{WC_i} \quad (10)$$

As can be seen from Eq. 10, the charge carrier mobility can be extracted from the plot of $\sqrt{I_d}$ against the gate voltage V_g (**Fig. 14 b**). The OFET mobility in the saturation regime can be obtained from the slope of the curve using Eq. 10.

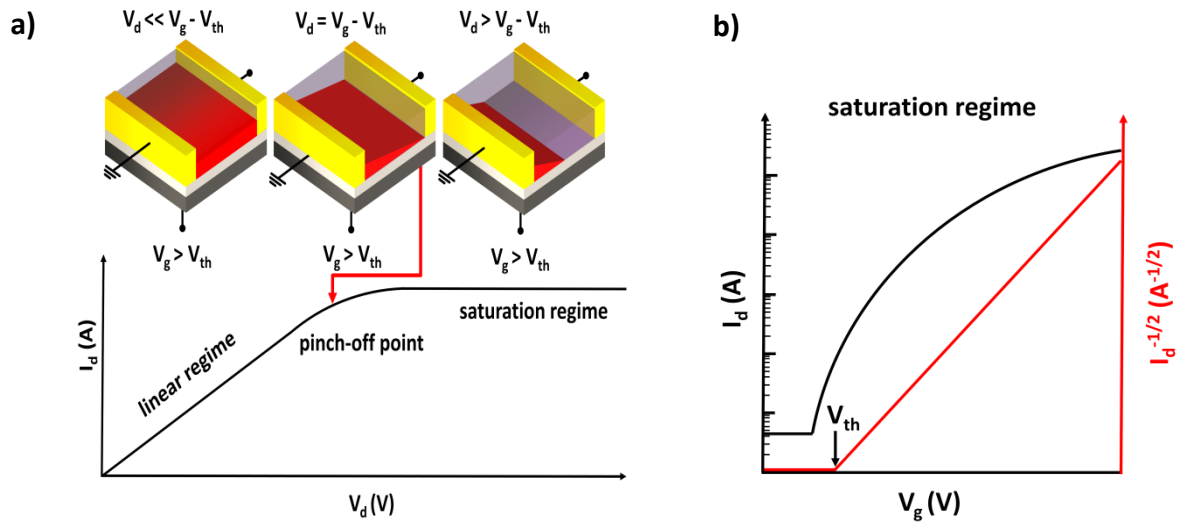


Fig. 14 a) Schematic illustration of the operation of an OFET at a gate voltage V_g above the threshold voltage V_{th} . (Adapted from Ref. 178) For low potentials at the drain electrode, a linear increase of the drain current I_d with the drain voltage V_d is observed (linear regime). At the pinch-off point the start of the saturation regime can be observed. For even higher voltages V_d the accumulation layer is depleted and the drain current saturates (saturation regime); b) Transfer curve of an OFET in the saturation regime (black) and the corresponding square-root drain current $\sqrt{I_d}$ (red) as a function of the gate voltage.

3 References

- 1 A. D. Jenkins, R. G. Jones, and G. Moad, *Pure Appl. Chem.*, 2010, **82**, 483.
- 2 T. Yokozawa and Y. Ohta, *Chem. Rev.*, 2016, **116**, 1950.
- 3 M. H. Stenzel and C. Barner-Kowollik, *Mater. Horiz.*, 2016, **3**, 471.
- 4 A. Kiriy, V. Senkovskyy, M. Sommer, *Macromol. Rapid Commun.*, 2011, **32**, 1503.
- 5 R. H. Lohwasser, G. Gupta, P. Kohn, M. Sommer, A. S. Lang, T. Thurn-Albrecht and M. Thelakkat, *Macromolecules*, 2013, **46**, 4403.
- 6 K.-Y. Jen, G. G. Miller and R. L. Elsenbaumer, *J. Chem. Soc., Chem. Commun.*, 1986, **17**, 1346.
- 7 R. D. McCullough and R. D. Lowe, *J. Chem. Soc., Chem. Commun.*, 1992, **1**, 70.
- 8 T.-A. Chen and R. D. Rieke, *J. Am. Chem. Soc.*, 1992, **114**, 10087.
- 9 A. Yokoyama, R. Miyakoshi and T. Yokozawa, *Macromolecules*, 2004, **37**, 1169.
- 10 E. E. Sheina, J. Liu, M. C. Iovu, D. W. Laird and R. D. McCullough, *Macromolecules*, 2004, **37**, 3526.
- 11 R. Miyakoshi, A. Yokoyama and T. Yokozawa, *J. Am. Chem. Soc.*, 2005, **127**, 17542.
- 12 M. C. Iovu, E. E. Sheina, R. R. Gil, R. D. McCullough, *Macromolecules*, 2005, **38**, 8649.
- 13 R. H. Lohwasser and M. Thelakkat, *Macromolecules*, 2011, **44**, 3388.
- 14 A. Krasovskiy, B. F. Straub and P. Knochel, *Angew. Chem. Int. Ed.*, 2006, **45**, 159.
- 15 S. Wu, L. Huang, H. Tian, Y. Geng and F. Wang, *Macromolecules*, 2011, **44**, 7558.
- 16 R. Miyakoshi, A. Yokoyama and T. Yokozawa, *Macromol. Rapid Commun.*, 2004, **25**, 1663.
- 17 M. Jeffries-El, G. Sauve, R. D. McCullough, *Macromolecules*, 2005, **38**, 10346.
- 18 R. Tkachov, V. Senkovskyy, H. Komber, J.-U. Sommer and A. Kiriy, *J. Am. Chem. Soc.*, 2010, **132**, 7803.
- 19 C. J. Hawker, A. W. Bosman and E. Harth, *Chem. Rev.*, 2001, **101**, 3661.
- 20 J. Nicolas, Y. Guillaneuf, C. Lefay, D. Bertin, D. Gigmes and B. Charleux, *Prog. Polym. Sci.*, 2013, **38**, 63.
- 21 K. Matyjaszewski and J. Xia, *Chem. Rev.*, 2001, **101**, 2921.
- 22 M. Kamigaito, T. Ando and M. Sawamoto, *Chem. Rev.*, 2001, **101**, 3689.
- 23 G. Moad, E. Rizzardo and S. H. Thang, *Aust. J. Chem.*, 2005, **58**, 379.
- 24 S. Perrier and P. Takolpuckdee, *J. Polym. Sci., Part A: Polym. Chem.*, 2005, **43**, 5347.
- 25 D. H. Solomon, E. Rizzardo and P. Cacioli, *P. Free radical polymerization and the produced polymers*, Commonwealth Scientific and Industrial Research Organization, Australia., 1985.
- 26 D. Benoit, V. Chaplinski, R. Braslau and C. J. Hawker, *J. Am. Chem. Soc.*, 1999, **121**, 3904.
- 27 H. Fischer, *Chem. Rev.*, 2001, 3581.
- 28 F. Chauvin, P.-E. Duflis, D. Gimes, Y. Guillaneuf, S. R. A. Marque, P. Tordo and D. Betin, *Macromolecules*, 2006, **39**, 5238.

-
- 29 R. McHalle, F. Aldabbach and P. B. Zetterlund, *J. Polym. Sci.: Part A: Polym. Chem.*, 2006, **45**, 2194.
- 30 D. Gigmes, D. Bertin, C. Lefay and Y. Guillaneuf, *Macromol. Theory Simul.*, 2009, **18**, 402.
- 31 T. Fukuda, T. Terauchi, A. Goto, K. Ohno, Y. Tsujii and T. Miyamoto, *Macromolecules*, 1996, **29**, 6393.
- 32 W. Tang, T. Fukuda and K. Matyjaszewski, *Macromolecules*, 2006, **39**, 4332.
- 33 A. Nabifar, N. T. McManus, E. Vivaldo-Limab, L. M. F. Lonac and A. Penlidis, *Chem. Eng. Sci.*, 2009, **64**, 304.
- 34 G. Moad, E. Rizzardo and S. H. Thang, *Acc. Chem. Res.*, 2008, **41**, 1133.
- 35 J. Chiefari, Y. K. Chong, F. Ercole, J. Krstina, J. Jeffery, T. P. T. Le, R. T. A. Mayadunne, G. F. Meijs, C. L. Moad, G. Moad, E. Rizzardo, S. H. Thang, *Macromolecules*, 1998, **31**, 5559.
- 36 G. Moad, E. Rizzardo and S. H. Thang, *Aust. J. Chem.*, 2009, **62**, 1402.
- 37 D. Charmot, P. Corpat, H. Adam, S. Z. Zard, T. Biadatti and G. Bouhadir, *Macromol. Symp.*, 2000, **150**, 23.
- 38 M. A. Harvison and A. B. Lowe, *Macromol. Rapid Commun.*, 2011, **32**, 779.
- 39 S. R. Gondi, A. P. Vogt and B. S. Sumerlin, *Macromolecules*, 2007, **40**, 474.
- 40 J. Vandenberg and T. Junkers, *Macromolecules*, 2014, **47**, 5051.
- 41 G. Gody, T. Maschmeyer, P. B. Zetterlund, S. Perrier, *Nat. Commun.*, 2013, **4**, 2505.
- 42 G. Gody, T. Maschmeyer, P. B. Zetterlund, S. Perrier, *Macromolecules*, 2014, **47**, 639.
- 43 G. Gody, T. Maschmeyer, P. B. Zetterlund, S. Perrier, *Macromolecules*, 2014, **47**, 3451.
- 44 H. C. Kolb, M. G. Finn and K. B. Sharpless, *Angew. Chem. Int. Ed.*, 2001, **40**, 2004.
- 45 V. V. Rostovtsev, L. G. Green, V. V. Fokin and K. B. Sharpless, *Angew. Chem. Int. Ed.*, 2002, **41**, 2596.
- 46 C. W. Tornøe, C. Christensen and M. Medal, *J. Org. Chem.*, 2002, **67**, 3057.
- 47 R. Huisgen, *Angew. Chem. Int. Ed.*, 1963, **11**, 633.
- 48 R. Huisgen, *Angew. Chem. Int. Ed.*, 1963, **10**, 565.
- 49 F. S. Bates and G. H. Fredrickson, *Annu. Rev. Chem.*, 1990, **41**, 525.
- 50 F. S. Bates, M. F. Schulz, A. K. Khaidpur, S. Förster, J. H. Rosedale, K. Almdal and K. Mortensen, *Faraday Discuss.*, 1994, **98**, 7.
- 51 P. J. Flory, *Principles of Polymer Chemistry*; Cornell University Press: Ithaca, New York, 1953.
- 52 P.-G. De Gennes, *Scaling Concepts in Polymer Physics*; Cornell University Press: Ithaca, New York, 1979.
- 53 F. S. Bates, *Science*, 1991, **251**, 898.
- 54 S. B. Darling, *Energy Environ. Sci.*, 2009, **2**, 1266.
- 55 W.-N. He, J.-T. Xu, *Prog. Polym. Sci.*, 2012, **37**, 1350.
- 56 M. Reenders, G. ten Brinke, *Macromolecules*, 2002, **35**, 3266.
- 57 B. Olsen, R. Segalman, *Mater. Sci. Eng. R Reports*, 2008, **62**, 37.

- 58 R. H. Lohwasser, G. Gupta, P. Kohn, M. Sommer, A. S. Lang, T. Thurn-Albrecht and M. Thelakkat, *Macromolecules*, 2013, **46**, 4403.
- 59 M. Sommer, S. Huettner, M. Thelakkat, *J. Mater. Chem.*, 2010, **20**, 10788.
- 60 D. Kipp, R. Verduzco and V. Ganesan, *Mol. Syst. Des. Eng.*, 2016, **1**, 353.
- 61 Y. Lee and E. D. Gomez, *Macromolecules*, 2015, **48**, 7385.
- 62 U. Scherf, A. Gutacker and N. Koenen, *Acc. Chem. Res.*, 2008, **41**, 1086.
- 63 P. D. Topham, A. J. Parnell, R. C. Hiorns, *J. Polym. Sci. Part B Polym. Phys.*, 2011, **49**, 1131.
- 64 A. Yassar, L. Miozzo, R. Girona, G. Horowitz, *Prog. Polym. Sci.*, 2013, **38**, 791.
- 65 K. Nakabayashi, H. Mori, *Materials*, 2014, **7**, 3274.
- 66 S. M. Lindner, S. Hüttner, A. Chiche, M. Thelakkat and G. Krausch, *Angew. Chem. Int. Ed.*, 2006, **45**, 3364.
- 67 M. Sommer, S. M. Lindner and M. Thelakkat, *Adv. Funct. Mater.*, 2007, **17**, 1493.
- 68 U. Stalmach, B. de Boer, C. Videlot, P. F. van Hutten and G. Hadziioannou, *J. Am. Chem. Soc.*, 2000, **122**, 5464.
- 69 B. de Boer, U. Stalmach, P. F. van Hutten, C. Melzer, V. V. Krasnikov and G. Hadziioannou, *Polymer*, 2001, **42**, 9097.
- 70 B. de Boer, U. Stalmach, C. Melzer and G. Hadziioannou, *Synth. Met.*, 2001, **121**, 1541.
- 71 M. H. van der Veen, B. de Boer, U. Stalmach, K. I. van de Wetering and G. Hadziioannou, *Macromolecules*, 2004, **37**, 3673.
- 72 S. Barrau, T. Heiser, F. Richard, C. Brochon, C. Ngov, K. van de Wetering, G. Hadziioannou, D. V. Anokhin and D. A. Ivanov, *Macromolecules*, 2008, **41**, 2701.
- 73 K. Sivula, Z. T. Ball, N. Watanabe and J. M. J. Fréchet, *Adv. Mater.*, 2006, **18**, 206.
- 74 J. U. Lee, A. Cirpan, T. Emrick, T. P. Russell and W. H. Jo, *J. Mater. Chem.*, 2009, **19**, 1483.
- 75 N. Sary, F. Richard, C. Brochon, N. Leclerc, P. Lévêque, J.-N. Audinot, S. Berson, T. Heiser, G. Hadziioannou and R. Mezzenga, *Adv. Mater.*, 2010, **22**, 763.
- 76 S. Miyanishi, Y. Zhang, K. Tajima and K. Hashimoto, *Chem. Commun.*, 2010, **46**, 6723.
- 77 S. Miyanishi, Y. Zhang, K. Hashimoto and K. Tajima, *Macromolecules*, 2012, **45**, 6424.
- 78 M. Hufnagel, M. Fischer, T. Thurn-Albrecht, M. Thelakkat, *Polym. Chem.*, 2015, **6**, 813.
- 79 M. Hufnagel, M. Thelakkat, *J. Polym. Sci. Part B: Polym. Phys.*, 2016, **54**, 1125.
- 80 M. Hufnagel, M. Fischer, T. Thurn-Albrecht, M. Thelakkat, *Macromolecules*, 2016, **49**, 1637.
- 81 M. Sommer, A. S. Lang, M. Thelakkat, *Angew. Chem. Int. Ed.*, 2008, **47**, 7901.
- 82 Q. Zhang, A. Cirpan, T. P. Russell, T. Emrick, *Macromolecules*, 2009, **42**, 1079.
- 83 S. Rajaram, P. B. Armstrong, B. J. Kim and J. M. J. Fréchet, *Chem. Mater.*, 2009, **21**, 1775.
- 84 M. J. Robb, S.-Y. Ku, C. J. Hawker, *Adv. Mater.*, 2003, **25**, 5686.
- 85 G. Tu, H. Li, M. Forster, R. Heiderhoff, L. J. Balk and U. Scherf, *Macromolecules*, 2006, **39**, 4327.

-
- 86 R. Verduzco, I. Botiz, D. L. Pickel, S. M. Kilbey, K. Hong, E. Dimasi, S. B Darling, *Macromolecules*, 2011, **44**, 530.
- 87 M. Sommer, H. Komber, S. Huettner, R. Mulherin, P. Kohn, N. C. Greenham, W., T. S. Huck, *Macromolecules*, 2012, **45**, 4142.
- 88 R. C. Mulherin, S. Jung, S. Huettner, K. Johnson, P. Kohn, M. Sommer, S. Allard, U. Scherf, N. C. Greenham, *Nano Lett.*, 2011, **11**, 4846.
- 89 C. Guo, Y.-H. Lin, M. D. Witman, K. A. Smith, C. W. A. Hexemer, J. Strzalka, E. D. Gomez and R. Verduzco, *Nano Lett.*, 2013, **13**, 2957.
- 90 V. D. Mitchell, E. Gann, S. Huettner, C. R. Singh, J. Subbiah, L. Thomsen, C. R. McNeill, M. Thelakkat and D. J. Jones, *Macromolecules*, 2017, **50**, 4942.
- 91 M. A. Brady, S.-Y. Ku, L. A. Perez, J. E. Cochran, K. Schmidt, T. M. Weiss, M. F. Toney, H. Ade, A. Hexemer, C. Wang, C. J. Hawker, E. J. Kramer and M. L. Chabiny, *Macromolecules*, 2016, **49**, 8187.
- 92 S. Y. Ku, M. A. Brady, N. D. Treat, J. E. Cochran, M. J. Robb, E. J. Kramer, M. L. Chabiny and C. J. Hawker, *J. Am. Chem. Soc.*, 2012, **134**, 16040.
- 93 S. Wang, Q. Yang, Y. Tao, Y. Guo, J. Yang, Y. Liu, L. Zhao, Z. Xie and W. Huang, *New. J. Chem.*, 2016, **40**, 1825.
- 94 K. Nakabayashi and H. Mori, *Macromolecules*, 2012, **45**, 9618.
- 95 J. Wang, M. Ueda and T. Higashihara, *ACS Macro Lett.*, 2013, **2**, 506.
- 96 J. Wang, M. Ueda and T. Higashihara, *J. Polym. Sci., Part A: Polym. Chem.*, 2014, **52**, 1139.
- 97 F. Nübling, H. Komber and M. Sommer, *Macromolecules*, 2017, **50**, 1909.
- 98 V. Senkovskyy, R. Tkachov, H. Komber, M. Sommer, M. Heuken, B. Voit, W. T. S. Huck, V. Kataev, A. Petr and Anton Kiriy, *J. Am. Chem. Soc.*, 2011, **133**, 19966.
- 99 A. A. Pollit, N. K. Obhi, A. J. Lough and D. S. Seferos, *Polym. Chem.*, 2017, **8**, 4108.
- 100 R. Verduzco, X. Li, S. L. Pesek and Gila E. Stein, *Chem. Soc. Rev.*, 2015, **44**, 2405.
- 101 M. Müllner and A. H.E. Müller, *Polymer*, 2016, **98**, 389.
- 102 S. W. Hong, W. Gu, J. Huh, B. R. Sveinbjornsson, G. Jeong, R. H. Grubbs and T. P. Russel, *ACS Nano*, 2013, **7**, 9684.
- 103 W. Gu, J. Huh, S. W. Hong, B. R. Sveinbjornsson, R. H. Grubbs and T. P. Russel, *ACS Nano*, 2013, **7**, 2551.
- 104 S. Ahn, D. L. Pickel, W. M. Kochemba, J. Chen, D. Uhrig, J. P. Hinestrosa, J.-M. Carrillo, M. Shao, C. Do, J. M. Messmann, W. M. Brown, B. G. Sumpter and S. M. Kilbey, *ACS Macro Lett.*, 2013, **2**, 761.
- 105 D. v. As, J. Subbiah, D. J. Jones and W. W. H. Wong, *Macromol. Chem. Phys.*, 2016, **217**, 403.
- 106 X. Pang, L. Zhao, C. Feng, R. Wu, H. Ma and Z. Lin, *Polym. Chem.*, 2013, **4**, 2025.
- 107 S. Ahn, J.-M. Y. Carrillo, J. K. Keum, J. Chen, D. Uhrig, B. S. Lokitz, B. G. Sumpter and S. M. Kilbey, *Nanoscale*, 2017, **9**, 7071.

-
- 108 D. Schiefer, R. Hanselmann and M. Sommer, *Polym. Chem.*, **8**, 2017, 4368.
- 109 W. J. Brittain and S. Minko, *J. Polym. Sci.: Part A: Polym. Chem.*, 2007, **45**, 3505.
- 110 M. Van der Waarden, *J. Colloid. Sci.*, 1950, **5**, 535.
- 111 M. Van der Waarden, *J. Colloid. Sci.*, 1951, **6**, 443.
- 112 E. L. Mackor, *J. Colloid. Sci.*, 1951, **6**, 492.
- 113 E. L. Mackor and J. H. van der Waals, *J. Colloid. Sci.*, 1952, **7**, 535.
- 114 E. J. Clayfield and E. C. Lumb, *J. Colloid. Interface Sci.*, 1966, **22**, 269.
- 115 E. J. Clayfield and E. C. Lumb, *J. Colloid. Interface Sci.*, 1966, **22**, 285.
- 116 S. Alexander, *J. Phys.*, 1977, **38**, 983.
- 117 P.-G. De Gennes, *J. Phys.*, 1976, **37**, 1445.
- 118 P.-G. De Gennes, *Macromolecules*, 1980, **13**, 1069.
- 119 M. S Kent, *Macromol. Rapid Commun.*, 2000, **21**, 243.
- 120 T. Cosgrove, T. G. Heath, K. Ryan and L. Crowley, *Macromolecules*, 1987, **20**, 2879.
- 121 E. Parsonage, M. Tirrell, H. Watanabe and R. Nuzzo, *Macromolecules*, 1991, **24**, 1987.
- 122 B. Zhao and W. J. Brittain, *Prog. Polym. Sci.*, 2000, 25, 677.
- 123 A. Granville and W. J. Brittain, *In Polymer Brushes*, Eds.: R. Advincula, W. J. Brittain, K. Caster, J. R  he, Wiley-VCH Verlag GmbH, Weinheim, Germany, 2004, 33.
- 124 V. Senkovskyy, N. Khanduyeva, H. Komber, U. Oertel, M. Stamm, D. Kuckling and A. Kiriy, *J. Am. Chem. Soc.*, 2007, **129**, 6626.
- 125 M. Tirrell, S. Patel and G. Hadziioannou, *Proc. Natl. Acad. Sci.*, USA 1987, **84**, 4725.
- 126 T. Wu, K. Efimenko and J. Genzer, *J. Am. Chem. Soc.*, 2002, **124**, 9394.
- 127 S. Yamamoto, M. Ejaz, Y. Tsujii, M. Matsumoto and T. Fukuda, *Macromolecules*, 2000, **33**, 5608.
- 128 S. Casalini, C. A. Bortolotti, F. Leonardi and F. Biscarini, *Chem. Soc. Rev.*, 2017, **46**, 40.
- 129 J. Alonzo, W. M. Kochemba, D. L. Pickel, M. Ramanathan, Z. Sun, D. Li, J. Chen, B. G. Sumpter, W. T. Hellera and S. M. Kilbey, *Nanoscale*, 2013, **5**, 9357.
- 130 E. L. Ratcliff, B. Zacher and N. R. Armstrong, *Phys. Chem. Lett.*, 2011, **2**, 1337.
- 131 G. S. Tulevski, Q. Miao, M. Fukuto, R. Abram, B. Ocko, R. Pindak, M. L. Steigerwald, C. R. Kagan and C. Nuckolls, *J. Am. Chem. Soc.*, 2004, **126**, 15048.
- 132 S. A. Ponomarenko, O. V. Borshchev, T. Meyer-Friedrichsen, A. P. Pleshkova, S. Setayesh, E. C. P. Smits, S. G. J. Mathijssen, D. M. de Leeuw, S. Kirchmeyer and A. M. Muzafarov, *Organometallics*, 2010, **29**, 4213.
- 133 E. C. P. Smits, S. G. J. Mathijssen, P. A. van Hal, S. Setayesh, T. C. T. Geuns, K. A. H. A. Mutsaers, E. Cantatore, H. J. Wondergem, O. Werzer, R. Resel, M. Kemerink, S. Kirchmeyer, A. M. Muzafarov, S. A. Ponomarenko, B. de Boer, P. W. M. Blom and D. M. de Leeuw, *Nature*, 2008, **455**, 956.
- 134 A. Ringk, X. Li, F. Gholamrezaie, E. C. P. Smits, A. Neuhold, A. Moser, C. V. der Marel, G. H. Gelinck, R. Resel, D. M. de Leeuw and P. Strohriegl, *Adv. Funct. Mater.*, 2012, **23**, 2016.

-
- 135 L. G. Whiting, H. J. Snaith, S. Khodabakhsh, J. W. Andreasen, D. W. Breiby, M. M. Nielsen, N. C. Greenham, R. H. Friend and W. T. S. Huck, *Nano Lett.*, 2006, **6**, 573.
- 136 T. Beryozkina, K. Boyko, N. Khanduyeva, V. Senkovskyy, M. Horecha, U. Oertel, F. Simon, M. Stamm and A. Kiriy, *Angew. Chem. Int. Ed.*, 2009, **48**, 2695.
- 137 N. Marshall, S. K. Sontag and J. Locklin, *Macromolecules*, 2010, **43**, 2137.
- 138 N. Khanduyeva, V. Senkovskyy, T. Beryozkina, M. Horecha, M. Stamm, C. Uhrich, M. Riede, K. Leo and A. Kiriy, *J. Am. Chem. Soc.*, 2009, **131**, 16445.
- 139 F. Boon, D. Moerman, D. Laurencin, S. Richeter, Y. Guari, A. Mehdi, P. Dubois, R. Lazzaroni and S. Clément, *Langmuir*, 2014, **30**, 11340.
- 140 N. Khanduyeva, V. Senkovskyy, T. Beryozkina, V. Bocharova, F. Simon, M. Nitschke, M. Stamm, R. Grötzschel and A. Kiriy, *Macromolecules*, 2008, **41**, 7383.
- 141 N. Khanduyeva, V. Senkovskyy, T. Beryozkina, M. Horecha, M. Stamm, C. Uhrich, M. Riede, K. Leo and A. Kiriy, *J. Am. Chem. Soc.*, 2009, **131**, 153.
- 142 P. Paoprasert, J. W. Spalanka, D. L. Peterson, R. E. Ruther, R. J. Hamers P. G. Evans and P. Gopalan, *J. Mater. Chem.*, 2010, **20**, 2651.
- 143 B. Yameen, C. Rodriguez-Emmenegger, C. M. Preuss, O. Pop-Georgievski, E. Verveniotis, V. Trouillet, B. Rezek, and C. Barner-Kowollik, *Chem. Commun.*, 2013, **49**, 8623.
- 144 F. Monnaie, L. Verheyen, J. De Winter, P. Gerbaux, W. Brullot, T. Verbiest and G. Koeckelberghs, *Macromolecules*, 2015, **48**, 8752.
- 145 D. Meng, J. Sun, S. Jiang, Y. Zeng, Y. Li, S. Yan, J. Geng and Y. Hang, *J. Mater. Chem.*, 2012, **22**, 21583.
- 146 N. Doubina, J. L. Jenkins, S. A. Paniagua, K. A. Mazzi, G. A. MacDonald, A. K.-Y. Jen, N. R. Armstrong, S. R. Marder and C. K. Luscombe, *Langmuir*, 2012, **28**, 1900.
- 147 J. Alonzo, W. M. Kochemba, D. L. Pickel, M. Ramanathan, Z. Sun, D. Li, J. Chen, B. G. Sumpter, W. T. Hellera and S. M. Kilbey, *Nanoscale*, 2013, **5**, 9357.
- 148 A. Roy, T. L. Bougher, R. Geng, Y. Ke, J. Locklin and B. A. Cola, *ACS Appl. Mater. Interfaces*, 2016, **8**, 25578.
- 149 W. Radke, in *Macromolecular Engineering Precise Synthesis, Material Properties, Applications*, ed. K. Matyjaszewski, Y. Gnanou, L. Leibler, Wiley-VCH Verlag GmbH & Co. KGaA, Weinheim, 2007, 1881.
- 150 D. Held, *The Column*, 2010, **6**, 16.
- 151 W. Radke, *Macromol. Theory Simul.*, 2001, **10**, 668.
- 152 Z. Grubisic, P. Remp and H. Benot, *Polym. Lett.*, 1967, **5**, 753.
- 153 D. Held, *The Column*, 2011, **7**, 20.
- 154 A. H. Soeriyadi, M. R. Wittaker, C. Boyer and T. P. David, *J. Polym. Sci.*, 2013, **51**, 1475.
- 155 L. Charles, *Mass Spectrom. Rev.*, 2014, **33**, 523.
- 156 A. S. Lang, A. Neubig, M. Sommer and M. Thelakkat, *Macromolecules*, 2010, **43**, 7001.
- 157 C. Barner-Kowollik, *Macromol. Rapid Commun.*, 2009, **30**, 1625.

-
- 158 R. Noriega, J. Rivnay, K. Vandewal, F. P. V. Koch, N. Stingelin, P. Smith, M. F. Toney and A. Salleo, *Nat. Mater.*, 2013, **12**, 1038.
- 159 I. Botiz and N. Stingelin, *Materials*, 2014, **7**, 2273.
- 160 R.-J. Joe, *Methods, of x-ray and neutron scattering in polymer science*, Oxford University Press, New York, 2000.
- 161 W. H. Bragg, W. L. Bragg, *Proc. R. Soc. Lond.*, 1913, **88**, 428.
- 162 *Progress in understanding polymer crystallization*, Eds.: G. Reiter, G. Strobl, Springer, Berlin, 2007.
- 163 B. Benjamin and S. Hsiao, *Chem. Rev.*, 2001, **101**, 1727.
- 164 P. Müller-Buschbaum, *Anal. Bioanal. Chem.*, 2003, **376**, 3.
- 165 V. Skypnychuck, G.-J. A. H. Wetzlar, P. I. Gordiichuck, S. C. B. Mannsfeld, A. Herrmann, M. F. Toney and D. R. Barbero, *Adv. Mater.*, 2016, **28**, 2359.
- 166 M. Rhee, *Macromol. Rapid Commun.*, 2014, **35**, 930.
- 167 P. Müller-Buschbaum, *Adv. Mater.*, 2014, **26**, 7692.
- 168 F. Laquai, G. Wegner and H. Bässler, *Phil. Trans. R. Soc. A*, 2007, **365**, 1473.
- 169 A. Köhler and H. Bässler, *Electronic Processes in Organic Semiconductors: An Introduction*, Wiley-VCH Verlag GmbH & Co. KGaA, Weinheim, 2015.
- 170 C. Tanase, E. J. Meijer, P. W. M. Blom and D. M. de Leeuw, *Phys. Rev. Lett.*, 2003, **91**, 216601.
- 171 S. Tiwari and N. C. Greenham, *Opt. Quant. Electron.*, 2009, **41**, 69.
- 172 A. Kokil, K. Yang and J. Kumar, *J. Polym. Sci. Part B.: Polym. Phys.*, 2012, **50**, 1130.
- 173 N. F. Mott and R. W. Gurney, *Electronic Processes in Ionic Crystals*; 1st Edition, Oxford University Press, Oxford, 1940.
- 174 G. Horowitz, *J. Mater. Res.*, 2004, **19**, 1946.
- 175 G. Horowitz, in *Semiconducting Polymers: Chemistry, Physics and Engineering, Vol. 2*, Eds.: G. Hadziannou and G. G. Malliaras, Wiley-VCH Verlag GmbH & Co. KGaA, Weinheim, 2007, 531.
- 176 A. R. Brown, C. P. Jarrett, D. M. de Leeuw and M. Matters, *Synt. Met.*, 1997, **88**, 37.
- 177 S. M. Sze and K. K. Ng, *Physics of Semiconductor Devices*, Wiley-VCH Verlag GmbH & Co. KGaA, Weinheim, 2007, 1.
- 178 J. Zaumseil and H. Sirringhaus, *Chem. Rev.*, 2007, **107**, 1296.
- 179 S. Kobayashi, T. Nishikawa, T. Takenobu, S. Mori, T. Shimoda, T. Mitani, H. Shimotani, N. Yoshimoto, S. Ogawa and Y. Iwasa, *Nat. Mater.*, 2004, **3**, 317.

Objective of the Thesis

The aim of this thesis is, on the one hand, the further development of modular synthetic strategies towards highly defined, novel semiconducting materials with a focus on the polymer architecture. On the other hand, the structure formation and its influence on the electronic properties of the materials were to be investigated. For this purpose, semiconducting diblock-, sidechain-, surface-grafted and bottle brush-copolymers were synthesized via a combination of different chain growth polymerization techniques and highly efficient polymer analogous click reactions. These novel polymers need to be tested for their efficiency in charge transport as well as structure formation with the help of various characterization methods and via application in devices.

Most semiconducting polymers used in organic electronics are made by step-growth polymerizations which allow only poor control over the molecular weight and dispersity of the material. Additionally, more complex architectures such as diblock copolymers are not accessible using polycondensation techniques. In order to understand the influences of the structure and structure formation, defined materials were designed and characterized in this thesis. Donor-acceptor diblock copolymers with defined structure and high comparability were to be synthesized and characterized. This was to be achieved by combining controlled chain growth polymerization techniques and polymer analogous reactions. Poly(3-hexylthiophene) shall be combined with a perylene bisimide sidechain polymer (PPBI) to obtain a block copolymer, P3HT-*b*-PPBI in order to study the influence of differently substituted PBI acceptor units on the structure formation. The molecular weights and volume fractions are so targeted to get microphase separated systems. Via this process, a defined morphology of the material can be achieved in addition to the defined molecular structure. A donor-acceptor material which forms a preferentially vertically aligned

ordered morphology in thin films is an interesting model material for organic photovoltaics (OPV). Diblock copolymers mostly align parallel to the substrate without post-processing. This may be overcome by synthesizing diblock brush copolymers. First, brush copolymers of P3HT shall be synthesized in order to test whether the electrical properties of the linear polymer can be retained and to establish design rules for the future better performing materials.

Semiconducting materials which are hydrophilic but not soluble in water are interesting for applications in bioelectronics. A novel sidechain polymer with hydrophilic phthalocyanine (CuPc) units shall be polymerized and characterized. The material shall be characterized in terms of solubility, thermal, structural and electrical properties. Here also the modular approach of click chemistry will be utilized.

Substrates with anchored semiconducting materials may be interesting interfacial materials due to their high stability and ultra-thin nature. Such substrate anchored brushes shall be synthesized by extending the aforementioned strategy from the post-functionalization of polymers to substrates by grafting-to method. A characterization of the structure of P3HT monolayers shall be conducted. The grafting density can be investigated by looking into the nature and extent of aggregation. Finally, the electrical properties shall be investigated in organic field effect transistors (OFETs).

In summary, a combination of controlled radical polymerization, KCTP and click reactions will be applied for the creation of a vast variety of complex semiconductor polymer architecture and their properties will be evaluated and compared.

Overview of the Thesis

This thesis focuses on the synthesis of novel semiconducting polymers with complex architectures and the influence of the architecture on the structure formation and the electrical properties. I show that click chemistry by copper catalyzed azide-alkyne cycloaddition (CuAAC) is a highly efficient way to synthesize novel semiconducting polymers and obtain highly comparable materials through the modularity of the strategy. By this I could precisely change one parameter and study its influence on the structure formation and electrical properties. The structure formation of donor-

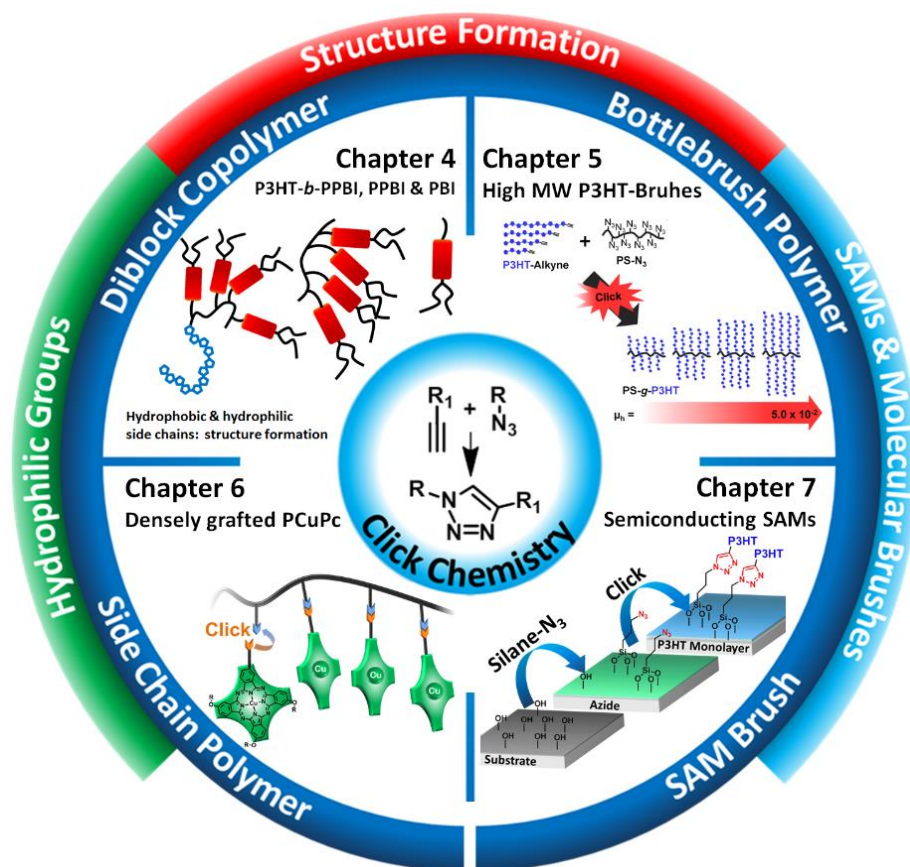


Fig. 1 Overview of the thesis including the four chapters: structure formation in donor-acceptor diblock copolymers with hydrophobic and hydrophilic group, synthesis and characterization of P3HT bottlebrush copolymers, P3HT self-assembled monolayers (SAMs) and a novel densely grafted copper phthalocyanine side chain polymer.

acceptor diblock copolymers containing solubilizing chains with different polarity (Chapter 4) and of bottlebrush polymers with different poly(3-hexylthiophene) (P3HT) side chain lengths (Chapter 5) was investigated (**Fig. 1**). The electronic properties of the bottlebrushes were measured and the concept was expanded to the synthesis and characterization of surface grafted P3HT monolayers (Chapter 8). Additionally, a novel liquid crystalline polymer with phthalocyanine side chains and hydrophilic solubilizing groups was synthesized and characterized (Chapter 7).

In the first section, two poly(3-hexylthiophene)-*block*-polyperylene bisimide diblock copolymers (P3HT-*b*-PPBI) incorporating P3HT as an electron donor and a polystyrene block with two different pendant perylene bisimides as electron acceptor blocks were synthesized and the interplay between phase separation, crystallization and glass transition was investigated. The diblock copolymers were synthesized by combining Kumada catalyst transfer polymerizations (KCTP), reversible addition-fragmentation chain transfer (RAFT) polymerization and CuAAC resulting in highly comparable polymers. I also synthesized low molecular weight model compounds and homopolymers with both PBIs to study the effect of the backbone glass transition on side chain crystallization in the acceptor block. The block copolymers were characterized by temperature dependent small- and wide-angle x-ray scattering (SAXS/WAXS) in combination with differential scanning calorimetry (DSC). The composition was selected to obtain P3HT cylinders in a PPBI matrix. Microphase separation in the liquid state led to a cylindrical morphology in both cases but the crystallization of the functional side chains depends strongly on the backbone transition.

For the second part, a series of well-defined P3HT grafted bottlebrushes were synthesized by a grafting-to approach using nitroxide mediated controlled radical polymerization (NMRP). Different P3HT chain lengths were incorporated to study the influence of the side chain length on the optical, thermal and electronic properties. The obtained properties were compared with the corresponding linear P3HT polymers. The optical, structural and electronic properties of the brushes strongly depend on the side chain lengths. A different trend as compared to linear P3HT could be observed in terms of crystallinity. For low molecular weight P3HT side chains, the brushes are

amorphous and exhibit very poor electronic properties. Highly crystalline materials are only obtained for longer side chains. For these brushes crystalline lamellar structures and high charge carrier mobilities could be observed. We report values that match the excellent electronic properties of linear polymers in the range of $10^{-2} \text{ cm}^2 \text{ V}^{-1} \text{ s}^{-1}$ and show that films of our bottlebrushes exhibit superior thermal stability at elevated temperatures.

Further, a new polymeric donor material with pendant copper phthalocyanine side chains (**PCuPc**) was synthesized by clicking **CuPc-N₃** to a poly(propargyloxy-styrene). FTIR and MALDI-ToF MS of **PCuPc** points towards quantitative grafting and due to the hydrophilic oligoethylene glycol swallow tails in the CuPc moiety, the polymer is soluble in most of the commonly used solvents such as ethyl acetate, THF and acetone. The absorption behavior (UV-Vis) as well as the electronic structure (cyclic voltammetry) were investigated and the thermal behavior could be elucidated via Flash-DSC. Liquid crystalline behavior could be observed and confirmed via X-ray diffraction (XRD) and polarization microscopy. The bulk transport of the polymer was determined by measuring the space charge limited current (SCLC) in diode configuration and PCuPc exhibited a decent charge carrier mobility which makes it a potential candidate for an application in organic electrochemical transistors (OECTs).

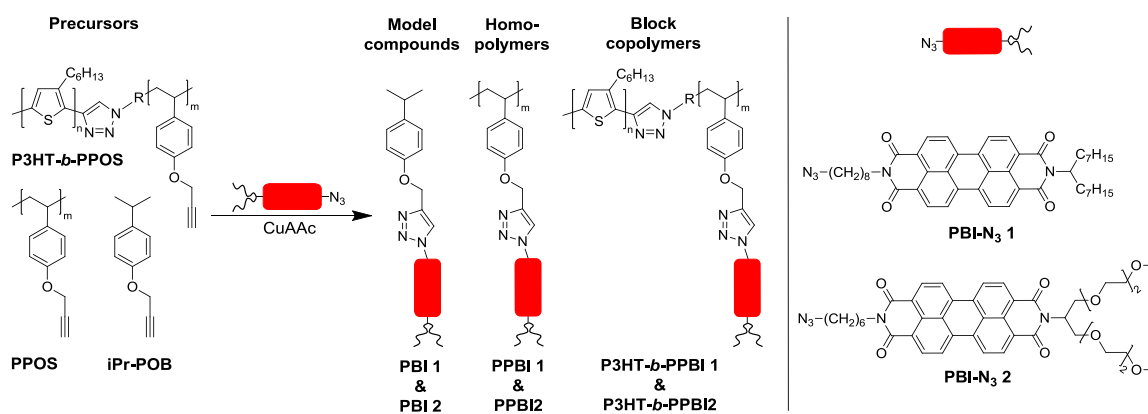
In the last part the concept of P3HT brushes is transferred from grafting to a polymeric backbone to the grafting onto a surface. Surface grafted P3HT monolayer brushes were prepared by CuAAC of alkyne-functionalized P3HT with a self-assembled monolayer (SAM) with azide functionality. I show the successful grafting of P3HT on the surface with AFM which makes it also possible to determine the film thickness of the layers. The grafting density, calculated from the thickness of the monolayer, is high enough that the monolayers are in the true brush regime and form aggregated films as evidenced by UV-Vis spectroscopy. The spectra are also compared to linear P3HT and the P3HT bottlebrush copolymer. SAM based organic field-effect transistors (SAMFETs) with a monolayer of grafted P3HT as active materials were tested. The measured field effect mobility of $1.6 \cdot 10^{-3} \text{ cm}^2 \text{ V}^{-1} \text{ s}^{-1}$ is nearly two orders of magnitude higher than previously reported values on P3HT based SAMFETs.

In the following an overview of the main results is given. The detailed description of the results can be found in the individual chapters:

Chapter 4: Impact of Molecular Dynamics on Structure Formation of Donor-Acceptor Block Copolymers

This study focuses on donor-acceptor block copolymers, synthesized by a novel modular approach, carrying different acceptor units and their structure property relationship.

Also the diblock copolymers are compared to respective homopolymers and their model compounds. Three alkynes (iPrPOB, PPOS and P3HT-*b*-PPOS) were grafted with two different azide functionalized perylene bisimide (PBI) molecules via a CuAAC click reaction (see **Scheme 1**). The influence of the complexity was gradually increased from small molecule model compounds (**PBI 1** and **2**) through the acceptor homopolymers (**PPBI 1** and **2**) to the donor-acceptor block copolymers (**P3HT-*b*-PPBI 1** and **2**). We could comparatively study the structure property relationship of these materials and obtain information about the influence of the complexity and the nature of acceptor units. This was possible only due to the applied modular synthetic approach, where the precursor polymers are identical. This ensured a high comparability of the materials. The model compounds are novel materials that were designed in order to resemble the repeating unit of both the acceptor homopolymers and the acceptor blocks of the diblock copolymers.



Scheme 1. Synthesis of perylene bisimide functionalized model compounds, homopolymers and block copolymers via CuAAC click chemistry. Three different precursors (left) are coupled with two different perylene bisimides (right).

The homopolymer **PPBI 1** was previously synthesized in our group. I additionally, synthesized the homopolymer **PPBI 2**. For both polymers **PPBI 1** and **2**, we measured the absolute molecular weights by MALDI ToF and confirmed quantitative grafting. We also employed this strategy to synthesize the donor-acceptor block copolymers. Our goal was to synthesize polymers with around 70 wt% acceptor block in order to obtain diblock copolymers with cylindrical microphase separation in which P3HT cylinders are embedded in a PPBI matrix. The value of 70% PPBI was obtained from previous studies in our group. A P3HT RAFT macroinitiator was synthesized which started the polymerization of a second functional polypropargyloxystyrene block. The second block was subsequently decorated with the PBI acceptor units by clicking PBI-azides, similar to the homopolymers. Two pure diblock copolymers could be retrieved after a column chromatography. By $^1\text{H-NMR}$ the composition of the obtained materials was confirmed.

The diblock copolymers were characterized via temperature dependent X-ray scattering measurements in collaboration with University of Halle in order to understand the structure evolution and the influence of the substituents and T_g of the acceptor block. The findings were supported by DSC, TEM and AFM measurements (**Fig. 2**). For **P3HT-*b*-PPBI 1** two crystallizations, first of the acceptor block and then of P3HT could be observed. In contrast, only a crystallization of the P3HT block is observable for **P3HT-*b*-PPBI 2**, since the PPBI 2 block is amorphous. In the small angle

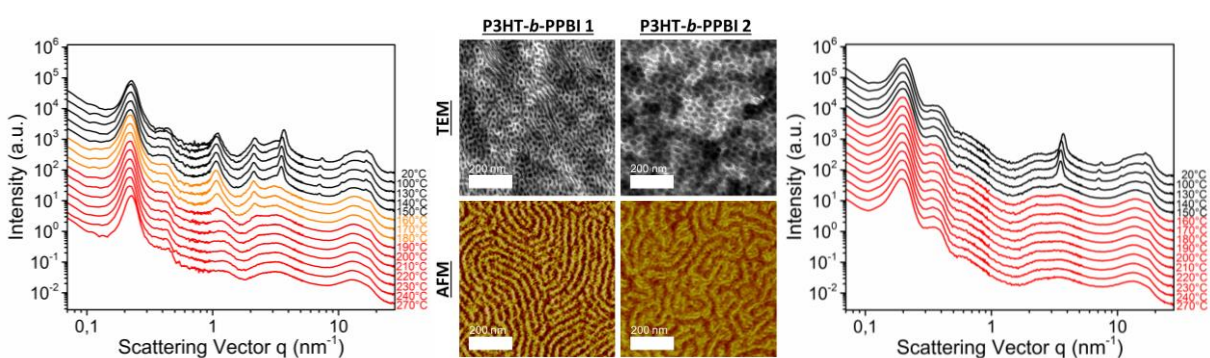


Fig. 2 Scattering intensity versus scattering vector q over full q -range of **P3HT-*b*-PPBI 1** (left) and **P3HT-*b*-PPBI 2** (right) at different temperatures during cooling. Temperatures at which the block copolymers are in the molten state are marked in red and temperatures at which only the PPBI block shows molecular ordering are marked in orange. Data were joined together from measurements at three sample-to-detector distances (curves shifted for clarity). TEM (Top) and AFM phase image (Bottom) of **P3HT-*b*-PPBI 1** (left) and **P3HT-*b*-PPBI 2** (right) after cooling from the molten state. For TEM the samples were annealed subsequently for 50h in chloroform vapor at 40 C and stained with RuO_4 .

scattering region both block copolymers show signals corresponding to a microphase separated structure which is identified as hexagonal cylinders of P3HT. This morphology is further supported by TEM and AFM. In the thin films a preferential orientation parallel to the substrate is observed by AFM. Additional DSC measurements reveal a significant amount of cold crystallization for both materials. The significant undercooling of the crystallization and the glass transitions temperatures of the PPBI-blocks, which are in the same temperature region explain the observed behavior.

Chapter 5: Poly(-3-hexylthiophene) Bottlebrush Copolymers with Tailored Side-Chain Lengths and High Charge Carrier Mobilities

In this chapter, the influence of the P3HT side chain lengths on the optical and electronical properties of P3HT bottlebrushes with polystyrene backbone is addressed. Four conjugated bottlebrush polymers with different P3HT side chain lengths were synthesized. Poly-(4-chloromethylstyrene) was synthesized and converted to poly-(4-azidomethylstyrene) upon substitution with sodium azide. Additionally, four alkyne end functionalized P3HT polymers **P3HT-Alkyne 1–4** and four reference polymers **P3HT 1–4** with molecular weights up to 11500 g mol⁻¹ were synthesized. The bottlebrushes were obtained by CuAAC of the P3HT-Alkynes with the backbone. The SEC traces of **Brush 3** and the corresponding precursor polymers are shown in **Fig. 3 a**. The SEC trace of the bottlebrush polymer is markedly shifted to high molecular weights and exhibits a rather narrow distribution. SEC curves of the series of purified bottlebrush polymers are shown in **Fig. 3 b**. The brush polymer with highest molecular weight (**Brush 4**) has side chains with a molecular weight of 11400 g mol⁻¹ (MALDI-ToF) resulting in very high molecular weight semiconductor polymers (144 000 g/mol in SEC). This is the P3HT bottlebrush with the longest side chains reported. ¹H-NMR spectroscopy provided information about the conversion in the case of the two smallest brushes. The estimated grafting density of these polymers is above 85 %. The high dilution of the backbone made it impossible to determine the grafting density for the two biggest brushes. I investigated the thermal and optical properties of the materials and found that a similar aggregation behavior in solution can be observed for the brushes compared to their linear counterparts. Unlike for the linear P3HTs, the crystallization is fully

suppressed for the two smallest brushes and kinetically hindered, due to the constraints imposed by the backbone, for the bigger brushes.

Organic field effect transistors (OFETs) were characterized with the P3HT brush polymers as active material in order to investigate the influence of the side chain length on the charge carrier mobility. For the OFET device of the melt crystallized **Brush 4**, a very high hole carrier mobility of $\mu_h = 4.95 \times 10^{-2} \text{ cm}^2 \text{ V}^{-1} \text{ s}^{-1}$, comparable to the highest values obtained for linear P3HT, was obtained. For both the brushes and the linear polymers higher charge carrier mobilities were obtained if the length of P3HT increased (**Fig. 3 c and d**). The films of the polymers, **Brush 3** and **4**, could be melt crystallized without dewetting. This makes these brushes also thermally more stable than films of the linear counterparts which can be of advantage for thin film applications.

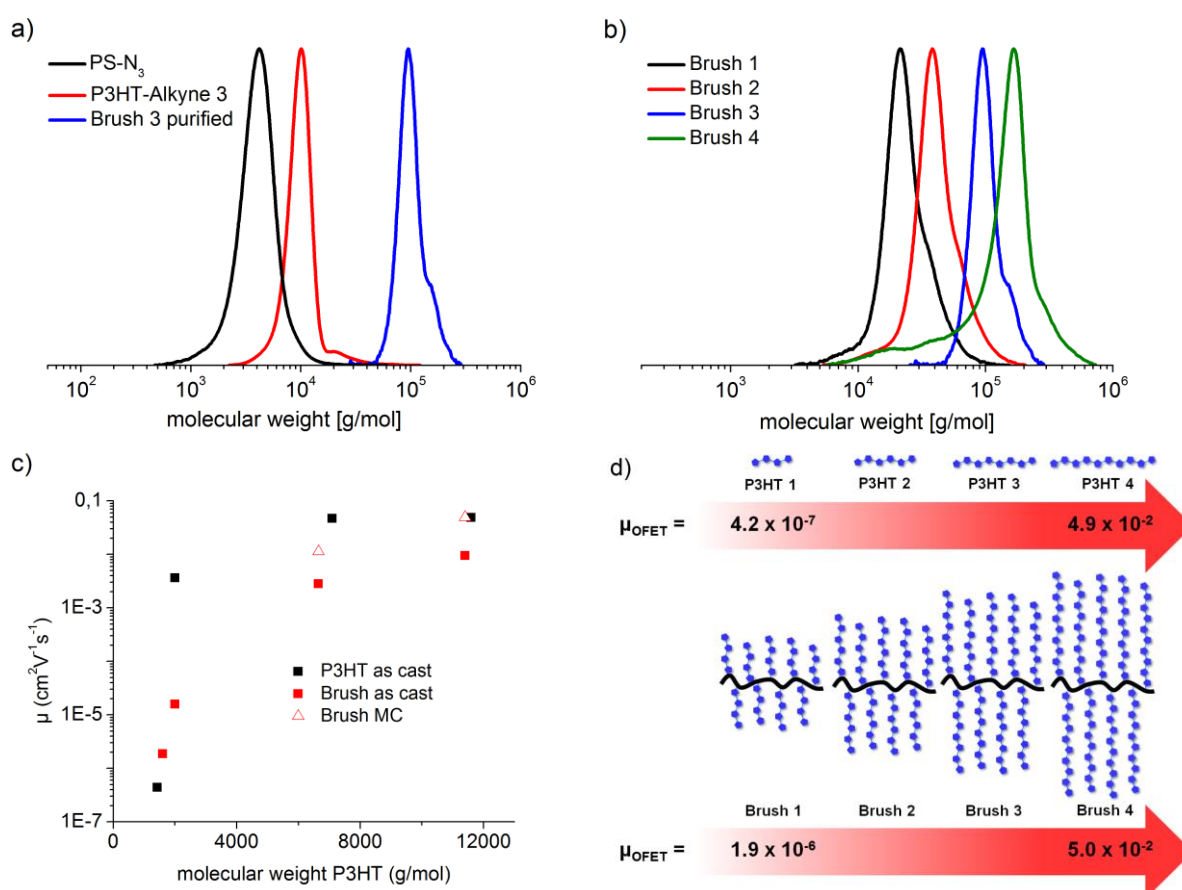


Fig. 3 a) Evolution of the SEC traces for **Brush 3** synthesized by the CuAAC of **PS-N₃** and **P3HT 3** as typical example; the raw product is purified from excess linear **P3HT 3** via preparative SEC; b) SEC traces of the four purified bottlebrush copolymers **Brush 1-4**; c) OFET hole mobilities μ plotted against the molecular weight $M_{n,\text{MALDI}}$ of the linear P3HT respectively the molecular weight $M_{n,\text{MALDI}}$ of the P3HT side-chain d) schematic diagram highlighting the dependency of μ_{OFET} on P3HT chain length.

Chapter 6: Densely Grafted Liquid Crystalline Copper Phthalocyanine Side Chain Polymer: Synthesis and Characterization

In this chapter, the bulky copper phthalocyanine azide (**CuPc-N₃**) was grafted to a poly-(4-propargyloxystyrene) (**PPOS**) backbone with high yields via CuAAC to obtain a donor semiconductor polymer. The solubility of the educts is crucial for quantitative grafting. Therefore, the **CuPc-N₃** with three swallow-tail oligo ethylene side chains was a promising candidate for the study as it is soluble in most solvents including water. SEC proved the successful grafting as the **PPOS** disappeared and the observed distribution was shifted to considerably higher molecular weights (**Fig. 4 a**) and the distribution was narrow and monomodal. The polymer had a good solubility (> 1 wt %) in technologically relevant solvents for environmentally benign processing (e. g. ethyl acetate). MALDI-ToF-MS of

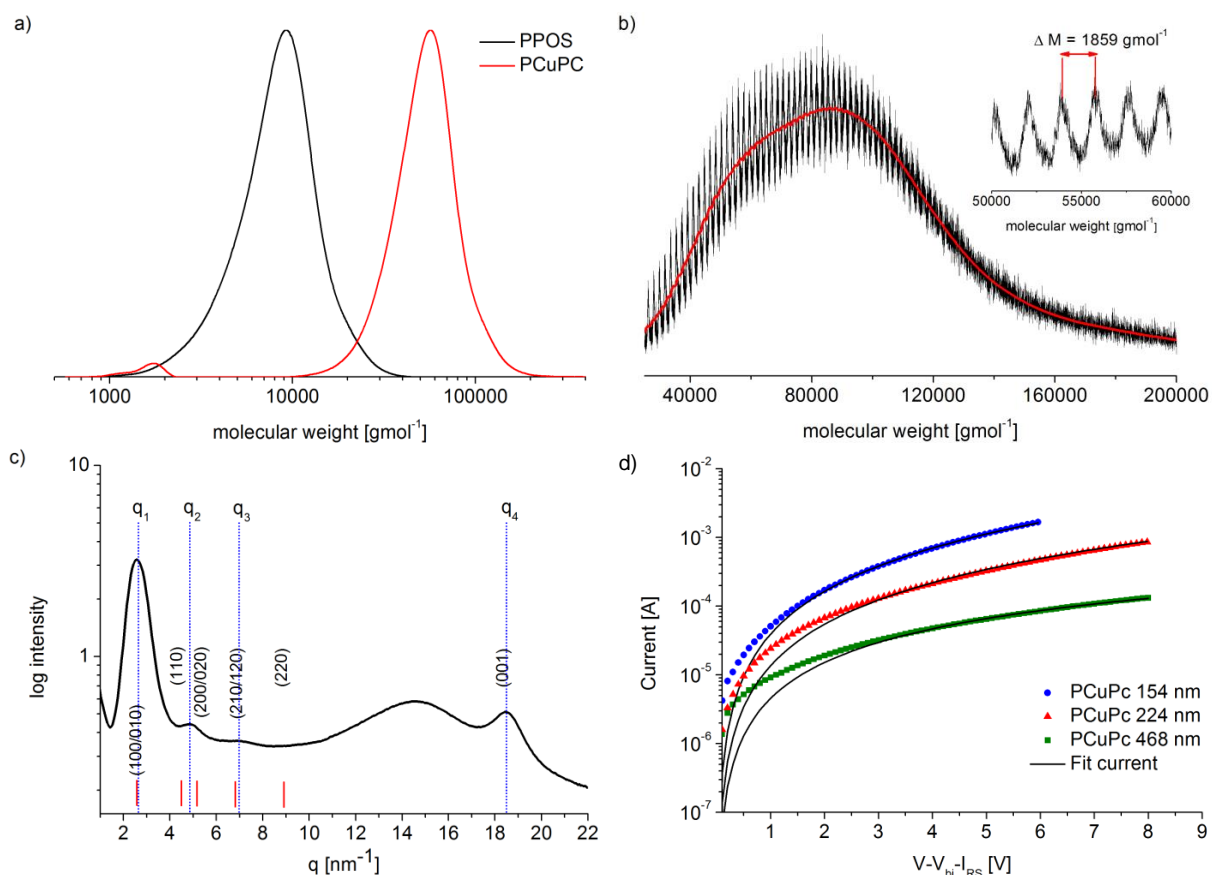


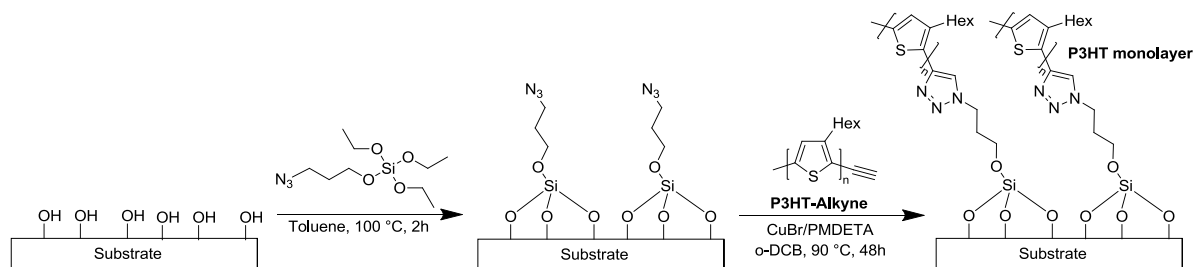
Fig. 4 a) SEC curves of the precursor polymer **PPOS** and the grafted polymer **PCuPc** after purification, b) MALDI-ToF MS of **PCuPc** with repeating units (inset); c) Diffraction pattern of the hexagonal mesophase (Col_h) of **PCuPc** measured at room temperature with the calculated reflection positions indicated by the red bars; d) I-V characteristics of as-cast films of **PCuPc** measured at room temperature. The I-V characteristics were corrected for the built in voltage (V_{bi}) and the voltage drop (IR) over the contacts.

PCuPc was possible with a resolution of the repeating units (**Fig. 4 b**). A single peak series is a strong indicator of quantitative grafting which is supported by the absence of the vibrational bands of both azide and alkyne functionality in IR spectroscopy.

Optical and electrochemical characterization via UV-Vis spectroscopy and cyclic voltammetry were conducted as well as thermal characterization via DSC and TGA. First, no phase transitions could be measured in DSC below the degradation temperature, a finding that seemed to contradict the observed birefringence in polarization microscopy. With ultrafast DSC (Flash-DSC) a melting above the degradation temperature was observed. The ordered phase at room temperature was investigated via wide angle X-ray scattering (WAXS) and determined to be columnar hexagonal (**Fig. 4 c**). Due to the high transition temperature the phase transition was not accessible. Additionally, the charge transport was measured in diode configuration. In contrast to other reports on phthalocyanines true SCLC behavior was observed. The semi-log plots of J vs. V indicate a V^2 dependency and for different thicknesses a L^{-3} dependence of J was observed (**Fig. 4 d**). A charge carrier mobility of $5.3 \cdot 10^{-6} \text{ cm}^2 \text{ V}^{-1} \text{ s}^{-1}$ was determined for **PCuPc**.

Chapter 7: Monolayer Brushes for Highly Efficient Polymeric SAMFETS

P3HT monolayers were obtained by grafting **P3HT-Alkyne** to an azide functionalized surface. The azide functionalized surface was prepared by silanization of a silicon oxide surface. Subsequently, the functional P3HT monolayers were synthesized by CuAAC click chemistry (see **Scheme 2**). By drying the monolayers from solvents with different boiling points the influence on the aggregation of the films was tested. AFM was used to follow the grafting process and determine the thicknesses of the grafted layers. Ultra-thin films with thicknesses between $h = 2.9\text{-}3.5 \text{ nm}$ were obtained. From the thicknesses, the grafting density values were obtained which proved the formation of continuous films in the true brush regime. UV-Vis spectroscopy was applied to gain insight in the aggregation of the grafted brushes and to compare them to thin spin-cast films of P3HT and P3HT bottlebrush copolymers (**Fig. 5 a**). The monolayers exhibit the aggregated spectra well known for P3HT. The monolayer dried from chloroform exhibited the highest aggregation strength as compared to the monolayers dried from



Scheme 2 Principle of the surface functionalization with P3HT. A substrate with hydroxy groups at the surface is functionalized with the azido silane. Subsequently the azido SAM reacts with P3HT-Alkyne to form the P3HT monolayer on the surface.

the other solvents (chlorobenzene and o-dichlorobenzene). In comparison to spin-cast films, the monolayers generally exhibited lower aggregation strengths.

To test electrical properties of the monolayers self-assembled-monolayer field-effect transistors (SAMFETS) were prepared. A very high charge carrier mobility of $1.6 \cdot 10^{-3} \text{ cm}^2 \text{ V s}^{-1}$ and an On/Off-Ratio of $8.9 \cdot 10^4$ for the grafted brushes dried from chloroform (see **Fig. 5 b**) were obtained. This is the highest mobility observed for surface grafted P3HT up to now and it represents the highest ever reported value for polymeric SAMFETs. The increased performance is attributed to the high molecular weight of the **P3HT-Alkyne**. In good agreement with the lower aggregation observed for the monolayers dried from chlorobenzene or dichlorobenzene a lower charge carrier mobilities in the SAMFETs dried from these solvents was observed. Thermal annealing revealed no improvement of the devices. By increasing the grafting density, the charge carrier mobility can be further improved in polymeric SAMFET devices.

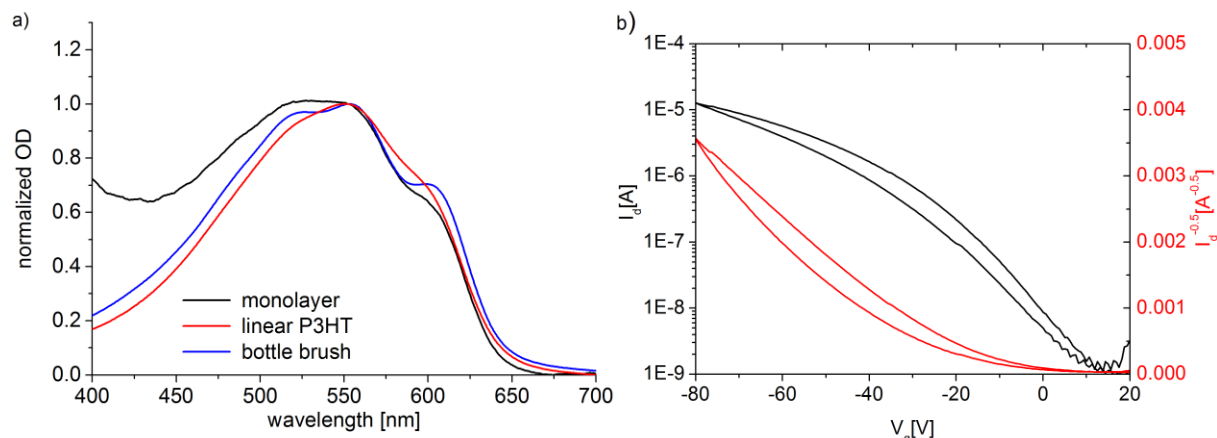


Fig. 5 a) UV-Vis spectra of the P3HT monolayer (dried from CHCl₃) and thin films of linear **P3HT** (as-cast) and **PS-g-P3HT** (MC at 240 °C); b) Transfer characteristics of the monolayer dried from CHCl₃ in saturation regime ($V_d = -80 \text{ V}$) at the bottom (d-f). The channel length was 20 μm in all cases.

Individual Contributions to Joint Publications

The following section specifies the individual contributions of the authors:

Chapter 4

“Impact of Molecular Dynamics on Structure Formation of Donor-Acceptor Block Copolymers”

by Matthias Fischer, Christian David Heinrich, Mukundan Thelakkat and Thomas Thurn-Albrecht.

This work is prepared for submission.

Matthias Fischer and I both contributed equally to this work. I designed and synthesized the diblock copolymers during my master thesis. The polymers were fully purified during the PhD thesis, characterized regarding their polymer properties using SEC, NMR etc. and AFM, TEM and DSC were also measured during my doctoral work. Matthias Fischer conducted the XRD measurements, interpreted the data and wrote the corresponding part and corrected the manuscript. I wrote the corresponding part and corrected the manuscript. Mukundan Thelakkat and Thomas Thurn-Albrecht supervised the project and corrected the final manuscript.

Chapter 5

“Poly(-3-hexylthiophene) Bottlebrush Copolymers with Tailored Side-Chain Lengths and High Charge Carrier Mobilities”

by Christian David Heinrich and Mukundan Thelakkat.

This work is published in the *Journal of Material Chemistry: C*, 2016, **4**, 5370-5378, doi: 10.1039/c6tc01029f.

I designed, synthesized and characterized the bottlebrush polymers and I wrote and corrected the manuscript. Mukundan Thelakkat supervised the project and corrected the manuscript.

Chapter 6

“Densely Grafted Liquid Crystalline Copper Phthalocyanine Side Chain Polymer: Synthesis and Characterization”

by Christian David Heinrich, Sinem Tuncel Kostakoğlu and Mukundan Thelakkat.

This work is published in the *Journal of Material Chemistry: C*, 2017, **5**, 6259-6268, doi: 10.1039/C7TC01234A.

I designed, synthesized and characterized the polymer and I wrote and corrected the manuscript. Sinem Tuncel Kostakoğlu synthesized the copper phthalocyanine monomer (CuPc-N₃) and corrected the manuscript. Mukundan Thelakkat supervised the project and corrected the final manuscript.

Chapter 7

“Monolayer Brushes for Highly Efficient Polymeric SAMFETs”

by Christian David Heinrich, Paul Max Reichstein and Mukundan Thelakkat.

This work is prepared for submission.

I synthesized the surface-grafted brushes and conducted the characterization in terms of AFM, UV-Vis and charge carrier transport. I wrote and corrected the manuscript. Paul Max Reichstein synthesized the P3HT-Alkyne, conducted preliminary tests to optimize the grafting procedure, measured the contact angle and corrected the manuscript. Mukundan Thelakkat supervised the project and corrected the final manuscript.

Impact of Molecular Dynamics on Structure Formation of Donor-Acceptor Block Copolymers

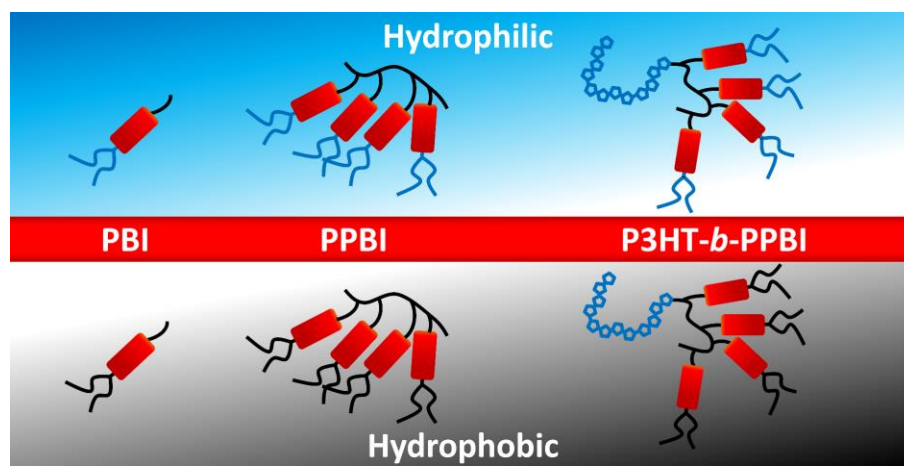
Matthias Fischer^{†§}, C. David Heinrich^{‡§}, Mukundan Thelakkat^{‡*}, Thomas Thurn-Albrecht^{†*}

[†] Experimental Polymer Physics Group, Martin Luther University Halle-Wittenberg, Von-Danckelmann-Platz 3, 06120 Halle, Germany

[‡] Applied Functional Polymers, Macromolecular Chemistry I, University of Bayreuth, Universitätsstr. 30, 95440 Bayreuth, Germany

*E-mail of corresponding authors: mukundan.thelakkat@uni-bayreuth.de, Thomas.thurn-albrecht@physik.uni-halle.de

§ Both authors contributed equally



Prepared for submission

Abstract

Donor-acceptor block copolymers (BCPs) are attractive model materials for studying morphology-dependent processes in organic photovoltaics due to their intrinsic property to form an equilibrium nanostructure on the length scale of the excitation diffusion length. As usually semiconductor polymers are crystalline or liquid crystalline and structure formation processes are complex in these BCPs. We here present a study of the interplay between phase separation, crystallization and glass transition of two poly(3-hexylthiophene)-*b*-polyperylene bisimide (**P3HT-*b*-PPBI 1** and **2**) diblock copolymers incorporation P3HT as a donor and a polystyrene with two different pendant perylene bisimides (**PBI-N₃ 1** and **2**) as acceptor blocks. These materials were synthesized by a modular approach, combining KCTP, controlled RAFT polymerization and click chemistry in order to obtain highly comparable polymers. We synthesized poly(3-hexylthiophene) (P3HT) with a high molecular weight ($M_{n,SEC} = 18300 \text{ g mol}^{-1}$), in a controlled manner, introduced a RAFT end group by click chemistry to form a macro initiator and subsequently polymerized propargyloxystyrene by sequential polymerization. In a post-polymerization step using click reaction, the polystyrene block was grafted with the PBI acceptor units. We obtained diblock copolymers with 70 wt% of the PBI block and 30 wt% P3HT. In order to study the effect of the backbone glass transition on side chain crystallization in the acceptor block, low molecular weight model compounds and homopolymers with both PBIs were also synthesized. The BCPs were characterized by temperature dependent small- and wide angle x-ray scattering (SAXS/WAXS) in combination with differential scanning microscopy (DSC) While microphase separation in the liquid state led to a cylindrical morphology in both cases, the crystallization of the functional side chains depend strongly on the backbone glass transition temperature as compared to the ordering temperature of the PBI unit.

Introduction

The combination of the controlled Kumada catalyst transfer polymerization (KTCP) of 3-hexylthiophene, controlled radical polymerization (CRP) of easily available monomers such as propargyloxystyrol and click chemistry of suitable semiconductor functionalities via copper-catalyzed azide-alkyne cycloaddition (CuAAC) opens a new versatile pathway towards defined donor-acceptor block copolymers (BCPs).¹⁻³ P3HT is one of the most studied conjugated polymers that can be polymerized in a controlled manner by the KTCP. McCullough *et al.*^{4,5} and Yokozawa *et al.*^{6,7} independently reported the controlled synthesis of P3HT. This method allows the synthesis of polymers with controlled end groups aside from being able to adjust the appropriate molecular weight for the intended application.^{8,9} In the field of organic electronics and organic solar cells absolute molecular weights of P3HT in the range of around $M_{n,MALDI} = 12000 \text{ gmol}^{-1}$ exhibit optimum material properties in terms of a high charge carrier mobility in organic field transistors (OFET)¹⁰ as well as in space charge limited current (SCLC) devices.¹¹ The first synthesis of acceptor polymers with pendant perylene bisimide side chains (PPBI) by a direct CRP of acrylate functionalized PBI monomer were reported in 2004 by Linder *et al.*¹² Bringing P3HT and the PPBI polymers in one block copolymer gives access to fully functionalized donor-acceptor BCPs. The equilibrium microstructure of nanoscale phase separated donor-acceptor BCPs with perpendicular alignment with respect to a substrate has been proposed to be a very interesting model system for organic photovoltaics (OPV).¹³ Such a structured material should in principle provide enough donor-acceptor interfaces, due to the small structure size, for charge separation as well as optimal pathways for charge carrier transport. Block copolymer microphase separation is well understood for amorphous blocks. The corresponding phase diagram in general depends on the incompatibility χN and the volume fraction.¹⁴ If crystalline or liquid crystalline blocks are involved, the self-assembly behavior becomes more complex since there is an additional competition between classical microphase separation and crystallization. Depending on the relative positions of the order-disorder transition temperature (T_{ODT}) and the crystallization temperature (T_c),

structure formation can either be induced by microphase separation or by crystallization. If crystallization starts from a microphase separated structure, the existing nanostructure can either remain intact (confined crystallization) or be destroyed (breakout crystallization).¹⁵

While the microphase separation in numerous BCPs of conjugated poly(alkylthiophene)s with an electronically inactive second block were reported,¹⁶⁻²⁰ reports on donor-acceptor polymers with well-ordered microphase separated structures are rare.²¹⁻²⁵ In previous publications we explored microstructure formation for several donor-acceptor BCPs containing a crystallizable donor block and a liquid crystalline acceptor block. Lohwasser *et al.* reported the synthesis of donor-acceptor BCPs, P3HT-*b*-PPBIs, which showed well-ordered lamellar and cylindrical microstructures as expected for the respective volume fractions.³ Lohwasser *et al.* pointed out the importance of the incompatibility factor χN for these systems.³ If χN , resp. the molecular weight, was high enough, microphase separation in the melt with subsequent confined crystallization during cooling was observed for a series of donor-acceptor BCPs consisting of P3HT and pendant PBIs attached to a polyacrylate backbone (cf. **Fig. 1 a**). In a later study the additional importance of chain mobility became clear.²⁴ In this case the acceptor block consisted of pendant phenyl-C₆₁-butyric acid methyl ester (PCBM) attached to a polystyrene backbone. This combination led to a strong increase of the glass transition temperature (T_g) of the acceptor block, which limited the microphase separation and formation of long-range order (cf. **Fig. 1 b**).^{24,26}

In our earlier report, for the synthesis of P3HT-*b*-PPBI, high molecular weight P3HT with alkyne end group was converted to a macro initiator for NMRP via CuAAC click chemistry. This initiator was used to directly synthesize the second block using PBI-acrylate monomers. The direct polymerization of this monomer is not trivial and the introduction of CuAAC in combination with a controlled radical polymerization gave easier access to defined PBI-pendant homopolymers.² This concept was first attempted by Tao *et al.* in 2009.²⁸ Lang *et al.* investigated this concept in detail by synthesizing poly(propargyloxystyrene) via nitroxide mediated radical polymerization (NMRP) and grafting this precursor polymer with different perylene bisimides with azide

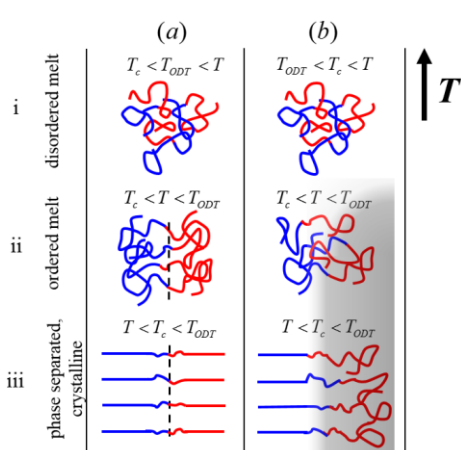


Fig. 1 Schematic illustration of the effect of the glass transition temperature on self-assembly and crystallization of a block copolymer with high T_g in one block. The gray color schematically indicates the temperature range with low molecular mobility of the acceptor block. (i) Above the order-disorder transition temperature (T_{ODT}), the BCP forms a disordered melt. (ii) While in case (a) the chain mobility is high in the relevant temperature range, so that a well ordered microphase separated state forms below T_{ODT} , microphase separation and the formation of long range order is limited by the high T_g in case (b). (iii) Below T_c crystallization takes place. It is confined for large segregation strengths. (For simplicity, it is assumed here that the crystallization temperature is the same for both blocks).

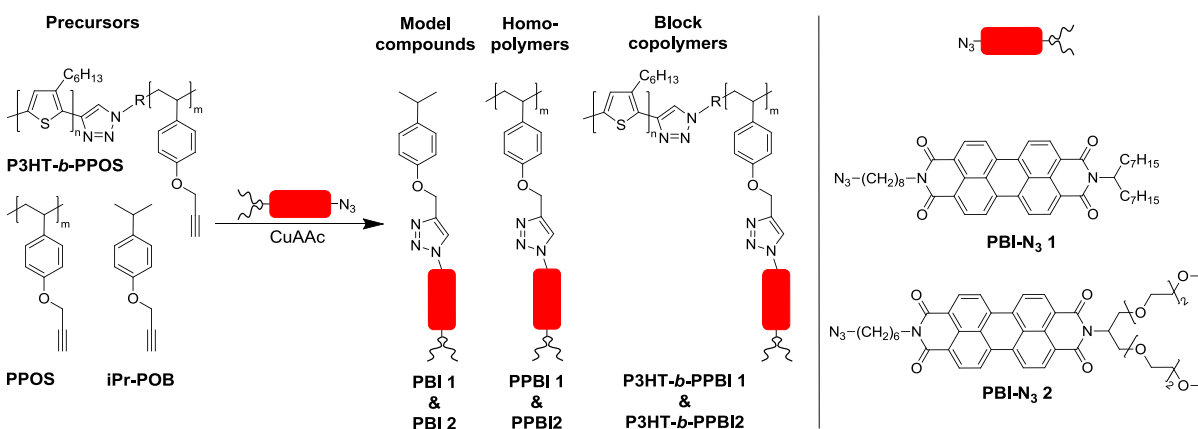
functionality.² A second study was concerned with the influence of the spacer length between the perylene bisimide core and the polymeric backbone and the influence of hydrophilic swallow tails on the thermal properties of the grafted polymers.²⁹ The hydrophilic PPBIs were amorphous materials and exhibited surprisingly high electron mobilities in SCLC devices.³⁰ Therefore, it is very interesting to incorporate such hydrophilic pendant blocks into BCPs and to study their microphase separation.

In the current study, based on the above facts, we have synthesized two comparable donor-acceptor BCPs with differently substituted PBI acceptor units by a modular approach. The PBIs are selected in such a manner that one carries the conventional hydrophobic alkyl swallow tail substituents, whereas the second one has flexible oligoethylene glycol (OEG) substituents. In addition, comparable sets of pendant PBI homopolymers and PBI model compounds were synthesized to study the structure formation in these respective systems and to understand the structure formation in BCPs, which may be complex. We use a combination of temperature dependent small- and wide-angle X-ray scattering (SAXS/WAXS), atomic force microscopy and transmission electron microscopy (AFM, TEM) to investigate the structure formation in BCPs with pendant PBIs attached to a polystyrene backbone. We expect that due to the lower T_g of the acceptor block microphase separation will again take place unhindered by molecular mobility.²⁹ Furthermore, the effect of different solubilizing group attached to the PBI unit is investigated.

Results and Discussion

Synthesis

The study focuses on the structure property relationship of donor-acceptor BCPs carrying different acceptor units and these are synthesized by a novel modular approach. Three alkynes (iPrPOB, PPOS and P3HT-*b*-PPOS) were grafted with two different azide functionalized PBI molecules via a CuAAC click reaction (see **Scheme 1**). The perylene bisimides were chosen due to the very promising electronic/ electrical properties of PBI homopolymers with these side chains.³⁰ The influence of the complexity on structure formation increasing from the small molecule model compounds (**PBI 1** and **2**) through the acceptor homopolymers (**PPBI 1** and **2**) and the donor-acceptor BCPs (**P3HT-*b*-PPBI 1** and **2**) can be studied. Due to the high comparability of the motive of the acceptor units as well as similar molecular weights obtained in the acceptor blocks and homo-polymers the system can be understood. Likewise, it is possible to investigate the influence of the different acceptor units **PBI-N₃ 1** and **2** on the grafting-to approach, as well as on structure formation. Two novel model compounds (**PBI 1** and **2**) were synthesized by CuAAC click reactions of the acceptor units **PBI-N₃ 1** and **2** with 1-isopropyl-4-propargyloxy-benzene.



Scheme 1. Synthesis of perylene bisimide functionalized model compounds, homopolymers and BCPs via CuAAC click chemistry. Three different precursors (left) are coupled with two different perylene bisimides (right).

Two novel model compounds (**PBI 1** and **2**) were synthesized by CuAAC click reactions of the acceptor units **PBI-N₃ 1** and **2** with 1-isopropyl-4-propargyloxybenzene. These compounds were designed to resemble the repeating unit of the acceptor polymers. The synthesis of similar homopolymers was first published by Lang and Thelakkat.²⁹ Very defined acceptor polymers with different PBI derivatives and excellent grafting densities can be synthesized with this strategy. Two clickable precursors, **PPOS 1** and **2**, were synthesized and converted into pendant PBI homopolymers, **PPBI 1** and **PPBI 2**. The first PBI homopolymer and its precursor (**PPB 1** and **PPOS 1**) were published by Lang and Thelakkat.²⁹ A comparable **PPBI 2** was synthesized by us from a new batch of precursor polymer **PPOS 2**. **PBI 1-2** and **PPBI1-2** serve as simple constituting moieties or blocks for the complex BCPs and help in elucidating the structure formation of the BCPs.

The efficiency of the grafting step via CuAAC click chemistry is crucial to obtain comparable materials. NMR and IR spectroscopy indicate a quantitative conversion of the alkynes. SEC measurement on the other hand cannot be readily used to make statements about the success of the grafting step.

Table 1 Overview of the synthesized polymers

	$M_{n,SEC}$ (g mol ⁻¹)	$M_{p,SEC}$ (g mol ⁻¹)	\bar{D}	$M_{n,NMR}$ (g mol ⁻¹)	$M_{p,MALDI}$ (g mol ⁻¹)	wt% (PPBI)
PPOS 1	7300	7800	1.11			
PPBI 1	59200	69900	1.09	41100 ^a	40800	
PPOS 2	7500	9100	1.20			
PPBI 2	79800	87500	1.14	53600 ^b	53800	
P3HT-Alkyne	18300	23000	1.19		13300	
P3HT-RAFT	18400	23600	1.18		13300	
P3HT-<i>b</i>-PTMSPOS	21900	29200	1.40	20500 ^c		
P3HT-<i>b</i>-PPOS	22300	28300	1.42	18000 ^c		
P3HT-<i>b</i>-PPBI 1	69500	87300	1.25	48100 ^c		72 ^d
P3HT-<i>b</i>-PPBI 2	77700	101200	1.23	49700 ^c		73 ^d

a) Calculated from M_p (**PPOS 1**) = 7800 g mol⁻¹ (~ DP = 44); b) Calculated from M_p (**PPOS 2**) = 9100 g mol⁻¹ (~ DP = 55); c) Calculated from and $M_{n,Maldi}$ (**P3HT-RAFT**) = 13300 g mol⁻¹ (~ DP = 80) and ratio of P3HT:PPOS (80:29) from NMR; d) Calculated from and $M_{n,Maldi}$ (**P3HT-RAFT**) = 13300 g mol⁻¹ (~ DP = 80) and ratio of P3HT:PPBI (80:37) from NMR.

In SEC a big shift of the apparent molecular weight combined with the absence of any signal at the position of the precursor indicates an efficient synthesis, but the significance of this measurement is reduced by the lack of a proper calibration (in this case a polystyrene standard was used). We additionally, measured MALDI-ToF mass spectrometry to obtain the absolute molecular weights of the grafted homopolymers and compared the absolute values with the expected molecular weights. The molecular weight of a densely grafted polymer can be calculated as the degree of polymerization (N) of the precursor polymers **PPOS 1** and **2** can be accurately determined by SEC. The molecular weight $M_{n,MALDI} = 40800 \text{ g mol}^{-1}$ obtained from the MALDI-ToF spectrum of **PPBI 1** (**Fig. 2**) is in very good agreement with the expected value ($M_{n,calc} = 41100 \text{ g mol}^{-1}$ from N taken from SEC)(see **Table 1**). The resolution of the MALDI spectrum is also still high enough to extract the repeating units of the polymer. Similarly, the molecular weight of **PPBI 2** ($M_{n,MALDI} = 53800 \text{ g mol}^{-1}$) obtained by MALDI (**Fig. S 1 a**) is also in very good agreement with the calculated molecular weight of $M_{n,calc} = 53600 \text{ g mol}^{-1}$. These measured absolute molecular weights are thus an additional strong support for the claim of quantitative grafting for both **PPBI 1** and **2**.

The click-reaction strategy employed for the homopolymer synthesis was adopted for the donor-acceptor BCPs as well. The objective was to obtain fully functionalized BCPs with a weight content of the acceptor block of around 70 wt% in order to obtain a diblock copolymer with cylindrical microphase separation. At first, an alkyne

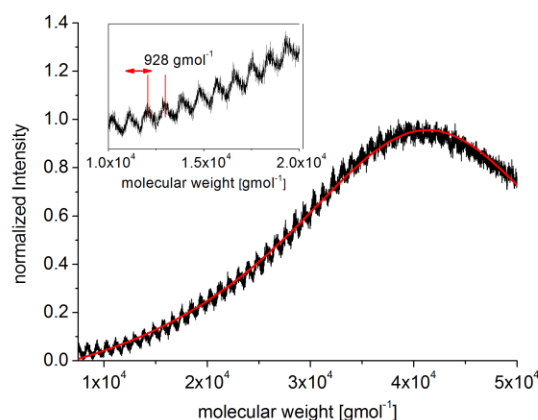
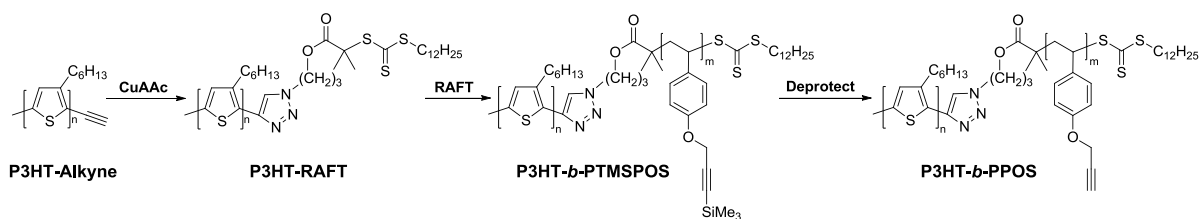


Fig. 2 MALDI-ToF spectrum of **PPBI 1** in linear positive mode with indol-3-acetic acid as matrix. The enlarged part in the inset shows the molecular mass of the repeating unit which is in very good agreement with the expected value of **PBI 1**.

functionalized P3HT polymer was synthesized via Kumada catalyst-transfer polymerization (KCTP) and it was converted to a macroinitiator by attaching a chain transfer agent suitable for the RAFT polymerization of the TMS-protected POS. This protected precursor block copolymer **P3HT-*b*-PTMSPOS** was subsequently deprotected to get **P3HT-*b*-PPOS** and grafted with the two different acceptor units, **PBI-N₃ 1** and **PBI-N₃ 2**. The synthesis of the precursor BCPs are shown schematically in a three step synthesis in **Scheme 2**.

Alkyne functionalized P3HT (**P3HT-Alkyne**) with high molecular weight was synthesized according to a published procedure.⁹ The absolute molecular weight of **P3HT-Alkyne** was determined by MALDI-ToF to be 13300 g mol⁻¹ which corresponds to a degree of polymerization N of 80 (**Fig. S 2 b**). **P3HT-Alkyne** was then converted to the macro initiator (**P3HT-RAFT**) for RAFT polymerization via CuAAC with an azide functionalized RAFT-agent. The successful functionalization with the RAFT end group can be detected by ¹H-NMR (**Fig. 3 a**). The signal of the alkyne proton at 3.50 ppm (**2**) cannot be detected any more after the click reaction and new signals which can be assigned to the RAFT end group (**a-d**) appear instead. We therefore assume that conversion from alkyne to RAFT end group was nearly quantitative.



Scheme 2. Synthesis of the precursor block copolymer **P3HT-*b*-PPOS**. **P3HT-Alkyne**, synthesized by Kumada catalyst-transfer polymerization (KCTP), is converted into the macro RAFT-agent **P3HT-RAFT** via CuAAC click chemistry. The PPOS block can be sequentially polymerized from **P3HT-RAFT** via a RAFT polymerization of trimethylsilyl protected 4-(propargyloxy)styrene. A deprotection of the alkyne group with TBAF results in the precursor polymer **P3HT-*b*-PPOS**.

The third step towards the fully functionalized BCPs was the polymerization of the second block. The second block was aimed to have about 30 repeating units in order to synthesize donor-acceptor BCPs with approximately 70 wt% non P3HT block. The RAFT polymerization leading to the block copolymer **P3HT-*b*-PTMSPOS** was optimized to achieve control of the N of the second block. At a [Monomer]:[P3HT-RAFT] ratio of 440:1 the polymerization gave reproducible results. The propargyloxy styrene monomer was polymerized with **P3HT-RAFT** initiator until a conversion of 6.7 % was reached. With the knowledge of the [Monomer]:[P3HT-RAFT] ratio and the conversion, a N of 30 was expected. This value is in excellent agreement with the one that can be obtained by calculating the **PTMSPOS** content via NMR. The molar ratio of P3HT:PTMSPOS is 2.8:1 and the N of the second block should therefore be 29. This calculation is only correct under the assumption that every single P3HT chain was bearing an alkyne end group that was also quantitatively converted to the RAFT group and started a new block. Also the small fraction of coupled P3HT (see **Fig. S 2a**) is neglected in this calculation. These points explain why the SEC curve of **P3HT-*b*-PTMSPOS** is not only shifted to higher molecular weights in comparison to the macro initiator **P3HT-RAFT**, but also shows a significant broadening of the distribution

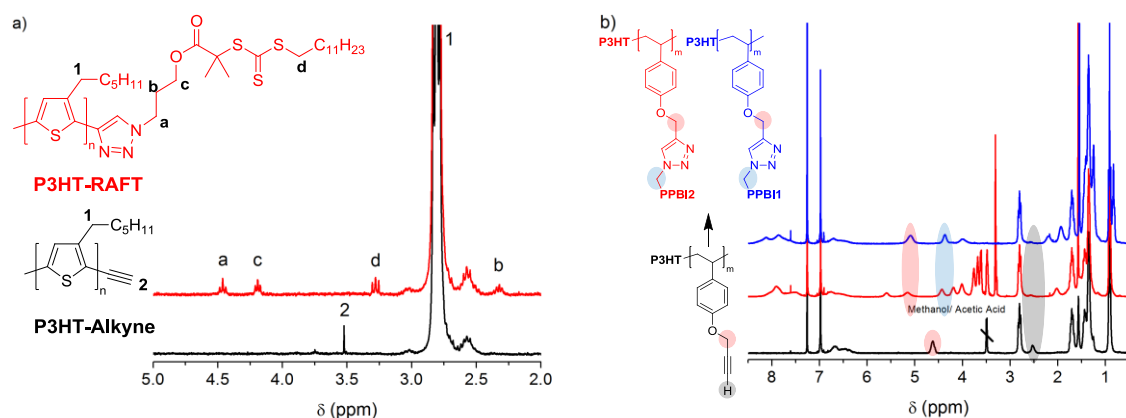


Fig. 3 a) Details of the $^1\text{H-NMR}$ spectral region of **P3HT-Alkyne** and the macroinitiator **P3HT-RAFT**. The Signal of the alkyne proton (**2**) disappears after the click reaction with the RAFT-agent and new signals (**a-d**) can be assigned to the new end group; b) $^1\text{H-NMR}$ spectra of **P3HT-*b*-PPOS**, and the donor-acceptor BCPs **P3HT-*b*-PPBI 1** and **2**. The position of the alkyne proton in **P3HT-*b*-PPOS** (grey), and the signals of the protons of the CH_2 groups adjacent to the triazole ring (blue and red) are highlighted.

(**Fig. 4 a**). The block copolymer **P3HT-*b*-PTMSPOS** had to be deprotected before the final grafting step. The trimethylsilyl group could be quantitatively cleaved at mild conditions with TBAF. The successful reaction could be monitored by $^1\text{H-NMR}$ (**Fig. S3 a**) and SEC (**Fig. 4 a**). This polymer was the precursor polymer (**P3HT-*b*-PPOS**) for the grafting with the acceptor PBI units.

In the final step, two fractions of the same precursor block copolymer were grafted with two different PBI- N_3 acceptors via CuAAC click reactions. These reactions were conducted at room temperature and resulted in a quantitative grafting of the second block. The complete conversion of the alkynes of the second block can be monitored via $^1\text{H-NMR}$ by the disappearance of the alkyne proton signal at 2.52 ppm (see **Fig. 3 b**). A new proton signal at 5.09 ppm is observed which is assigned to the CH_2 on the acceptor side adjacent to the triazoles ring. The strongest indicator for quantitative grafting is the shift of signal of the methylene protons directly adjacent to the oxygen atom of the propargyloxystyrene. This O-CH_2 proton signal appears at 4.62 ppm in case of the precursor **P3HT-*b*-PPOS** and is shifted markedly to lower field (5.09 ppm) for both donor-acceptor BCPs (**P3HT-*b*-PPBI 1** and **2**).

The SEC curves of the grafted material before final purification (**Fig. S3 b**) exhibit a clear low molecular weight peak even though the grafting of the second block was highly efficient. This peak appears at the exact position of the precursor polymer. Its presence stems from one of the aforementioned non-quantitative reactions during the

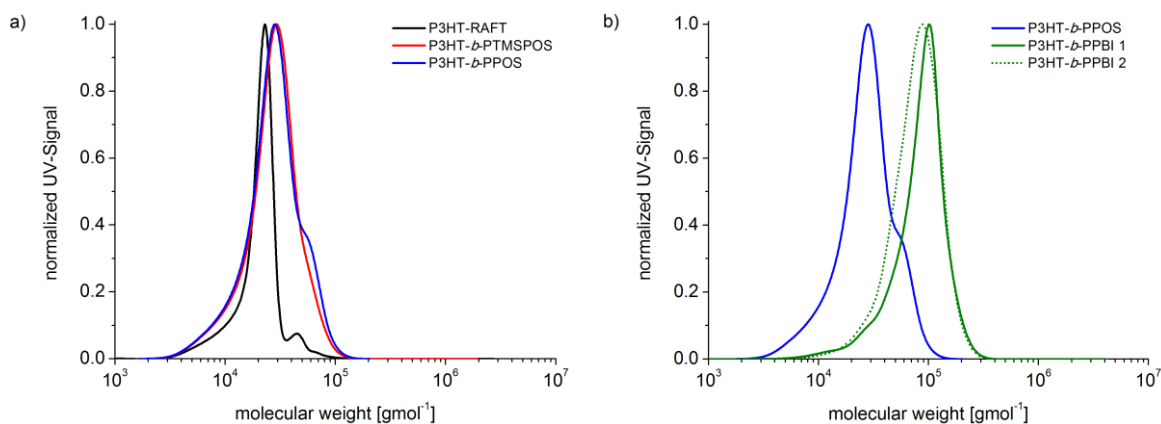


Fig. 4 SEC traces of P3HT-RAFT and the BCPs **P3HT-*b*-PTMSPOS** and **P3HT-*b*-PPOS** (a) and the two purified donor-acceptor BCPs **P3HT-*b*-PPBI 1** and **2** after CuAAC click reaction of **P3HT-*b*-PPOS** with the **PBI-Azides 1** and **2** (b).

previous steps e.g. that not all P3HT chains were functionalized with an alkyne end group. These side products could be efficiently separated from the final BCPs via a silica gel column. The strong interaction of the perylene bisimide containing polymers with the stationary phase was successfully utilized for this. Any residual P3HT polymers could be selectively washed from the column with toluene while residual **PBI-N₃ 1** and **2** could be washed down with chloroform. The pure BCPs could finally be retrieved from the column by a 95:5 (v:v) mixture of chloroform: methanol with high yield. The SEC curves of the purified polymers (**Fig. 4 b**) are monomodal with no sign of residual P3HT or precursor block copolymer. The molar composition of the BCPs can be extracted from ¹H-NMR analysis of **P3HT-*b*-PPBI 1** and **2** with a value of 2.16:1 for both polymers. This means that the second block constitutes 72 wt% (**P3HT-*b*-PPBI 1**) and 73 wt% (**P3HT-*b*-PPBI 2**) of the overall mass of the block copolymer. The N for the acceptor block was calculated as 37. The overall efficiency of the end group modification of P3HT and the initiation of the second block can be determined by comparing this value with the calculated DP of the precursor **P3HT-*b*-PTMSPOS** (DP = 29). The increased DP after purification therefore means that about 80 % of the P3HT chains, formed during the initial P3HT polymerization, were functionalized with an alkyne, transformed to a macro initiator and subsequently started the polymerization of the styrene monomer. Altogether the described synthetic strategy gave access to highly comparable donor-acceptor BCPs with precise control over the composition. Especially the highly efficient quantitative grafting with different acceptor units and the lack of unreacted precursors or P3HT homopolymers ensures the structural purity and high comparability of the final BCPs.

Structure Formation in P3HT-*b*-PPBI 1 and 2

The diblock copolymers **P3HT-*b*-PPBI 1** and **2** are characterized via temperature dependent X-ray scattering measurements in order to understand the structure formation of the polymers. Additionally, the findings will also be supported by DSC, TEM and AFM measurements. **Fig.5** depicts temperature dependent X-ray scattering measurements. The scattering curves can be divided into two regions: At larger scattering vectors ($q > 1 \text{ nm}^{-1}$) the Bragg reflections of the individual phases can be studied, while at small scattering vectors ($q < 1 \text{ nm}^{-1}$) the signals of the BCP nanostructure can be found. Two separate crystallization events take place in **P3HT-*b*-PPBI 1** during cooling. First, at 180°C two scattering peaks form at 1.07 nm^{-1} and 2.14 nm^{-1} . These peak positions are in agreement with a lamellar liquid crystalline morphology as proposed for the corresponding PPBI homopolymer.²⁹ Additionally, a second crystallization event takes place at 150°C . At this temperature, the typical scattering pattern of P3HT with the (100)-reflection at 3.7 nm^{-1} together with its higher order signals and the π - π -stacking signal at $\approx 16.6 \text{ nm}^{-1}$ appears.^{31,32} In contrast, only one crystallization event is observed in **P3HT-*b*-PPBI 2**. Here only P3HT crystallizes at 150°C , and the PPBI block stays in an amorphous state. While the behavior of the PPBI block is in agreement with the corresponding homopolymer,²⁹ the reason for its amorphous state is still topic of further investigation. In the region of small scattering

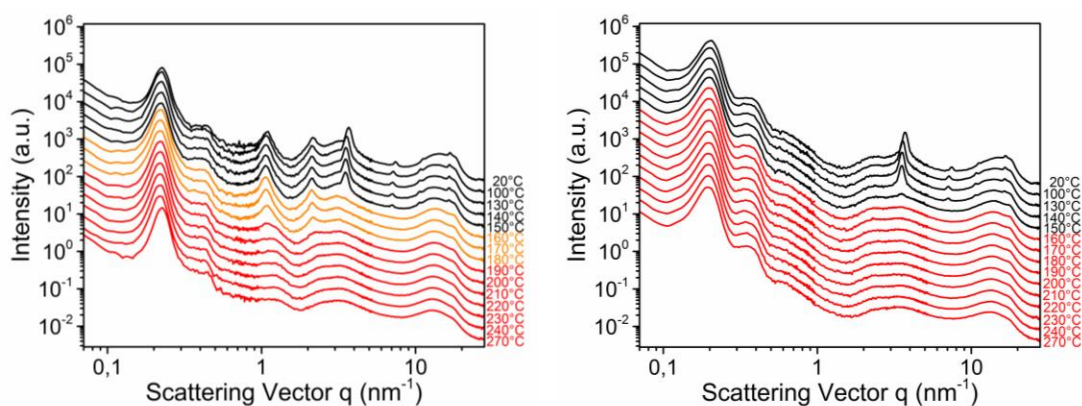


Fig. 5: Scattering intensity versus scattering vector q over full q -range of **P3HT-*b*-PPBI 1** (left) and **P3HT-*b*-PPBI 2** (right) at different temperatures during cooling. Temperatures at which the BCPs are in the molten state are marked in red and temperatures at which only the PPBI block shows molecular ordering are marked in orange. Data were joined together from measurements at three sample-to-detector distances (curves shifted for clarity).

vectors ($q < 1 \text{ nm}^{-1}$) both BCPs show scattering signals corresponding to the BCP microstructure. The signals consist of a strong scattering peak at around 0.2 nm^{-1} accompanied by higher order signals which are a clear indication for a microphase separated structure. It is worth to point out that the BCP nanostructure (SAXS peak shape and position) keeps unchanged over the whole temperature range studied from $270 \text{ }^\circ\text{C}$ to $20 \text{ }^\circ\text{C}$ (except for a minor shift due to thermal expansion). This observation carries two implications: (i) The order disorder transition temperature is higher than $270 \text{ }^\circ\text{C}$ and (ii) confined crystallization without breakout takes place within the morphology of the BCP nanostructures.

In order to determine the BCP morphology, we performed a closer analysis of the SAXS patterns of both samples at $20 \text{ }^\circ\text{C}$ after cooling from the molten state. Based on the chemical composition of 72 and 73 wt.% PPBI for **P3HT-*b*-PPBI 1** and **2** respectively, a cylindrical morphology would be expected (hexagonally ordered P3HT cylinders in PPBI matrices) according to the classical phase diagram of coil-coil BCPs assuming that P3HT and the PPBIs have a similar density. **Fig. 6** shows the small angle X-ray scattering data together with an empirical model function consisting of a power law background and three Gaussians with a common FWHM to describe the peaks up to the third order. Even though the higher order peaks are too close to be well separated the peak positions fit to a ratio of $1:\sqrt{3}:2$ consistent with the expected lattice of hexagonal cylinders. From the position of the first order reflections the distance between the (100)-planes can be calculated to be 28 nm and 31 nm (i.e. a cylinder-to-cylinder

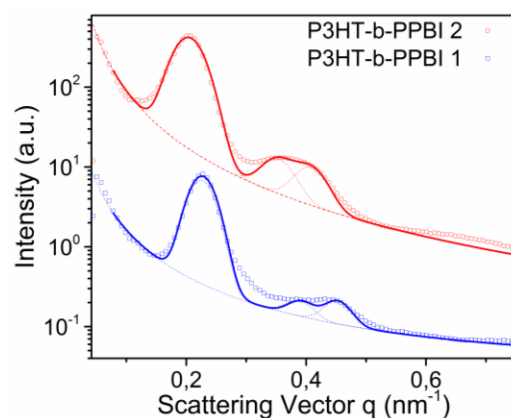


Fig. 6 Small angle X-ray scattering intensity versus scattering vector q of **P3HT-*b*-PPBI 1** (blue) and **P3HT-*b*-PPBI 2** (red) at $20 \text{ }^\circ\text{C}$ with a model function consisting of a power law background intensity and three Gaussians to describe the peaks. Curves of **P3HT-*b*-PPBI 2** are shifted by a factor of 10 for clarity.

distance of 32.5 nm and 36 nm) for **P3HT-*b*-PPBI 1** and **2** respectively. The FWHM of the SAXS peaks is a factor of 1.9 and 2.3 above the resolution limit of the instrument for **P3HT-*b*-PPBI 1** and **2** respectively, indicating that the long range order is limited within the samples. While usually the peak width is given by the resolution of the instrument for a microphase separated sample, the existence of higher order SAXS signals are a clear indication for an ordered microphase separated structure.

The cylindrical BCP morphology is further supported by TEM and AFM measurements as shown in **Fig. 7**. In the TEM images of both BCPs an arrangement of cylinders can be observed. The samples are stained with RuO₄, which is known to selectively stain P3HT.²⁸ In agreement with the chemical composition with P3HT as minority component of the BCP, the P3HT-cylinders appear in dark in the bright matrix of PPBI. While in the TEM images most of the cylinders are cross-cut (except of a few lying cylinders in **P3HT-*b*-PPBI 1**) the AFM images of both materials show the common orientation of flat lying cylinders caused by interaction with the surface.³³

In agreement with the temperature dependent X-ray experiments, the DSC measurements also show melting and crystallization in both BCPs (**Fig. 8**). One melting and one crystallization peak can be observed within the DSC traces of each sample. The

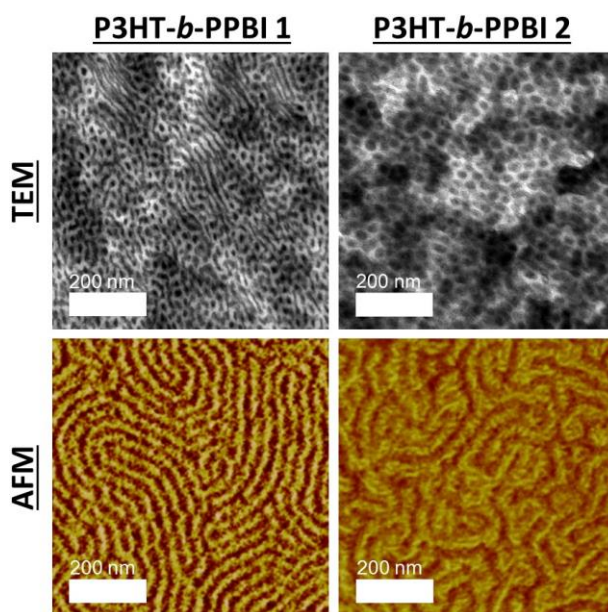


Fig. 7 TEM (Top) and AFM phase image (Bottom) of **P3HT-*b*-PPBI 1** (left) and **P3HT-*b*-PPBI 2** (right) after cooling from the molten state. For TEM the samples were annealed subsequently for 50h in chloroform vapor at 40 C and stained with RuO₄

peak temperatures of melting/crystallization are 228 °C/146 °C and 222 °C/140 °C for **P3HT-*b*-PPBI 1** and **2** respectively. Taking differences in the thermal program between the X-ray and the DSC measurements into account (stepwise vs. direct cooling), the crystallization temperatures are in good agreement with the crystallization of P3HT as observed in the temperature dependent X-ray measurements. It is unclear why no separate crystallization/melting of the PPBI-block can be observed in the DSC traces of **P3HT-*b*-PPBI 1**. Possible explanations are that either the transition enthalpy of the liquid-crystalline ordering is too weak to be detected, or that within the thermal program of the DSC the PPBI block crystallizes together with the P3HT.

The difference of around 80 °C between the melting and crystallization peak also shows that a considerable amount of undercooling is necessary in order to induce crystallization in the BCPs, which is in agreement to previous similar examples.^{24,25,26} Additionally, to the melting and crystallization peaks, both BCPs show a significant amount of cold crystallization between 60 °C and 170 °C, most likely due to the significant undercooling needed to induce crystallization. According to Lang *et al.*, the glass transitions temperatures of the PPBI-blocks are with 166 °C and 142 °C (applicable for **P3HT-*b*-PPBI 1** and **P3HT-*b*-PPBI 2**) respectively in the temperature window of cold crystallization.²⁹ Since both phenomena are superimposing each other, the glass transition of the acceptor block is not visible in the DSC measurements of the BCPs.

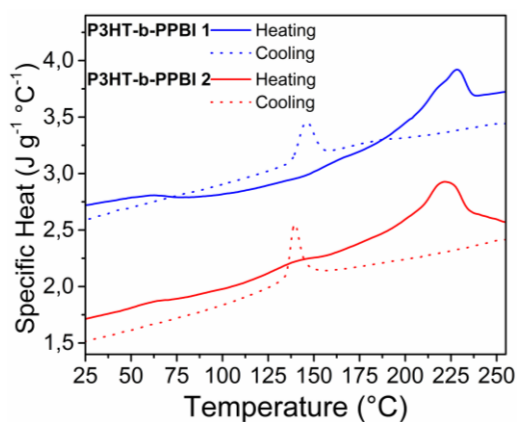


Fig. 8 DSC traces of **P3HT-*b*-PPBI 1** and **2** measured with a heating/cooling rate of 10 K min⁻¹. Curves of **P3HT-*b*-PPBI 1** are shifted by 1 J g⁻¹ °C⁻¹ for clarity.

Conclusion

We synthesized two donor-acceptor BCPs **P3HT-*b*-PPBI 1** and **2**, the corresponding side chain perylene bisimide homopolymers (**PPBI 1** and **2**) and PBI model compounds by a modular approach. We could show that the side chain grafting with different perylene bisimides is quantitative for the homopolymers as well as the diblock copolymers. The critical step is therefore, the end functionalization of P3HT and the sequential polymerization of the second block. We could show that about 80 % of the P3HT started a second block and we found a convenient way to separate the homopolymers from the **P3HT-*b*-PPBI 1** and **2**. We explored the interplay between microphase separation and molecular dynamics in two donor-acceptor BCPs consisting of P3HT-*b*-PPBI and confirmed the expectation that the decrease of the glass transition temperature as compared with a previously examined sample containing PCBM in the acceptor block facilitates the formation of a well-defined microphase separated structure. Inside the existing block copolymer nanostructure confined crystallization without alteration of the cylindrical morphology occurred. The morphology of the individual blocks was found to be the same as in the corresponding homopolymers. The results demonstrate that for efficient material design of phase separated donor-acceptor BCPs, a number of different criteria have to be considered ranging from the optoelectronic function and thermodynamics of self-assembly up to the molecular mobility.

Associated Content

Supporting Information: Experimental details, additional MALDI-ToF MS spectra, ¹H-NMR spectra and SEC curves.

Acknowledgements

The authors acknowledge financial support from the Bavarian State Ministry of Education, Science and the Arts under the research network "Solar technologies go hybrid" (SolTech). We thank Martin Hufnagel and Hubertus Burchhardt for the measurement of the MALDI-ToF MS spectra and Carmen Kunert for the TEM measurements.

References and Notes

- 1 M. Sommer, A. S. Lang and M. Thelakkat, *Angew. Chem. Int. Ed.*, 2008, **47**, 7901,
- 2 A. S. Lang, A. Neubig, M. Sommer and M. Thelakkat, *Macromolecules*, 2010, **43**, 7001.
- 3 R. H. Lohwasser, G. Gupta, P. Kohn, M. Sommer, A. S. Lang, T. Thurn-Albrecht and M. Thelakkat, *Macromolecules*, 2013, **46**, 4403.
- 4 E. E. Sheina, J. Liu, M. C. Iovu, D. W. Laird and R. D. McCullough, *Macromolecules*, 2004, **37**, 3526.
- 5 M. C. Iovu, E. E. Sheina, R. R. Gil and R. D. McCullough, *Macromolecules*, 2005, **38**, 8649.
- 6 A. Yokoyama, R. Miyakoshi and T. Yokozawa, *Macromolecules*, 2004, **37**, 1169.
- 7 R. Miyakoshi, A. Yokoyama and T. Yokozawa, *J. Am. Chem. Soc.*, 2005, **127**, 17542.
- 8 R. H. Lohwasser and M. Thelakkat, *Macromolecules*, 2011, **44**, 3388.
- 9 M. Jeffries-El, G. Sauvé and R. D. McCullough, *Macromolecules*, 2005, **38**, 10346.
- 10 R. Zhang, B. Li, M. C. Iovu, M. Jeffries-El, G. Sauvé, J. Cooper, S. Jia, S. Tristram-Nagle, D. M. Smilgies, D. N. Lambeth, R. D. McCullough and T. Kowalewski, *J. Am. Chem. Soc.*, 2006, **128**, 3480.

- 11 C. R. Singh, G. Gupta, R. H. Lohwasser, S. Engmann, J. Balko, M. Thelakkat, T. Thurn-Albrecht and H. Hoppe, *J. Polym. Sci.: Part B: Polym. Phys.*, 2013, **51**, 943.
- 12 S. M. Lindner and M. Thelakkat, *Macromolecules*, 2004, **37**, 8832.
- 13 M. Sommer, S. Huettner and M. Thelakkat, *J. Mater. Chem.*, 2010, **20**, 10788.
- 14 F. S. Bates and G. H. Fredrickson, *Annu. Rev. Phys. Chem.*, 1990, **41**, 525.
- 15 W.-N. He and J.-T. Xu, *Prog. Polym. Sci.*, 2012, **37**, 1350.
- 16 C. Dai, W. Yen, Y. Lee, C. Ho and W. Su, *J. Am. Chem. Soc.*, 2007, **129**, 11036.
- 17 B. W. Boudouris, C. D. Frisbie and M. A. Hillmyer, *Macromolecules*, 2008, **41**, 67.
- 18 T. Higashihara and M. Ueda, *Macromolecules*, 2009, **42**, 8794.
- 19 V. Ho, B. W. Boudouris, B. L. McCulloch, C. G. Shuttle, M. Burkhardt, M. L. Chabiny, and R. A. Segalman, *J. Am. Chem. Soc.*, 2011, **133**, 9270.
- 20 J. Park, K. S. Lee, C. Choi, J. Kwak, H. C. Moon and J. K. Kim, *Macromolecules*, 2016, **49**, 3647.
- 21 R. Verduzco, I. Botiz, D. L. Pickel, S. L. Kilbey, K. Hong, E. Dimasi and S. B. Darling, *Macromolecules*, 2011, **44**, 530.
- 22 M. Sommer, H. Komber, S. Huettner, R. Mulherin, P. Kohn, N. C. Greenham and W. T. S. Huck, *Macromolecules*, 2012, **45**, 4142.
- 23 C. Guo, Y.-H. Lin, M. D. Witman, K. A. Smith, C. Wang, A. Hexemer, J. Strzalka, E. D. Gomez and R. Verduzco, *Nano Lett.*, 2013, **13**, 2957.
- 24 M. Hufnagel, M. Fischer, T. Thurn-Albrecht and M. Thelakkat, *Polym. Chem.*, 2015, **6**, 813.
- 25 R. J. Ono, A. D. Todd, Z. Hu, D. A. Vanden Bout and C. W. Bielawski, *Macromol. Rapid. Commun.*, 2014, **35**, 204.
- 26 M. Hufnagel, M. Fischer, T. Thurn-Albrecht and M. Thelakkat, *Macromolecules*, 2016, **49**, 1637.
- 27 H. C. Kolb, M. G. Finn and K. B. Sharpless, *Angew. Chem., Int. Ed.*, 2001, **40**, 2004.
- 28 Y. Tao, B. McCulloch, S. Kim and R. A. Segalman, *Soft Matter*, 2009, **5**, 4219.
- 29 A. S. Lang and M. Thelakkat, *Polym. Chem.*, 2011, **2**, 2213.
- 30 A. S. Lang, M.-A. Muth, C. D. Heinrich, M. Crassco-Orozco and M. Thelakkat, *J. Polym. Sci., Part B: Polym. Phys.*, 2013, **51**, 1480.
- 31 T. J. Prosa, M. J. Winokur, J. Moulton, P. Smith and A. J. Heeger, *Macromolecules*, 1992, **25**, 4364.
- 32 F. P. V. Koch, J. Rivnay, S. Foster, C. Müller, J. M. Downing, E. Buchaca-Domingo, P. Westacott, L. Yu, M. Yuan, M. Baklar, Z. Fei, C. Luscombe, M. A. McLachlan, M. Heeney, G. Rumbles, C. Silva, A. Salleo, J. Nelson, P. Smith and N. Stingelin, *Prog. Polym. Sci.*, 2013, **38**, 1978.
- 33 S. H. Kim, M. J. Misner and T. P. Russell, *Adv. Mater.*, 2008, **20**, 4851.

Supporting Information

Materials

EthynylMgCl (0.6 M in THF/Toluene) and t-BuMgCl (1.7 M in THF) were purchased from Acros and titrated according to Krasovskiy and Knochel.¹ Azobisisobutyronitrile (AIBN, > 98%), CuBr (> 98 %), CuI (> 98 %), N,N,N',N'',N''-pentamethyldiethylenetriamine (PMDETA, 99 %), tetrabutylammonium fluoride trihydrate (TBAF, > 98 %), 4-isopropylphenol (98%) and 18-crown-6 (> 99 %) were purchased from Fluka. *N,N*-Diisopropyl-ethylamine (DIPEA, > 99 %) and propargylbromide (80 % in toluene) were purchased from Sigma-Aldrich. [1,3-Bis(diphenylphosphino)propane]-dichloronickel(II) (Ni(dppp)Cl₂),² N-(1,3-Bis(2-(2-(2-methoxy)ethoxy)ethoxy)propyl),N'-(hexyl-6'-azido)perylene-3,4,9,10-tetracarboxylic acid bisimide (**PBI-N₃ 2**),⁶ 2,5-dibromo-3-hex-ylthiophene,^{3,4} 2-dodecylsulfanylthiocarbonylsulfanyl-2-methylpropionicacid-3-azido-propylester,⁵ N-(1-heptyloctyl),N'-(octyl-8'-azido)-perylene-3,4,9,10-tetracarboxylic acid bisimide (**PBI-N₃ 1**),⁶ 4-(3'-trimethylsilylpropargyloxy)-styrene,^{6,7} *N-t*-butyl-*O*-[1-[4-(chloro-methyl)-phenyl]ethyl]-*N*-(2-methyl-1-phenylpropyl)hydroxylamine⁸ and 2,2,5-trimethyl-4-phen-yl-3-azahexane-3-nitroxide⁸ were synthesized according to published procedures. AIBN was recrystallized from ethanol and DIPEA and PMDETA were distilled prior to use. All other reagents were used without further purification. A CuBr/PMDETA stock solution was prepared for all CuAAC reactions. For this a dry Schlenk flask was charged with CuBr (50 mg, 0.035 mmol) and 5 mL 1,2,4-trichlorobenzene and the solution was degassed with N₂ for 20 min and degassed PMDETA (180 mg, 1.05 mmol) was added.

Methods

¹H-NMR (300 MHz) spectra were recorded on a Bruker AC 300 spectrometer and calibrated to the solvent peak (CDCl₃ δ = 7.26 ppm). Fourier transform infrared (FTIR) spectra were recorded on a Perkin Elmer Spectrum 100 FTIR spectrometer in attenuated total reflection (ATR) mode. Size exclusion chromatography (SEC)

measurements were carried out in THF with two Varian MIXED-C columns (300 x 7.5 mm) at room temperature and at a flow rate of 0.5 mL min⁻¹ using a UV (Waters model 468) detector with 254 nm wavelength. The SEC was calibrated with polystyrene as external standard and 1,2-dichlorobenzene as internal standard. MALDI-TOF mass spectra were recorded in linear positive mode on a Bruker Reflex III with dithranol or indol-3-acetic acid as matrix. Differential scanning calorimetry measurements were prepared on a Mettler Toledo DSC 2, calibrated with indium and zinc at a heating rate of 10 Kmin⁻¹ under continuous nitrogen flow. Thermogravimetric measurements were performed on a Mettler Toledo TGA/SDTA 851 at heating rates of 10 K min⁻¹ under nitrogen. X-ray scattering experiments were performed in transmission using a SAXSLAB laboratory setup (Retro-F) equipped an AXO microfocus X-ray source with an AXO multilayer X-ray optic (ASTIX) as monochromator for Cu K_α radiation ($\lambda = 0.154$ nm). A DECTRIS PILTUS3 R 300K detector was used to record the 2D scattering patterns. As sample holders two millimeter thick aluminum discs with a central hole were used. The measurements were performed in vacuum at and fitted together from three sample to detector distances to cover a wider q -range ($q = 0.05$ -1 nm⁻¹; $q = 0.65$ -5.2 nm⁻¹ and $q = 4.3$ -29 nm⁻¹). For temperature control, a LINKAM hotstage was used with a common heating/cooling rate of 10 K min⁻¹. Atomic force microscopy (AFM) images were recorded in intermittent contact mode on a Dimension 3100 Nanoscope V a hybrid closed loop XYZ tip scanner (5120 x 5120 pixels). The measured films were prepared by spin casting at 2000 rpm on silicon substrates from a 1 wt% chloroform solution (14.8 mg mL⁻¹), heated to 270 °C and cooled rapidly to room temperature. For transmission electron microscopy (TEM) the **P3HT-*b*-PPBI 1** sample was annealed in chloroform vapor for 50 h at 40 °C and the **P3HT-*b*-PPBI 2** sample was annealed at 260 °C for 15 min and cooled down to room temperature at 1 °C min⁻¹. Both samples were cut with an ultramicrotome and stained with RuO₄ for 10 min. The samples were measured at a Zeiss 9220 mega TEM.

Synthesis

Diblock copolymers

Alkyne Functionalized P3HT (P3HT-Alkyne): P3HT-Alkyne was synthesized according to a reported procedure.⁹ A 0.5 M LiCl solution was prepared by weighing 1.06 g LiCl into a Schlenk flask and subsequently drying for 4 h *in vacuo* at 140 °C. 50 mL anhydrous THF was added and the solution was stirred overnight to assure a complete dissolution of the LiCl. A dry Schlenk flask was charged with 6.15 g (18.86 mmol) 2,5-dibromo-3-hexyl-thiophene under N₂ atmosphere. 37.8 mL of the 0.5 M LiCl solution in THF were added. 14.8 mL (18.10 mmol) of a 1.25 M solution of t-BuMgCl in THF were added and the reaction mixture was stirred for 24 h to ensure the complete formation of the active Grignard species. The solution was diluted with 136 mL THF and the polymerization was started by adding 98.8 mg (118.60 μmol) Ni(dppp)Cl₂ suspended in 2 mL THF. The polymerization was terminated by adding 8 mL (3.77 mmol) of a 0.5 M solution of EthynylMgCl in THF/Toluene after 33 min. The solution was stirred for further 15 min and the polymer was subsequently precipitated in methanol. The polymer was dried and redissolved in CHCl₃. The solution was filtered over a short aluminum oxide column to remove residual LiCl and Ni(dppp)Cl₂, evaporated with the rotary evaporator to get a concentrated solution, and precipitated again in methanol. $m = 2.18$ g, $M_{n,SEC} = 18300$ g mol⁻¹, PDI = 1.19. ¹H NMR (300 MHz, CHCl₃): δ (ppm) 6.98 (s, 1H), 3.52 (s, 1H), 2.81 (t, 2H, J = 7.7 Hz), 1.80-1.60 (m, 2H), 1.50-1.25 (m, 6H), 0.98-0.83 (m, 3H); IR (ATR): ν(cm⁻¹) 3310 (C≡C-H₂), 2095 (C≡C)

P3HT-Macro RAFT-agent (P3HT-RAFT): A dry flask was charged with 1.6 g (133.0 μmol) **P3HT-Alkyne** and 596.4 mg (1.33 mmol) 2-Dodecylsulfanylthiocarbonylsulfanyl-2-methylpropionicacid-3-azido-propylester. The reagents were dissolved in 400 mL THF and the solution was degassed with N₂ for 20 min. 8 mL (47.04 mmol) DIPEA and 190.6 mg (1.33 mmol) equivalents CuI were added. The mixture was stirred at 40 °C for 6 days. The solution was filtered over a short aluminum oxide column to remove the catalyst and dried *in vacuo*. The polymer was precipitated

from concentrated chloroform solutions in methanol (twice) and hexanes. $m = 1.40$ g, $M_{n,SEC} = 18400$ g mol⁻¹, PDI = 1.18. ¹H NMR (300 MHz, CHCl₃): δ (ppm) 6.98 (s, 1H), 2.81 (t, 2H, $J = 7.7$ Hz), 1.80-1.60 (m, 2H), 1.50-1.25 (m, 6H), 0.98-0.83 (m, 3H); IR (ATR): ν (cm⁻¹) 1738 (C=O).

P3HT-*b*-poly(4-(3'-trimethylsilylpropargyloxystyrene) (P3HT-*b*-PTMSPOS):

A dry Schlenk flask was charged with 675 mg (56.23 μ mol) **P3HT-RAFT** agent, 5.18 g (22.5 mmol) (3'-trimethylsilylpropargyloxy)-styrene and 3.69 mg (22.5 μ mol) AIBN. The reagents were dissolved in 23 mL 1,2,4-Trichlorobenzene and the solution was degassed with N₂ for 20 min. The polymerization was started by immersing the Schlenk flask into an 80 °C warm oil bath. The conversion was controlled *via* NMR. After the projected conversion was achieved the polymerization was terminated by immersing the flask into liquid nitrogen. The resulting polymers were precipitated in methanol, redissolved in the smallest possible amount of chloroform and precipitated in hexane. $m = 950$ mg, $M_{n,SEC} = 22200$ g mol⁻¹, PDI = 1.37, Conversion = 6.7 %. ¹H NMR (300 MHz, CHCl₃): δ (ppm) 6.98 (s, 1H), 6.8-6.15 (br, 4H), 4.70-4.50 (br, 2H), 2.81 (t, 2H, $J = 7.7$ Hz), 1.78-1.60 (m, 2H), 1.50-1.20 (m, 9H), 0.97-0.83 (m, 3H), 0.18 (s, 9H); IR(ATR): ν (cm⁻¹) 2180 (C \equiv C), 1731 (C=O).

Synthesis of P3HT-*b*-poly(4-propargyloxystyrene) (P3HT-*b*-PPOS): 1.36 g **P3HT-*b*-TMSPPOS** was dissolved in 175 mL THF and the solution was degassed with N₂ for 20 min. 245 mg acetic acid and 12.9 mL of a degassed 0.5 M TBAF solution in THF was added with a syringe. The solution was stirred at room temperature for 48 h. The polymer was precipitated in methanol. $m = 822$ mg, $M_{n,SEC} = 21900$ g mol⁻¹, PDI = 1.42. ¹H NMR (300 MHz, CHCl₃): δ (ppm) 6.98 (s, 1H), 6.8-6.15 (br, 4H), 4.72-4.52 (br, 2H), 2.80 (t, 2H, $J = 7.7$ Hz), 2.58- 2.45 (br, 1H), 1.80-1.60 (m, 2H), 1.50-1.20 (m, 9H), 0.99-0.79 (m, 3H); IR (ATR): ν (cm⁻¹) 2180 (C \equiv C), 1731 (C=O).

P3HT-*b*-PPBI 1: A dry Schlenk flask was charged with 200 mg **P3HT-*b*-PPOS** and 257 mg (343 μmol , 1.1 eq.) **PBI-N₃ 1**. The reagents were dissolved in 60 mL 1,2-dichlorobenzene and the solution was degassed for 20 min with N₂. 15 drops of the CuBr/PMDETA stock solution were added and the mixture was stirred at rt for 72 h. The polymer was filtered over aluminum oxide, precipitated in ethyl acetate and dried. The polymer was purified by column chromatography (toluene, ethylacetate, CHCl₃, CHCl₃: methanol 98:2) and subsequently precipitated in methanol from a concentrated CHCl₃ solution. $m = 372$ mg, $M_{n,SEC} = 69500$ g mol⁻¹, PDI = 1.25. ¹H NMR (300 MHz, CHCl₃): δ (ppm) 8.54-7.41 (br, 9H), 6.98 (s, 1H), 6.91-6.21 (br, 4H), 5.37-4.82 (br, 3H), 4.51-4.24 (br, 2H), 4.15-3.82 (br, 2H), 2.80 (t, 2H, $J = 7.7$ Hz), 2.35-1.07 (m, 47H), 0.99-0.75 (m, 9H); IR (ATR): $\nu(\text{cm}^{-1})$ 3058, 2953, 2923, 2854, 2166, 1695, 1654, 1594, 1579, 1508, 1456, 1437, 1404, 1377, 1340, 1244, 1215, 1174, 1125, 1109, 1087, 1047, 1008, 962, 851, 825, 810, 795, 746, 722.

P3HT-*b*-PPBI 2: A dry Schlenk flask was charged with 150 mg **P3HT-*b*-PPOS** and 211 mg (257 μmol , 1.1 eq.) **PBI-N₃ 2**. The reagents were dissolved in 22.5 mL 1,3,5-trichlorobenzene and the solution was degassed for 20 min with N₂. 8 drops of the CuBr/PMDETA stock solution were added and the mixture was stirred at rt for 72 h. The polymer was filtered over aluminum oxide, precipitated in ethyl acetate and dried. The polymer was purified by column chromatography (toluene, ethylacetate, CHCl₃, CHCl₃: methanol 98:2) and subsequently precipitated in methanol from a concentrated CHCl₃ solution. $m = 254$ mg, $M_{n,SEC} = 77700$ g mol⁻¹, PDI = 1.23. ¹H NMR (300 MHz, CHCl₃): δ (ppm) 8.30-7.32 (br, 9H), 6.98 (s, 1H), 7.00-6.31 (br, 4H), 5.74-5.46 (br, 1H), 5.33-4.96 (br, 2H), 4.56-4.31 (br, 2H), 4.31-3.86 (br, 6H), 3.86-3.38 (m, 16H), 3.38-3.19 (br, 6H), 2.80 (t, 2H, $J = 7.7$ Hz), 2.16-1.06 (m, 19H), 0.99-0.77 (m, 3H); IR (ATR): $\nu(\text{cm}^{-1})$ 3056, 2953, 2923, 2856, 2167, 2051, 1694, 1654, 1593, 1578, 1508, 1437, 1404, 1341, 1302, 1245, 1200, 1178, 1100, 1049, 851, 825, 810, 793, 745.

Homopolymers

Synthesis of PTMSPOS: 4-(3'-trimethylsilylpropargyloxy)styrene (**TMSPoS**) (75 eq), *N*-*t*-butyl-*O*-[1-[4-(chloromethyl)-phen-yl]ethyl]-*N*-(2-methyl-1-phenylpropyl)-hydroxylamine (1 eq, Hawker-Initiator) and 2,2,5-trimeth-yl-4-phenyl-3-azahexane-3-nitroxide (0.1 eq, free nitroxide) were dissolved in 1.6 mL *o*-DCB per 1 g monomer and degassed by three freeze-pump-thaw cycles. The polymerization was started by the immersion of the reaction vessel in a 125 °C warm oil bath. The reaction was quenched by cooling in liquid nitrogen and precipitated into cold methanol twice from a concentrated THF solution. **PTMSPOS 1:** 654 mg, $M_{n,SEC} = 9100 \text{ g mol}^{-1}$, PDI = 1.32; $^1\text{H NMR}$ (300 MHz, CHCl_3): δ (ppm) 6.9–6.18 (br, 4H), 4.63 (s, 2H), 1.79–0.92 (br, 2H), 0.23 (s, 9H). **PTMSPOS 2:** 1.2 g, $M_{n,SEC} = 9300 \text{ g mol}^{-1}$, PDI = 1.11; $^1\text{H NMR}$ (300 MHz, CHCl_3): δ (ppm) 6.9–6.18 (br, 4H), 4.63 (s, 2H), 1.79–0.92 (br, 2H), 0.23 (s, 9H)

Synthesis of PPOS: **PTMSPOS 1/ PTMSPOS 2** was dissolved in THF, cooled to 0 °C and degassed by purging with nitrogen. 3 eq. of a degassed 0.5 M solution of tetrabutylammonium fluoride trihydrate in THF and 3 eq. of acetic acid were added via syringe. The mixture was stirred overnight and the polymer was precipitated in methanol twice from a concentrated THF solution. **PPOS 1:** 330 mg, $M_{n,SEC} = 7400 \text{ g mol}^{-1}$, PDI = 1.11; $^1\text{H NMR}$ (300 MHz, CHCl_3): δ (ppm) 6.9–6.18 (br, 4H), 4.63 (s, 2H), 2.52 (br, 1H), 1.79–0.92 (br, 2H); IR (ATR): $\nu(\text{cm}^{-1})$ 3286 ($\text{C}\equiv\text{C-H}$), 2120 ($\text{C}\equiv\text{C}$). **PPOS 2:** 500 mg, $M_{n,SEC} = 7500 \text{ g mol}^{-1}$, PDI = 1.21; $^1\text{H NMR}$ (300 MHz, CHCl_3): δ (ppm) 6.9–6.18 (br, 4H), 4.63 (s, 2H), 2.52 (br, 1H), 1.79–0.92 (br, 2H); IR (ATR): $\nu(\text{cm}^{-1})$ 3286 ($\text{C}\equiv\text{C-H}$), 2120 ($\text{C}\equiv\text{C}$).

PPBI 1: The synthesis of **PPBI 1** was published by Lang and Thelakkat.⁶ The polymer was synthesized according to the general method above and extracted with methyl ethyl ketone. 50 mg, $M_{n,SEC} = 59200 \text{ g mol}^{-1}$, PDI = 1.09; $^1\text{H NMR}$ (300 MHz, CHCl_3): δ (ppm) 8.45–7.40 (br, 9H), 7.00–6.10 (br, 4H), 5.35–4.86 (br, 3H), 4.50–4.24 (br, 2H), 4.18–3.80 (br, 2H), 2.40–1.00 (m, 39H), 0.83 (br, 6H).

PPBI 2: A dry Schlenk flask was charged with 49.8 mg **PPOS 2** and 287.7 mg (362 μmol , 1.5 eq.) **PBI-N₃ 2**. The reagents were dissolved in 20 mL 1,2-dichlorobenzene and the solution was degassed for 20 min with N_2 . 10 drops of the CuBr/PMDETA stock solution were added and the mixture was stirred at 40 °C for 5 days. The polymer was filtered over aluminum oxide, precipitated in methanol. The polymer was purified via extraction with a soxleth apparatus with methyl ethyl ketone. 254 mg, $M_{n,SEC} = 43500 \text{ g mol}^{-1}$, PDI = 1.14; $^1\text{H NMR}$ (300 MHz, CHCl_3): δ (ppm) 8.30–7.32 (br, 9H), 7.05–6.20 (br s, 4H), 5.72–5.40 (br, 1H), 5.30–4.95 (br, 2H), 4.54–4.25 (br, 2H), 4.25–4.10 (br, 2H), 4.10–3.85 (br, 4H), 3.85–3.40 (m, 16H), 3.30 (m, 6H) 2.39–1.40 (m, 11H).

Model Compounds

1-Isopropyl-4-propargyloxybenzene: 5.00 g (36.71 mmol) p-isopropylphenole and 50 mL acetone were added to a 250 mL Schlenk flask. 9.56g (73.42 mmol) KCO_3 and 1.94 g (7.34 mmol) 18-Crown-6 were added and the mixture was refluxed. 8.19 g (55.07 mmol) of a 80 wt% solution of propargylbromide in toluene was added and the mixture was stirred at 60 °C for 20 h. 200 mL water and 80 mL chloroform were added and the organic phase was separated. The aqueous phase was extracted 3 more times with 80 mL chloroform each. The combined organic phases were washed 3 times with water and subsequently dried over Na_2SO_4 and the solvent wash evaporated in *vacuo*. The crude product was purified by distillation in *vacuo*. Yield = 5.8 g (33.29 mmol, 91 %); $^1\text{H NMR}$ (300 MHz, CHCl_3): δ (ppm) 7.23–7.12 (m, 2H), 6.98–6.87 (m, 2H), 4.68 (d, $J = 2.4 \text{ Hz}$, 2H), 2.98 (dq, $J = 7.0 \text{ Hz}$, 1H), 2.53 (t, $J = 2.4 \text{ Hz}$, 1H), 1.25 (d, $J = 7.0 \text{ Hz}$, 6H).

PBI 1: A dry Schlenk flask was charged with 63.9 mg (398 μmol , 1.5 eq) 1-isopropyl-4-propargyloxybenzene and 200.0 mg (265 μmol) **PBI-N₃ 1** and 15 mL THF. The solution was degassed for 20 min with N₂ and 6 drops of the CuBr/PMDETA stock solution were added. The mixture was stirred at 40 °C for 24 h. The mixture was filtered over aluminum oxide and the product was precipitated in methanol. The product was freeze dried from benzene and dried in *vacuo* at 80 °C. The product was obtained as red solid. m =204 mg; ¹H NMR (300 MHz, CHCl₃): δ (ppm) 8.76–8.51 (m, 8H), 7.60 (s, 1H), 7.18–7.09 (m, 2H), 6.98–6.84 (m, 2H), 5.29–5.09 (s, 3H), 4.35 (t, J = 7.2 Hz, 2H), 4.19 (t, J = 7.5 Hz, 4H), 2.85 (dq, J = 7.0 Hz, 1H), 2.34–2.14 (m, 2H), 2.00–1.80 (m, 4H), 1.80–1.67 (m, 2H), 1.52–1.08 (m, 28H), 1.21 (d, J =7.0 Hz, 6H), 0.87–0.78 (m, 6H).

PBI 2: A dry Schlenk flask was charged with 95.0 mg (546 μmol , 2.9 eq) 1-isopropyl-4-propargyloxybenzene and 150.0 mg (189 μmol) **PBI-N₃ 2** and 20 mL THF. The solution was degassed for 20 min with N₂ and 6 drops of the CuBr/PMDETA stock solution were added. The mixture was stirred at 40 °C for 24 h. The mixture was filtered over aluminum oxide and the solvent was removed with the rotary evaporator. The excess 1-isopropyl-4-propargyloxybenzene was removed in *vacuo* at 80°C for 12 h. The product was obtained as dark red solid after freeze drying from benzene. m =137 mg; ¹H NMR (300 MHz, CHCl₃): δ (ppm) 8.63–8.36 (m, 8H), 7.63 (s, 1H), 7.23–7.12 (m, 2H), 6.98–6.87 (m, 2H), 5.78–5.63 (m, 1H), 5.18 (s, 2H), 4.43–4.33 (t, J = 7.2 Hz, 2H), 4.27–4.14 (m, 4H), 4.04–3.95 (m, 2H), 3.80–3.52 (m, 12H), 3.30–3.24 (m, 4H), 3.32–3.25 (s, 6H), 2.94–2.75 (dq, J = 7.0 Hz, 1H), 2.05–1.88 (m, 2H), 1.87–1.70 (m, 2H), 1.58–1.37 (m, 4H), 1.20 (d, J = 7.0 Hz, 6H).

Additional Figures

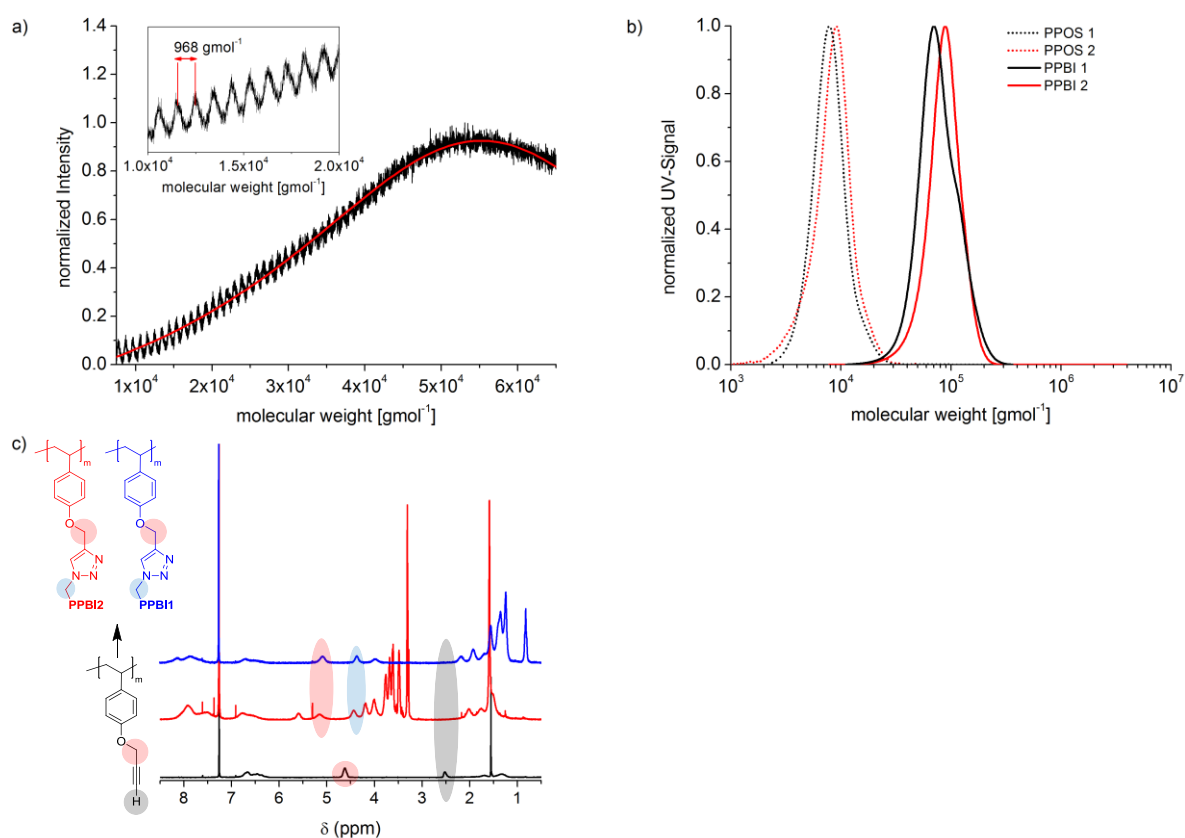


Fig. S 1. MALDI-ToF spectrum in linear positive mode with indol-3-acetic acid as matrix, of **PPBI 2**. The enlarged part in the inset shows the molecular mass of the repeating unit which is in very good agreement with the expected value (a) and SEC of the PPBI homopolymers **PPBI 1** and **2** and the corresponding precursor polymers **PPOS 1** and **2** (b). c) $^1\text{H-NMR}$ spectra of **PPOS 1**, **PPBI 1** and **PPBI 2**.

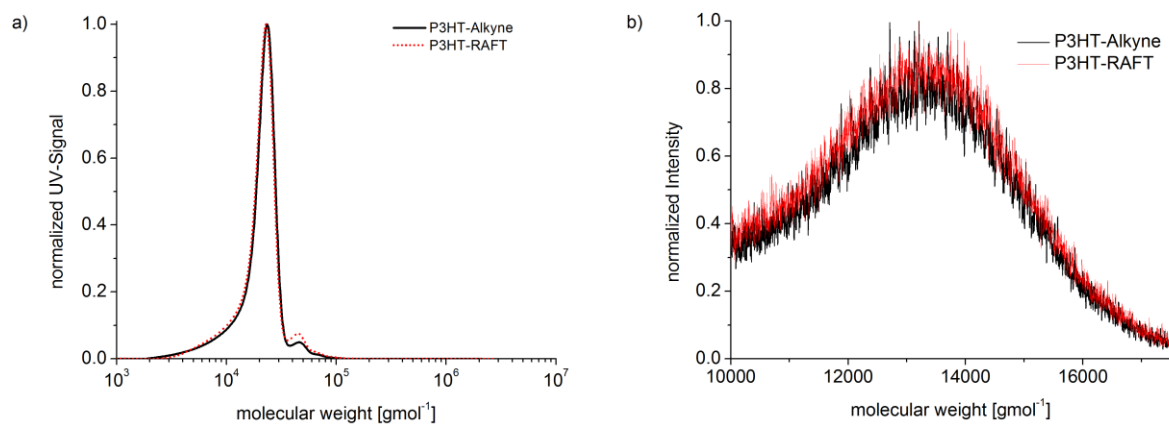


Fig. S 2 SEC traces (a) and MALDI-ToF Spectra in linear positive mode with dithranol as matrix (b) of **P3HT-Alkyne** and **P3HT-RAFT**.

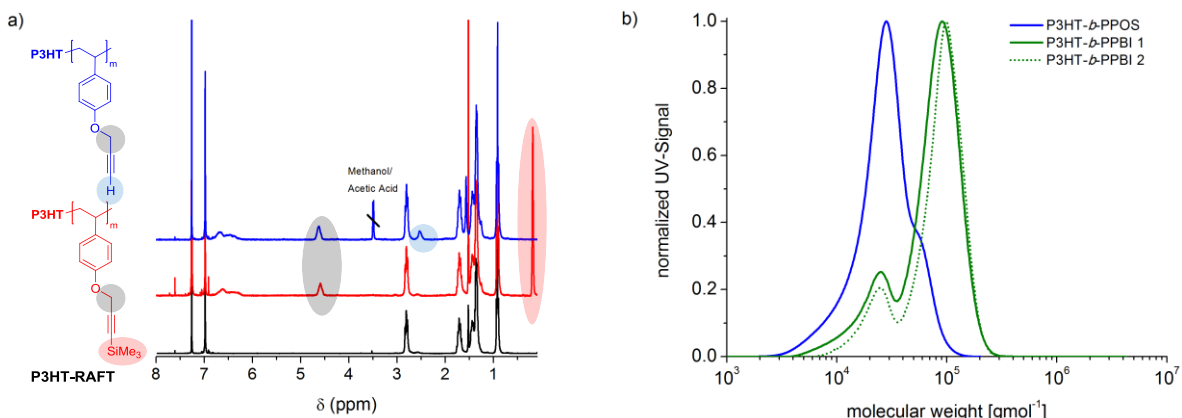


Fig. S 3 a) $^1\text{H-NMR}$ spectra of **P3HT-RAFT** and the BCPs **P3HT-*b*-PPTMSPOS** and **P3HT-*b*-PPOS**, b) SEC traces of the two unpurified donor-acceptor BCPs **P3HT-*b*-PPBI 1** and **2** after CuAAC click reaction of **P3HT-*b*-PPOS** with the **PBI-Azides 1** and **2**.

References

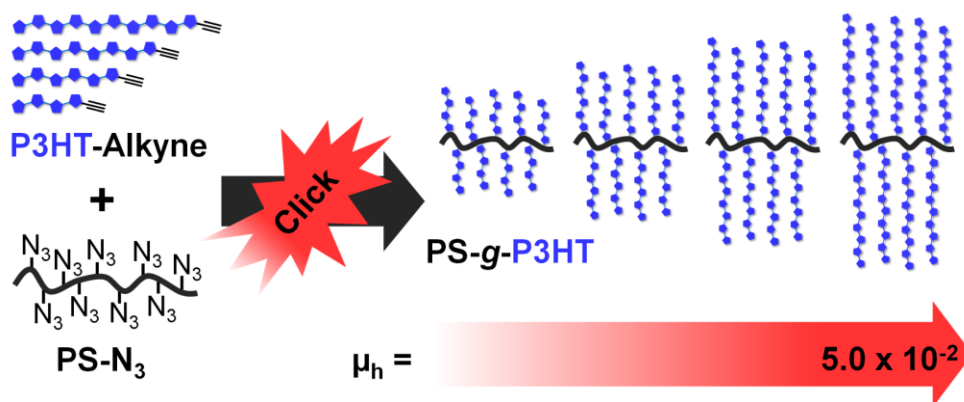
- 1 A. Krasovskiy and P. Knochel, *Synthesis*, 2006, **5**, 890.
- 2 G. R. Van Hecke and W. Horrocks, *Inorg. Chem.*, 1966, **5**, 1968.
- 3 M. C. Iovu, E. E. Sheina, R. R. Gil and R. D. McCullough, *Macromolecules*, 2005, **38**, 8649.
- 4 C. Van Pham, H. B. Mark Jr. and H. Zimmer, *Synthetic Communications*, 1986, **16**, 689.
- 5 S. R. Gondi, A. P. Vogt and B. S. Sumerlin, *Macromolecules*, 2007, **40**, 474.
- 6 A. S. Lang and M. Thelakkat, *Polym. Chem.*, 2011, **2**, 2213.
- 7 S. Fleischmann, H. Komber and B. Voit, *Macromolecules*, 2008, **41**, 5255.
- 8 D. Benoit, V. Chaplinski, R. Braslau and C. J. Hawker, *J. Am. Chem. Soc.*, 1999, **121**, 3904.
- 9 R. H. Lohwasser and M. Thelakkat, *Macromolecules*, 2012, **45**, 3070.

Poly-(3-hexylthiophene) Bottlebrush Copolymers with Tailored Side-Chain Lengths and High Charge Carrier Mobilities

C. David Heinrich, Mukundan Thelakkat*

Applied Functional Polymers, Macromolecular Chemistry I, University of Bayreuth,
Universitätsstr. 30, 95440 Bayreuth, Germany

*E-mail of corresponding author: mukundan.thelakkat@uni-bayreuth.de



Published in *Journal of Material Chemistry C*,
Reproduced with permission from *J. Mater. Chem. C*, 2016, **4**, 5370-5378.
Copyright 2016 The Royal Society of Chemistry

Abstract

A series of well-defined Poly(3-hexylthiophene) (P3HT) grafted bottlebrushes PS-*g*-P3HT with different P3HT chain lengths were synthesized by a grafting to approach using nitroxide mediated controlled radical polymerization. The influence of the side-chain length on the optical, thermal and electronic properties in these polymers are systematically studied and compared with the corresponding linear P3HTs. It can be shown that the optical, structural and electronic properties of the brushes depend heavily on the side chain lengths. The results of DSC, UV-Vis and AFM measurements reveal two important things. The brush polymers with low molecular weight P3HT side-chains do not crystallize and therefore exhibit very poor electronic properties. With an increase of the side-chain length, highly crystalline materials are obtained and a brush with a high molecular weight (144 kg/mol) carrying long P3HT side chains (17000 g mol⁻¹) is necessary to obtain crystalline lamellar structures and the best charge transport properties. For the first time P3HT brush polymers are reported that can match the excellent electronic properties of its linear counterparts in the range of 10⁻² cm² V⁻¹ s⁻¹. Additionally, the brush polymers exhibit better thin film stability at elevated temperatures compared to linear P3HTs.

Introduction

Bottlebrush polymers consist of polymeric backbones which are densely grafted with regularly spaced side-chains. A high grafting density forces the backbone into an extended chain through steric repulsion.^{1,2} Moreover, the densely packed side chains causes the polymer backbones to be stiffened and the persistence length of the brush chain increases with increasing side chain density. Therefore this architecture leads to unique material properties. Thus, bottlebrush polymers have far higher polymer chain mobilities than linear polymers with comparable molecular weights due the absence of chain entanglements.³ Therefore, bottlebrush polymers with conjugated, electronically

active poly(3-hexylthiophene) (P3HT), which can add up the benefits of the brush architecture and the good electronic properties of linear P3HT, should be interesting materials for organic electronics. Surprisingly, there are no reports on charge carrier mobilities in semiconductor polymer brushes.

In contrast to most other polymeric organic semiconductors, the synthesis of linear P3HT can be conducted in a highly controlled manner. The Kumada catalyst transfer polymerization which was independently reported by McCullough *et al.*^{4,5} and Yokozawa *et al.*^{6,7} allows the synthesis of polymers with defined molecular weight and controlled end groups.^{8,9} In addition, very high molecular weights can be easily achieved in bottlebrushes which may have advantages in terms of mechanical properties, especially in thin film applications. The correlation of molecular weight and mechanical properties is well-studied in linear semiconductor polymers, whereas very little is known in semiconductor bottlebrushes.¹⁰ Thus the brush architecture can improve the film stability even at high temperatures against delamination simply by the inherent increase in molecular weight in these systems. Another interesting and important property of chain orientation/alignment might also be positively influenced by this architecture. It was proposed that in organic photovoltaics (OPV), a nanoscale phase-separated donor-acceptor diblock copolymer could have ideal microstructures that could provide optimal pathways for charge collection.¹¹ Such a microphase separated system must be preferentially vertically aligned to the substrate; otherwise the structure would consist of effective charge blocking layers. As a first breakthrough the synthesis of micro phase separated fully conjugated polymers could be reported¹² but the alignment of such a system is not yet accomplished. However, thin films of diblock copolymer bottlebrushes were found to form vertical aligned micro structures without the need of difficult post processing and alignment procedures.¹³ Therefore, donor-acceptor brush block copolymers may be possible candidates to solve this issue. This motivated us to investigate in details opto-electronic properties concerning P3HT bottle brushes. At first, it is of course imperative to synthesize P3TH brushes in a well-controlled way and to study those alone in order to investigate what design rules are necessary to retain or improve the electronic properties in the donor component. There

are several examples of surface grafted P3HT brushes synthesized either by grafting-from^{14,15} or grafting-to^{16,17} processes but the synthesis of P3HT bottlebrushes was only reported a few times up to now. In 2013 Lin et al.¹⁸ reported the synthesis of PS-*g*-P3HT by grafting P3HT onto a polystyrene backbone by CuAAC click chemistry. P3HT bottlebrushes were also reported by a grafting-from¹⁹ and a grafting-through polymerization.^{20,21} For the grafting-through route *exo*-norbornenyl-functionalized P3HT macromonomers were polymerized by a controlled ring opening metathesis polymerization (ROMP). The molecular weights of these P3HT side-chains were relatively low, in the range of only 2,000 to 11,000 g mol⁻¹ (as measured by SEC). Moreover, up to now, no comparative study was conducted to understand the structure property relationship, which correlates the length of P3HT side chains and charge carrier mobility in these systems and compares them with those in linear polymers. Even though OFET devices with linear P3HT as semiconductor have already delivered charge carrier mobilities of up to 0.1 cm² V⁻¹ s⁻¹, no hole mobility data is available for P3HT brushes at all.²²⁻²⁶ We hypothesized that in order to obtain bottlebrush polymers containing P3HT, with properties that meet the requirements for applications in OFET or OPV devices, we would need a higher molecular weight of the P3HT side-chains than previously reported.

Several groups reported a correlation between the molecular weight of linear P3HT and the charge carrier mobility in OFET devices.²⁶⁻²⁸ Generally, the measured charge carrier mobilities increased by several orders of magnitude when the molecular weight P3HT was increased. Zhang et al. reported a distinct correlation between the molecular weight the nanostructure of P3HT and the charge carrier mobility in OFET devices.²⁹ A similar correlation was observed by Singh et al. in SCLC devices.³⁰ Both reports give indications for an optimum absolute molecular weight of P3HT, in terms of charge carrier mobility, between 10,000 and 15,000 g mol⁻¹. The electrical properties of P3HT are dependent on the polymer's ability to crystallize and the size of the crystalline nanofibrils. AFM and XRD measurements show that the long period of P3HT nanofibers increases as P3HT becomes longer. The long period and simultaneously the charge carrier mobility reach a plateau when the P3HT chains are so long that chain-folding occurs.³⁰ If a similar dependence of charge transport on molecular weight exists in the

case of bottlebrush polymers as well, then previously reported studies were ignoring this important point of having polymers with sufficient molecular weight of the side-chains. A previous study by Wong et al.,²¹ varied the side-chain length, but also changed the molecular weight of the backbone making an investigation regarding the influence of the length of P3HT side-chains for a given backbone length difficult.

The aim of our study was therefore to elucidate the influence of the chain lengths of P3HT in brush polymers on charge carrier mobility without varying the molecular weight of the backbone. This is highly required to understand the correlations of optical and electronic properties with the molecular weight in P3HT brushes. We demonstrate that brush polymers can have comparable optical and electronic properties and superior film stability as compared to linear P3HT, if higher molecular weight P3HT is grafted.

Experimental Section

Materials and Methods

All commercial reagents were, unless otherwise noted, used without further purification. The linear polymers **P3HT 1-4**,⁸ *N-t*-Butyl-*O*-[1-[4-(chloromethyl)-phenyl]ethyl]-*N*-(2-methyl-1-phenylpropyl)hydroxylamine,³¹ 2,2,5-Trimethyl-4-phenyl-3-aza-hexane-3-nitroxide³¹ were synthesized in our group according to a published procedure. The synthesis of other polymers reported is outlined in the ESI. ¹H-NMR (300 MHz) spectra were recorded on a Bruker AC 300 spectrometer and calibrated to the solvent peak (CDCl₃ δ = 7.26 ppm). Fourier transform infrared (FTIR) spectra were recorded on a Perkin Elmer Spectrum 100 FTIR spectrometer in attenuated total reflection (ATR) mode. Size exclusion chromatography (SEC) measurements were carried out in THF with two Varian MIXED-C columns (300 x 7.5 mm) at room temperature and at a flow rate of 0.5 mL min⁻¹ using a UV (Waters model 468) detector with 254 nm wavelength. The SEC was calibrated with polystyrene as external standard and 1,2-dichlorobenzene as internal standard. MALDI-TOF mass spectra were recorded on a Bruker Reflex III with dithranol as matrix. Differential scanning calorimetry measurements were prepared on a Mettler Toledo DSC 2, calibrated with indium and zinc at a heating rate of 10 Kmin⁻¹ under continuous nitrogen flow.

Absorption measurements were carried out on a JASCO V-670. Solutions containing CHCl₃/EtOAc mixtures were used at concentrations of 0.02 mg/mL⁻¹. Different solutions were prepared by adding CHCl₃ and EtOAc to a polymer stock solution in CHCl₃ with a concentration of 0.2 mg mL⁻¹. Polymer films for optical characterization were prepared by spin casting on ODS treated glass substrates (the substrates were prepared in an identical procedure as the OFET devices) from 6 mg mL⁻¹ chloroform solutions. Atomic force microscopy images were recorded in intermittent contact mode on a Dimension 3100 Nanoscope V with a Nanoscope V controller and a hybrid closed loop XYZ tip scanner (5120 x 5120 pixels).

Device Preparation and Characterization

Bottom gate / bottom contact organic field effect transistors (OFET Gen4) were purchased from Fraunhofer IPMS. N-doped silicon (doping at the surface $n \approx 3 \cdot 10^{17} \text{ cm}^{-3}$) was used as surface and gate electrode. The dielectric consists of a $230 \pm 10 \text{ nm}$ layer of silicon oxide. Each substrate consisted of 16 devices with a constant channel width of 10 mm and a varying channel length of $2.5\text{-}20 \text{ }\mu\text{m}$. The source and drain electrodes were 30 nm thick gold on a 10 nm ITO adhesion layer. The devices were prepared by cleaning in acetone and subsequently *iso*-propanol in an ultrasonic bath for 10 min , followed by a 15 min treatment in an ozone oven at 50°C and subsequent silanization by a 45 min treatment in a bath of $1 \text{ wt}\%$ octadecyltrichlorsilane (ODTS) in toluene at 60°C . The devices were rinsed with toluene and *iso*-propanol and dried. Thin polymer films were spin cast from 6 mg mL^{-1} chloroform solutions at a spinning speed of $4,000 \text{ rpm}$ under ambient conditions. All devices were stored and measured under nitrogen atmosphere. The IV-characteristics were measured using an Agilent B1500 Semiconductor Parameter Analyzer. The devices were annealed at 10 K above the melting temperature and slowly cooled down ($\sim 1 \text{ K min}^{-1}$) to room temperature. All annealing experiments were conducted under nitrogen atmosphere. Using Equation (1) the charge carrier mobilities were calculated from the slope of the $(I_d)^{0.5}\text{-}V_g$ plots.

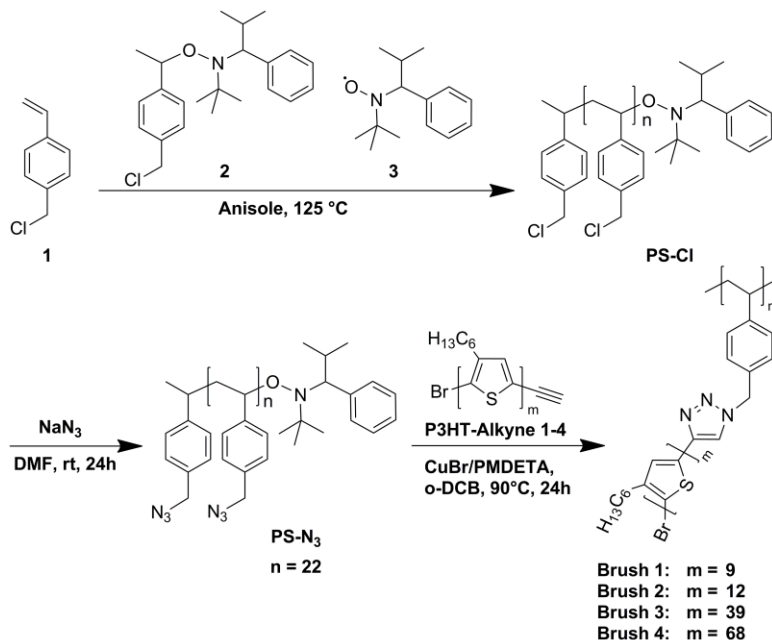
$$I_d \approx \frac{W}{2L} C_i \mu (V_g - V_T)^2 \quad (1)$$

Results and Discussion

Synthesis

Our study focuses on the influence of the length of the P3HT side-chains on optical and electronic properties while keeping the polystyrene backbone identical. This was done in order to see if a similar trend of the optical, thermal and electronic properties as for linear P3HTs could also be observed for brush polymers. Four conjugated bottlebrush polymers with different P3HT side-chain lengths and having an identical polystyrene backbone were synthesized in a procedure similar to the one published by Lin *et al.*¹⁸ We identified the grafting-to process as the ideal synthesis method to obtain highly comparable polymers as one backbone polymer can be used for the whole series of brush polymers.

As shown in **Scheme 1** the polymeric backbone of the brush is synthesized first. Poly-(4-chloromethylstyrene) (**PS-Cl**) is synthesized by nitroxide mediated radical polymerization (NMRP) utilizing a chlorine functionalized derivative of the well-known Hawker initiator.³¹ **PS-Cl** can be easily converted to poly-(4-azidomethylstyrene) **PS-N₃**



Scheme 1 Scheme of synthesis of Poly-4-chloromethylstyrene (**PS-Cl**) via NMP followed by the polymer analogous substitution of chlorine with sodium azide in order to obtain Poly-4-azidomethylstyrene (**PS-N₃**). The conjugated P3HT bottlebrush polymers, **Brush 1-4** were obtained by linking up **PS-N₃** and four alkyne terminated P3HT polymers (**P3HT-Alkyne 1-4**) with different chain lengths via CuAAC reaction.

upon substitution with sodium azide. The quantitative conversion can be observed in $^1\text{H-NMR}$ by the shift of the methyl protons adjacent to the chlorine in **PS-Cl** versus the azide group in **PS-N₃** (see **Fig. S1**, ESI). First **PS-N₃** with a molecular weight of $M_{n,SEC} = 3600$ g mol⁻¹ and low $\bar{D} = 1.20$ (**Table 1**) is obtained and is utilized as the precursor polymer for all click reactions to synthesize the bottlebrush polymers **PS-g-P3HT**. Additionally, four alkyne end functionalized P3HT polymers **P3HT-Alkyne 1-4** were synthesized according to an optimized procedure.³² Functionalization with the alkyne end groups was analytically proven by MALDI-ToF mass spectrometry (see **Fig. S2**, ESI) MALDI-ToF mass spectrometry is also the most reliable measurement to obtain the absolute molecular weights of P3HT. Molecular weights $M_{n,MALDI}$ between 1600 g mol⁻¹ for **P3HT-Alkyne 1** and 11400 g mol⁻¹ for **P3HT-Alkyne 4** were obtained. SEC on the other hand is a relative method and it was already reported that the SEC values, when calibrated against polystyrene, are always overestimated for P3HT.³³ **Table 1** gives a comparison of the M_n values obtained by SEC and MALDI-ToF for the alkyne functionalized polymers **P3HT-Alkyne 1-4** and a series of unfunctionalized P3HT polymers **P3HT 1-4** used in this study.

Table 1 Summary of the synthesized Polystyrene derivatives **PS-Cl** and **PS-N₃**, the four different alkyne-functionalized P3HT polymers **P3HT-Alkyne 1-4**, the resulting bottlebrush polymers **Brush 1-4** and the unfunctionalized linear polymers **P3HT 1-4**.

	$M_{n,SEC}^a$ (g mol ⁻¹)	\bar{D}	$M_{n,MALDI}$ (g mol ⁻¹)	μ_{max} (cm ² V ⁻¹ s ⁻¹)	I_{on}/I_{off} ratio	$T_{m,peak}^b$ (°C)	ΔH_m^b (J g ⁻¹)	$T_{c,peak}^b$ (°C)	T_g^b (°C)
PS-Cl	3200	1.21							77
PS-N₃	3600	1.21							35
P3HT-Alkyne 1	2000	1.57	1600						-15
P3HT-Alkyne 2	3800	1.36	2000						1
P3HT-Alkyne 3	9300	1.13	6650			210	18.8	176	
P3HT-Alkyne 4	17400	1.15	11400			225	19.3	189	
Brush 1	21000	1.21		1.88×10^{-6}	4.21×10^2				-5
Brush 2	36500	1.22		1.58×10^{-3}	2.69×10^3				3
Brush 3	97000	1.09		1.13×10^{-2}	3.37×10^5	205	15.3	165	
Brush 4	144000	1.37		4.95×10^{-2}	1.45×10^5	219	14.9	173	
P3HT 1^c	1400	1.18	1430	4.42×10^{-7}	3.31×10^2	22.3	18.7	-10	
P3HT 2^c	4100	1.16	2000	3.62×10^{-3}	5.28×10^4	156	7.2	137	
P3HT 3^c	10300	1.09	7100	4.69×10^{-2}	8.36×10^4	221/227	26.4	198	
P3HT 4^c	15900	1.11	11600	4.88×10^{-2}	4.75×10^5	229/238/247	22.3	203	

^a Measured in THF with a polystyrene calibration and o-dichlorobenzene as internal standard; ^b measured via DSC with a heating/cooling rate of 10 K min⁻¹; ^c linear P3HT reference polymers

The linear polymers **P3HT 1–4** without an active alkyne end group were later used for comparison with the brush polymers. They were synthesized according to a reported procedure in ref. 8 and are highly comparable to their functionalized counterparts **P3HT-Alkyne 1–4** as can be seen from their properties given in **Table 1**. The bottlebrushes PS-*g*-P3HT were obtained by a grafting-to process. For this, the alkyne end groups of **P3HT-Alkyne 1–4** reacted in a copper catalyzed reaction with the azide groups of **PS-N₃**. The copper catalyzed azide–alkyne reaction (CuAAC) is highly efficient, which is usually conducted at low temperature and is well known as the workhorse of “click-chemistry”.³⁴ It was nevertheless necessary to conduct the reaction at elevated temperatures of 90 °C to obtain high conversions. The success of grafting can easily be monitored by SEC. The SEC traces of **Brush 3**, as one typical example, and the corresponding precursor polymers are shown in **Fig. 1 a**. After the synthesis of the bottlebrush polymer the SEC trace is markedly shifted to high molecular weights. A rather narrow distribution is also an indicator of excellent conversion *i.e.* high grafting density. A tailing in the low molecular weight region would be otherwise expected if the reaction were incomplete. But this is not observed. A second peak from the P3HT precursor can be observed. This is the case for all synthesized brush polymers because P3HT-Alkyne is always added to the reaction in an excess of 1.1–1.5 equivalents (see **Fig. S3 a**, ESI). The raw products could be purified by preparative SEC in the case of **Brushes 1–3**. The solubility of **Brush 4** in THF was found to be too low for preparative SEC but most of the residual P3HT-Alkyne could be removed by washing the

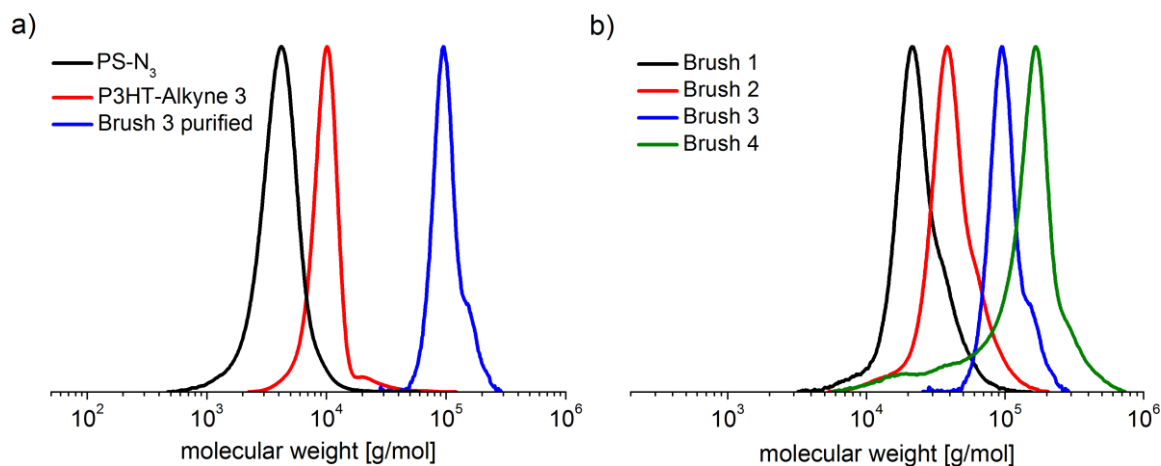


Fig. 1 a) Evolution of the SEC traces for **Brush 3** which is synthesized by the CuAAC of **PS-N₃** and **P3HT 3** as a typical example; the raw product is purified from the excess of the linear **P3HT 3** via preparative SEC; b) SEC traces of the four purified bottlebrush copolymers **Brush 1–4**.

polymer with THF, which predominantly dissolves the linear polymer. The SEC series of the series of purified bottlebrush polymers are shown in **Fig. 1 b. Brush 4** with an $M_{n,SEC}$ of 144000 g mol⁻¹ having side-chains of 11400 g mol⁻¹ in absolute terms (MALDI) is thus the conjugated P3HT bottlebrush polymer with the longest side-chain reported until now. In comparison Wong *et al.* reported bottlebrushes of P3HT synthesized by ROMP from a P3HT macromonomer with molecular weights of up to only $M_{n,SEC} = 11\,200$ g mol⁻¹, which may correspond to approximately 8000 g mol⁻¹ in absolute terms.²¹

The SEC measurements alone are not sufficient to make a statement about the grafting density in the final polymers. In the case of **Brushes 1 and 2**, ¹H-NMR spectroscopy can provide this missing information and make it possible to estimate the conversion. By examining the ¹H-NMR of **Brush 1** (see **Fig. S3 b**, ESI), we find that the peak of the methyl protons adjacent to the azide in **PS-N₃** is shifted from 4.4 ppm to 5.4 ppm due to the formation of triazole after the click reaction. Additionally, a new peak emerges at around 7.6 ppm. This peak can be assigned to the only proton of the triazole ring itself. The grafting density can be estimated by comparing the integrals at 4.4 ppm and 5.4 ppm. We estimate the grafting density of the polymers, **Brushes 1 and 2**, where this calculation is possible, to be 85% for **Brush 1** and 90% for **Brush 2**. Lin *et al.*¹⁸ claimed nearly quantitative grafting of different poly(4-azidomethylstyrene) backbones with a relatively short P3HT-Alkyne ($M_{n,SEC} = 4100$ g mol⁻¹) without being able to observe the peak at 5.4 ppm or at 7.6 ppm in ¹H-NMR. The assignment of the peak at 4.4 ppm to the proton at the triazole ring is questionable and is not in agreement with findings in low molecular weight model compounds with a similar chemical structure at the triazole ring.³⁵ The polystyrene backbone in the bigger brush polymers, **Brushes 3 and 4**, on the other hand is already so diluted in relation to P3HT that a quantitative statement about the grafting density is not possible.

Thermal Properties

The thermal properties were examined *via* DSC measurements. The linear reference polymers are all semicrystalline and the melting and crystallization temperatures increase considerably for higher molecular weights. The dependency of the melting temperature on the length of the backbone has been described theoretically for polyolefins^{36,37} and it was shown that P3HT follows the same trend.^{38,39} The small brush polymers on the other hand exhibit a different thermal behavior. The two brushes with very short P3HT chains (**Brushes 1** and **2**) do not crystallize at all. Both polymers are apparently amorphous and only glass transitions below room temperature are observed (T_g of -5 °C for **Brush 1** and 3 °C for **Brush 2** respectively; see also **Fig. S4 a** and **b**, ESI). We suggest that this is due to the influence of the polystyrene backbone, which in the case of the short brushes makes up for about 8 wt% of the overall brush polymer, and the very low T_m expected for low molecular weight P3HT.⁴⁰ The connection to the polystyrene backbone greatly reduces the mobility of the P3HT chains. An additional higher glass transition that could be assigned to the polystyrene backbone cannot be observed and it is unclear if the backbone in such a high dilution can vitrify separately. The difference in the glass transition temperatures of the precursor polymers **PS-Cl** (77 °C) and **PS-N₃** (35 °C) also shows that even a relatively small change of the substituents of the polystyrene has a pronounced effect on the thermal properties. A comparison of the P3HT precursors **P3HT-Alkyne 1** and **2** with linear **P3HT 1** and **2** can help understand the system more. Even the influence of the end groups in very

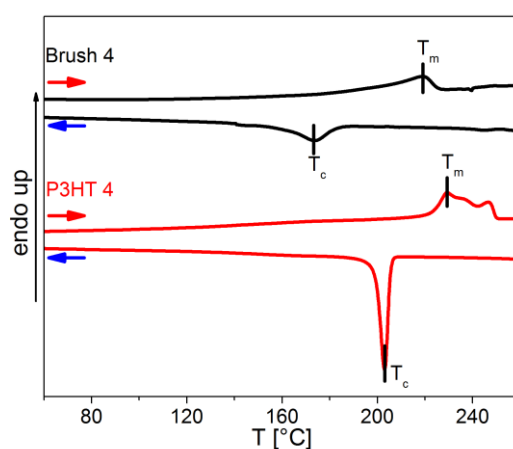


Fig. 2 DSC measurements of **Brush 4** and the linear equivalent P3HT 4 as example at a heating/cooling rate of 10 K min^{-1} .

short polymers can be very big. **P3HT-Alkyne 1** and **2** for instance are amorphous with a T_g of $-15\text{ }^\circ\text{C}$ and $-1\text{ }^\circ\text{C}$ whereas **P3HT 1** and **2** are crystalline. A different behavior can be observed for longer brush polymers, **Brushes 3** and **4**. In both cases, melting and crystallization of the P3HT side-chains can be clearly observed. In **Fig. 2 Brush 4** and the linear reference polymer **P3HT 4** are compared as an example. It can be clearly seen that the melting temperature T_m and the enthalpy ΔH_m as well as the kinetics of crystallization are different for the brushes. The T_c ($173\text{ }^\circ\text{C}$) of **Brush 4** is about 30 K lower than that for the linear counterpart **P3HT 4** ($203\text{ }^\circ\text{C}$) which is an indication for a kinetically hindered crystallization due to the reduced mobility of the polymer side-chains. Additionally, the enthalpy of phase transition ΔH_m is reduced from 22.3 J g^{-1} in **P3HT 4** to 14.9 J g^{-1} in **Brush 4**. This corresponds to a reduction of enthalpy by 40 % and therefore cannot be explained by the diluting effect of the backbone alone which only makes up 1.5 % of the overall mass of the bottlebrush. This means, that the steric hindrance which is induced through the change in the polymer architecture must be the cause for a reduced overall crystallinity. If the published $\Delta H_m^\infty = 33\text{ J g}^{-1}$ value for linear P3HT is taken into account, then **Brush 4** can be considered to be 45% crystalline.⁴¹ The behavior of **Brush 3** is comparable to **Brush 4**. The only difference is a lower T_c and T_m for both linear and brush polymers due to shorter side-chains. **Brush 3** also has a very similar degree of crystallinity of 46%.

Optical spectroscopy in solutions and films

Further information about the aggregation properties of the bottlebrush polymers can be extracted from UV-spectroscopy. UV-Vis spectra of either thin films or solutions of linear P3HT can easily be qualitatively analyzed for a possible aggregation of the polymer. According to Spano *et al.*⁴² P3HT forms weak H-aggregates in thin films or in bad solvents. The aggregates have a distinctly different absorption spectrum in comparison to non-aggregated P3HT coils giving rise to the possibility of deconvoluting the spectra and even estimating the fraction of aggregates.⁴³ The solution spectra of P3TH exhibit one broad peak which shows a bathochromic shift when the polymer mass increases, indicating that the conjugated system grows. This saturates at a certain molecular weight *i.e.* a further increase of the molecular weight of the polymer will not induce additional changes to the spectra. The saturation value can be observed at around 450 nm (**Fig. S5 a**, ESI). If aggregates are

present a bathochromic shift of nearly 100 nm occurs and three distinct peaks can be observed.

The solution behavior of the bottlebrush polymers was characterized first. The first question was if **Brushes 1 to 4** would form non-aggregated solutions or if the large molecular weight and the different architectures of brushes would lead to irreversible aggregates as it was observed in brushes with a polynorbornene backbone.²⁰ UV-Vis spectra of the chloroform solutions of all four brush polymers were measured (see **Fig. S5 a**, ESI). All four spectra resemble the spectra of coiled P3HT in solution and aggregation was not observed. The peak maximum shifts as expected with the increase of the P3HT side-chain length from **Brushes 1 to 4** from 432 nm to 454 nm.

We also investigated the influence of the solvent nature in a similar manner as reported for linear P3HT⁴⁴ by using mixtures of a good solvent (chloroform) and a bad solvent (ethyl acetate) without changing the overall polymer concentration. As an example the aggregation of **Brush 4** in solution is shown in **Fig. 3 a** for increasing amounts of non-solvent ethyl acetate. The P3HT side-chains in pure chloroform solution are in a non-aggregated state. Adding 15 vol% EtOAc already induces a big change. Here the spectrum is a superposition of a fraction of coiled P3HT and of the aggregated species. The spectra of the aggregates are characterized by the three peaks at 524 nm, 560 nm and 608 nm which can be identified as the 0-2, 0-1 and the 0-0 transition. According to Spano *et al.* the ratio of the absorbance of the 0-0 peak and the 0-1 peak can be used to determine the quality or the degree of aggregation. A high 0-0 to 0-1 ratio is an indicator of a higher order.⁴³ A qualitative examination of the spectra of **Brush 4** for increasing amounts of non-solvent shows that while the fraction of aggregates increases (as evidenced by the decrease of the peak from the coiled P3HT at 454 nm), the aggregates must be less ordered as the relative intensity of the 0-0 absorption decreases with respect to the 0-1 transition. The ratio of 0-0 to the 0-1 absorption decreases from $A_{0-0} : A_{0-1} = 0.78$ for 15 vol% of the nonsolvent ethyl acetate to $A_{0-0} : A_{0-1} = 0.59$ when the ethyl acetate amount is increased to 80 vol% (see **Fig. 3 a**). **Brush 3** also forms aggregates in solution and an increase of the fraction of aggregates can be observed with increasing content of the non-solvent ethyl acetate. We cannot observe a distinct change in the shape of the spectra in this case (see **Fig. S5 b**, ESI). The ratio of 0-0 to the 0-1 absorption increases only slightly from $A_{0-0} : A_{0-1} = 0.55$ for

20 vol% of the nonsolvent ethyl acetate to $A_{0-0} : A_{0-1} = 0.55$ with an ethyl acetate content of 80 vol%. That means, that in contrast to **Brush 4** the quality of the aggregates in **Brush 3** does not change with the solvent quality. A similar investigation of the short brushes, **Brushes 1** and **2**, was conducted but no spectral changes for the different solvent mixtures

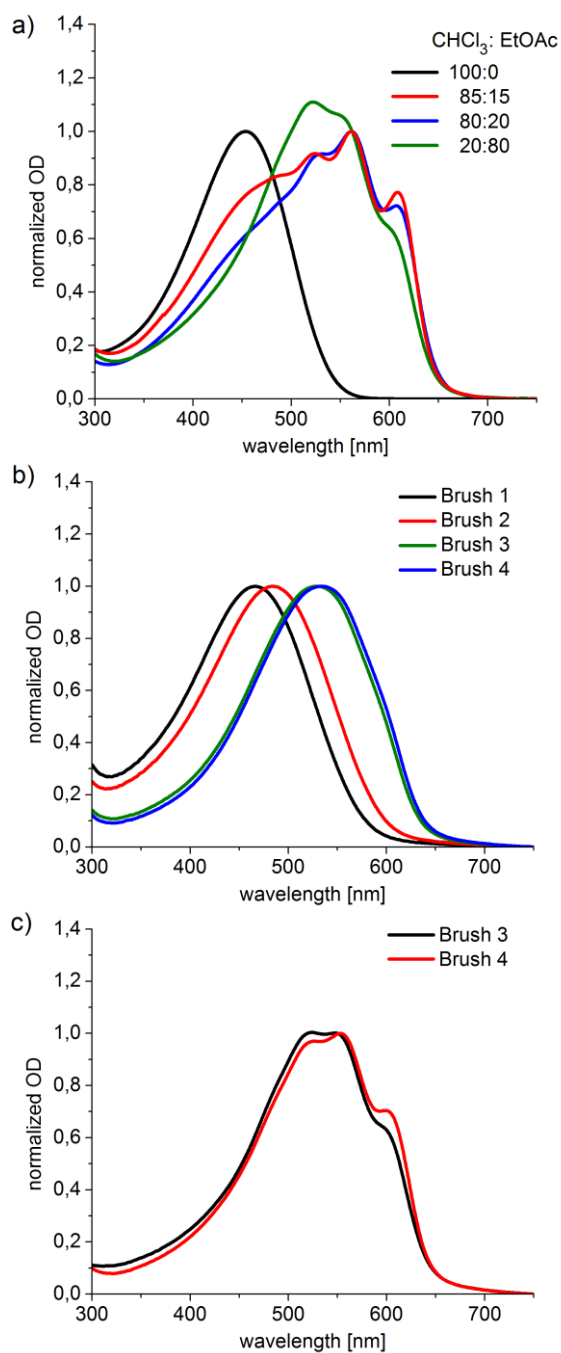


Fig. 3 a) UV-Vis spectra of **Brush 4** in a mixture of good solvent (CHCl_3) and bad solvent (EtOAc) exhibiting pronounced aggregation with increasing EtOAc content; b) UV-Vis spectra of the brush polymers Brush 1-4 in as cast films and c) of **Brush 3** and **4** after melt crystallization.

were detected. **Brushes 1** and **2** can therefore not aggregate at all even in 90 vol% ethyl acetate solution. This result is also in agreement with bulk DSC measurements, which showed that these polymers could not crystallize.

We were further interested in the thin film properties of brush polymers. To be able to compare the results with the OFET measurements later, we conducted the following experiments on comparable films. We ensured that the substrate had the same properties as in the OFET devices by the hydrophobization of the surface with octadecyltrimethoxysilane (ODTS) and prepared the films by spin casting chloroform solutions. In **Fig. 3 b**, the UV-Vis spectra of all four brushes are shown directly after spin casting. The spectra of the films of **Brushes 1–4** are unstructured but a bathochromic shift can be observed in comparison to the corresponding spectra of the chloroform solutions of these polymers. The peak maxima of the small brushes, **Brushes 1** and **2**, are red-shifted by 32 nm and 45 nm in thin films. The shift of the maxima of **Brushes 3** and **4** in thin films is larger with approximately 80 nm for both polymers. The onset of absorption at around 650 nm for **Brushes 3** and **4** is the same as expected for aggregated linear P3HTs. The films of these two brush polymers (**Brushes 3** and **4**) are therefore to some extent aggregated. If compared to linear **P3HT 1–4** a different behavior can be observed (**Fig. S5 c**, ESI). While the spectrum of the as-cast film of **P3HT 1** resembles the non-aggregated solution spectrum in chloroform, the as-cast films of **P3HT 2–4** with higher molecular weights exhibit structured spectra in which three vibrational bands can be observed.

Spin casting polymer films from low boiling solvents such as chloroform leads to films with low crystallinity as the film solidifies very fast. All polymer films were therefore also melt-crystallized in order to have maximum aggregation due to improved crystallization. However, the films of the linear polymers **P3HT 1–4** and the small brush polymers, **Brushes 1** and **2**, were not stable on the highly hydrophobic surface and showed dewetting behavior. **Brushes 3** and **4** on the other hand, formed high quality films due to their high molecular weight that showed no signs of dewetting. The spectra of the melt crystallized films of **Brushes 3** and **4** (**Fig. 3 c**) do now show structured curves expected for well-aggregated P3HT. While the as-cast films of **Brushes 3** and **4** were nearly identical to their order of aggregation, the ratio of the 0–0 band at around 605 nm to the 0–1 band at 560 nm for the melt crystallized film of **Brush 4** is higher ($A_{0-0} : A_{0-1} = 0.70$) as compared to **Brush 3**

($A_{0-0} : A_{0-1} = 0.62$). This is, as mentioned before, an indicator of a higher order of the melt-cast film of high molecular weight **Brush 4**.

Atomic Force Microscopy

A linear P3HT is known to form lamellar crystallites which can be observed by either atomic force microscopy (AFM)^{30,45} or transmission electron microscopy (TEM).⁴⁶ For grafted P3HT bottlebrush polymers, no optical characterization has been reported in the literature. We therefore investigated **Brushes 3** and **4**, where we already observed crystallization in DSC and UV-Vis, by AFM. **Fig. 4** shows the observed structures for the linear P3HT (**P3HT 4**) in comparison to the brush polymers with similar side-chains (**Brush 4**). A highly ordered lamellar structure is observed for the linear polymer. Interestingly, the brush polymer forms very similar structural features, but with less order. The long period, that means the thickness of the crystalline lamellae (bright color) and the amorphous part (dark color) combined, can be roughly estimated to be 25 nm for both polymers. This is in the range of the contour length of stretched P3HT chains with a molecular weight of around 12 000 g mol⁻¹ (MALDI). This is in good agreement with the reported values of Singh *et al.*, where extended P3HT chains were observed in melt-crystallized samples up to molecular weights of 12 000 g mol⁻¹ (MALDI).³⁰ This is the first report on the brush polymer that crystallizes in a similar manner to its linear counterpart in the high molecular weight range. Though the AFM picture of the brush shows a lower order as well as a smaller length of the crystalline lamellae. This is consistent with the already

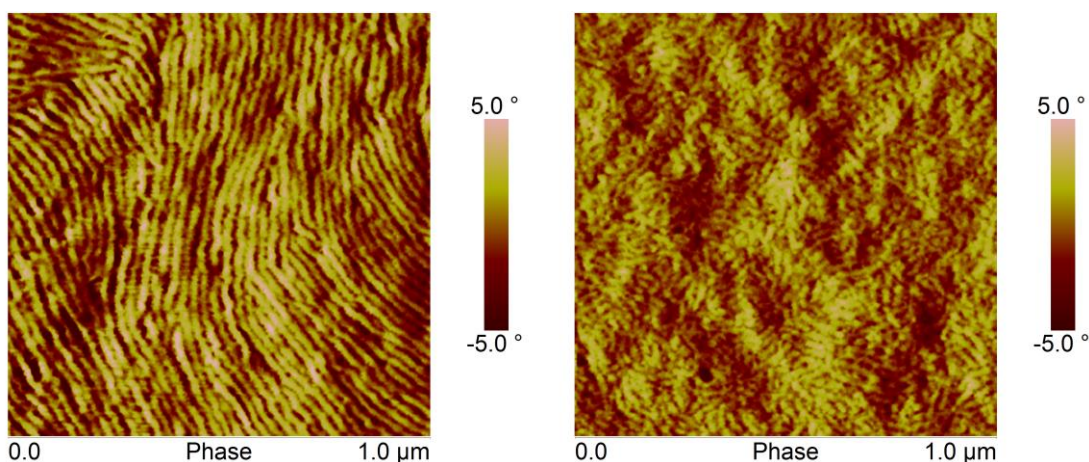


Fig. 4 AMF phase image of **P3HT4** (left) and **Brush 4** (right) after melt crystallization.

observed differences between the linear and the brush polymers that we discussed in DSC and UV-Vis measurements and is yet another indication of a hindered crystallization due to mobility restrictions induced by the immobilization of one chain end on the polystyrene backbone. In the investigation of **Brush 3** and its linear counterpart **P3HT 3**, on the other hand, we could not observe a clear structure for the brush (see **Fig. S6**, ESI). This is unexpected due to the otherwise similar characteristics of aggregation (UV-Vis, DSC) in comparison to **Brush 4**.

Charge carrier mobilities

The influence of the side-chain length on the charge carrier mobilities of P3HT brush polymers was investigated in organic field effect transistors (OFETs). We prepared devices in a bottom gate/bottom contact configuration. The detailed description of the preparation and device structure is given in the Experimental section. Herein we compare the charge carrier mobilities of **Brushes 1–4** with those of the linear counterparts **P3HT 1–4**. We show the p-type output curves and the p-type transfer curves of melt crystallized **Brush 4** (**Fig. 5 a** and **b**) as a sample with the highest measured mobility within the series of tested polymers. The OFET device with the melt crystallized **Brush 4** as an active material reached a hole carrier mobility of $\mu_h = 4.95 \times 10^{-2} \text{ cm}^2\text{V}^{-1} \text{ s}^{-1}$. This value is comparable to the highest values that we could achieve for the linear polymers and it is also in the range of the best reported mobilities for P3HT.²⁵ The measurements of the hole mobilities of **P3HT 1–4** show a high dependency of the hole mobility on the molecular weight.³⁰ An increase of the molecular weight from 1400 g mol⁻¹ to 11 600 g mol⁻¹ (MALDI) increases the hole mobility by five orders of magnitude. Earlier reports suggest that a further increase of the molecular weight above approximately 12 000 g mol⁻¹ (MALDI) will not increase the charge carrier mobility, measured by SCLC, in the film.³⁰ Attempts to further improve the OFET device with linear P3HT by thermal annealing were not successful. The thin films of the linear P3HT polymers were not stable on the hydrophobic surface and showed dewetting behavior. The PS-*g*-P3HT bottlebrushes under investigation also showed a similar dependency of the hole mobilities on the molecular weights of the conjugated P3HT side-chains (see **Fig. 5 c**). The measured mobilities of as-cast films of **Brushes 1–4** were lower than the as-cast films of the corresponding linear polymers. Thus the decrease in order/crystallinity in brush polymers

discussed above negatively influences the charge carrier mobility in the brush polymers to a certain extent. The devices with brush polymers were also thermally annealed above the melting temperature. The polymers, **Brushes 3** and **4**, were stable even after melt crystallization and a marked increase in the charge carrier mobilities could be measured for both polymers after annealing. **Brush 4** thus exhibited the best mobility compared to excellent film stability. These results are in accordance with the UV-Vis measurements which show an increase of the crystallinity after melt crystallization. These results clearly show that PS-*g*-P3HT bottlebrushes with high molecular weight side-chains are necessary if the excellent electronic properties comparable to the linear systems are to be obtained. Moreover, the improved wetting behavior and higher thermal stability of the high molecular weight brushes are of advantage for thin film applications.

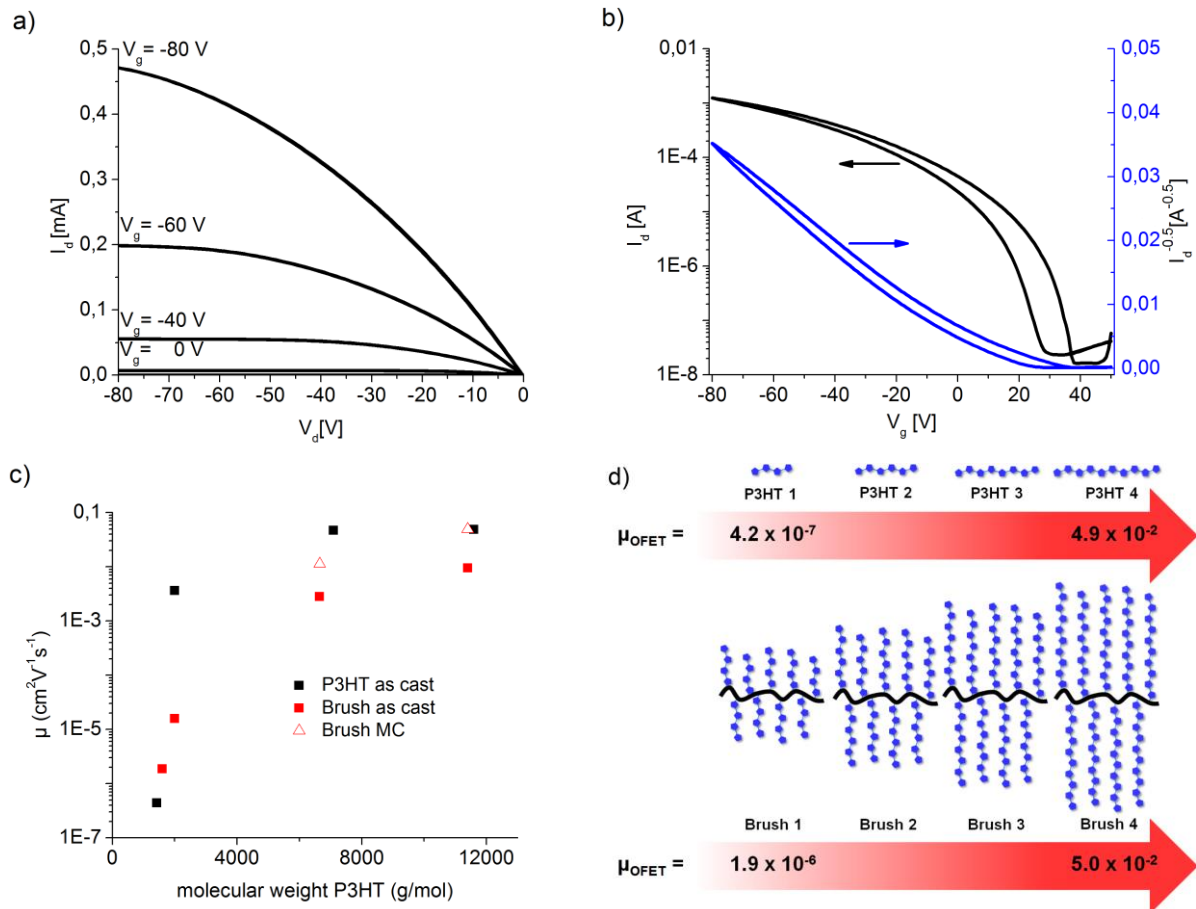


Fig. 5 a) p-output curves and b) p-transfer curves of the melt crystallized **Brush 4** and c) measured OFET hole mobilities μ plotted against the molecular weight $M_{n, \text{MALDI}}$ of the linear P3HT respectively the molecular weight $M_{n, \text{MALDI}}$ of the P3HT side-chain in case of the bottlebrush polymers d) schematic diagram highlighting the dependency of μ_{OFET} on P3HT chain length.

Conclusions

We have demonstrated that there is a strong correlation between the charge carrier mobility of PS-*g*-P3HT bottlebrushes and their side-chain lengths. In order to investigate the influence of the side-chains on the optical and electronic properties we synthesized a series of PS-*g*-P3HT bottlebrushes *via* a grafting-to approach using nitroxide mediated controlled radical polymerization, where only the length of the side-chains was varied. Synthetically we could achieve brushes from 21 000 to 144 000 g mol⁻¹ (SEC), with the highest molecular weight P3HT side-chains being 17 400 g mol⁻¹ (SEC), which is equivalent to 11400 g mol⁻¹ in MALDI-TOF analysis. Charge carrier mobility measurements demonstrated that high molecular weight is necessary to obtain a high charge carrier mobility of $5.0 \times 10^{-2} \text{ cm}^2 \text{ V}^{-1} \text{ s}^{-1}$ that is competitive with linear P3HTs. We also investigated the structure formation of the grafted polymers in bulk, solution and thin film. The results of DSC, UV-Vis and AFM measurements reveal two important things. The brush polymers with low molecular weight P3HT side-chains do not crystallize and therefore exhibit very poor electronic properties. With an increase of the side-chain length, highly crystalline materials are obtained. These investigations indicate crystallization and aggregation behavior in brushes, which is similar to the linear P3HTs. Lamellar crystallites are for example observed in AFM for the first time for brushes. The excellent thermal stability of the brushes in thin films can be an additional advantage for applications.

Acknowledgements

The authors acknowledge financial support from DFG (SFB 840), GRK 1640 (DFG) and the Bavarian State Ministry of Education, Science and the Arts (Solar technologies go hybrid). We also thank practical students Alexander Krimalowski, Tobias Jurczyk and Marius Feldmann for their contribution to synthesis.

References

- 1 M. Wintermantel, M. Gerle, K. Fischer, M. Schmidt, L. Wataoka, H. Urakawa, K. Kajiwara and Y. Tsukahara, *Macromolecules*, 1996, **29**, 978.
- 2 M. Zhang and A. H. E. Müller, *J. Polym. Sci., Part A: Polym. Chem.*, 2005, **43**, 3461.
- 3 M. Hu, Y. Xia, G. B. McKenna, J. A. Kornfield and R. H. Grubbs, *Macromolecules*, 2011, **44**, 6935.
- 4 E. E. Sheina, J. Liu, M. C. Iovu, D. W. Laird and R. D. McCullough, *Macromolecules*, 2004, **37**, 3526.
- 5 M. C. Iovu, E. E. Sheina, R. R. Gil and R. D. McCullough, *Macromolecules*, 2005, **38**, 8649.
- 6 A. Yokoyama, R. Miyakoshi and T. Yokozawa, *Macromolecules*, 2004, **37**, 1169.
- 7 R. Miyakoshi, A. Yokoyama and T. Yokozawa, *J. Am. Chem. Soc.*, 2005, **127**, 17542.
- 8 R. H. Lohwasser and M. Thelakkat, *Macromolecules*, 2011, **44**, 3388.
- 9 M. Jeffries-El, G. Sauve and R. D. McCullough, *Macromolecules*, 2005, **38**, 10346.
- 10 F. P. V. Koch, J. Rivnay, S. Foster, C. Müller, J. M. Downing, E. Buchaca-Domingo, P. Westacott, L. Yu, M. Yuan, M. Baklar, Z. Fei, C. Luscombe, M. A. McLachlan, M. Heeney, G. Rumbles, C. Silva, A. Salleo, J. Nelson, P. Smith and N. Stingelin, *Prog. Polym. Sci.*, 2013, **38**, 1978.
- 11 M. Sommer, S. Huettner and M. Thelakkat, *J. Mater. Chem.*, 2010, **20**, 10788.
- 12 R. H. Lohwasser, G. Gupta, P. Kohn, M. Sommer, A. S. Lang, T. Thurn-Albrecht and M. Thelakkat, *Macromolecules*, 2013, **46**, 4403.
- 13 S. W. Hong, W. Gu, J. Huh, B. R. Sveinbjornsson, G. Jeong, R. H. Grubbs and T. P. Russell, *ACS Nano*, 2013, **7**, 9684.
- 14 N. Khanduyeva, V. Senkovskyy, T. Beryozkina, M. Horecha, M. Stamm, C. Uhrich, M. Riede, K. Leo and A. Kiriy, *J. Am. Chem. Soc.*, 2009, **131**, 153.
- 15 N. Khanduyeva, V. Senkovskyy, T. Beryozkina, V. Bocharova, F. Simon, M. Nitschke, M. Stamm, R. Grötzschel and A. Kiriy, *Macromolecules*, 2008, **41**, 7383.
- 16 P. Paoprasert, J. W. Spalenka, D. L. Peterson, R. E. Ruther, R. J. Hamers, P. G. Evans and P. Gopalan, *J. Mater. Chem.*, 2010, **20**, 2651.
- 17 D. Meng, J. Sun, S. Jiang, Y. Zeng, Y. Li, S. Yan, J. Geng and Y. Huang, *J. Mater. Chem.*, 2012, **22**, 21583.
- 18 X. Pang, L. Zhao, C. Feng, R. Wu, H. Ma and Z. Lin, *Polym. Chem.*, 2013, **4**, 2025.
- 19 S. Samanta, D. P. Chatterjee, R. K. Layek and A. K. Nandi, *J. Mater. Chem.*, 2012, **22**, 10542.
- 20 S. Ahn, D. L. Pickel, W. M. Kochemba, J. Chen, D. Uhrig, J. P. Hinstrosa, J.-M. Carillo, M. Shao, C. Do, J. M. Messmann, W. M. Brown, B. G. Sumpter and S. M. Kilbey, *ACS Macro Lett.*, 2013, **2**, 761.

- 21 D. v. As, J. Subbiah, D. J. Jones and W. W. H. Wong, *Macromol. Chem. Phys.*, 2016, **217**, 403.
- 22 Z. Bao, A. Dodabalapur and A. J. Lovinger, *Appl. Phys. Lett.*, 1996, **69**, 4108.
- 23 H. Sirringhaus, N. Tessler and R. H. Friend, *Science*, 1998, **290**, 1741.
- 24 H. Sirringhaus, P. J. Brown, R. H. Friend, M. M. Nielsen, K. Bechgaard, B. M. W. Langeveld-Voss, A. J. H. Spiering, R. A. J. Janssen, E.W. Meijer, P. Herwing and P.M. de Leeuw, *Nature*, 1999, **401**, 685.
- 25 J.-F. Chang, B. Sun, D. W. Breiby, M. M. Nielsen, T. J. Sölling, M. Giles, J. McCulloch and H. Sirringhaus, *Chem. Mater.*, 2004, **16**, 4772.
- 26 R. J. Klein, M. D. McGehee, E. N. Kadnikova, J. Liu, J. M. J. Fréchet and M. F. Toney, *J. Am. Chem. Soc.*, 2006, **128**, 3480.
- 27 R. J. Kline, M. D. McGehee, E. N. Kadnikova, J. Liu and J. M. J. Fréchet, *Adv. Mater.*, 2003, **15**, 1519.
- 28 A. Zen, J. Pflaum, S. Hirschmann, W. Zhuang, F. Jaiser, U. Asawapirom, J. P. Rabe, U. Scherf and D. Neher, *Adv. Funct. Mater.*, 2004, **14**, 757.
- 29 R. Zhang, B. Li, M. C. Iovu, M. Jefries-EL, G. Sauv e, J. Cooper, S. Jia, S. Tristram-Nagle, D. M. Smilgies, D. N. Lambeth, R. D. McCullough and T. Kowalewski, *J. Am. Chem. Soc.*, 2006, **128**, 3480.
- 30 C. R. Singh, G. Gupta, R. Lohwasser, S. Engmann, J. Balko, M. Thelakkat, T. Thurn-Albrecht and H. Hoppe, *J. Polym. Sci., Part B: Polym. Phys.*, 2013, **51**, 943.
- 31 D. Benoit, V. Chaplinski, R. Braslau and C. J. Hawker, *J. Am. Chem. Soc.*, 1999, **121**, 3904.
- 32 R. H. Lohwasser and M. Thelakkat, *Macromolecules*, 2012, **45**, 3070.
- 33 J. Liu, R. S. Loewe and R. D. McCullough, *Macromolecules*, 1999, **32**, 5777.
- 34 V. V. Rostovtsev, L. G. Green, V. V. Fokin and K. B. Sharpless, *Angew. Chem., Int. Ed.*, 2002, **41**, 2596.
- 35 K. Lorincz, P. Kele and Z. Novak, *Synthesis*, 2009, 3527.
- 36 W. E. Garner, K. V. B. Bibber and A. M. King, *J. Chem. Soc.*, **1931**, 1533.
- 37 M. G. Broadhurst, *J. Chem. Phys.*, 1962, **36**, 2578.
- 38 F. P. V. Koch, M. Heeney and P. Smith, *J. Am. Chem. Soc.*, 2013, **135**, 13699.
- 39 C. R. Snyder, R. C. Nieuwendaal, D. M. DeLongchamp, C. K. Luscombe, P. Sista and S. D. Boyd, *Macromolecules*, 2014, **47**, 3942.
- 40 Z. Wu, A. Petzhold, T. Henze, T. Thurn-Albrecht, R. H. Lohwasser, M. Sommer and M. Thelakkat, *Macromolecules*, 2010, **43**, 4646.
- 41 J. Balko, R. H. Lohwasser, M. Sommer, M. Thelakkat and T. Thurn-Albrecht, *Macromolecules*, 2013, **46**, 9642.
- 42 J. Clark, C. Silva, R. H. Friend and F. C. Spano, *Phys. Rev. Lett.*, 2007, **98**, 206406.
- 43 J. Clark, J.-F. Chang, F. C. Spano, R. H. Friend and C. Silva, *Appl. Phys. Lett.*, 2009, **94**, 163306.

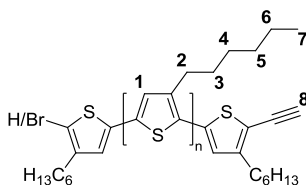
- 44 C. Scharsich, R. H. Lohwasser, M. Sommer, U. Asawapirom, U. Scherf, M. Thelakkat, D. Neher and A. Köhler, *J. Polym. Sci., Part B: Polym. Phys.*, 2012, **50**, 442.
- 45 Z. Wu, A. Petzold, T. Henze, T. Thurn-Albrecht, R. H. Lohwasser, M. Sommer and M. Thelakkat, *Macromolecules*, 2010, **43**, 4646.
- 46 M. Brinkmann and P. Rannou, *Macromolecules*, 2009, **42**, 1125.

Supporting Information (ESI)

1. Synthesis

1.1. Synthesis of P3HT-Alkyne:

General procedure for the synthesis of alkyne functionalized P3HT (P3HT-Alkyne 1-4):



The alkyne functionalized P3HT polymers were synthesized according to a reported procedure.¹ A 0.5 M LiCl solution was prepared first by weighing LiCl into a Schlenk flask and subsequently drying for 4 h *in vacuo* at 140 °C. Anhydrous THF was added and the solution was stirred overnight to assure a complete dissolution of the LiCl. The Grignard reagents *t*-BuMgCl and EthynylMgCl were titrated prior to their use according to a published procedure.² A dry Schlenk flask was charged with one equivalent 2,5-dibromo-3-hexyl-thiophene under N₂ atmosphere. 2 mL of the 0.5 M LiCl solution in THF were added for every mmol 2,5-dibromo-3-hexylthiophene. 0.96 equivalents *t*-BuMgCl were added and the solution was stirred for 24 h to ensure the complete formation of the active Grignard species. The solution was diluted with 7.2 mL THF for every mmol 2,5-dibromo-3-hexylthiophene and the polymerization was started by adding Ni(dppp)Cl₂ (suspension in THF). It is possible to adjust the molecular weight of the polymer by changing the ratio of monomer:Ni(dppp)Cl₂ due to the controlled nature of the polymerization. The polymerization was terminated by adding 0.2 equivalents EthynylMgCl after 30 min. The solution was stirred for further 15 min and the polymer was subsequently precipitated in methanol. The polymer was dried and redissolved in CHCl₃. The solution was filtered over a short aluminum oxide column to remove residual LiCl and Ni(dppp)Cl₂, evaporated with the rotary evaporator to get a concentrated solution, and precipitated again in methanol.

Synthesis of P3HT-Alkyne 1 and 2: The polymerization was carried out at a monomer:Ni(dppp)Cl₂ ratio of 1: 0.06. The major part of obtained P3HT-Alkyne coupled

after precipitation as observed by SEC. The raw product was fractionated to recover the uncoupled product. Two fractions **P3HT-Alkyne 1** and **2** were obtained. **P3HT-Alkyne 1** with a lower molecular weight was soluble in Acetone and **P3HT-Alkyne 2** was soluble in a 1:1 mixture of Acetone:Hexane. Both fractions were freeze dried from benzene and obtained as red sticky solids. The residual polymer contained mainly coupled species and was discarded.

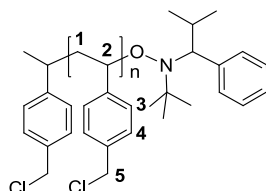
P3HT-Alkyne 1: $m = 589$ mg, $M_{n,SEC} = 2000$ g mol⁻¹, $M_{n,MALDI} = 1600$ g mol⁻¹, $\mathcal{D} = 1.57$; ¹H NMR (300 MHz, CHCl₃): δ (ppm) 6.97 (s, 1H, H-1), 3.53 (s, 1H, H-8), 2.85-2.4 (t, 2H, H-2), 1.80-1.60 (m, 2H, H-3), 1.50-1.25 (m, 6H, H-4 H-5 H-6), 0.98-0.83 (m, 3H, H-7); IR(ATR): $\nu(\text{cm}^{-1})$ 3310 (C≡C-H₂), 2095 (C≡C)

P3HT-Alkyne 2 $m = 450$ mg, $M_{n,SEC} = 3,800$ g/mol, $M_{n,MALDI} = 2,000$ g/mol, $\mathcal{D} = 1.36$; ¹H NMR (300 MHz, CHCl₃): δ (ppm) 6.98 (s, 1H, H-1), 3.52 (s, 1H, H-8), 2.85-2.4 (m, 2H, H-2), 1.80-1.60 (m, 2H, H-3), 1.50-1.25 (m, 6H, H-4 H-5 H-6), 0.98-0.83 (m, 3H, H-7); IR(ATR): $\nu(\text{cm}^{-1})$ 3311 (C≡C-H), 2096 (C≡C)

Synthesis of P3HT-Alkyne 3: The polymerization was carried out at a monomer:Ni(dppp)Cl₂ ratio of 1: 0.02. The polymer was obtained as a dark solid after one additional precipitation in hexane. $m = 695$ mg, $M_{n,SEC} = 9300$ g mol⁻¹, $M_{n,MALDI} = 6650$ g mol⁻¹, $\mathcal{D} = 1.13$; ¹H NMR (300 MHz, CHCl₃): δ (ppm) 6.98 (s, 1H, H-1), 3.52 (s, 1H, H-8), 2.85-2.4 (m, 2H, H-2), 1.80-1.60 (m, 2H, H-3), 1.50-1.25 (m, 6H, H-4 H-5 H-6), 0.98-0.83 (m, 3H, H-7); IR(ATR): $\nu(\text{cm}^{-1})$ 3313 (C≡C-H), 2096 (C≡C)

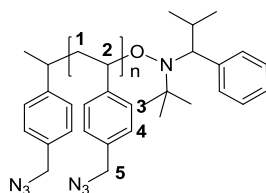
Synthesis of P3HT-Alkyne 4: The polymerization was carried out at a monomer:Ni(dppp)Cl₂ ratio of 1: 0.0125. 2.75 g, $M_{n,SEC} = 17400$, $M_{n,MALDI} = 11400$ g/mol; $\mathcal{D} = 1.15$; ¹H NMR (300 MHz, CHCl₃): δ (ppm) 6.98 (s, 1H, H-1), 3.53 (s, 1H, H-8), 2.85-2.4 (m, 2H, H-2), 1.80-1.60 (m, 2H, H-3), 1.50-1.25 (m, 6H, H-4 H-5 H-6), 0.98-0.83 (m, 3H, H-7); IR(ATR): $\nu(\text{cm}^{-1})$ 3312 (C≡C-H), 2096 (C≡C).

1.2. Synthesis of Poly(4-chloromethylstyrene) (PS-Cl)



A dry 10 mL Schlenk flask was charged with 123.4 mg (0.33 mmol) *N-t*-Butyl-*O*-[1-[4-(chloromethyl)phenyl]ethyl]-*N*-(2-methyl-1-phenylpropyl)hydroxylamine (**2**), 726.1 μg (3.3 μmol) 2,2,5-Trimethyl-4-phenyl-3-azahexane-3-nitroxide (**3**) and 1,445.6 mg 4-chloromethyl-styrene (**1**). 1.3 mL anisole were added and the solution was degassed by four freeze-pump-thaw cycles. The polymerization was initiated by immersion into an oil bath at 125 °C. The conversion was monitored via NMR and the reaction was terminated after 180 min (Conversion = 85 %) by the immersion of the reaction vessel into liquid nitrogen. The polymer was obtained by precipitation into methanol. $m = 1.1$ g, $M_{n,SEC} = 3100$ g mol⁻¹; $D = 1.25$; ¹H NMR (300 MHz, CHCl₃): δ (ppm) 7.2-6.2 (b, 4H, H-3,H-4), 4.6-4.2 (b, 2H, H-5), 2.6-0.4 (m, 3H, H-1, H-2).

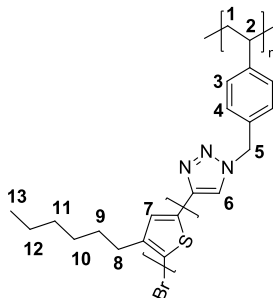
1.3. Synthesis of Poly(4-azidomethylstyrene) (PS-N₃)



In a dry 25 ml Schlenk flask 400 mg (2.62 mmol chlorine groups) of polymer **4** was dissolved in 10 mL dimethylformamide and 1.7 g (26.2 mmol) sodium azide was added. The reaction was stirred at room temperature for 24 h. After that 15 mL pentane was added and the mixture was washed twice with distilled water. Dichloromethane was added to the turbid organic layer and the mixture was filtered. The polymer was obtained after precipitation from methanol. 183.7 mg, $M_{n,SEC} = 3600$ $D = 1.21$; ¹H NMR (300 MHz, CHCl₃): δ (ppm) 7.2-6.2 (b, 4H, H-3,H-4), 4.4-4.0 (b, 2H, H-5), 2.6-0.4 (m, 3H, H-1, H-2); IR(ATR): $\nu(\text{cm}^{-1})$ 2086 (N₃).

1.4. Synthesis of Poly(4-methylstyrene)-*g*-P3HT (Brush 1-4)

General procedure for **Brush 1-4**:



A dry roundbottom flask was charged with poly(4-azidomethylstyrene) (**5**) and with 1.1–1.5 equivalents of an alkyne functionalized P3HT (**P3HT-Alkyne 1-4**). The polymers were dissolved in *o*-dichlorobenzene. The solution was degassed by purging with nitrogen for 20 min and was heated to 90 °C. After that a degassed stock solution of CuBr/PMDETA was added and the reaction was stirred for 24 h. The reaction mixture was filtered over a short aluminum oxide column and the raw polymers were obtained after precipitation in methanol.

Synthesis of Brush 1: 375 mg ($3.1 \cdot 10^{-1}$ mmol) **P3HT-Alkyne 1** and 42.0 mg ($2.6 \cdot 10^{-1}$ mmol azide groups) poly(4-azidomethylstyrene) (**5**) were dissolved in 15 mL *o*-dichlorobenzene. 0.25 mL of the catalyst stock solution were added. The raw product could be purified from the excess of linear P3HT by preparative SEC. $m = 68$ mg, $M_{n,SEC} = 21000$ g mol $^{-1}$, $D = 1.21$; $^1\text{H NMR}$ (300 MHz, CHCl $_3$): δ (ppm) 8.4–7.4 (b, 1H; H-6), 7.2–6.0 (4H, H-1, H-2), 6.96 (s, 1H, H-7), 6.0–5.0 (b, 2H, H-5), 2.85–2.4 (t, 2H, H-8), 1.80–1.60 (m, 2H, H-9), 1.50–1.25 (m, 6H, H-10 H-11 H-12), 0.98–0.83 (m, 3H, H-13); IR(ATR): $\nu(\text{cm}^{-1})$ 2095 (C \equiv C).

Synthesis of Brush 2: 270 mg ($1.1 \cdot 10^{-1}$ mmol) **P3HT-Alkyne 2** and 14.7 mg ($9.3 \cdot 10^{-2}$ mmol azide groups) poly(4-azidomethylstyrene) (**5**) were dissolved in 10 mL *o*-dichlorobenzene. 0.25 mL of the catalyst stock solution were added. The raw product could be purified from the excess of linear P3HT by preparative SEC. $m = 108$ mg, $M_{n,SEC} = 36500$ g mol $^{-1}$, $D = 1.22$; $^1\text{H NMR}$ (300 MHz, CHCl $_3$): δ (ppm) 8.4–7.4 (b, 1H; H-6), 7.2–

6.0 (4H, H-1, H-2), 6.96 (s, 1H, H-7), 6.0-5.0 (b, 2H, H-5), 2.85-2.4 (t, 2H, H-8), 1.80-1.60 (m, 2H, H-9), 1.50-1.25 (m, 6H, H-10 H-11 H-12), 0.98-0.83 (m, 3H, H-13); IR(ATR): $\nu(\text{cm}^{-1})$ 2096 ($\text{C}\equiv\text{C}$).

Synthesis of Brush 3: 110 mg ($1.5 \cdot 10^{-2}$ mmol) **P3HT-Alkyne 3** and 2679 μg ($1.6 \cdot 10^{-2}$ mmol azide groups) poly(4-azidomethyl-styrene) (**5**) were dissolved in 10.2 mL o-dichlorobenzene. 1 mL of the catalyst stock solution was added. The raw product could be purified from the excess of linear P3HT by preparative SEC. $m = 90$ mg, $M_{n,\text{SEC}} = 97000$ g mol $^{-1}$, $D = 1.09$; $^1\text{H NMR}$ (300 MHz, CHCl_3): δ (ppm) 8.0-7.6 (b, 1H; H-6), 7.2-6.0 (4H, H-1, H-2), 6.98 (s, 1H, H-7), 6.0-5.0 (b, 2H, H-5), 2.85-2.4 (t, 2H, H-8), 1.80-1.60 (m, 2H, H-9), 1.50-1.25 (m, 6H, H-10 H-11 H-12), 0.98-0.83 (m, 3H, H-13).

Synthesis of Brush 4: 500 mg ($4.3 \cdot 10^{-2}$ mmol) **P3HT-Alkyne 4** and 5282 μg ($2.4 \cdot 10^{-2}$ mmol azide groups) poly(4-azidomethyl-styrene) (**5**) were dissolved in 20.4 mL o-dichlorobenzene. 2 mL of the catalyst stock solution were added. The raw product could be purified from the excess of linear P3HT by washing the polymer with THF at room temperature. $m = 139.2$ mg, $M_{n,\text{SEC}} = 144000$ g mol $^{-1}$, $D = 1.37$; $^1\text{H NMR}$ (300 MHz, CHCl_3): δ (ppm) 6.98 (s, 1H, H-7), 2.85-2.4 (t, 2H, H-8), 1.80-1.60 (m, 2H, H-9), 1.50-1.25 (m, 6H, H-10 H-11 H-12), 0.98-0.83 (m, 3H, H-13).

2. Additional Measurements

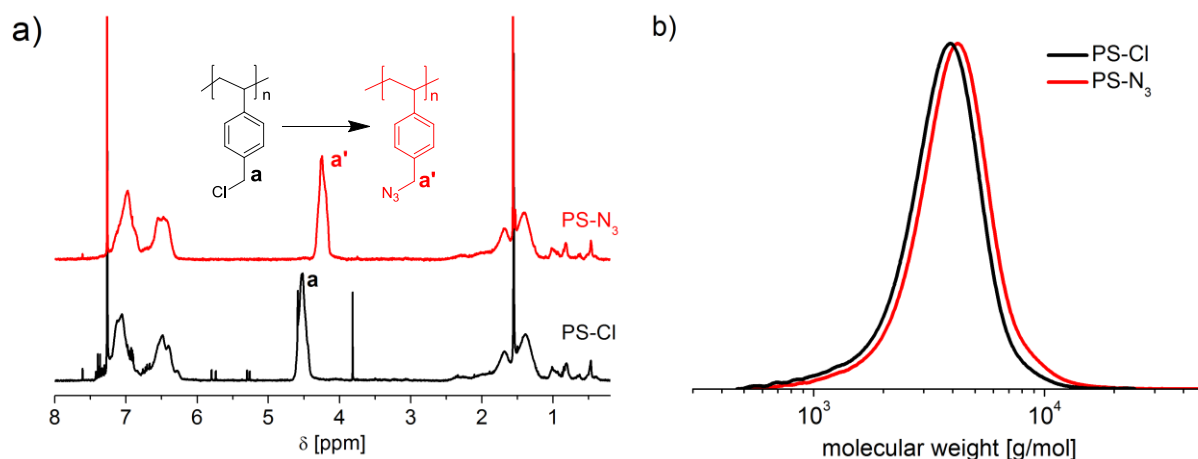


Fig. S 1 a) $^1\text{H-NMR}$ spectra of PS-Cl and PS- N_3 , the shift of the peak at around 4.4 ppm (**a**) in PS- N_3 to 4.2 ppm (**a'**) in PS-Cl is a strong indicator for a quantitative substitution of chlorine with azide; b) SEC traces of PS-Cl and PS- N_3 .

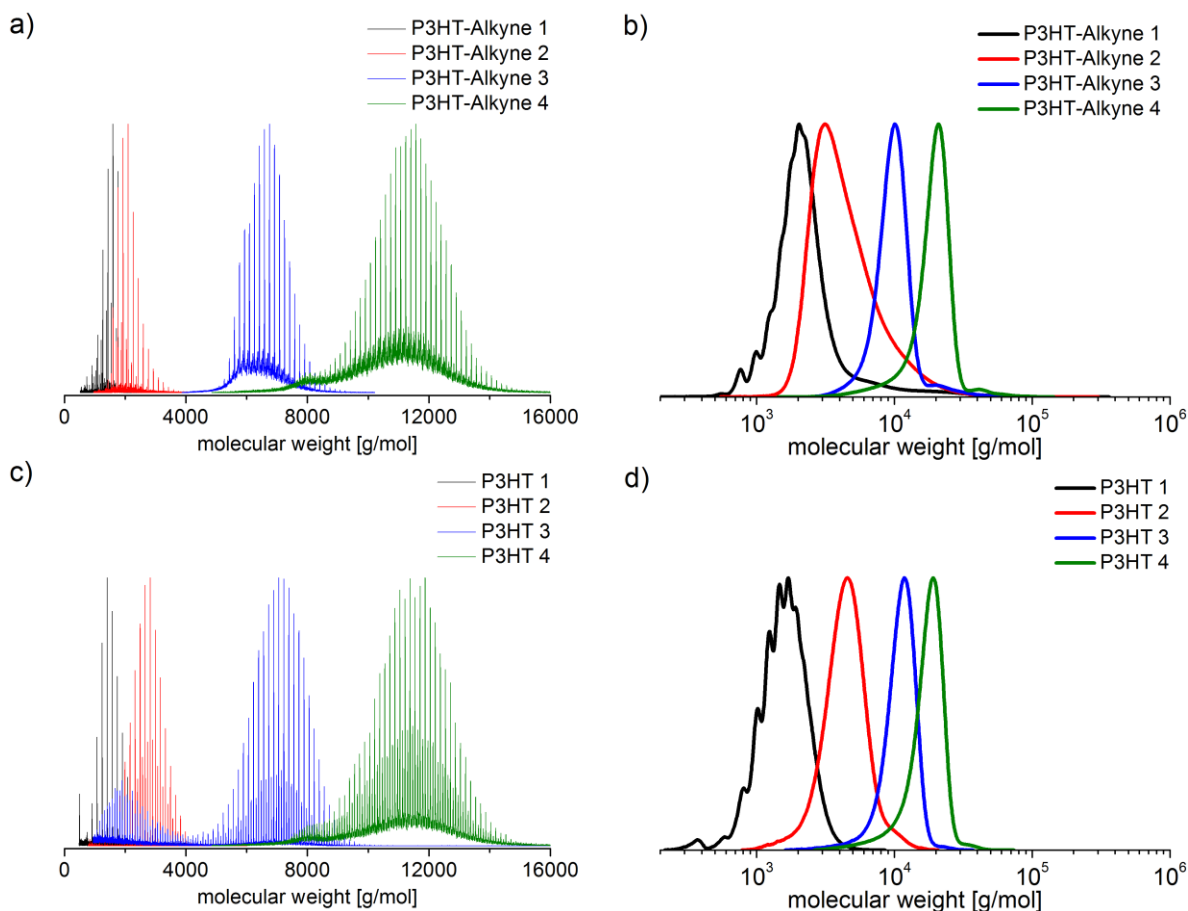


Fig. S 2 MALDI-ToF MS of **P3HT-Alkyne 1-4** (a) and **P3HT 1-4** (c) and SEC traces of **P3HT-Alkyne 1-4** (b) and **P3HT 1-4** (d).

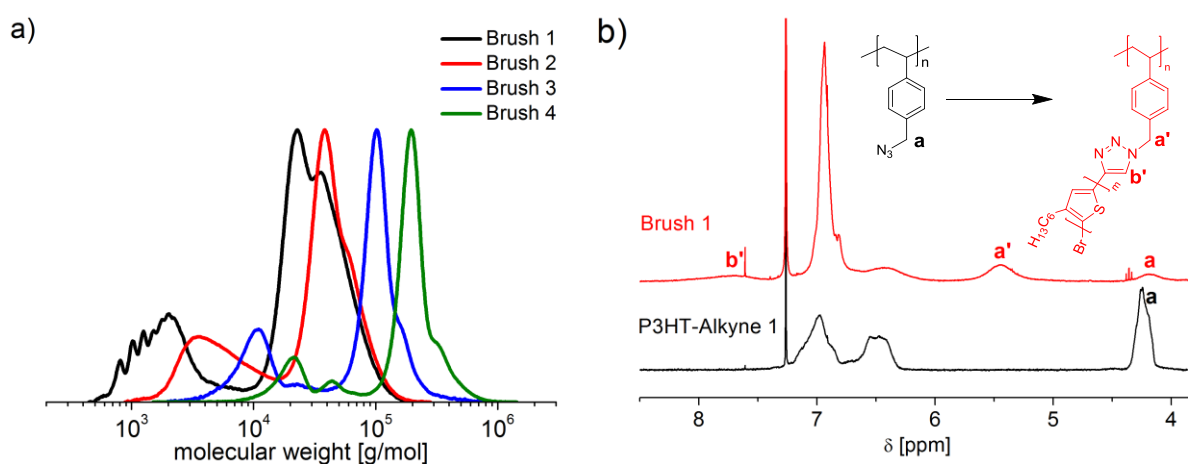


Fig. S 3 a) SEC traces of the raw brush polymers **Brush 1-4**. All unpurified brush polymers still contain P3HT-Alkyne. b) Detail of the $^1\text{H-NMR}$ spectra of **P3HT-Alkyne 1** and **Brush 1** between 3.5 and 8.5 ppm. Two new peaks emerge in the brush polymer. The peak at 5.4 ppm (**a'**) belongs to the methyl group next to the triazole and the peak at above 7.5 ppm (**b'**) is assigned to the triazole itself. The peak at 4.4 ppm (**a**) is an indicator for a non-quantitative reaction as it can be found in the same position in **PS-N₃**.

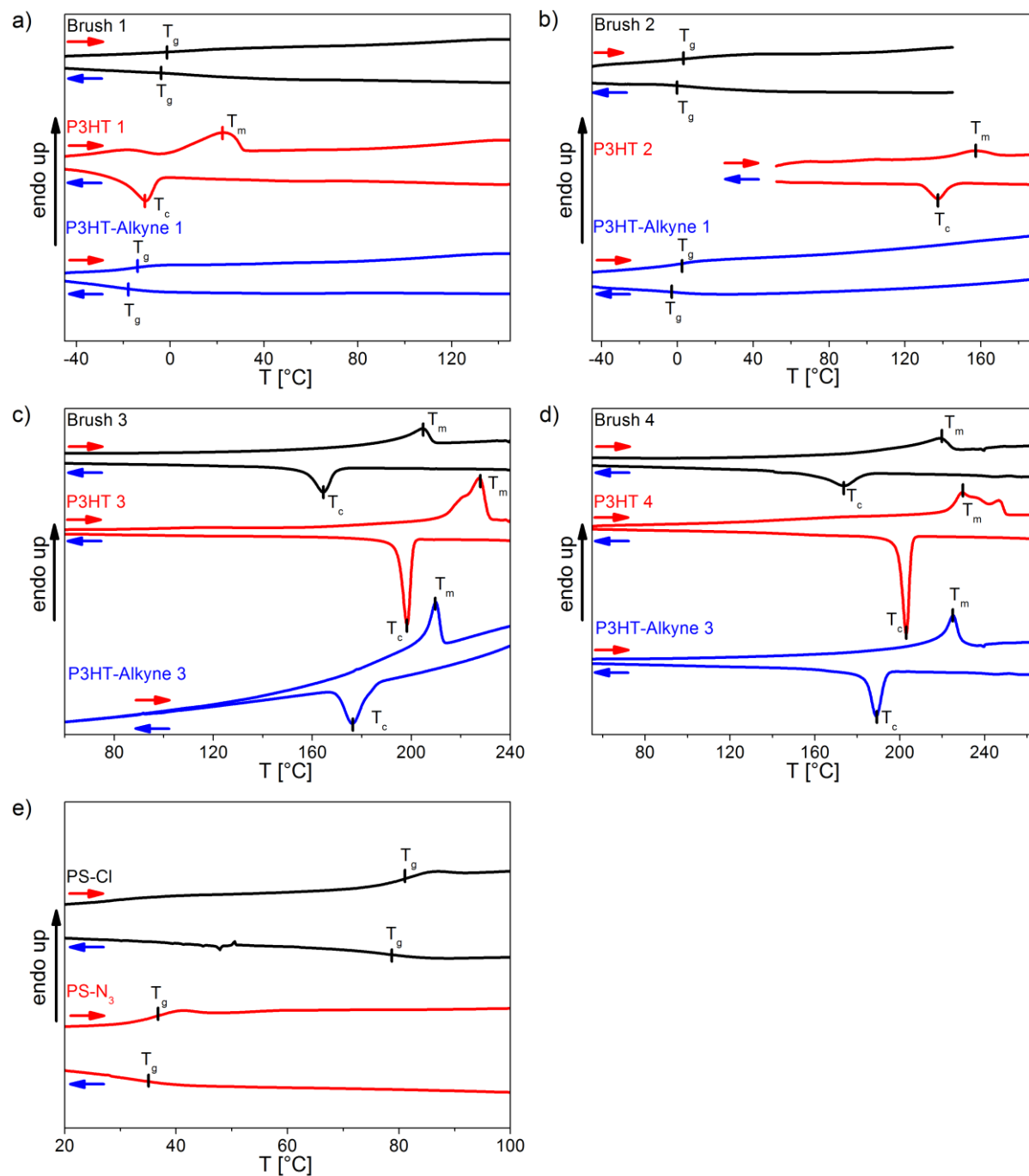


Fig. S 4 DSC measurements of **Brush 1-4**, **P3HT-Alkyne 1-4** and **P3HT 1-4** (a-d) and **PS-Cl** and **PS-N₃** (e) at a heating/cooling rate of 10 K min⁻¹

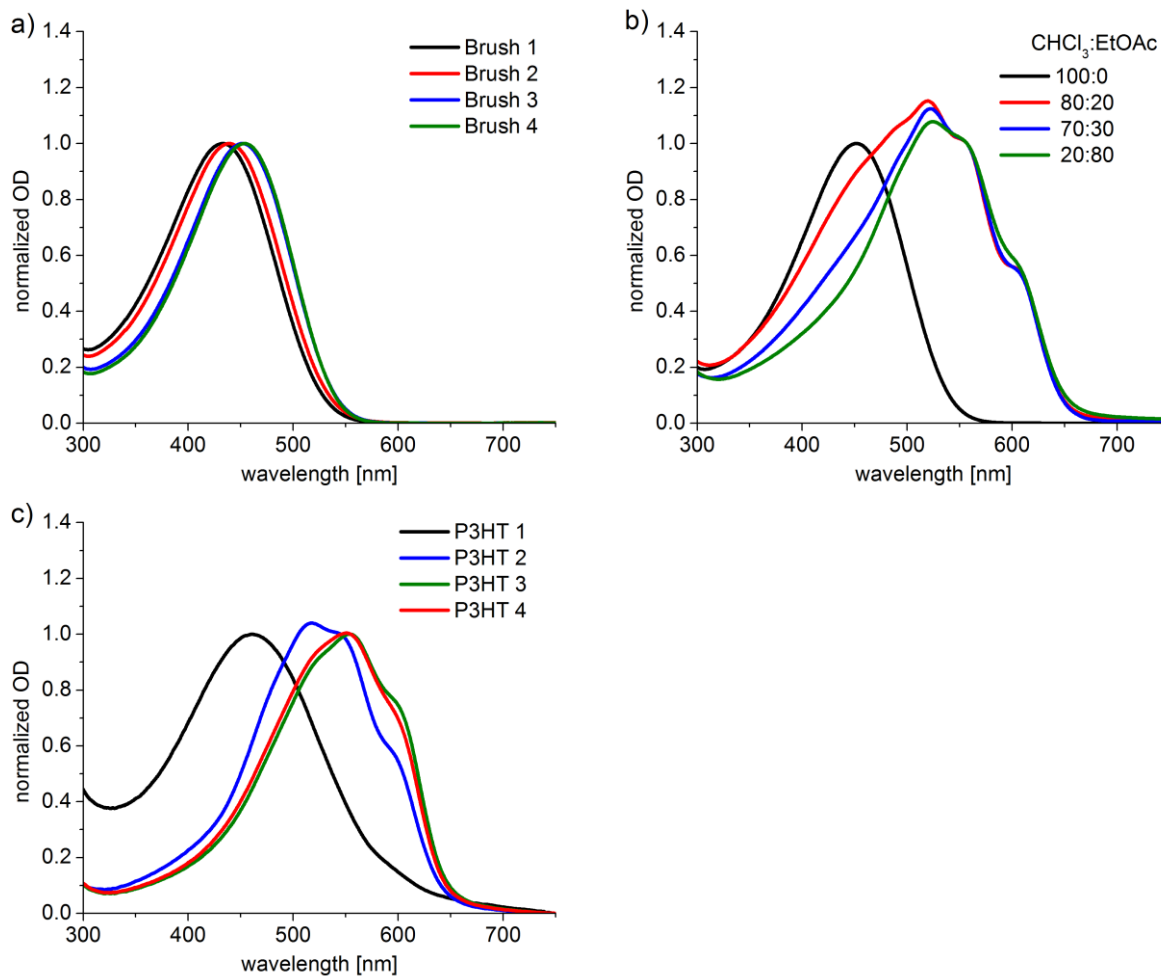


Fig. S 5 a) normalized UV-Vis spectra of **Brushes 1-4** in chloroform solutions; b) UV-Vis spectra of **Brush 3** in a mixture of good solvent (CHCl_3) and a bad solvent (EtOAc); c) as-cast films of **P3HT 1-4** on ODTs treated glass substrates

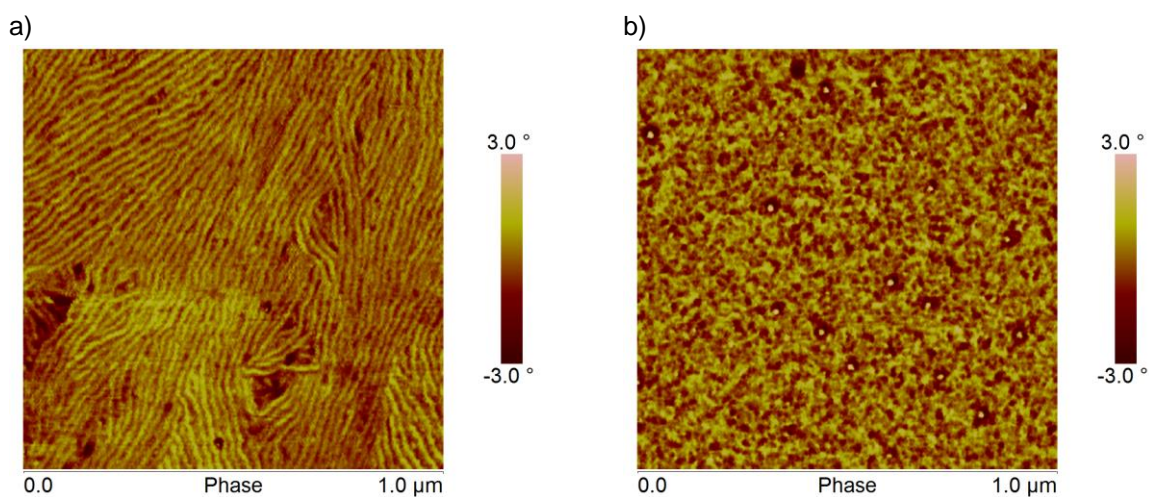
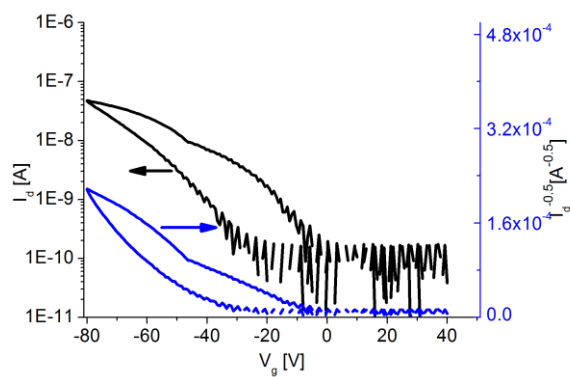
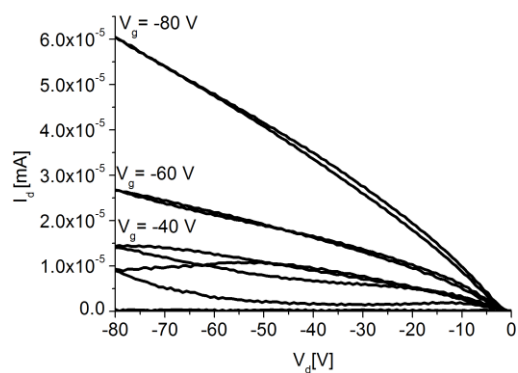
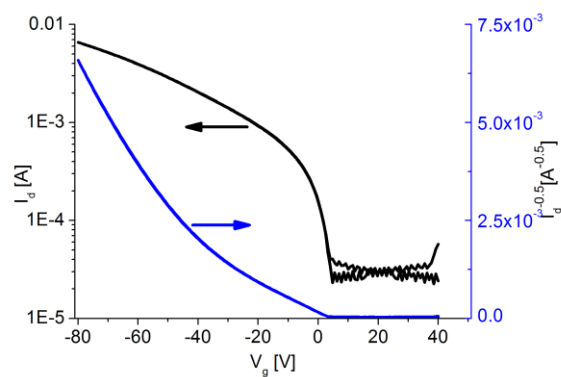
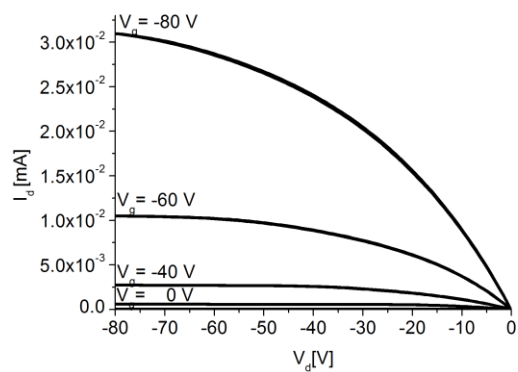


Fig. S 6 AMF phase image of **P3HT 3** (a) and **Brush 3** (b) after melt crystallization

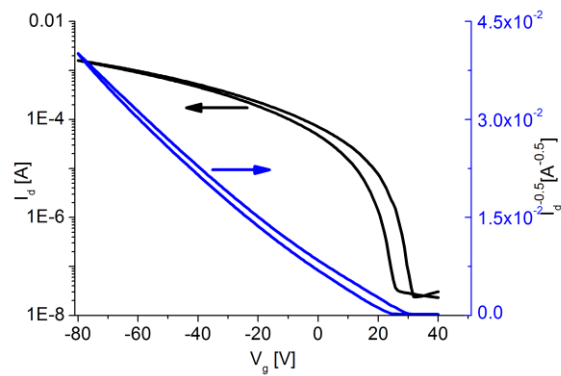
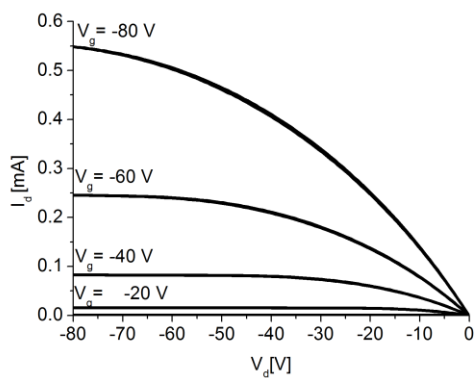
P3HT1



P3HT 2



P3HT 3



P3HT 4

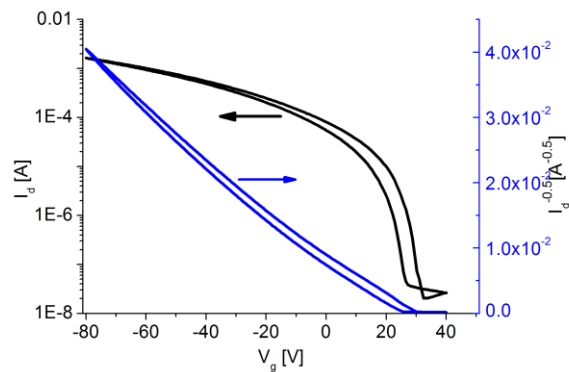
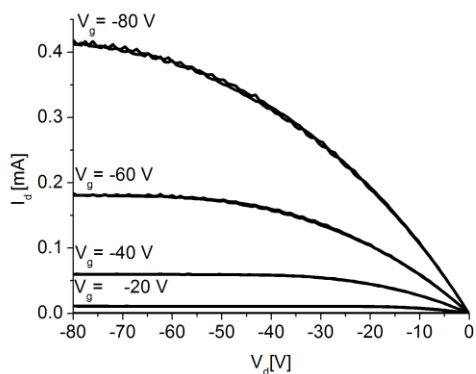


Fig. S 7 p-output curves (left) and p-transfer curves (right) of the as-cast P3HT 1-4

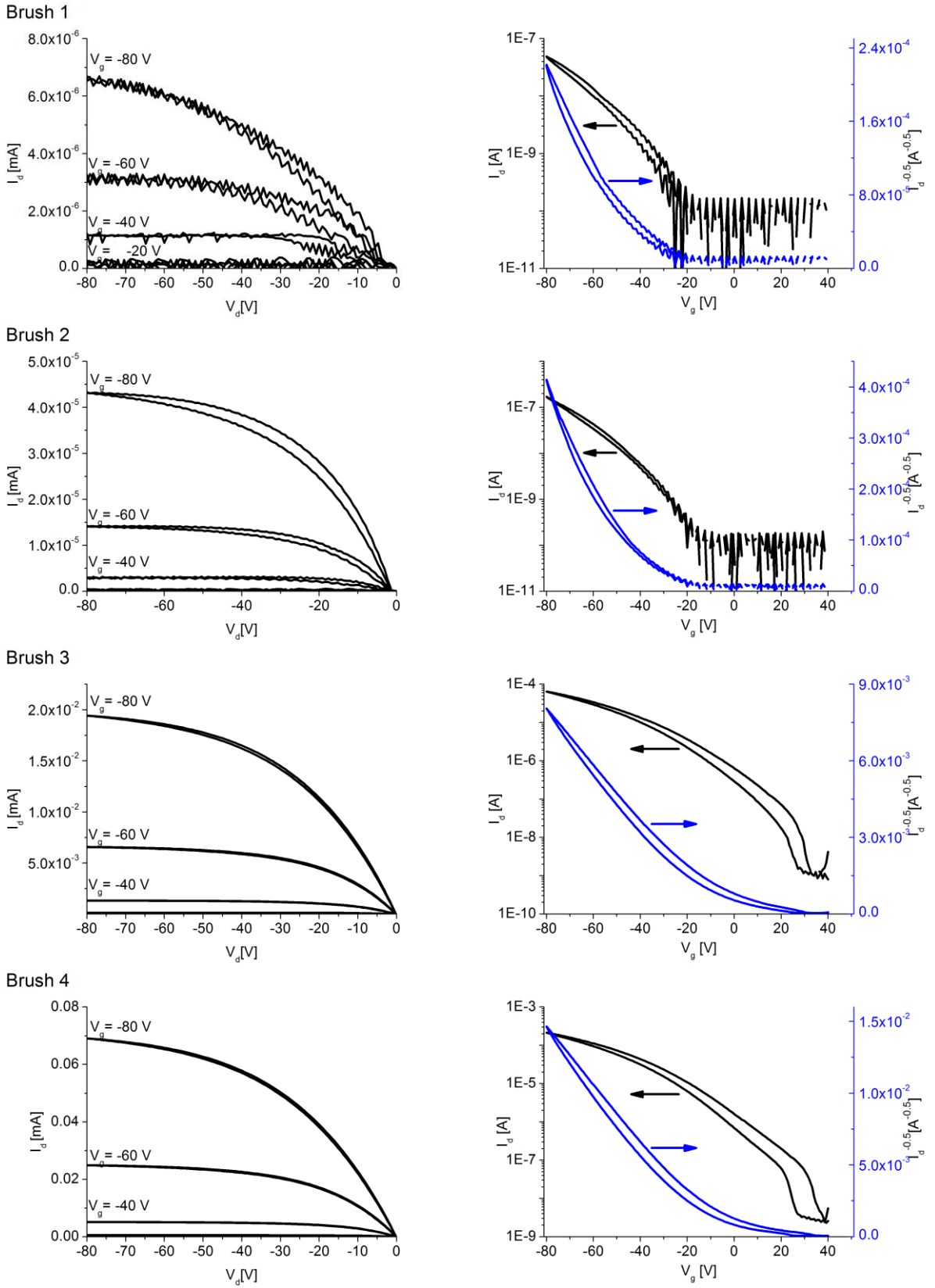


Fig. S 8 p-output curves (left) and p-transfer curves (right) of the as-cast **Brush 1-4**

Brush 3 melt crystallized

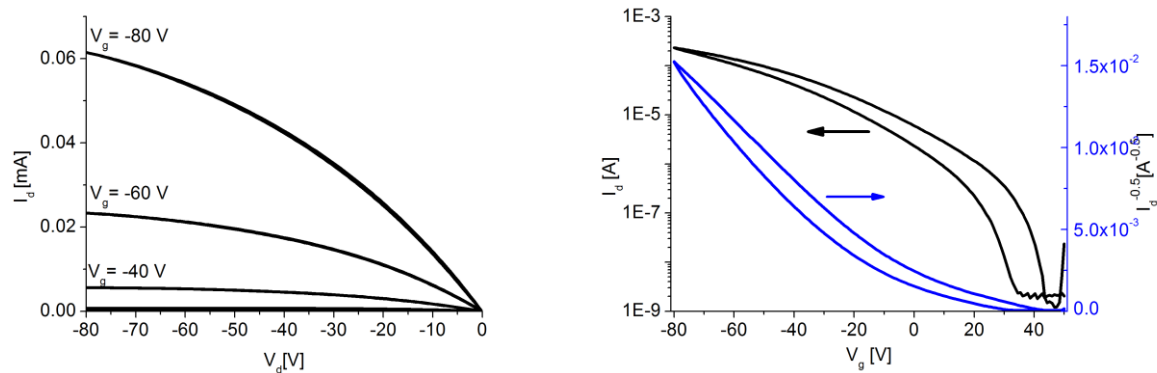


Fig. S 9 p-output curve (left) and p-transfer curve (right) of the melt crystallized **Brush 3**

2. References

- 1 R.H. Lohwasser and M. Thelakkat, *Macromolecules*, 2012, **45**, 3070.
- 2 A. Krasovskiy and P. Knochel, *Synthesis*, 2006, **5**, 0890.

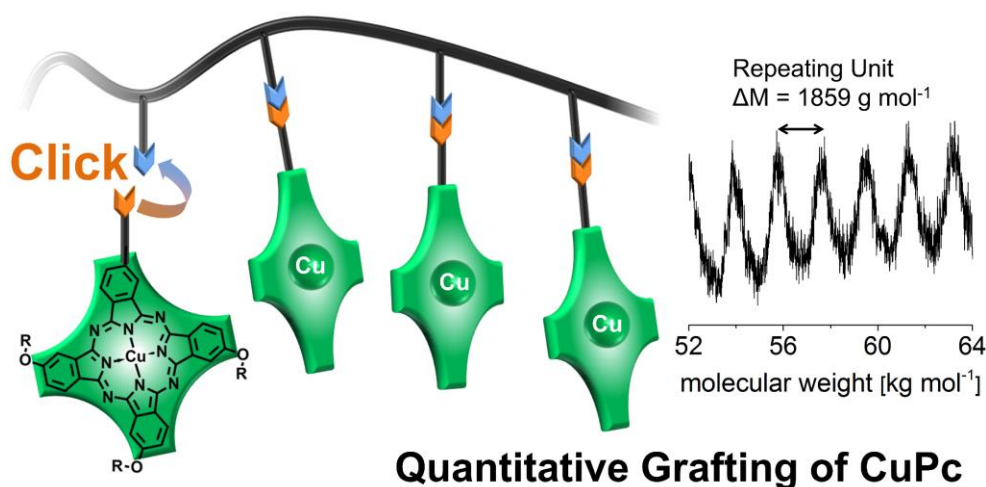
Densely Grafted Liquid Crystalline Copper Phthalocyanine Side Chain Polymer: Synthesis and Characterization

C. David Heinrich^a, Sinem Tuncel Kostakoğlu^{a,b} and Mukundan Thelakkat^{*a}

^a Applied Functional Polymers, Macromolecular Chemistry I and Bavarian Polymer Institute, University of Bayreuth, Universitätsstr. 30, 95440 Bayreuth, Germany.

^b Department of Chemistry, Gebze Technical University, 41400 Gebze, Turkey.

*E-mail of corresponding author: mukundan.thelakkat@uni-bayreuth.de



Published in *Journal of Material Chemistry C*,
Reproduced with permission from *J. Mater. Chem. C*, 2017, 5, 6259-6268.
Copyright 2017 The Royal Society of Chemistry

Abstract

A new polymeric donor material with pendant copper phthalocyanine side chains (**PCuPc**) was synthesized. The excellent suitability of a grafting-to approach, combining the controlled radical polymerization of propargyloxystyrene followed by “click” chemistry, was demonstrated. A polymer with a high molecular weight ($M_n = 88000 \text{ g mol}^{-1}$) and a narrow distribution $\mathcal{D} = 1.20$ was synthesized. FTIR and high resolution MALDI-ToF MS of **PCuPc** points towards quantitative grafting. The PCuPc is soluble in most of the commonly used solvents such as ethyl acetate, THF and acetone. The absorption behavior and electronic structure was investigated via UV-Vis spectroscopy and cyclic voltammetry. The thermal behavior could be elucidated via Flash-DSC and liquid crystalline behavior could be observed and confirmed via XRD and polarization microscopy. The bulk transport was determined by the SCLC method.

Introduction

The combination of controlled radical polymerization (CRP) and “click”-chemistry has been proved to be a highly versatile and robust way for the synthesis of novel highly defined polymeric materials.¹ Our group successfully applied this strategy in the synthesis of electronically active materials designed for applications in organic electronics and organic solar cells. We reported pendant side chain polymers,² block-copolymers³ and defined brush polymers.⁴ During our work we came to appreciate the comparability and versatility that arises from the modularity and high yield of grafting of this concept.⁴⁻⁶ The first step for the design of those materials is the synthesis of backbone polymers. These can be derivatives of standard thermoplastic polymers like polystyrene (PS) or polymethylmethacrylate (PMMA) which are accessible for the well-established types of CRP. Three methods, namely atom transfer radical polymerization (ATRP),⁷ reversible addition fragmentation chain transfer polymerization (RAFT)⁸ and nitroxide mediated radical polymerization (NMRP)⁹ are commonly used to control radical polymerizations. All three have in common that narrow distributions and a control over the molecular weight can be obtained by reducing the concentration of

active radical species during the poly-merization.¹⁰ By this, the amount of termination reactions, which would otherwise lead to ill-defined polymers with broad distributions, is drastically reduced. We chose NMRP for our study as it is well established for styrene derivatives and the synthesis of propargyloxystyrene has been previously optimized.⁵ Propargyloxystyrene, a styrene derivative with alkyne functionality in para-position of the styrene, can be coupled to organic azides via the copper-catalyzed azide-alkyne cyclo-addition (CuAAC). Since the concept “click-chemistry” was proposed in 2002¹¹ it has been widely used not only in biochemistry but also materials science.¹² The CuAAC, the copper catalyzed version¹³ of the Huisgen-reaction,¹⁴ is its most common representative and was instrumental in the recognition and spreading of the “click” concept. The extra-ordinary efficiency of this reaction, even at low temperature, makes it an excellent choice for polymer analogous reactions with high sterical demand.^{4,12}

Phthalocyanines (Pcs) are a long known class of macrocyclic compounds.¹⁵ Metal complexes of Pcs like the insoluble CuPc, also known as phthalocyanine blue, are widely used as blue or green pigments.¹⁶ The first reports on the synthesis of Pcs were published in the early 20th century¹⁵ and the semiconducting behavior has been known since 1948.¹⁷ In 1996 Pcs were used for the first time in organic photovoltaics (OPV) as the donor material in combination with fullerene as acceptor.¹⁸ Pcs were first used in vacuum deposited devices and optimized systems have reached power conversion efficiencies (PCEs) higher than 4 %.¹⁹ With solution-processible Pcs, which are desirable due the lower costs in device preparation by coating and printing methods, comparable PCEs could be achieved.²⁰ Very recently, de Oliveira *et al.* reported on water-gated phthalocyanine transistors showing that Pcs may also be interesting materials in bio electronics.²¹

One great benefit of using a polymeric semiconductor material is the superior film forming ability of polymers in comparison to small molecules. The synthesis of Pc semiconductor polymers carrying Pc as side chains via a grafting-to process utilizing CuAAC is therefore an attractive way to obtain such materials. Earlier, two materials synthesized in this way were reported, but only low grafting densities were targeted and thus obtained.²² A third report by López-Duarte *et al.* is the only one that claims a

densely grafted polymer.²³ There are indications of the successful grafting (IR- and UV-Vis spectroscopy) but neither the polymer characteristic (degree of polymerization and distribution) nor the structure formation were investigated. The ring opening metathesis polymerization (ROMP) of norbornene is a competing strategy towards defined functional polymers. The ROMP of functional norbornene monomers is a representative for a grafting-through process which inherently leads to densely grafted polymers.²⁴ A first report by Kimura *et al.* showed the shortcomings of this method though, as only oligomers could be synthesized.²⁵ Escoursa *et al.* could achieve higher molecular weights but were limited by the low solubility of the resulting polymers and similar to the first report only poor control was achieved which resulted in a rather high dispersity of the polymers ($\text{Đ} > 2$).²⁶ The solubility of Pcs can be tuned by the substitution of the PC-core with different side-groups. Both symmetrical and asymmetrical PCs, substituted with oligo ethylene glycol substituents, were reported.²⁷ Our goal therefore was to establish a way to synthesize Pc side chain polymers with high grafting density, high solubility as well as a defined molecular weight.

Here we report the synthesis and characterization of a highly soluble, hydrophilic semiconductor using grafting-to of an unsymmetrical copper phthalocyanine derivative with azide functionality (**CuPc-N₃**) to a styrene backbone. The hydrophilic swallow tail oligo ethylene glycol substituents allow the processing of the material from eco-friendly solvents such as THF, ethyl acetate etc. Additionally, this material is an interesting candidate for applications in bioelectronics.

Experimental Section

Materials and Methods

CuBr (> 98%), CuCl₂ (99%), mesyl chloride (> 99.7%), N,N,N', N'',N''-pentamethyldiethylenetriamine (PMDTA, 99%), sodium azide and trimethylamine (> 99%) were purchased from Sigma-Aldrich, N,N-dimethylaminoethanol (DMAE, > 98%) and tetra-butylammonium fluoride trihydrate (TBAF, > 98%) were purchased from Fluka. 4-(6-hydroxyhexylsulfanyl)-1,2-dicyanobenzene²⁸ and 4-{2-[2-(2-ethoxyethoxy)-ethoxy]-1-[2-((2-ethoxy-ethoxy)ethoxy)ethoxymethyl]ethoxy}-1,2-dicyanobenzene,²⁹ 4-(3'-trimethylsilylpropargyloxy)styrene,^{30,5} *N-t-butyl-O*-[1-[4-(chloromethyl)phenyl]-ethyl]-*N*-(2-methyl-1-phenylpropyl)-hydroxylamine³¹ and 2,2,5-trimethyl-4-phenyl-3-azahexane-3-nitroxide³¹ were synthesized according to published procedures. A CuBr/PMDTA stock solution was prepared for the CuAAC reaction. For this a dry Schlenk flask was charged with CuBr (50 mg, 0.35 mmol) and 5 mL 1,2-dichlorobenzene and the solution was degassed with N₂ for 20 min and degassed PMDTA (60 mg, 0.35 mmol) was added. ¹H-NMR (300 MHz) spectra were recorded on a Bruker AC 300 spectrometer and calibrated to the solvent peak (CDCl₃, δ = 7.26 ppm). Fourier transform infrared (FTIR) spectra were recorded on a Perkin Elmer Spectrum 100 FTIR spectrometer in attenuated total reflection (ATR) mode. Differential scanning calorimetry measurements were prepared on a Mettler Toledo Flash 1 under continuous nitrogen flow. Thermogravimetric measurements were performed on a Netzsch STA 409 C at a heating rate of 10 K min⁻¹ under nitrogen. Absorption measurements were carried out on a JASCO V-670 spectro-photometer. Optical properties in solution were measured in DCM at a path length of 10 mm; films were spin-coated onto glass slides from a 7.4 mg mL⁻¹ chloroform solution at 1500 rpm. Size exclusion chromatography (SEC) measurements were carried out in THF with two Varian MIXED-C columns (300 x 7.5 mm) at room temperature and at a flow rate of 0.5 mL min⁻¹ using a UV (Waters model 468) detector with 254 nm wavelength. The SEC was calibrated with polystyrene as external standard and 1,2-dichlorobenzene as internal standard. MALDI-ToF mass spectra were recorded on a Bruker Reflex III with

dithranol as matrix. All WAXS data reported here were measured using the x-ray system “Double Ganesha AIR” (SAXSLAB, Denmark). The x-ray source of this laboratory-based system is a rotating anode (copper, MicoMax 007HF, Rigaku Corporation, Japan) providing a micro-focused beam at $\lambda = 0.154$ nm. The data are recorded by a position sensitive detector (PILATUS 300K, Dectris). To cover the range of scattering vectors between 0.05 - 22.5 nm⁻¹ different detector positions were used. Cyclic voltammetry was carried out under moisture- and oxygen-free conditions using a standard three-electrode assembly connected to a potentiostat and a PC at a scanning rate of 100 mV s⁻¹. The working electrode was a solid Pt electrode (cross-section area 0.0314 cm², AMETEK Advanced Measurement Technology). A platinum wire in DCM with conducting salt was used as counter electrode and the quasi-reference electrode consisted of a silver wire and AgNO₃ in acetonitrile (0.1 M). Tertbutylammoniumhexafluorophosphate (Bu₄NPF₆) was used as conducting salt (0.1 M) and DCM as solvent. Each measurement was calibrated against the internal standard ferrocene/ferrocenium. The values of the ionization potential and the electron affinity are calculated from the half wave potential of the first oxidation or the first reduction respectively according to Gräf *et al.*:³²

$$E^{\text{IP}}(\text{X}) = \left[-e \left(E_{\text{ox1}}^{1/2}(\text{X vs. Ag/AgNO}_3) - E_{\text{ox1}}^{1/2}(\text{Fc/Fc}^+ \text{ vs. Ag/AgNO}_3) \right) \right] + E^{\text{IP}}(\text{Fc/Fc}^+ \text{ vs. zero vacuum level}) \quad (1)$$

$$E^{\text{EA}}(\text{X}) = \left[-e \left(E_{\text{red1}}^{1/2}(\text{X vs. Ag/AgNO}_3) - E_{\text{ox1}}^{1/2}(\text{Fc/Fc}^+ \text{ vs. Ag/AgNO}_3) \right) \right] + E^{\text{IP}}(\text{Fc/Fc}^+ \text{ vs. zero vacuum level}) \quad (2)$$

X: measured compound; $E_{\text{ox1}}^{1/2}/E_{\text{red1}}^{1/2}$: half-wave potential of the 1st oxidation/reduction potential; $E^{\text{IP}}(\text{Fc/Fc}^+ \text{ vs. zero vacuum level}) = -5.16$ eV: value of the ionization potential of ferrocene vs. vacuum level in DCM.

Device Preparation and Characterization

Single carrier space-charge-limited-current (SCLC) devices in diode configuration were prepared for charge carrier mobility determination of holes within the layer stack of glass/ITO/PEDOT:PSS/Polymer/Mo/Au. A hole-injecting layer of PEDOT:PSS (HTL solar (38 nm) from Clevios) was spin coated onto cleaned patterned ITO glass

substrates. The polymer solution (3.25 mg mL⁻¹ in chloroform) was doctor bladed on top, with different blade speeds (A higher blade speed will result in a thicker film.), under inert conditions resulting in film thicknesses in the range of 150 – 500 nm. The thickness was measured after the measurements of the *I*-*V* characteristics with a Veeco Dektak 150 profilometer. Subsequently, MoO₃ and the top Au electrodes were thermally evaporated onto the polymer layer under high vacuum. The devices had an active area of 9 mm² which is determined by the overlap of the ITO and the evaporated top electrode. Dark current-voltage *I*-*V* measurements were made under inert environment at room temperature with a Keithley 2400 source measure unit. For mobility evaluation, forward bias voltages, that is, hole injection from PEDOT:PSS were considered. The charge carrier mobilities were evaluated by fitting measured *I*-*V* characteristics in a voltage range from 2 to 8 V using the Murgatroyd formula.³³ Prior to fitting, the measured *I*-*V* characteristics were corrected for the built in voltage (*V*_{bi}) and the voltage drop (*IR*) across contacts.

Synthesis

CuPc-OH A mixture of 4-{2-[2-(2-ethoxyethoxy)ethoxy]-1-[2-((2-ethoxyethoxy)ethoxy)ethoxymethyl] ethyloxy}-1,2-dicyano-benzene (2.35 g, 5.2 mmol), 4-(6-hydroxyhexyl-sulfanyl)-1,2-dicyanobenzene (153 mg, 0.58 mmol) and anhydrous CuCl₂ (522 mg, 3.9 mmol) were refluxed in anhydrous N,N-dimethylaminoethanol (10 mL) for 24 h under argon atmosphere. N,N-dimethylaminoethanol was removed by adding hexane to the reaction mixture, the crude product was precipitated. The solid was dissolved in dichloromethane, filtered to remove inorganic impurities, and then concentrated. The crude product was purified by column chromatography over silica gel using dichloromethane:ethanol 25:1 and then dichloromethane:ethanol 10:1 as eluent. The desired phthalocyanine was obtained as green solid. 120 mg (12%). C₈₃H₁₁₈N₈O₂₂SCu, M_w = 1675.48 g mol⁻¹. MALDI-ToF-MS (matrix DHB): *m/z* 1675.6 [M]⁺, 1698.6 [M+Na]⁺. IR (ATR): ν (cm⁻¹) 3400 (OH), 3040 (ArCH), 2985-2860 (CH₂, CH₃), 1654 (C=N), 1608 (ArC=C), 1507, 1472, 1400, 1345, 1278, 1233, 1120-1085 (C-O-C).

CuPc-Mes CuPc-OH (230 mg, 0.14 mmol) and triethylamine (2 mL, 14.4 mmol) were stirred in dichloromethane (10 mL) in an ice bath, then mesyl chloride (1 mL, 12.9 mmol) was added dropwise over 10 min. The stirring continues overnight at room temperature. The reaction mixture was washed by a dilute solution of potassium carbonate and subsequently with water. The organic phase was dried on sodium sulfate, concentrated and loaded on a silica gel column for chromatography (eluent: dichloromethane then dichloro-methane/ethanol with increasing polarity). The desired phthalocyanine was obtained as green solid. 210 mg (87%). $C_{84}H_{120}N_8O_{24}S_2Cu$, $M_w = 1753.57 \text{ g mol}^{-1}$. MALDI-ToF-MS (matrix DHB): m/z 1753.85 [M]⁺. IR (ATR): ν (cm^{-1}) 3070 (ArCH), 2974-2864 (CH_2 , CH_3), 1608 (C=N), 1507 (ArC=C), 1481, 1398, 1344, 1231, 1174 (S=O), 1098 (C-O-C).

CuPc-N₃ CuPc-Mes (210 mg, 0.12 mmol) and NaN₃ (31 mg, 0.48 mmol) were stirred in 10 mL DMF at 80 °C overnight. Water was added to the cooled reaction mixture and the resulting precipitate was filtrated, recovered in dichloromethane and purified by a silica gel column chromatography (eluent: dichloromethane then dichloromethane/ethanol with increasing polarity). The desired phthalocyanine was obtained as green solid. 195 mg (96%). $C_{83}H_{117}N_{11}O_{21}SCu$, $M_w = 1700.49 \text{ g mol}^{-1}$. MALDI-ToF-MS (matrix DHB): m/z 1700.48 [M]⁺. IR (ATR): ν (cm^{-1}) 3072 (ArCH), 2966-2862 (CH_2 , CH_3), 2094 (N=N), 1606 (C=N), 1510 (ArC=C), 1477, 1398, 1344, 1261, 1240, 1099 (C-O-C).

PPOS 2.75 g 4-(3'-trimethylsilylpropargyloxy)styrene (11.9 mmol), 51.8 mg *N*-*t*-butyl-*O*-[1-[4-(chloromethyl)-phenyl]-ethyl]-*N*-(2-methyl-1-phenylpropyl)hydroxylamine (159.0 μmol) and 5.2 mg 2,2,5-trimethyl-4-phenyl-3-azahexane-3-nitroxide (15.9 μmol) were dissolved in 1.5 mL *o*-DCB monomer and degassed by three freeze-pump-thaw cycles. The polymerization was started by the immersion of the reaction vessel in a 125 °C warm oil bath. The reaction was quenched by cooling in liquid nitrogen after 326 min and precipitated into cold methanol twice from a concentrated THF solution. The protected polymer was dissolved in 5mL THF, cooled to 0 °C and degassed by purging with nitrogen. 5ml of a degassed solution of 2.1 g tetrabutylammonium fluoride trihydrate (6.5 mmol) and 0.4 mg of acetic acid (6.5 mmol) in THF were added via syringe. The mixture was stirred overnight and the

polymer was precipitated in methanol twice from a concentrated THF solution. 500 mg, $M_{n,SEC} = 7500 \text{ g mol}^{-1}$, $M_{p,SEC} = 9100 \text{ g mol}^{-1}$, PDI = 1.21. $^1\text{H NMR}$ (300 MHz, CHCl_3): δ (ppm) 6.9–6.18 (br, 4H), 4.63 (s, 2H), 2.52 (br, 1H), 1.79–0.92 (br, 3H). IR (ATR): $\nu(\text{cm}^{-1})$ 3286 ($\text{C}\equiv\text{C-H}$), 2120 ($\text{C}\equiv\text{C}$).

PCuPc A dry round bottom flask was charged with 18.5 mg (117.6 μmol alkyne groups) propargyloxystyrene (PPOS), 230 mg (135.3 μmol) CuPc- N_3 and 5 mL DCM. The solution was degassed by four freeze-pump-thaw cycles and 0.1 mL of the CuBr/PMDTA stock solution were added. The reaction vessel was immersed into a 35 $^\circ\text{C}$ warm oil bath. The mixture was filtered over a short aluminum oxide column to remove the catalyst and dialyzed against methanol for 11 days. The polymer was precipitated from a concentrated solution into diethyl ether. The precipitate was obtained by centrifugation and washed several times with diethyl ether. The purified product was dissolved in benzene, after a second precipitation, centrifugation and washing step, and obtained as green solid after freeze drying. 128 mg (58%) of the pure product were obtained. $M_{n,SEC} = 56800 \text{ g mol}^{-1}$; $\text{Đ} = 1.26$; $M_{n,MALDI} = 88000 \text{ g mol}^{-1}$; IR (ATR): $\nu(\text{cm}^{-1})$ 2862, 1607, 1508, 1231, 1099.

Results and Discussion

Synthesis

With the powerful tool of “click”-chemistry in hand, we were able to synthesize a new grafted donor polymer with copper phthalocyanine as donor units. Synthetically we were interested whether the extraordinarily bulky copper phthalocyanine azide (**CuPc-N₃**) could be grafted to a polymer backbone with sufficient yields via CuAAC. Poly(4-propargyl-oxystyrene) (**PPOS**) was chosen as a suitable backbone polymer comparable to the one of the grafted poly perylene bisimides synthesized in our group.⁵ The solubility of the educts and the product plays a crucial role for the grafting to be successful and quantitative. The **CuPc-N₃** with three swallow-tail oligo ethylene side chains is therefore an excellent candidate for our study. This compound is soluble in most solvents including water. We were confident that this would be the basis for a high solubility of the grafted polymer and that this would ensure a good solubility and accessibility of the active sites throughout the grafting-to “click” reaction. The CuAAC was conducted under very mild conditions in DCM at 35 °C with CuBr/PMDTA used as catalyst system (**Scheme 1**). The success of the reaction was proven with SEC after a reaction time of 24 h. The peak at 9000 g mol⁻¹ (**PPOS**) disappeared and was shifted to considerably higher molecular weights. The narrow monomodal distribution was first an indicator of the successful grafting. The raw product was still contaminated with **CuPc-N₃** which was used in slight excess, but the extraordinary solubility of the CuPC units resulted in a grafted polymer which is soluble in solvents such as acetone, chloroform, DCM, DMF, ethyl acetate and THF. Thus, unlike many reported semiconductor polymers, this polymer is soluble in a number of non-halogenated solvents. Additionally, its solubility (> 1 wt %) in technologically relevant processing solvents such as ethyl acetate and THF allows environmentally benign processing conditions. First attempts to purify the polymer via dialysis proved to be ineffective. Among the common solvents only water and diethyl ether were found to be only solvents in which the polymer could be precipitated from a concentrated solution. Precipitation in diethyl ether was not optimal as the polymer precipitated as an extremely fine powder which could not be filtrated. Only by a combination of several precipitations in diethyl ether in combination with centrifugation,

Table 1 Molecular weight, thermal, optical and electrochemical properties of **PPOS** and **PCuPc**

	$M_{p,SEC}$ [g mol ⁻¹]	\bar{D}	$M_{n,calc}^a$ [g mol ⁻¹]	$M_{n,MALDI}$ [g mol ⁻¹]	T_{dec}^b [°C]	T_g^c [°C]	T_m^d [°C]	T_c^d [°C]	$E_{g,fund}^e$ [eV]	IP^e [eV]	EA^e [eV]
PPOS	9100	1.20			416	55					-
PCuPc	56800	1.20	102000	88000	315		314	270	1.66	-5.40	3.74

^a Theoretical molecular weight calculated with a degree of polymerization of **PPOS** of 55 under the assumption of a quantitative grafting. ^b Decomposition onset measured via thermogravimetric analysis under N₂ atmosphere. ^c Measured by differential scanning calorimetry at 10 Kmin⁻¹ under N₂ atmosphere. ^d Measured by differential scanning calorimetry at 1000 Ks⁻¹ under N₂ atmosphere. ^e Calculated with equation (1) and (2) from the half-wave potential of the first oxidation/reduction

We believe that the discrepancy between the calculated value and the experimentally obtained one is not an effect of non-quantitative grafting but rather an artifact from the mass spectrometry itself. Even though the dispersity of the polymer is fairly low it is close to what is considered a broad distribution for MALDI-ToF ($\bar{D} > 1.2$). MALDI-ToF measurements of polymers with higher dispersities exhibit underestimated molecular weights as the low molecular weight fractions are preferentially ionized.³⁴ Additionally, the expected molecular weight of **PCuPc** is already at the upper limit of this technique but the resolution of the mass spectrum is still high enough to detect the repeating units of the polymer. By measuring the difference between two peaks a value of 1859 g mol⁻¹ is obtained which is almost exactly the expected value for the Pc repeating unit. This observation of a single peak series is only possible in case of a nearly quantitative grafting leading to each repeat unit carrying a Pc unit. If the grafting was lower the difference between the two peaks would not only be lower but the

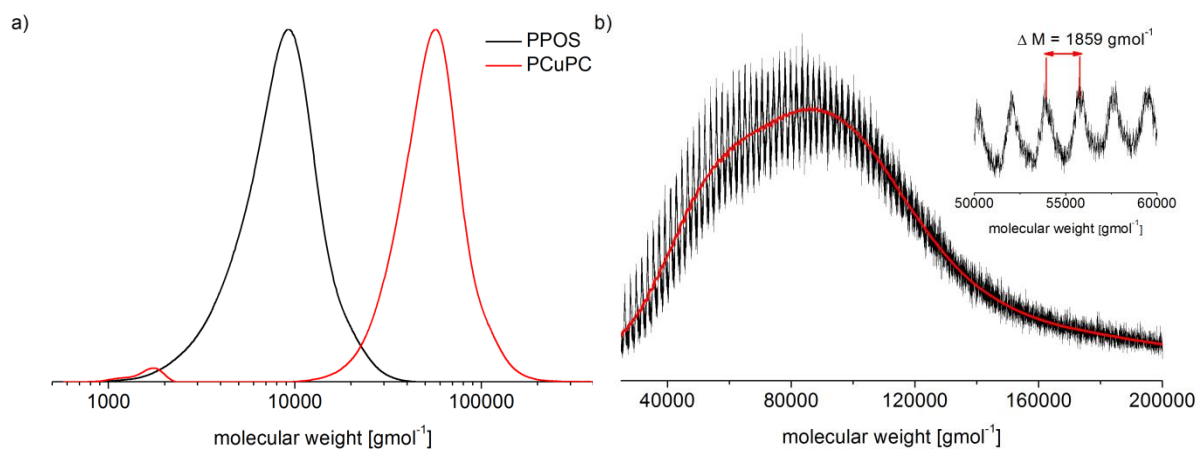


Fig.1 a) SEC curves of the precursor polymer PPOS and the grafted polymer PCuPC after purification, b) MALDI-ToF MS of PCuPC with observable repeating units (inlet).

repeating units would certainly not be observable anymore. A grafting of 85 %, as indicated by the peak molecular weight, would not result in phthalocyanine groups being attached to 85 % of the active sites in every chain but rather to a distribution of chains with higher and lower grafting densities. In effect this would blur the peaks of the repeating units and only the overall weight distribution would be observable.

The strong line broadening impedes a reasonable characterization via $^1\text{H-NMR}$ (Fig. S1, ESI). IR-spectroscopy on the other hand can be applied to monitor the presence of alkyne and azide groups. The absence of the vibrational bands of both functionalities (N_3 at 2095 cm^{-1} and alkyne at 3290 cm^{-1}) in the spectrum of **PCuPC** (Fig. 2) is another evidence for the purity of the polymer (absence of N_3) as well as the successful quantitative grafting (absence of alkyne).

Optical and Electrochemical Characterization

The UV-Vis spectra of porphyrins - phthalocyanines are nitrogen-substituted derivatives of this class of macrocycles - consist of two distinct sets of peaks. In the region between 300-500 nm the Soret- or B-bands can be observed which are ascribed to the $S_0 \rightarrow S_2$ transition.³⁵ The Q-bands which are ascribed to the $S_0 \rightarrow S_2$ transition are shifted to considerably higher wavelengths. The position, quantity and relative intensities of the Q-bands are strongly influenced

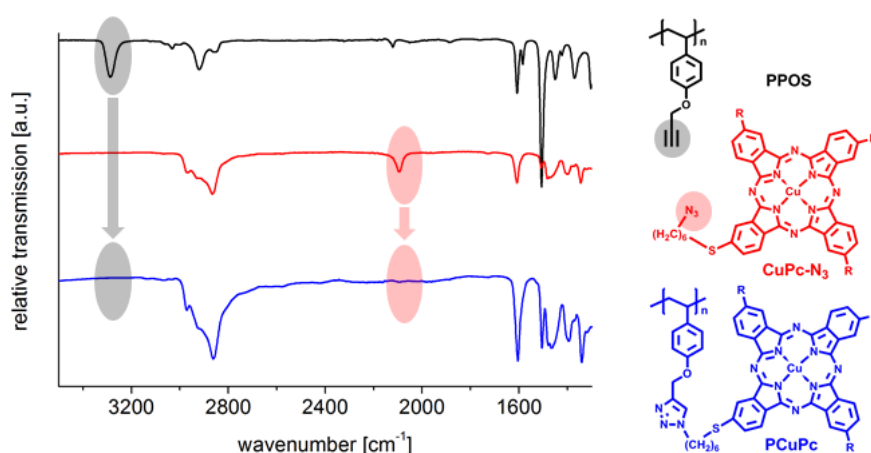


Fig. 1 IR spectra of the precursors PPOS (black) and CuPc-N_3 (red) and the grafted polymer PCuPC (blue). The band at 3290 cm^{-1} which is present in PPOS and is assigned to the alkyne (gray ellipse) cannot be detected in PCuPC. Similarly, the band at 2095 cm^{-1} which is present in CuPc-N_3 and is assigned to the azide (red ellipse) can also not be detected in PCuPC.

by the symmetry of the molecule, whether or not the macrocycle is complexed by a metal cation, and by the nature of the complexing metal.³⁶ The solution spectrum in DCM of the CuPc derivative **CuPc-N₃** used in this study has two Soret-bands at 339 nm and 394 nm. The Q-bands can be observed at 615 nm and 685 nm with the lower energy transition showing a considerably higher absorption (**Fig. 3a**). This is the expected spectrum for a CuPc in a good solvent i.e. the molecules are fully dissolved and in their non-aggregated state.³⁷

The solution spectrum of **PCuPc** is very similar compared to **CuPc-N₃** in the Soret-band region (334 nm and 394 nm) but shows a distinctly different behavior in the Q-band region. The position of the peak maxima is shifted slightly (629 nm and 680 nm) but even more noticeable is the change in peak intensities. Whereas the lower energy transition in **CuPc-N₃** has a nearly 4 times stronger absorption than the higher energy Q-band, the ratio in **PCuPc** is nearly 1:1 with the lower energy transition being the one with the smaller absorption. This behavior can be explained by the formation of H-aggregates formed by π - π -stacking of the phthalocyanine side chain units.³⁸ We propose that this aggregation is observed due to the forced proximity of the phthalocyanine units which are densely grafted to the polymer backbone. This assertion can be validated by measuring the polymer at different concentrations (**Fig. S2**, ESI). We observed no concentration dependence of the **PCuPc** spectra in DCM which is indicative of intra-molecular aggregation unlike **CuPc-N₃**. Additionally, **PCuPc** was measured in thin film in order to get first indications whether any additional

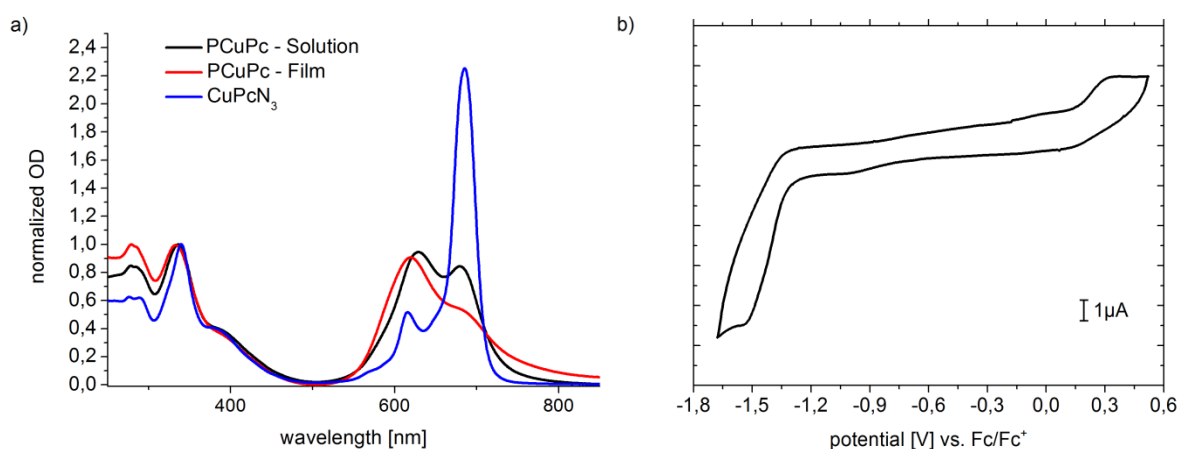


Fig. 2 a) UV-Vis Spectra of PCuPc in solution (DCM) and in thin film in comparison to the phthalocyanine monomer CuPc-N₃, b) cyclic voltammetry of PCuPc in DCM.

aggregation can be observed in the solid state. Again the only changes were observed for the Q-bands. The peak maxima are observed at 618 nm and 680 nm and the lower energy peak is further reduced in intensity in comparison to the spectrum in solution. The aggregation in thin films is therefore increased in relation to the solution and it can be expected that at least some kind of order is present in the solid state. We will address this question further in the next part after we have a look at the electronic structure of **PCuPc**. Cyclic voltammetry was performed to study the redox process of **PCuPc** and to approximate the fundamental gap $E_{g,\text{fund}}$ which relates to the energy difference between the ionization potential IP and the electron affinity EA.³⁹ We could observe both the first oxidation and the first reduction of **PCuPc** in DCM solution. The first oxidation was observed at a half wave potential of $E_{\text{Ox}}^{1/2}(\text{PCuPc vs. Ag/AgNO}_3) = 240$ mV and the first reduction was observed at a half wave potential of $E_{\text{Red}}^{1/2}(\text{PCuPc vs. Ag/AgNO}_3) = -1420$ mV. With equation (1) and (2) in the methods section we can calculate the ionization potential IP and the electron affinity EA in relation to the vacuum level. IP was determined to be -5.40 eV and EA -3.70 eV, respectively. The difference between these two represents the fundamental gap $E_{g,\text{fund}} = 1.66$ eV. The value of the fundamental gap is very good agreement with reported values on no polymer bound CuPcs.⁴⁰

Structure and Thermal Properties

The high complexity of the grafted polymer on the one hand with its very bulky and sterically demanding side groups and on the other hand dense grafting of discotic-type units as side chains offer an interesting system in terms of structural order/disorder. Therefore, we were interested in the question whether some kind of order/periodicity in structure could be observed. We also had first indications of a stacking of the side chain units in solid state. Thermogravimetric analysis (TGA) was conducted first to probe the thermal stability of the system. We could determine the onset of degradation at a heating rate of 10 K min⁻¹ under inert atmosphere to be 315 °C (**Fig. 4a**). The weight loss in the first step (40 wt % at about 300°C) corresponds to the same weight

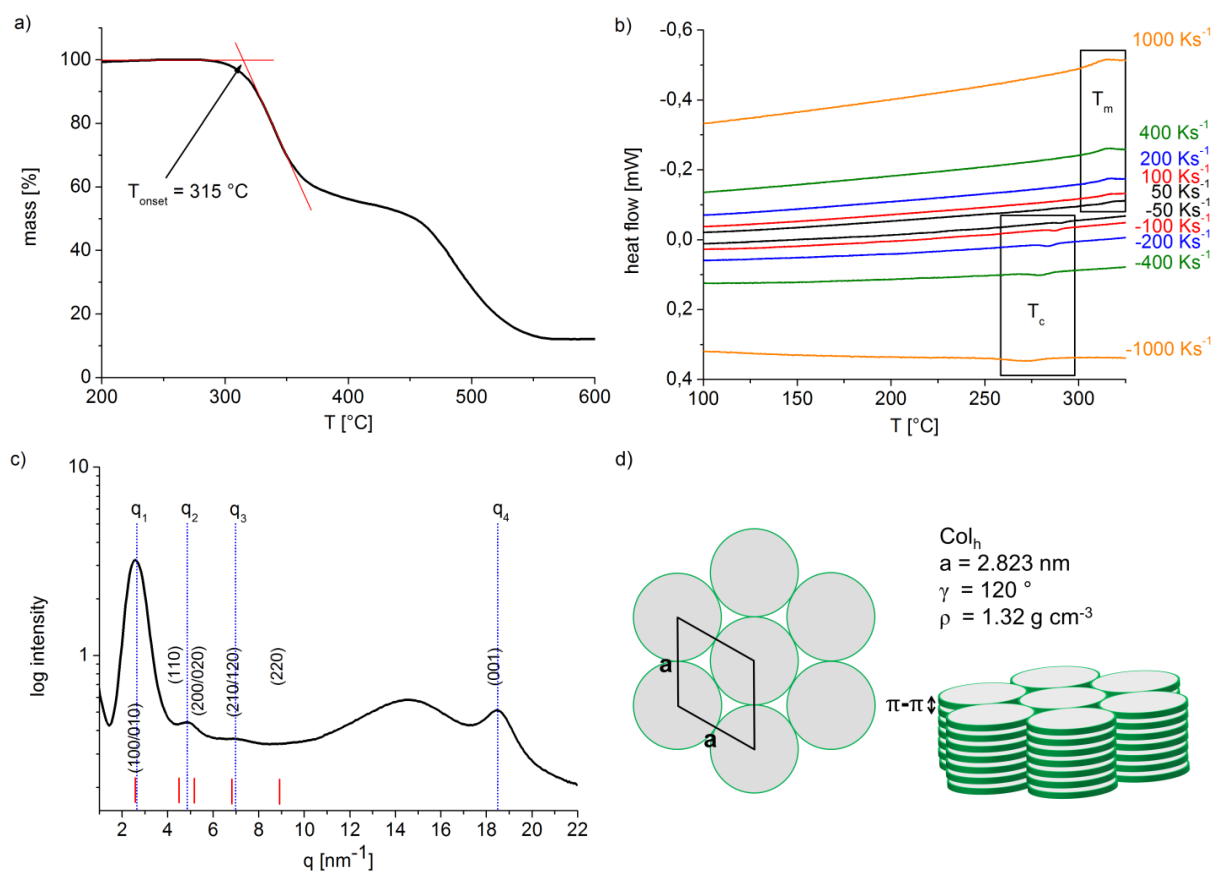


Fig. 3 a) Thermal stability of PCuPC obtained via TGA at 10 K min^{-1} under N_2 atmosphere. b) DSC curves of PCuPC at K s^{-1} measured via Flash-DSC. (c) Diffraction pattern of the hexagonal mesophase (Col_h) of PCuPC measured at room temperature with the calculated reflection positions indicated by the red bars. (d) Illustration of the lattice and the main parameters.

percentage as of OEG side chains and therefore, is most likely due to the decomposition of the OEG side chains. This is also supported by the fact that polyethylene glycol decomposes at about 300 °C with a mass loss of 100%. The second major step of decomposition happens above 450 °C with a mass loss of 40 wt%. This can be attributed to decomposition of the CuPc pendant groups. Secondly, we tried to access the phase transition temperatures with a standard DSC measurement at a 10 K min^{-1} heating rate. Within the accessible range below the degradation temperature no transitions could be observed even though birefringence was found with polarization microscopy (**Fig. S3**, ESI), which indicated the existence of an ordered phase at room temperature. Hence we were certain that some kind of phase transition should be observable. We therefore switched to a Flash-DSC which allows measurements with extremely high

heating rates up to several thousand K s^{-1} .⁴¹ These heating rates can be realized by reducing the sample size to just a few nanograms. While this technique was developed to probe the kinetics of phase transitions, we use the fact that stress on the material is very low due to the very short time that the sample is subject to high temperatures. This makes it possible to even measure phase transitions that are above the decomposition temperature at normal conditions. The measured DSC curves at heating rates from $50 - 1000 \text{ K s}^{-1}$ are plotted in **Fig 4b**. We were now able to detect first order phase transitions above $300 \text{ }^\circ\text{C}$. The melting transition at a heating rate of 1000 K s^{-1} is as high as $314 \text{ }^\circ\text{C}$ and crystallization is observed during cooling at $270 \text{ }^\circ\text{C}$. The nature of the ordered phase at room temperature was investigated via wide angle X-ray scattering (WAXS) with a q range of about $q \approx 1\text{-}22 \text{ nm}^{-1}$. The structure above the transition temperature was not accessible due to the same reasons as for the standard DSC measurements. However, the diffraction pattern of the **PCuPc** at room temperature (**Fig. 4c**) clearly exhibits three peaks in the low q region till 10 nm^{-1} , one very broad peak in the range of $10 - 20 \text{ nm}^{-1}$ and an additional peak at 18.50 nm^{-1} . A structure model was obtained by the following considerations. The presence of a low number of broad peaks and absence of further peaks is indicative of a liquid crystalline mesophase. As the formation of columnar π - π -stacking is commonly observed for disc-like mesogenes, such as phthalocyanines, we investigated if such a structure could explain the observed pattern. Additionally, the fact that the order is mainly expected in the lateral direction, with a more liquid-like packing along the stacking direction, makes it possible to describe the system by a 2D model.

We started with the system showing the highest symmetry, which is the hexagonal one. The unit cell of a hexagonal 2D lattice is defined by the lattice constant a and the angle $\gamma = 120 \text{ }^\circ$. The q -values q_{hk0} for different miller indices can be calculated as follows:

$$q_{hk0} = 2\pi \sqrt{\frac{4}{3} \left(\frac{h^2 + k^2 + hk}{a^2} \right)} \quad (3)$$

The lattice constant \mathbf{a} was determined from the first peak q_1 under the assumption that it represented the (100) reflection of the hexagonal unit cell. The lattice constant was calculated for a value of $\mathbf{a} = 2.823$ nm. The higher reflections in a hexagonal system are expected at $\sqrt{3}q_1$, $\sqrt{4}q_1$ and $\sqrt{7}q_1$.⁴² All calculated reflexes are indicated in **Fig. 4d** by red bars. It can be seen that there is a very good agreement of calculated positions and the observed pattern. The appearance of the (110) and the (200)/(020) reflexes as only one is most likely due to overlap as result of the peak broadening. The broad peak at $10 - 20$ nm⁻¹ represents the amorphous parts of the polymer. The reflex with the highest q -value can be assigned to the π - π -stacking and the position relates to a stacking distance of 0.34 nm. The validity of our model is ultimately determined by calculation of the crystallographic density:

$$\rho = \frac{nM}{N_A a^2 c \sin \gamma} \quad (4)$$

In our case the molar weight M is the molecular mass of the repeating unit ($M = 1858.69$ g mol⁻¹), N_A is the Avogadro's constant and $n = 1$ is the number of molecules within the unit cell. A reasonable density value of $\rho = 1.32$ g cm⁻³ was obtained. The room temperature mesophase of **PCuPc** is therefore determined to be columnar hexagonal Col_h although the strong broadening of the reflexes indicates lack of perfect order. The existence of the Col_h mesophase is also in good agreement with the structure of the CuPc moiety itself. XRD and polarization microscopy reveal the existence of a room temperature Col_h mesophase for **CuPc-OH** (**Fig. S4**, ESI).

Space Charge Limited Current Mobility (SCLC)

We measured the I-V characteristics of hole-only devices with different thicknesses to extract the mobility in bulk in the space charge limited current regime. The determination of the mobility values requires the fitting of the measured curves. We used the empirical Murgatroyd (**Equation 5**) formula, which considers a field dependence of the mobility in the SCLC regime.

$$J = \frac{9}{8} \epsilon_r \epsilon_0 \mu_0 e^{0.89} \gamma_L^{\frac{V}{L}} \frac{V^2}{L^3} \quad (5)$$

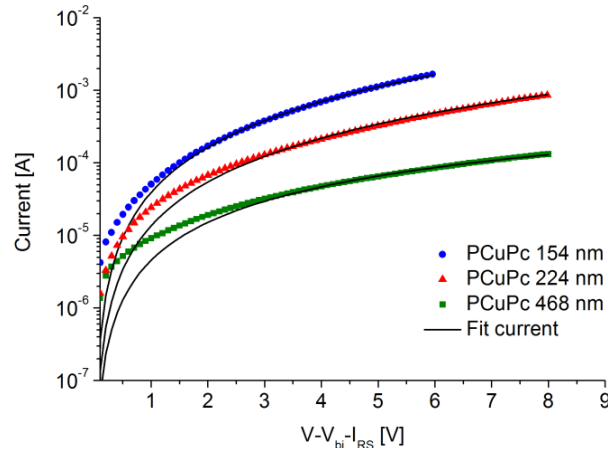


Fig. 4 I-V characteristics of as-cast films of **PCuPc** measured at room temperature. The I-V characteristics were corrected for the built in voltage (V_{bi}) and the voltage drop (IR) over the contacts.

The current density J is measured against the voltage V . The semi-log plots of J vs. V indicate a V^2 dependency regime and for different thicknesses a L^{-3} dependence of J is observed (**Fig. 5**). The relative permittivity ϵ_r (~ 3.5), the vacuum permittivity ϵ_0 and the thickness of the polymer film L are fixed parameters. The I-V curves are fitted with the zero field mobility μ_0 and the empirical parameter γ in the range of space charge limited transport which is characterized by $J \sim V^2$. The log-log plot of the I-V shows that no slopes greater 2 are observed which are indicative of trap limited transport (**Fig. S5a**, ESI).⁴³ In contrast to other reports on the mobility of PCs measured in diode configuration we only observed true SCLC behavior for **PCuPc**.⁴⁴ This was validated by the aforementioned quadratic dependency of the current density on the voltage but also cubic on the inverse active layer thickness ($J \sim \frac{1}{L^3}$) (**Fig. S5b**, ESI). We therefore assured the reproducibility and validity of the calculated mobility values for three devices with a different active layer thickness (**Table S1**, ESI). For reporting the bulk mobility of **PCuPc** in a consistent way, we determine an effective mobility μ at the same electric field ($F = \frac{V}{L} = 1.5 \cdot 10^7 \text{ Vm}^{-1}$) as given by the Poole-Frenkel relationship (**Equation 6**).

$$\mu = \mu_0 e^{\gamma \frac{V}{L}} \quad (6)$$

The relative mobility for **PCuPc** was determined to be $5.3 \cdot 10^{-6} \text{ cm}^2 \text{ V}^{-1} \text{ s}^{-1}$. This value is lower than reported values on low molecular liquid crystalline CuPc and ZnPc, but no true SCLC behavior was observed in those cases.⁴⁴ Many of the reported SCLC values do not verify the presence of SCLC regime or L^{-3} dependence. The main charge transport channel in such a material will occur along the π - π stacking direction. A columnar liquid crystal provides an efficient and flexible conduction pathway along the column. Even though the hydrophilic swallow tails improve the solubility and is required for processing the materials, it does not contribute towards electronic charge transport. Thus OEG substituents and main chain polystyrene which are insulating materials dilute the amount of the electronically active Pc core. This can lower the charge carrier mobility.⁴⁵

Conclusions

We have synthesized a new phthalocyanine donor polymer in which Pc moieties are densely grafted to a polystyrene backbone and observed the high efficiency of the grafting process via CuAAC. We were therefore able to synthesize a defined functional polymer ($\mathcal{D} = 1.20$) with high molecular weight (88000 g mol^{-1}). The high solubility of both the azide and the polymer was essential for the almost quantitative grafting which in turn is responsible for the observed structure formation. Surprisingly, we could obtain a good quality MALDI-ToF spectrum with a resolution of the repeating units. We found that **PCuPc** forms intramolecular aggregates in solution due to the forced proximity of the phthalocyanine side chains. Bulk studies revealed the liquid crystalline nature of the polymer which forms a Col_h phase. A phase transition could be observed only at high temperatures, with Flash-DSC at ultra-fast heating rates. Measurements of the space charge limited current of the material in a diode setup exhibited rather low bulk hole-mobilities of $5.3 \cdot 10^{-6} \text{ cm}^2 \text{ V}^{-1} \text{ s}^{-1}$. We believe that this material is an interesting candidate for applications in bioelectronics and currently we are testing its applicability for organic electrochemical transistors (OECTs).

Acknowledgements

We thank Dr. Martin Dulle (PC I, University of Bayreuth) for the XRD measurement, Hubertus Burchardt and Martin Hufnagel for the MALDI-ToF measurements, Tina Weller for the DSC measurement and Dr. Chetan R. Singh for help with the SCLC measurements. We acknowledge funding from the Bavarian State Ministry of Education, Science and the Arts under the program “Solar technologies go hybrid” (SolTech). Sinem Tuncel Kostakoğlu gratefully acknowledges funding from TUBITAK-BIDEB (2219-International Postdoctoral Research Fellowship Programme).

References

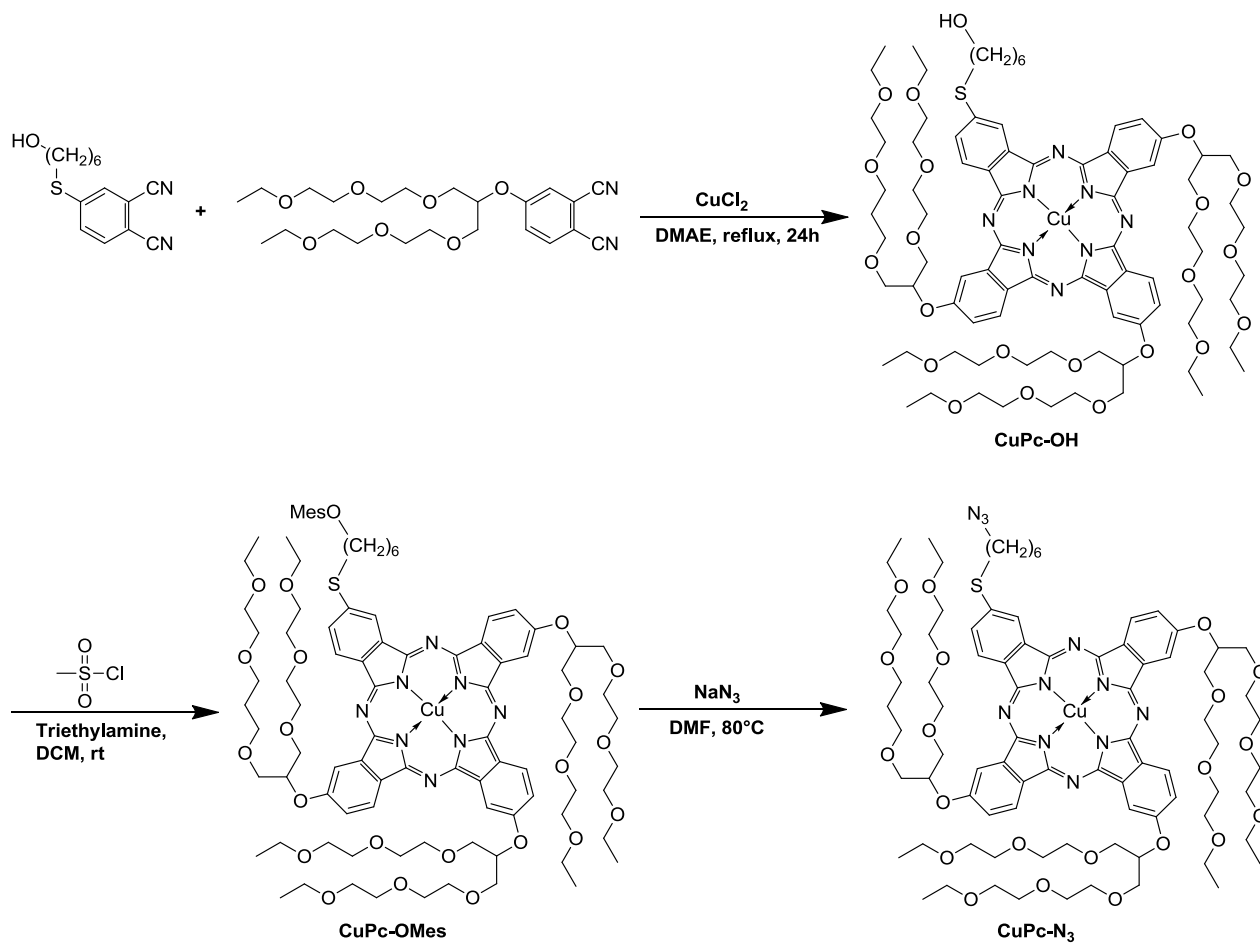
- 1 G. Delaittre, N. K. Guimard and C. Barner-Kowollik, *Acc. Chem. Res.*, 2015, **48**, 1296.
- 2 A. S. Lang, A. Neubig, M. Sommer and M. Thelakkat, *Macromolecules*, 2010, **43**, 7001; M. Hufnagel, M.A. Muth, J. Brendel and M. Thelakkat, *Macromolecules*, 2014, **47**, 2324.
- 3 R.H. Lohwasser, G. Gupta, P. Kohn, M. Sommer, A.S. Lang, T. Thurn-Albrecht and M. Thelakkat, *Macromolecules*, 2013, **46**, 4403; M. Hufnagel, M. Fischer, T. Thurn-Albrecht and M. Thelakkat, *Polym. Chem.*, 2015, **6**, 813.
- 4 C.D. Heinrich and M. Thelakkat, *J. Mater. Chem. C*, 2016, **4**, 5370.
- 5 A. S. Lang and M. Thelakkat, *Polym. Chem.*, 2011, **2**, 2213.
- 6 P. Reichstein, S. Gödrich, G. Papastravou and M. Thelakkat, *Macromolecules*, 2016, **49**, 5484.
- 7 V. Ladmiral, G. Mantovani, G. J. Clarkson, S. Cauet, J. L. Irwin and D.M. Haddleton, *J. Am. Chem. Soc.*, 2006, **128**, 4823; H. Gao and K. J. Matyjaszewski, *J. Am. Chem. Soc.*, 2007, **129**, 6633.
- 8 D. Quemener, M. L.Hellaye, C. Bissett, T. P. Davis, C. Barner Kowollik and M. H. Stenzel, *J. Polym. Sci., Part A: Polym. Chem.*, 2008, **46**, 155; X. Zhang, X. Lian, L. Liu, J. Zhang and H. Zhao, *Macromolecules*, 2008, **41**, 7863; G. Moad, E. Rizzardo and S. H. Thang, *Aust. J. Chem.*, 2009, **62**, 1402.

- 9 M. Malkoch, R. J. Thibault, E. Drockenmuller, M. Messerschmidt, B. Voit, T. P. Russell and C. J. Hawker, *J. Am. Chem. Soc.*, 2005, **127**, 14942; S. Fleischmann, H. Komber, and B. Voit, *Macromolecules*, 2008, **41**, 5255.
- 10 E. Mastan, X. Li and S. Zhu, *Progress Polym. Sci.*, 2015, **45**, 71.
- 11 H. C. Kolb, M. G. Finn and K. B. Sharpless, *Angew. Chem. Int. Ed.*, 2001, **40**, 2004.
- 12 W. H. Binder and R. Sachsenhofer, *Macromol. Rapid Commun.*, 2008, **29**, 952.
- 13 V. V. Rostovtsev, L. G. Green, V. V. Fokin and K. B. Sharpless, *Angew. Chem. Int. Ed.*, 2002, **41**, 2596; C. W. Tornøe, C. Christensen and M. Medal, *J. Org. Chem.*, 2002, **67**, 3057.
- 14 R. Huisgen, *Angew. Chem. Int. Ed.*, 1963, **10**, 633; R. Huisgen, *Angew. Chem. Int. Ed.*, 1963, **11**, 565.
- 15 A. Braun and J. Tcherniac, *Ber. Dtsch. Chem. Ges.*, 1907, **40**, 2709.
- 16 H. d. Diesbach and E. Von der Weid, *Helvetica Chimica Acta*, 1927, **10**, 886.
- 17 A. T. Vartanyan, *Zh. Fiz. Khim.*, 1948, **22**, 769.
- 18 K. Murata, S. Ito, K. Takahashi and B. M. Hoffman, *Appl. Phys. Lett.*, 1996, **68**, 427.
- 19 Z. Wang, T. Miyadera, Y. Yamanari and Y. Yoshida, *ACS Appl. Mater. Interfaces*, 2014, **6**, 6369.
- 20 Q. D. Dao, T. Hori, K. Fukumura, T. Masuda, T. Kamikado, A. Fujii, Y. Shimizu and M. Ozaki, *Appl. Phys. Lett.*, 2012, **101**, 263301.
- 21 R. F. de Oliveira, L. Mercedes, T. P. Vello and C. C. Bof Bufon, *Org. Electron.*, 2016, **31**, 217.
- 22 B. J. Campo, J. Duchateau, C. R. Ganivet, B. Ballesteros, J. Gilot, M. M. Wienk, W. D. Oosterbaan, L. Lutsen, T. J. Cleij, G. de la Torre, R. A. Janssen, D. Vanderzande and T. Torres, *Dalton Trans.*, 2011, **40**, 3979; H. Mert, H. Dinçer, E. Çalışkan, B. N. Şen and Y. H. Gürsel, *J. Appl. Polym. Sci.*, 2015, **132**, 41574.
- 23 I. López-Duarte, M. V. M. Díaz, E. Schwartz, M. Koepf, P. H. J. Kouwer, A. E. Rowan, R. J. M. Nolte and T. Torres, *Chem. Plus Chem.*, 2012, **77**, 700.
- 24 J. A. Johnson, Y. Y. Lu, A. O. Burts, Y.-H. Lim, M. G. Finn, J. T. Koberstein, N. J. Turro, D. A. Tirrell and R. H. Grubbs, *J. Am. Chem. Soc.*; 2011, **133**, 559; Y. C. Teo and Y. Xia, *Macromolecules*, 2015, **48**, 5656; S. Ahn, D. L. Pickel, W. M. Kochemba, J. Chen, D. Uhrig, J. P. Hinestrosa, J.-M. Carrillo, M. Shao, C. Do, J. M. Messman, W. M. Brown, B. G. Sumpter and S. M. Kilbey, *ACS Macro Lett.*, 2013, **2**, 761.
- 25 M. Kimura, H. Ueki, K. Ohta, K. Hanabusa, H. Shirai, and N. Kobayashi, *Langmuir*, 2002, **18**, 7683.
- 26 A. de la Escorusa, M. V. Martínez-Díaz, T. Torres, R. H. Grubbs, D. M. Guldi, H. Neugebauer, C. Winder, M. Drees and N. S. Sariciftci, *Chem. Asian. J.*, 2006, **1-2**, 148.

- 27 E. N. Kaya, S. Tuncel, T.V. Basova, H. Banimuslem, A. Hassan, A. G. Gürek, V. Ahsen and M. Durmuş, *Sens. Actuator B-Chem.*, 2014, **199**, 277; B. Kadem, M. Göksel, A. Şenocak, E. Demirbaş, D. Atilla, M. Durmuş, T. Basova, K. Shanmugasundaram, A. Hassan, *Polyhedron*, 2016, **110**, 37.
- 28 M. N. Yaraşır, M. Kandaz, A. Koca and B. Salih, *J. Porphyrins Phthalocyanines*, 2006, **10**, 1022.
- 29 M. M. Ayhan, G. A. Özpınar, M. Durmuş, A. G. Gürek, *Dalton Trans.*, 2013, **42**, 14892.
- 30 S. Fleischmann, H. Komber, and B. Voit, *Macromolecules*, 2008, **41**, 5255.
- 31 D. Benoit, V. Chaplinski, R. Braslau and C. J. Hawker, *J. Am. Chem. Soc.*, 1999, **121**, 3904.
- 32 K. Gräf, M. A. Rahim, S. Das and M. Thelakkat, *Dyes and Pigments*, 2013, **99**, 1101.
- 33 P. N. Murgatroyd, *J. Phys. D: Appl. Phys.*, 1970, **3**, 151.
- 34 D. C. Schriemer and L. Li, *Anal. Chem.*, 1997, **69**, 4169; K. Martin, J. Spickermann, H. J. Rader and K. Müllen, *Rapid Commun. Mass Spectrom.*, 1996, **10**, 1471.
- 35 M. Gouterman, *The Porphyrins, Physical Chemistry Part A, Vol. III*, ed. D. Dolphin, Academic Press: New York, 1978, Chapter 1, 1-165; J. Mack, M. J. Stillman and N. K. Kobayashi, *Coord. Chem. Rev.*, 2007, **251**, 429.
- 36 T. Fukuda and N. Kobayashi, *Handbook of Porphyrin Science: Vol 9*, ed. K. M. Kadish, K. M. Smith and R. Guilard, World Scientific Publishing Co. Pte. Ltd., Singapore, 2010, 1-644; N. Kobayashi, S. Nakajima, H. Ogata and T. Fukuda, *Chem. Eur. J.*, 2004, **10**, 6294.
- 37 R. Bayrak, K. Karaoglu, Y. Ünver, K. Sancak, F. Duumludag and I. Degirmencio, *J. Organomet. Chem.*, 2012, **712**, 57.
- 38 P. Batat, M. Bayar, B. Pur, E. Çoker, V. Ahsen, F. Yuksel and A. L. Demirel, *Phys. Chem. Chem. Phys.*, 2016, **18**, 15574
- 39 J.-L. Bredas, *Mater. Horiz.*, 2014, **1**, 17.
- 40 N. Zharnikova, N. Usol'tseva, E. Kudrik and M. Thelakkat, *J. Mater. Chem.*, 2009, **19**, 3161.
- 41 Y. L. Gaoa, E. Zhuravlev, C. D. Zoua, B. Yanga, Q. J. Zhai and C. Schick, *Thermochimica Acta*, 2009, **482**, 1; V. Mathot, M. Pydaa, T. Pijpers, G. V. Poel, E. van de Kerkhoff, S. van Herwaardeng, F. van Herwaardeng and A. Leenaers, *Thermochimica Acta*, 2011, **522**, 36.
- 42 A. Omenat, J. Barbera, J. L. Serrano, S. Houbrechts and A. Persoons, *Adv. Mater.*, 1999, **11**, 1292.
- 43 N. F. Mott and R. W. Gurney, 1940, *Electronic Processes in Ionic Crystals* (London: Oxford University Press); B. Li, J. Chen, D. Yang and D. Ma, *Semicond.*

- Sci. Technol.*, 2011, **26**, 115006; A. M. Saleh, A. K. Hassan and R. D. Gould, *J. Phys. Chem. Solids*, 2003, **64**, 1297.
- 44 P. Apostol, J. Eccher, M. E. R. Dotto, C. B. Costa, T. Cazati, E. A. Hillard, H. Bock and I. H. Bechthold, *Phys. Chem. Chem. Phys.*, 2015, **17**, 32390; I. H. Bechthold, J. Eccher, G. C. Faria, H. Gallardo, F. Molin, N. R. S. Gobo, K. T. de Oliveira and H. J. von Seggern, *J. Phys. Chem. B*, 2012, **116**, 13554.
- 45 T. Wöhrle, I. Wurzbach, J. Kirres, A. Kostidou, N. Kapernaum, J. Litterscheidt, J. C. Haenle, P. Staffeld, A. Baro, F. Giesselmann and S. Laschat, *Chem. Rev.*, 2016, **116**, 1139.

Supporting Information (ESI)

Scheme S 1 Synthesis of **CuPc-N₃**.

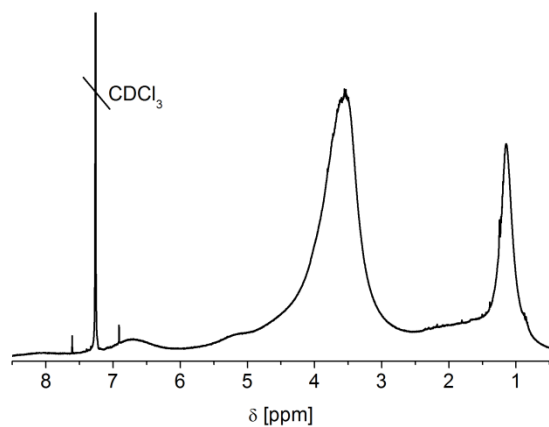


Fig. S 1 ¹H-NMR spectrum of **PCuPc**.

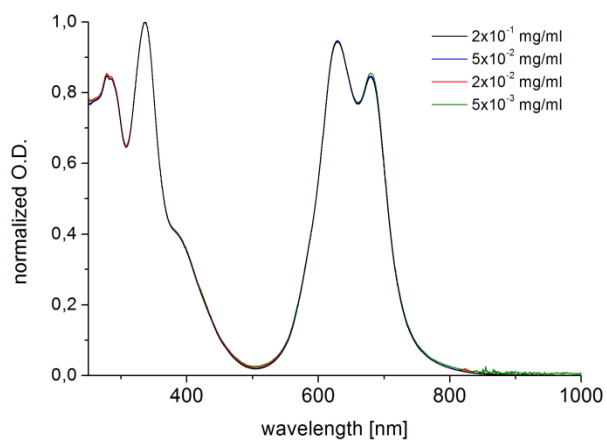


Fig. S 2 Normalized UV-Vis spectra of solutions of **PCuPc** in DCM in a concentration range from $2 \cdot 10^{-1}$ – $5 \cdot 10^{-3}$ mg mL⁻¹. No difference of the spectra at different concentrations can be detected.

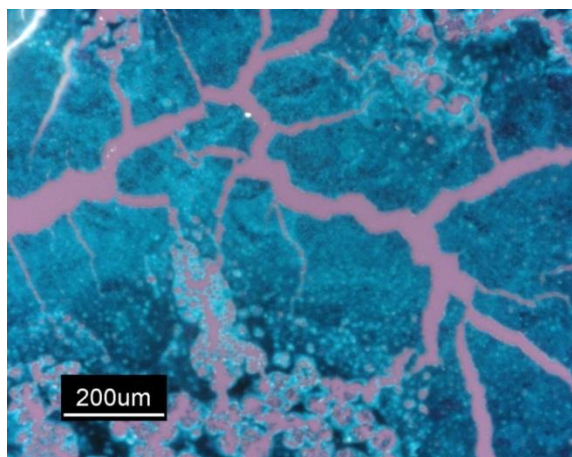


Fig. S 3 Polarization microscopy picture of **PCuPc** at room temperature.

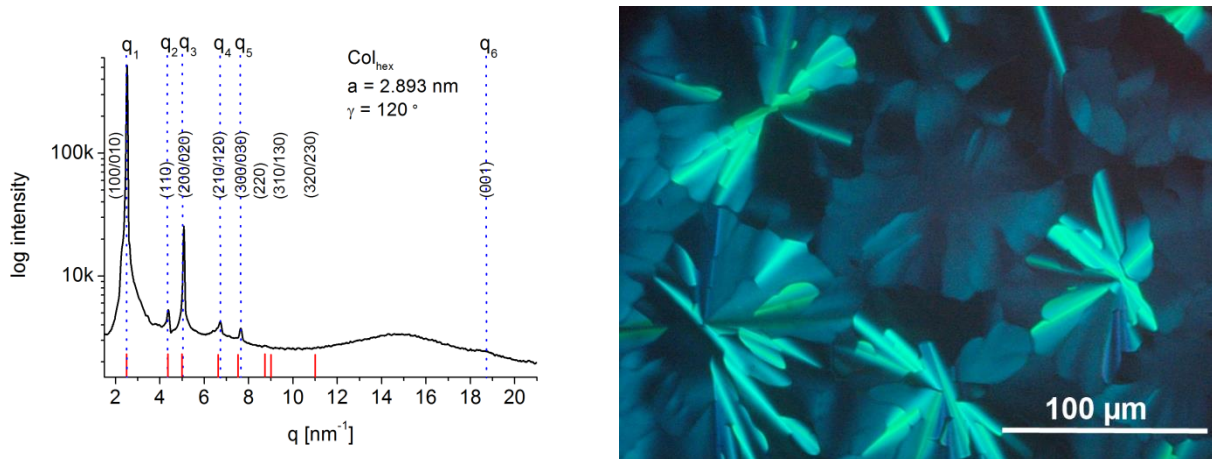


Fig. S 4 (left) Diffraction pattern of the hexagonal mesophase (Col_{hex}) of **CuPc-OH** measured at room temperature with the calculated reflection positions indicated by the red bars (measured at a Bruker Advanced D8 diffractometer). (right) Polarization microscopy picture of **CuPc-OH** at room temperature. The phase transition behavior of CuPc-OH was observed by means of a polarizing optical microscope (Leitz Wetzler Orthoplan-pol.) equipped with a hot stage (Linkam TMS 93) and a temperature controller (Linkam LNP).

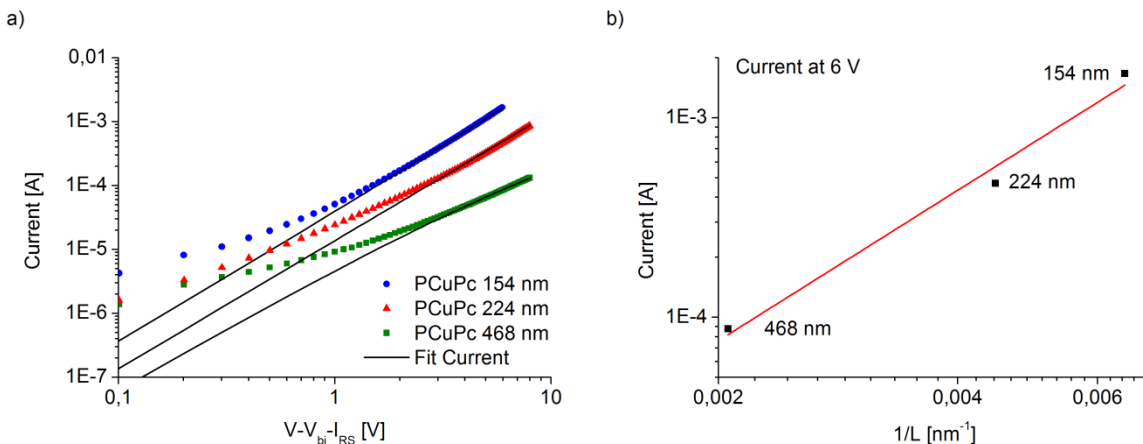


Fig. S 5 a) Log-log plot of I-V characteristics of as-cast films of **PCuPc** measured at room temperature. The I-V characteristics were corrected for the built-in voltage (V_{bi}) and the voltage drop (IR) over the contacts. The fits are calculated with equation (5) and the parameters given in **Table S 1**. b) Dependency of the current at a fixed voltage (6 V) on the film thickness L . The fit corresponds to L^3 .

Table S 1 Active layer film thicknesses and fitting parameter for the SCLC devices.

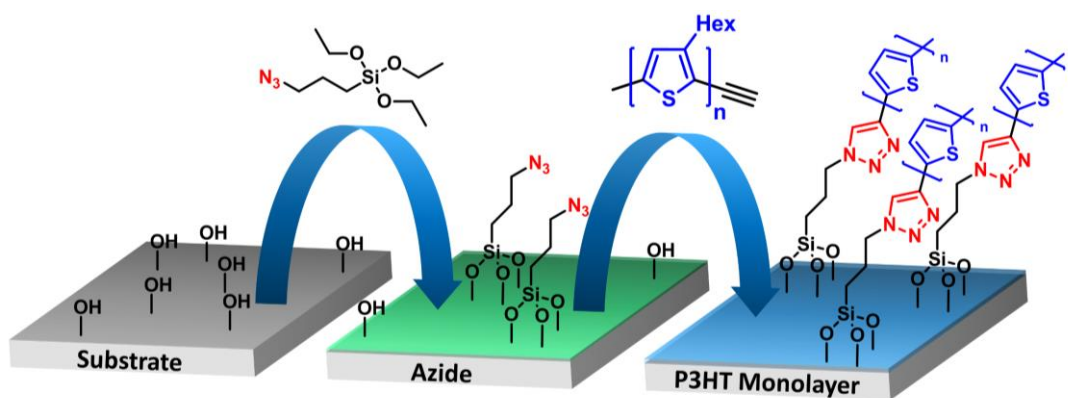
	Thickness [nm]	Fitted mobility [$cm^2 V^{-1} s^{-1}$]	Fitted γ [$V^{-0.5} m^{-0.5}$]	Mobility at $F = 1.5 \cdot 10^7 V m^{-1}$ [$cm^2 V^{-1} s^{-1}$]
Device 1	154	$4.1 \cdot 10^{-5}$	$-4.7 \cdot 10^{-5}$	$4.9 \cdot 10^{-6}$
Device 2	224	$5.0 \cdot 10^{-6}$	0	$5.0 \cdot 10^{-6}$
Device 3	468	$2.3 \cdot 10^{-5}$	$-3.4 \cdot 10^{-4}$	$6.2 \cdot 10^{-6}$

Monolayer Brushes for Highly Efficient Polymeric SAMFETs

C. David Heinrich, Paul M. Reichstein, Mukundan Thelakkat*

Applied Functional Polymers, Macromolecular Chemistry I, University of Bayreuth,
Universitätsstr. 30, 95440 Bayreuth, Germany

*E-mail of corresponding author: mukundan.thelakkat@uni-bayreuth.de



Prepared for submission

Abstract

Densely surface grafted poly(3-hexylthiophene) (P3HT) monolayer brushes were prepared by click-chemistry. For this, alkyne-functionalized P3HT was coupled to a surface immobilized self-assembled monolayer (SAM) with azide functionality. The grafted **P3HT-Alkyne** with a molecular weight of $M_{n,MALDI} = 11400 \text{ g mol}^{-1}$ (SEC: 17400 g mol^{-1}) and a narrow distribution of $\mathcal{D} = 1.15$, has the highest reported molecular weight for surface immobilized P3HT brushes. We show the successful grafting of P3HT on the substrate surface with AFM. From the film thickness, we could calculate a grafting density that is high enough to form a monolayer in the true brush regime. The aggregation behavior of the films is characterized by UV-Vis spectroscopy and compared to linear **P3HT** and the bottlebrush copolymer **PS-g-P3HT**. SAM based organic field-effect transistors (SAMFETs) with P3HT as active materials were optimized, and characterized. A high field effect mobility of $1.6 \cdot 10^{-3} \text{ cm}^2 \text{ V}^{-1} \text{ s}^{-1}$ was achieved, which is nearly two orders of magnitude higher than reported values on polymer based SAMFETs.

Introduction

The spontaneous organization of molecules on a surface –self-assembly- is widely used for creating functional surfaces. For example, self-assembled monolayers (SAMs) are used in organic electronics to functionalize surfaces with materials of minimal thickness.¹ In the field of organic photovoltaics, these self-assembled layer function as charge extraction layers for holes or electrons.^{2,3} In organic field effect transistors (OFETs) SAMs are routinely used to treat the oxidic dielectric in order to tune the wettability of the substrate and to reduce the amount of redox active reactive sites at the interface between the dielectric and the active semiconductor material.⁴ Materials for SAMs consist of an anchoring group which chemisorbs on the surface and a linker for example an aliphatic chain.⁵ Established anchoring groups for oxide substrates are

chlorosilanes, methoxysilanes and ethoxysilanes for SiO₂, phosphonic acids for Al₂O₃ and thiols for gold.^{6,7} Backbones with functional end groups can be used instead of a hydrophobic aliphatic chain in order to tune the wettability.⁷ Paoprasert *et al.*⁸ developed an azide functionalized silane, thereby introducing a reactive functional group, which can be used to fabricate active surfaces which can be further modified by copper-catalyzed alkyne-azide cycloaddition (CuAAC).⁹

While SAMs are predominantly used to tune the interface between the substrate and the semiconductor material,¹⁰ it is also possible for SAMs to act as the active material in the organic semiconductor devices themselves. Several SAM based organic field effect conductors (SAMFETs) have been reported.^{11,12} Different kinds of SAMs (p- or n-type) can be used according to the desired type of charge transport. Highly efficient p-type SAMFETs and integrated circuits based on small molecule oligothiophene derivatives with charge carrier mobilities up to $2.0 \cdot 10^{-2} \text{ cm}^2 \text{ V}^{-1} \text{ s}^{-1}$ have been reported by Blom & de Leeuw *et al.*¹² However, the highest charge carrier mobilities of a SAMFET based on poly(3-hexylthiophene) (P3HT)⁸ was reported to be $5 \cdot 10^{-5} \text{ cm}^2 \text{ V}^{-1} \text{ s}^{-1}$ which is several orders of magnitude lower than the reported values of thicker spin-cast films.¹³ This is mainly due to low degree of grafting in self-assembled mono-layers and lack of enough pi-pi stacking in such ultra-thin layers. The best n-type SAMFETs on the other hand were reported by Ringk *et al.* with a mobility of $1.5 \cdot 10^{-3} \text{ cm}^2 \text{ V}^{-1} \text{ s}^{-1}$.¹⁴ The inherent advantage of an end-on aligned polymeric semiconductor for charge transport is realizable in a SAM only with a high degree of grafting as in the brush regime.

Aside from applications as transistors, SAMs of organic semiconductors may also be used as charge extraction layers for organic photovoltaics (OPV).^{2,3} or to modify the work function of metals in order to minimize the energy barriers for injection or extraction of charges.¹⁵ Such interlayers are used to improve the wettability and the contact with the active material and introduce a selectivity of the electrode towards positive or negative charges. Chemical bound interlayers which are inherently very thin and stable towards a solution based processing of the active layer may be beneficial in terms of performance and processing of the device.³

The click chemistry concept proposed by Paoprasert *et al.* can be used to introduce any kind of acceptor or donor material with an alkyne functionality.⁸ P3HT was chosen as we could report high charge carrier mobilities in molecular bottle-brush type polymers.¹⁶ For this, P3HT with a high molecular weight (11400 g mol⁻¹) was chosen. In this molecular weight range P3HT shows the best electrical properties in linear polymers^{17,18} as well as brush systems.¹⁶ We characterized the absorption of the grafted films to gain information about the success of the grafting process. The occurrence of aggregation in these thin films can indicate a dense grafting and can be crucial for a lateral charge transport along the π - π stacked molecules. Record charge carrier mobility was obtained for SAMFETs using surface-grafted conjugated polymer, P3HT.

Experimental Section

Materials

All commercial reagents were, unless otherwise noted, used without further purification. (3-Chloropropyl)triethoxysilane (> 95%), CuBr (>98%), 6-iodo-1-hexyne (97%), sodium azide, N,N,N',N'',N''-pentamethyl-diethylene-triamine (PMDETA, 99%), were purchased from Sigma-Aldrich. A CuBr/PMDETA stock solution was prepared for all CuAAC reactions. For this a dry Schlenk flask was charged with CuBr (150 mg, 0.105 mmol) and 15 mL 1,2-dichlorobenzene and the solution was degassed with N₂ for 20 min and degassed PMDETA (540 mg, 3.15 mmol) was added. The polymers **P3HT** and **PS-g-P3HT** were published by our group as P3HT 4 and Brush 4 respectively.¹⁶

Methods

¹H-NMR (300 MHz) spectra were recorded on a Bruker AC 300 spectrometer and calibrated to the solvent peak (CDCl₃ δ = 7.26 ppm). Fourier transform infrared (FTIR) spectra were recorded on a Perkin Elmer Spectrum 100 FTIR spectrometer in attenuated total reflection (ATR) mode. Differential scanning calorimetry measurements were prepared on a Mettler Toledo DSC 2, calibrated with indium and zinc at a heating rate of 10 K min⁻¹ under continuous nitrogen flow. Thermogravimetric measurements were performed on a Mettler Toledo TGA/SDTA 851 at heating rates of 10 Kmin⁻¹ under nitrogen. Absorption measurements were carried out on a JASCO V-670. The reflection and transmission measurements were conducted with a 60 mm integrating sphere (ISN-723 UV-Visible-NIR). Bottom gate / bottom contact organic field effect transistors (OFET Gen4) were purchased from Fraunhofer IPMS. N-doped silicon (doping at the surface n ≈ 3·10¹⁷ cm⁻³) was used as surface and gate electrode. The dielectric consists of a 230 ± 10 nm layer of silicon oxide. Each substrate consisted of 16 devices with a constant channel width of 10 mm and a varying channel length of 2.5-20 μm. The source and drain electrodes were 30 nm thick gold on a 10 nm ITO adhesion layer. The charge carrier mobilities were calculated from the slope of the

(I_d)^{0.5}-V_g plots:

$$I_d \approx \frac{W}{2L} C_i \mu (V_g - V_T)^2 \quad (1)$$

Atomic force microscopy (AFM) images were recorded in intermittent contact mode on a Dimension 3100 Nanoscope V with a Nanoscope V controller and a hybrid closed loop XYZ tip scanner (5120 x 5120 pixels). Si cantilever tips from Bruker (Model OTESPA-R3) with a resonant frequency of 300 kHz with a force constant of 26 N/m were used.

Synthesis

3-(Azidopropyl)triethoxysilane:⁸ 20 g (83.3 mmol) (3-chloropropyl)triethoxysilane was dissolved in 200 mL DMF and 10.9 g (167.2 mmol) sodium azide was added and the mixture was heated to 60°C for 12 h. After cooling to rt 200 mL diethyl ether was added and the organic phase was washed with 200 mL water. The water phase was extracted two times with 50 mL diethyl ether. The combined organic phase was washed 3 times with water. The solvents were removed at the rotary evaporator and the obtained product was used without further purification. $m = 17.25$ g (84%) ¹H NMR (300 MHz, CHCl₃): δ (ppm) 3.82 (q, 6H, $J = 7.9$ Hz), 3.26 (t, 2H, $J = 7.0$ Hz), 1.71 (m, 2H), 1.23 (t, 9H, $J = 7.0$ Hz), 0.67 (m, 2H). IR (ATR): $\nu(\text{cm}^{-1})$ 2094 (N₃).

Preparation of substrates with Azide functionality: The glass or OFET substrates were cleaned twice in an ultrasonic bath in acetone and subsequently cleaned with oxygen plasma for 10 min. The cleaned substrates were functionalized by immersion in a 1 vol% 3-(azido-propyl)triethoxysilane solution in toluene at 100 °C for 2 h. The substrates were washed with toluene and cleaned three times, 5 min each, in an ultrasonic bath in toluene to remove any unbound silane. The dried substrates were stored in the dark.

P3HT-Alkyne: The alkyne functionalized P3HT polymers were synthesized according to a reported procedure.¹⁹ A 0.5 M LiCl solution was prepared first by weighing LiCl into a Schlenk flask and subsequently drying for 4 h *in vacuo* at 140 °C. Anhydrous THF was added and the solution was stirred overnight to assure a complete dissolution of the LiCl. The Grignard reagents *t*-BuMgCl and EthynylMgCl were titrated prior to their use according to a published procedure.²⁰ A dry Schlenk flask was charged with 7.86 g (24.10 mmol) 2,5-dibromo-3-hexyl-thiophene under N₂ atmosphere. 48 mL of the 0.5 M LiCl solution in THF were added. 17.9 mL (1.3 M in THF, 23.14 mmol) *t*-BuMgCl were added and the solution was stirred for 24 h. The solution was diluted

with 175 mL THF and the polymerization was started by adding 159.3 mg (0.289 mmol) Ni(dppp)Cl₂ (suspension in 2 mL THF). The polymerization was terminated after 25:30 min by adding 12.3 mL (0.47 M in THF, 5.82 mmol) EthynylMgCl. The solution was stirred for further 11 min and the polymer was subsequently precipitated in methanol. The polymer was dried and redissolved in CHCl₃. The solution was filtered over a short aluminum oxide column to remove residual LiCl and Ni(dppp)Cl₂, evaporated with the rotary evaporator to get a concentrated solution, and precipitated again in hexanes. $m = 2.75$ g, $M_{n,SEC} = 17400$ g mol⁻¹, $M_{n,MALDI} = 11400$ g mol⁻¹; $\bar{D} = 1.15$; ¹H NMR (300 MHz, CHCl₃): δ (ppm) 6.98 (s, 1H), 3.53 (s, 1H), 2.85-2.4 (m, 2H), 1.80-1.60 (m, 2H), 1.50-1.25 (m, 6H), 0.98-0.83 (m, 3H); IR(ATR): ν (cm⁻¹) 3312 (C≡C-H), 2096 (C≡C).

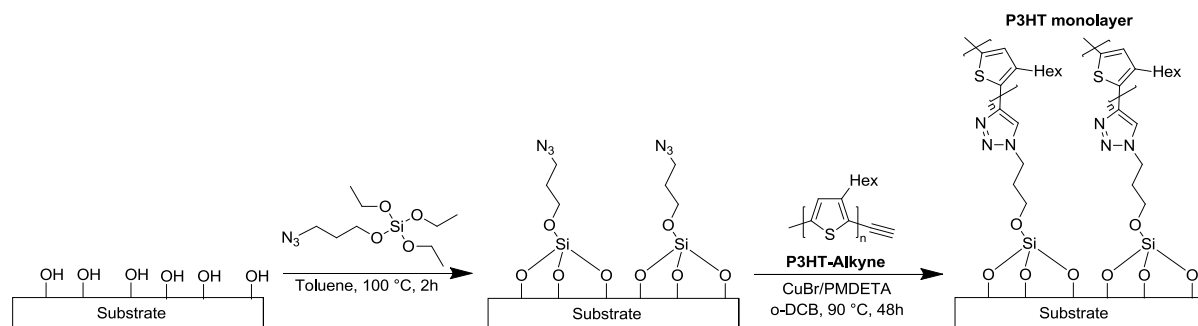
Grafting with P3HT-Alkyne: A custom made flat bottom Schlenk flask was charged with the azido functionalized substrates and 28.5 mg ($2.5 \cdot 10^{-3}$ mmol) **P3HT-Alkyne**. The flask was degassed and 40 mL dry o-dichlorobenzene were added. 0.5 mL of a 0.07 mol L⁻¹ solution of CuBr/PMDETA in o-dichlorobenzene was added and the solution was stirred for 48 h at 90 °C. The substrates were washed with chloroform and cleaned three times, 5 min each, in an ultrasonic bath in chloroform to remove any unbound alkyne compound. Subsequently the substrates were immersed in chloroform, chlorobenzene or o-dichlorobenzene and dried after removal from the solvent.

Results and Discussion

Synthesis of P3HT-Alkyne and Surface Grafting

P3HT-Alkyne was synthesized according to a reported procedure.¹⁹ We used the identical material, named P3HT-Alkyne, to form P3HT monolayers grafted on a surface. The monolayers are compared to linear **P3HT** and a P3HT bottlebrush (**PS-g-P3HT**) having the same length and dispersity for P3HT.¹⁶ The **P3HT-Alkyne** and **P3HT** possess a narrow distribution ($\mathcal{D} < 1.15$) and have a comparable, high molecular weight of $M_{n, \text{MALDI}} \sim 11500 \text{ g mol}^{-1}$. **PS-g-P3HT** was synthesized by grafting **P3HT-Alkyne** to a polystyrene backbone according to published procedures.^{16,21} All the SEC and MALDI-TOF data of all the polymers are given in **Table 1**.

The grafted P3HT monolayers were obtained after a two-step process. First, an azide functionalized surface was made by silanization and subsequently functional P3HT monolayers were synthesized by CuAAC click chemistry using **P3HT-Alkyne** (see **Scheme 1**). Ethoxysilane can form SAMs on a number of substrates, with hydroxygroups at the surface. We functionalized glass substrates for the UV-Vis measurements and SiO₂ surfaces in a similar way for the OFET fabrication. To remove any organic impurities from the pristine substrate surface and to obtain a hydrophilic surface the substrates were cleaned twice in an ultrasonic bath with acetone and subsequently cleaned for 10 min with oxygen plasma. The cleaned substrates were functionalized directly afterwards by immersion in a 100 °C warm 1 wt% solution of 3-(azidopropyl)triethoxysilane in toluene.



Scheme 1 Principle of the surface functionalization with P3HT. A substrate with hydroxy groups at the surface is functionalized with the azido silane. Subsequently the azido SAM reacts with P3HT-Alkyne to form the P3HT monolayer on the surface.

Table 1 SEC – and MALDI-TOF data and thermal properties of **P3HT-Alkyne**, linear **P3HT** and the bottle brush **PS-*g*-P3HT**.

	$M_{n,SEC}$ [g mol ⁻¹]	\bar{D}	$M_{n,Maldi}$ [g mol ⁻¹]	$T_{m,peak}$ [°C]	ΔH_m [J g ⁻¹]	$T_{c,peak}$ [°C]
P3HT-Alkyne	17400	1.15	11400	225	19.3	189
P3HT	15900	1.11	11600	229/238/247	22.3	203
PS-<i>g</i>-P3HT	144000	1.37		219	14.9	173

After 2 h the substrates were removed from the solution, washed with toluene and cleaned three times, 10 min each, in an ultrasonic bath with toluene to remove any silane molecule which was not chemically bound to the surface. The azide-functionalized substrates were stored in the dark before the next synthetic step was initiated. For the CuAAC reaction of **P3HT-Alkyne**, we applied the optimized procedure which was also used for the synthesis of molecular P3HT brushes.¹⁶ We conducted the reaction at an elevated temperature of 90 °C to ensure a dense grafting of the high molecular weight **P3HT-Alkyne**. After the reaction, the surface grafted brushes and the blank substrate were washed with chloroform and cleaned three times, 10 min each, in an ultrasonic bath with chloroform to remove any unreacted **P3HT-Alkyne**, copper catalyst and ligand. The crystallinity of P3HT bulk and thin films has a pronounced effect on its optical and electronic properties. We dipped the substrates in chloroform (bp = 61°C), chlorobenzene (bp = 132 °C) or o-dichlorobenzene (bp = 179 °C), removed them from the solvent and let them dry. All three solvent are good solvent for P3HT but have different boiling points therefore, possibly influencing the time of drying and giving the monolayer more or less time to crystallize. The functionalization of the glass substrates was followed by AFM. In **Fig. 1 a)** the height image of a cleaned glass substrate is shown. A smooth surface with a roughness of $R_{RMS} = 1.21$ nm is observed. After the silanization the roughness slightly increases ($R_{RMS} = 1.64$ nm) and structures with a height of 10-25 nm appear. These are most likely cross-linked aggregates formed by the azidosilane which could not be washed from the substrates. The roughness increases further after the grafting with P3HT ($R_{RMS} = 1.84$ nm) and the structures are still present. AFM was also used to measure the film thickness of the monolayers grafted onto the OFET devices by scratching the film and measuring the step height. The

average measured thicknesses for the grafted monolayers are between $h = 2.9\text{-}3.5$ nm (see **Table 2**). With the obtained values of the thickness, the grafting density can be calculated from $\sigma = h\rho N_A/M_n$, where h is the film thickness, ρ the density of P3HT ($\rho = 1.11$ g cm⁻³),²² N_A the Avogadro's number and $M_n = 11500$ g mol⁻¹ the molecular weight of the polymer. The grafting density of the monolayers in the range of $\sigma = 0.17\text{-}0.2$ chains / nm² is high enough for the monolayers to be in the true brush regime. This can be quantified by the reduced tethered density $\Sigma = \sigma\pi R_g^2$ which corresponds to the number of chains present in an area that would be occupied by one non overlapping polymer chain at the same conditions (solvent, temperature). At low grafting densities ($\Sigma < 1$) the grafted layer is in the mushroom regime which is characterized by single chains that do not form a continuous film. For higher values ($1 < \Sigma < 5$) a transition from the mushroom- to the brush-regime occurs and at $\Sigma > 5$ the density is high enough to form a true densely packed brush, where the polymers are forced into a chain extended configuration.²³ In order to calculate Σ , the gyration radius R_g in *o*-dichlorobenzene (*o*-DCB) has to be obtained. McCulloch *et al.* reported that P3HT in *o*-DCB can be described as a wormlike chain and R_g can be therefore be calculated from $R_g^2 = 1/3 Ll_p$ where l_p is

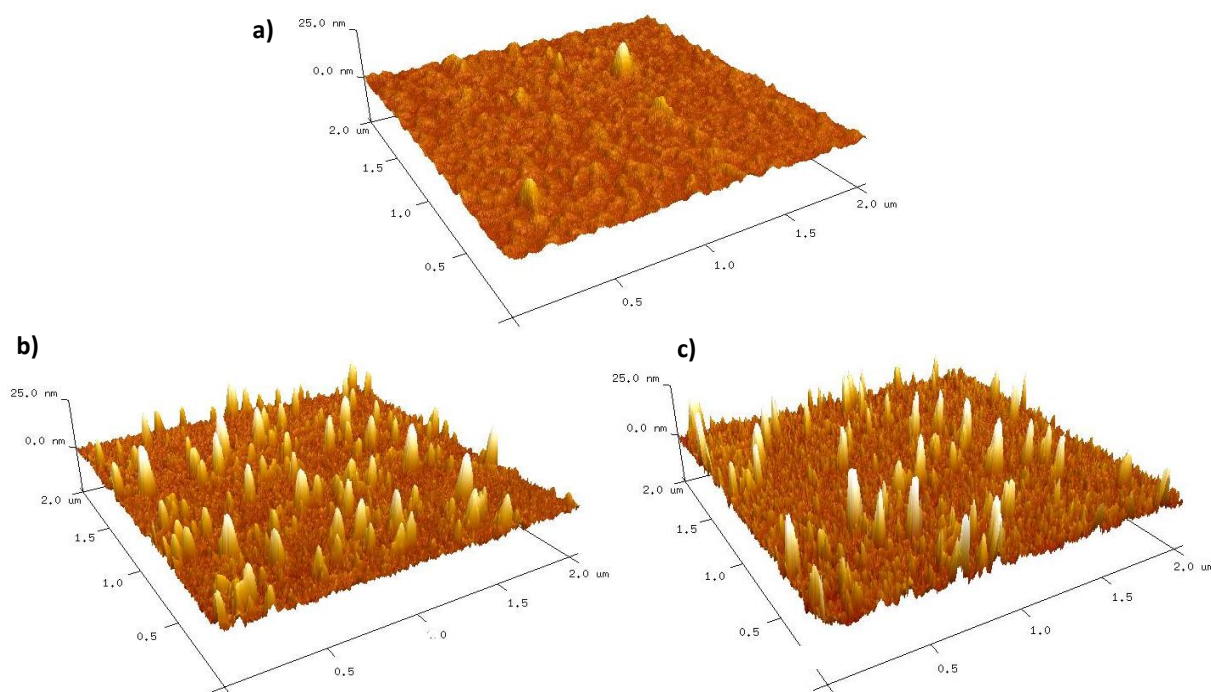


Fig. 1 Atomic force microscopy pictures (height image) of the glass substrate (a) the azido silane surface (b) and the P3HT monolayer (c).

the persistence length and L the contour length.²⁴ The contour length L is the length of the stretched polymer and for **P3HT-Alkyne** with $M_n = 11400 \text{ g mol}^{-1}$ ($N = 68$) $L = N L_{\text{monomer}} = 26.2 \text{ nm}$ (with $L_{\text{monomer}} = 0.385 \text{ nm}$) is obtained.²⁵ The value for $l_p = 2.2 \text{ nm}$ was measured by McCulloch *et al.* in *o*-DCB at $90 \text{ }^\circ\text{C}$ and the gyration Radius is subsequently calculated to be $R_g = 4.4 \text{ nm}$.²⁴ from these values, we obtain values for the reduced tethered density of $\Sigma = 10.3\text{-}12.1$, which is indicative of the monolayer being within the true brush regime and form a continuous film. On grafting the substrates with P3HT, the hydrophobicity of the surface increases drastically. This was monitored by contact angle measurements (see **Fig. S 1**). For example, the clean ITO surface has a contact angle around $50\text{-}60^\circ$, whereas after the azide modification and cleaning, it changes to $75\text{-}80^\circ$ and after grafting a monolayer of P3HT, it increases almost to 100° . This clearly indicates the increase in hydrophobicity of the surface after grating P3HT. We also did not observe any influence of chain length on the contact angle. Additionally, the P3HT grafted substrates are visibly colored purple which is a second indicator of the successful reaction and UV-Vis spectroscopy was preformed to quantify the absorption.

UV-Vis Spectroscopy

For the accurate measurement of very thin films by UV-Vis spectroscopy possible errors have to be considered. In a standard setup only the transmission is measured, neglecting the different reflection of the substance film and the substrate. In very thin films interference patterns, which overlay the absorption of the measured film, are also frequently observed. Additionally, scattered light at a rough surface may also be falsely interpreted as the materials' absorption. These effects have about the same magnitude as the absorption for films with a thickness of only a few nm. We, therefore, calculated the absorption of the thin grafted monolayers of **P3HT-Alkyne** from the transmission and the reflection, which were measured with an integrating sphere. By this, we obtained accurate values for the optical density without any of the aforementioned errors. In **Fig. 2 a** the absorption spectra of **P3HT-Alkyne** grafted onto glass substrates and dried from different solvents are shown. In all three cases structured spectra with an onset of absorption of around 650 nm can be observed. This observation

corresponds to a spectrum which would be expected for aggregated linear P3HT. The aggregation is characterized by the peaks for the 0-2, 0-1 and 0-0 transition at 524 nm, 560 nm and 605 nm, respectively. In order, to compare the aggregation of the three grafted monolayers the spectra were normalized to the 0-1 transition. The aggregation can be described by the theory of Spano *et al.* which describes the aggregation of P3HT as weakly bound H-aggregates where the aggregation strength can be determined by the relative intensity of the 0-0 and the 0-1 transition.²⁶ For a stronger aggregated sample the ratio $A_{0-0}:A_{0-1}$ is expected to be higher. The strongest aggregation can be observed for the monolayer which was dried from chloroform ($A_{0-0}:A_{0-1} = 0.62$). The quality of the aggregates decreases when the films were dried from the solvents with higher boiling points. The lowest value was observed for chlorobenzene ($A_{0-0}:A_{0-1} = 0.50$) and a slightly higher value was observed for o-dichlorobenzene ($A_{0-0}:A_{0-1} = 0.55$). No strong correlation of the solvents boiling point and the drying time was observed. On the contrary, aggregation is strongest for monolayer dried from chloroform.

The monolayer dried from chloroform was also compared with the spectra of spin-cast films of linear **P3HT** and **PS-g-P3HT**. For the comparison, films were prepared in the same way as the respective OFET devices for which we observed the best performances.¹⁶ For **P3HT** this was an as-cast film spin coated from chloroform and for the **PS-g-P3HT**, the film was additionally melt crystallized at 240 °C. The spectra of the cast films have a comparable onset of absorption at 650 nm just as the

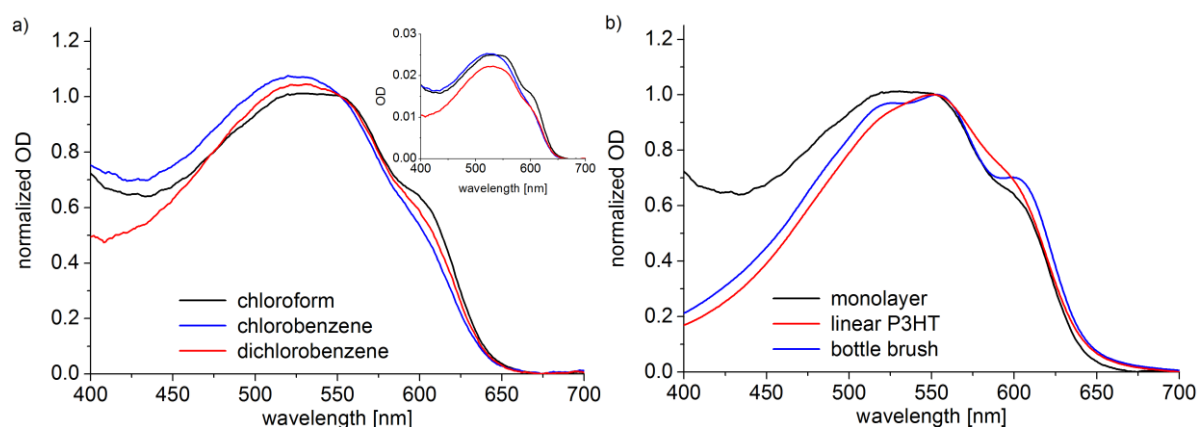


Fig. 2 a) Normalized UV-Vis spectra of P3HT monolayers on glass substrates dried from different solvents (inlet: the same spectra are shown without normalization). b) Comparison of the UV-Vis spectra of the P3HT monolayer (dried from chloroform) with thin films of linear **P3HT** (as-cast) and **PS-g-P3HT** (MC at 240°C).

monolayer but for both materials higher aggregation strengths can be observed. We calculate a ratio of $A_{0-0}:A_{0-1} = 0.67$ for the linear **P3HT** and $A_{0-0}:A_{0-1} = 0.70$ for **PS-g-P3HT** which is higher than the 0.62 obtained for the monolayer dried from chloroform.

Organic Field Effect Transistors (OFETs)

The electrical properties of the monolayers were investigated in p-type SAMFETs. We used commercial bottom-gate (Si), bottom-contact (Au) devices with a silicon oxide layer as dielectric. The P3HT monolayers were directly prepared on the oxide layer as described before. The output and transfer characteristics of the monolayer dried from chloroform are shown in **Fig. 1 a** and **d**. By plotting the gate voltage of the transfer curve against the square root of the drain current, the mobility can be extracted (see **Equation (1)**). We achieved a mobility of $1.6 \cdot 10^{-3} \text{ cm}^2 \text{ V s}^{-1}$ and an On/Off-Ratio of $8.9 \cdot 10^4$ (see **Table 2**), which are remarkable values for a thin film $< 4 \text{ nm}$. The mobility is nearly two orders of magnitude higher in comparison to previously reported surface immobilized P3HT brushes and in general any polymeric SAMFET.⁸ In comparison lower mobility values were obtained when the monolayers were dried from chlorobenzene or o-DCB (see **Fig. S 2**). This finding is in good agreement with the lower aggregation which can be observed for these monolayers in absorption studies. In order to understand the influence of thermal annealing on device characteristics, they were annealed for 10 min at $100 \text{ }^\circ\text{C}$ in the glove box and measured. Unfortunately, currents decreased and the threshold voltage strongly shifted from $V_{G,Th} \sim 10 \text{ V}$ for the monolayer dried from CHCl_3 to $V_{G,Th} \sim -20 \text{ V}$ for the annealed device. Additional annealing of the same device at $150 \text{ }^\circ\text{C}$ led to a further decrease in current (see **Fig. S 3**). Thus the best devices are, obtained by drying the monolayers from chloroform. UV-Vis spectroscopy revealed a lower aggregation for the other tested solvents (chlorobenzene and o-DCB) which can explain the lower performances of these SAMFET devices. The considerably higher molecular weight that we used, in comparison to previous a report,⁸ is most likely the reason for the high mobility of $1.6 \cdot 10^{-3} \text{ cm}^2 \text{ V s}^{-1}$ which was observed for the monolayer dried from chloroform. For linear **P3HT**^{17,18} as well as **PS-g-P3HT**¹⁶ the very high mobilities are only observed for high molecular weight P3HT. The long period or lamellar width of the crystallites and

correspondingly the charge carrier mobility in P3HT were found to increase continuously with molecular weight and at about 12000 g mol^{-1} absolute molecular weight ($\sim 20000 \text{ g mol}^{-1}$ in GPC with PS calibration), the chains start folding resulting in saturation of both long period and charge carrier mobility.^{18,27} Thus P3HT samples with sufficient molecular weights in the above-mentioned ranges are required for high mobility applications. We demonstrate that P3HT grafted monolayers can be produced with excellent electrical properties if the molecular weight is high enough and the grafting density is sufficient. But the device performance of the monolayer SAMFETs is still lower than those compared to the OFETs made from spin coated thin layers of similar polymers (see **Fig. 3**). For example, the hole mobilities for linear **P3HT** and a bottle-brush polymer, **PS-g-P3HT** having a similar molecular weight of P3HT are 4.9×10^{-2} and $5.0 \times 10^{-2} \text{ cm}^2 \text{ V}^{-1} \text{ s}^{-1}$ respectively.

The most distinct difference between the monolayer OFETs and the devices prepared via spin casting is the thickness of the active layer and possible differences in the alignment of polymeric chain on the substrate. Even though a direct comparison of the device performance does not deliver any conclusive inference, we like to elaborate the

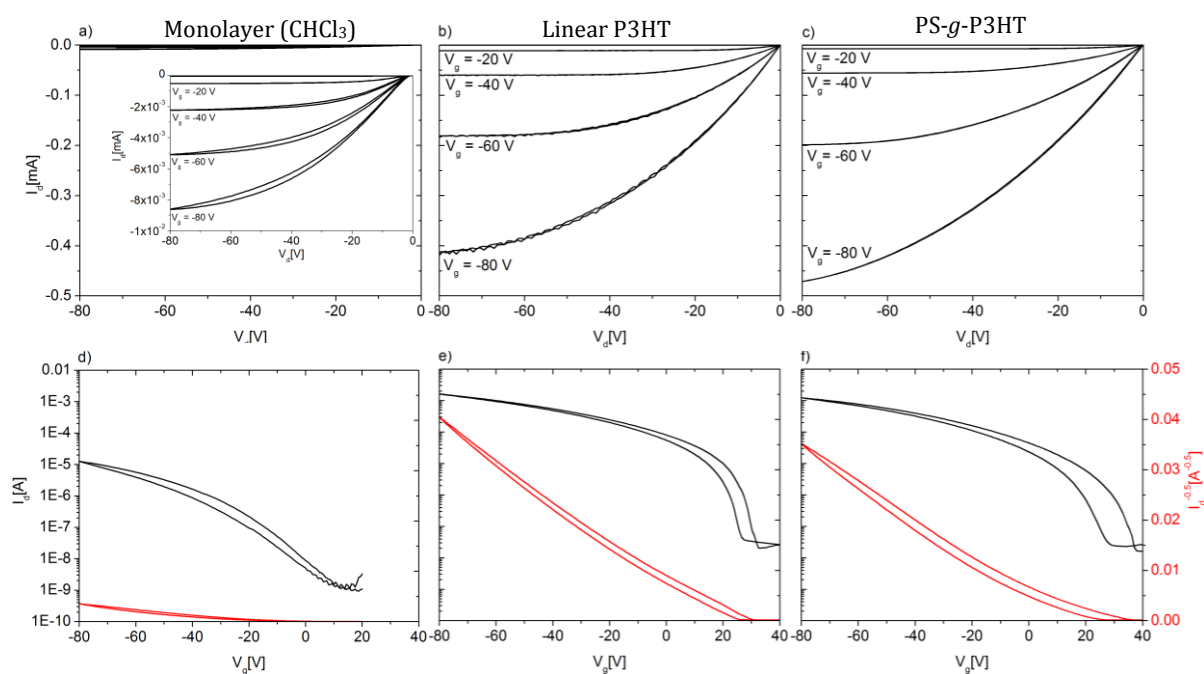


Fig. 3 Representative OFET I-V-curves of the monolayer dried from chloroform, linear **P3HT** and **PS-g-P3HT**. The p-output characteristics are shown at the top (a-c) and the transfer characteristics in saturation regime ($V_d = -80\text{V}$) at the bottom (d-f). The channel length was $20 \mu\text{m}$ in all cases.

peculiarities and differences in both cases. The spin cast layers have a thickness of about 25 nm while the SAMs have a thickness of only up to 3.5 nm. Joshi *et al.* showed for very thin films (thickness > 10 nm), the OFET mobility for P3HT is constant ($\mu_h \sim 10^{-6} \text{ cm}^2 \text{ V}^{-1} \text{ s}^{-1}$).²⁸ In a recent study the dependence of the charge carrier mobility of OFETs with different layer thicknesses was reported for a range of high molecular weight P3HTs ($M_n = 34\text{-}170 \text{ kDa}$).²⁹ It was shown that OFETs with a thickness of the P3HT layer < 8 nm have dramatically lower charge carrier mobilities, μ being in the range of $1 \times 10^{-3} \text{ cm}^2 \text{ V}^{-1} \text{ s}^{-1}$ - $3 \times 10^{-3} \text{ cm}^2 \text{ V}^{-1} \text{ s}^{-1}$. For such thin layers only 2D transport is possible and any defects or trapping sites at the interface are detrimental for the device performance. The reported mobility $2.0 \times 10^{-3} \text{ cm}^2 \text{ V}^{-1} \text{ s}^{-1}$ for sub 8 nm layers is in good agreement with the mobility of the monolayer dried from chloroform. The device performance of the monolayers could not be improved by post processing annealing steps Improving the devices further depends on the possibility to increase the grafting density by adopting other surface chemistry of suitable spacers.

Table 2 Average charge carrier mobility values, I_{ON}/I_{OFF} for channel lengths 5-20 μm and layer thickness h for the monolayers after different solvent/thermal treatments and best values obtained for linear **P3HT** and **Ps-g-P3HT**.

	μ [$\text{cm}^2 \text{ V}^{-1} \text{ s}^{-1}$]	I_{ON}/I_{OFF}	h [nm]
Monolayer (CHCl₃)	1.6×10^{-3}	8.9×10^4	3.5
Monolayer (CB)	6.9×10^{-4}	1.9×10^5	2.9
Monolayer (o-DCB)	5.6×10^{-4}	1.2×10^5	3.3
Monolayer (100°C)	4.0×10^{-4}	1.7×10^5	
Monolayer (150°C)	5.7×10^{-5}	2.6×10^3	
Linear P3HT	4.9×10^{-2}	4.8×10^5	25
PS-g-P3HT	5.0×10^{-2}	1.5×10^5	23

Conclusions

We have demonstrated dense surface grafting of P3HT-Alkyne with a high molecular weight of about $M_{n,MALDI} = 11400 \text{ g mol}^{-1}$ via CuAAC click reaction on surface anchored azide groups. By measuring the film thickness with AFM we can show that the grafting density is high enough that the P3HT layer is in the true brush regime. By measuring the reflection and transmission of the grafted films with an integrating sphere, we were able to accurately measure the absorption in ultra-thin films and compare the spectra with linear **P3HT** and **PS-g-P3HT**. The spectra of the grafted SAM strongly resemble those of the spin cast films. The strongest aggregation was observed when the films were rinsed and dried from chloroform. Accordingly, SAMFETs with monolayers dried from chloroform exhibited the highest charge carrier mobilities ($1.6 \cdot 10^{-3} \text{ cm}^2 \text{ V s}^{-1}$). This is the highest value reported for surface grafted P3HT brushes and polymeric SAMFET in general. The charge carrier mobility cannot be further improved by thermal annealing. However, further improvements are possible if the grafting density can be drastically increased by tuning the surface anchoring chemistry and using the optimum spacer length.

Acknowledgements

We acknowledge funding from the Bavarian State Ministry of Education, Science and the Arts under the program “Solar technologies go hybrid” (SolTech).

References and Notes

- 1 S. Casalini, C. A. Bortolotti, F. Leonardi and F. Biscarini, *Chem. Soc. Rev.*, 2017, **46**, 40.
- 2 J. Alonzo, W. M. Kochemba, D. L. Pickel, M. Ramanathan, Z. Sun, D. Li, J. Chen, B. G. Sumpter, W. T. Hellera and S. M. Kilbey, *Nanoscale*, 2013, **5**, 9357.
- 3 E. L. Ratcliff, B. Zacher and N. R. Armstrong, *Phys. Chem. Lett.*, 2011, **2**, 1337.
- 4 S. Kobayashi, T. Nishikawa, T. Takenobu, S. Mori, T. Shimoda, T. Mitani, H. Shimotani, N. Yoshimoto, S. Ogawa and Y. Iwasa, *Nature Materials*, 2004, **3**, 317.

- 5 T. Schmaltz, G. Sforazzini, T. Reichert and H. Frauenrath, *Adv. Mater.*, 2017, 1605286.
- 6 A. Ulman, *Chem. Rev.*, 1996, **96**, 1533; J. C. Love, L. A. Estroff, J. K. Kriebel, R. G. Nuzzo and G. M. Whitesides, *Chem. Rev.*, 2005, **105**, 1103.
- 7 F. Schreiber, *Prog. Surf. Sci.*, 2000, **65**, 151.
- 8 P. Paoprasert, J. W. Spalenka, D. L. Peterson, R. E. Ruther, R. J. Hamers P. G. Evans and P. Gopalan, *J. Mater. Chem.*, 2010, **20**, 2651.
- 9 A. S. Lang, A. Neubig, M. Sommer and M. Thelakkat, *Macromolecules*, 2010, **43**, 7001; C. D. Heinrich, S. Tuncel Kostakoğlu and M. Thelakkat, *J. Mater. Chem. C*, 2017, **5**, 6259.
- 10 M. Halik, H. Klauk, U. Zschieschang, G. Schmid, C. Dehm, M. Schutz, S. Maisch, F. Effenberger, M. Brunnbauer and F. Stellacci, *Nature*, 2004, **431**, 963; H. Klauk, U. Zschieschang, J. Pflaum and M. Halik, *Nature*, 2007, **445**, 745.
- 11 G. S. Tulevski, Q. Miao, M. Fukuto, R. Abram, B. Ocko, R. Pindak, M. L. Steigerwald, C. R. Kagan and C. Nuckolls, *J. Am. Chem. Soc.*, 2004, **126**, 15048.
- 12 S. A. Ponomarenko, O. V. Borshchev, T. Meyer-Friedrichsen, A. P. Pleshkova, S. Setayesh, E. C. P. Smits, S. G. J. Mathijssen, D. M. de Leeuw, S. Kirchmeyer and A. M. Muzafarov, *Organometallics*, 2010, **29**, 4213; E. C. P. Smits, S. G. J. Mathijssen, P. A. van Hal, S. Setayesh, T. C. T. Geuns, K. A. H. A. Mutsaers, E. Cantatore, H. J. Wondergem, O. Werzer, R. Resel, M. Kemerink, S. Kirchmeyer, A. M. Muzafarov, S. A. Ponomarenko, B. de Boer, P. W. M. Blom and D. M. de Leeuw, *Nature*, 2008, **455**, 956.
- 13 Z. Bao, A. Dodabalapu and A. J. Lovinger, *Appl. Phys. Lett.*, 1996, **69**, 4108.
- 14 A. Ringk, X. Li, F. Gholamrezaie, E. C. P. Smits, A. Neuhold, A. Moser, C. V. der Marel, G. H. Gelinck, R. Resel, D. M. de Leeuw and P. Strohriegel, *Adv. Funct. Mater.*, 2012, **23**, 2016.
- 15 G. Heimel, L. Romaner, E. Zojer and J. L. Bredas, *Acc. Chem. Res.*, 2008, **41**, 721; C.-C. Chueh, C.-Zhi Li and A. K.-Y. Jen, *Energy Environ. Sci.*, 2015, **8**, 1160.
- 16 C. D. Heinrich and M. Thelakkat, *J. Mater. Chem. C*, 2016, **4**, 5370.
- 17 R. J. Klein, M. D. McGehee, E. N. Kadnikova, J. Liu, J. M. J. Fréchet and M. F. Toney, *J. Am. Chem. Soc.*, 2006, **128**, 3480; R. J. Kline, M. D. McGehee, E. N. Kadnikova, J. Liu and J. M. J. Fréchet, *Adv. Mater.*, 2003, **15**, 1519; A. Zen, J. Pflaum, S. Hirschmann, W. Zhuang, F. Jaiser, U. Asawapirom, J. P. Rabe, U. Scherf and D. Neher, *Adv. Funct. Mater.*, 2004, **14**, 757;
- 18 C. R. Singh, G. Gupta, R. Lohwasser, S. Engmann, J. Balko, M. Thelakkat, T. Thurn-Albrecht and H. Hoppe, *J. Polym. Sci., Part B: Polym. Phys.*, 2013, **51**, 943.
- 19 R. H. Lohwasser and M. Thelakkat, *Macromolecules*, 2012, **45**, 3070.
- 20 A. Krasovskiy and P. Knochel, *Synthesis*, 2006, **5**, 0890.
- 21 X. Pang, L. Zhao, C. Feng, R. Wu, H. Ma and Z. Lin, *Polym. Chem.*, 2013, **4**, 2025.

- 22 T. J. Prosa, M. J. Winokur, J. Moulton, P. Smith and A. J. Heeger, *Macromolecules*, 1992, **25**, 4364.
- 23 W. J. Brittain and S. Minko, *J. Polym. Sci.: Part A: Polym. Chem.*, 2007, **45**, 3505; T. Wu, K. Efimenko and J. Genzer, *J. Am. Chem. Soc.*, 2002, **124**, 9394.
- 24 B. McCulloch, V. Ho, M. Hoarfrost, C. Stanley, C. Do, W. T. Heller and R. Segalman, *Macromolecules*, 2013, **46**, 1899.
- 25 M. Brinkmann, J. C. Wittmann, *Adv. Mater.*, **2006**, 18, 860.
- 26 J. Clark, C. Silva, R. H. Friend and F. C. Spano, *Phys. Rev. Lett.*, 2007, **98**, 206406; J. Clark, J.-F. Chang, F. C. Spano, R. H. Friend and C. Silva, *Appl. Phys. Lett.*, 2009, **94**, 163306.
- 27 R. Zhang, B. Li, M. C. Iovu, M. Jefries-EL, G. Sauv e, J. Cooper, S. Jia, S. Tristram-Nagle, D. M. Smilgies, D. N. Lambeth, R. D. M McCullough and T. Kowalewski, *J. Am. Chem. Soc.*, 2006, **128**, 3480.
- 28 S. Joshi, S. Grigorian, U. Pietsch, P. Pingel, A. Zen, D. Nehera and U. Scherf, *Macromolecules*, 2008, **41**, 6800.
- 29 L. Janasz, M. Gradzka, D. Chlebosz, W. Zajaczkowski, T. Marszalek, A. Kiersnowski, J. Ulanski and W. Pisula, *Langmuir*, 2017, **33**, 4189.

Supporting Information

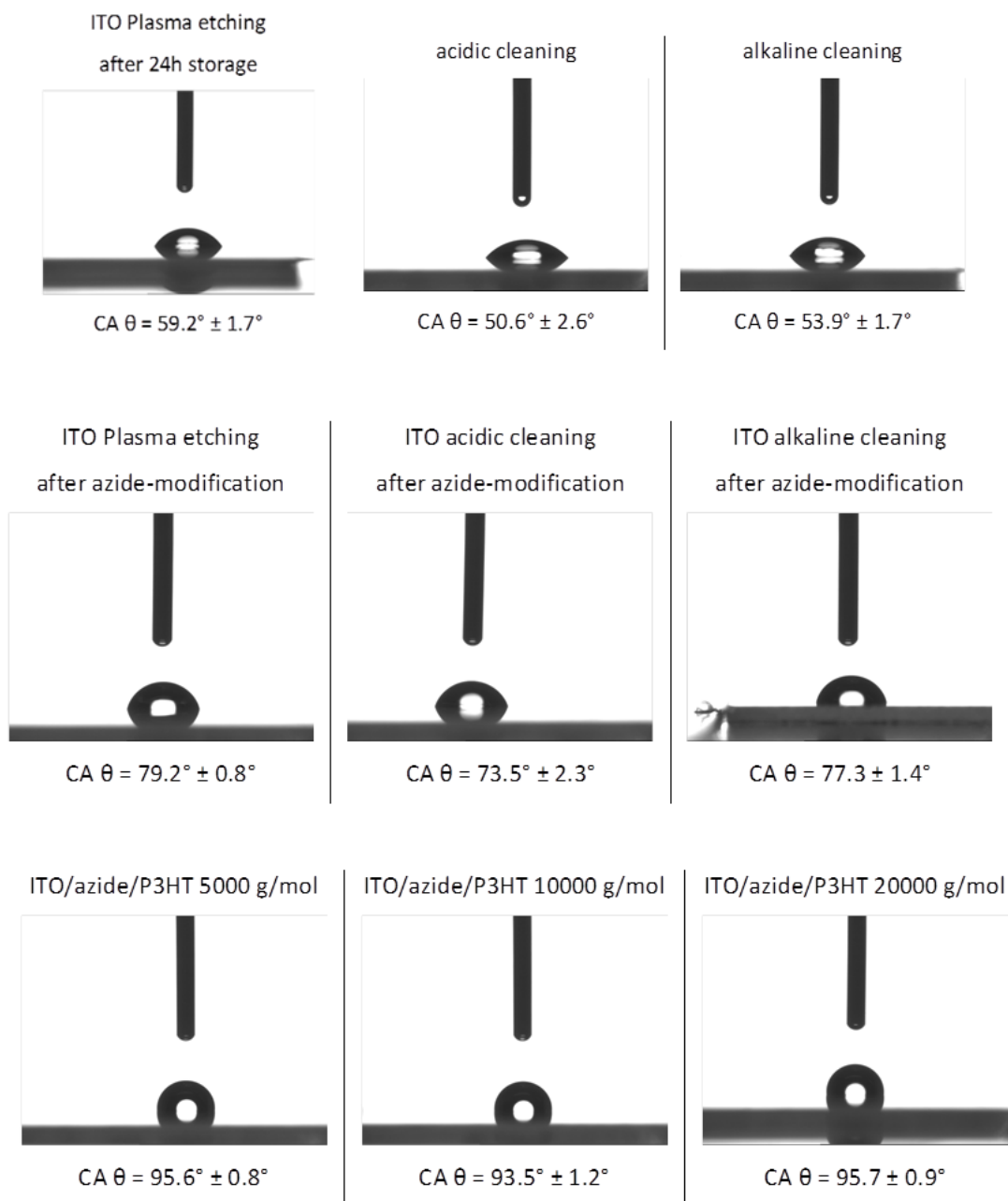


Fig. S 1 *Top*: The clean ITO surface has a contact angle around 50-60°. *Middle row*: After the azide modification and cleaning, it changes to 75-80°. *Bottom*: after grafting a monolayer of P3HT, it increases almost to 100°. This clearly indicates the increase in hydrophobicity of the surface after grating P3HT. We also did not observe any influence of chain length on the contact angle

Table S 1 Charge carrier mobility values, I_{ON}/I_{OFF} for for the monolayers after different solvent/thermal treatments and best values obtained for linear **P3HT** and **Ps-g-P3HT**.

	μ [$\text{cm}^2 \text{V}^{-1} \text{s}^{-1}$]	I_{ON}/I_{OFF}	Channel [μm]
Monolayer (CHCl₃)	1.82×10^{-3}	9.30×10^4	5
	1.52×10^{-3}	7.98×10^4	5
	8.78×10^{-4}	2.15×10^4	10
	1.45×10^{-3}	4.31×10^4	10
	1.18×10^{-3}	3.26×10^4	10
Monolayer (CB)	2.04×10^{-4}	1.76×10^4	20
	2.28×10^{-4}	1.68×10^4	20
	5.99×10^{-4}	1.08×10^5	10
	3.36×10^{-4}	5.56×10^4	10
	1.08×10^{-3}	3.44×10^5	5
Monolayer (o-DCB)	2.04×10^{-4}	1.19×10^4	20
	1.30×10^{-4}	7.33×10^3	20
	5.42×10^{-4}	7.47×10^4	10
	4.23×10^{-4}	5.73×10^4	10
	1.01×10^{-3}	2.81×10^5	5
	1.04×10^{-3}	2.81×10^5	5
Monolayer (100°C)	2.04×10^{-4}	1.30×10^4	20
	1.51×10^{-4}	2.00×10^4	20
	3.63×10^{-4}	8.80×10^4	10
	3.63×10^{-4}	8.00×10^4	10
	5.53×10^{-4}	3.20×10^5	5
Monolayer (150°C)	2.09×10^{-5}	2.0×10^2	20
	4.35×10^{-5}	2.0×10^2	20
	3.11×10^{-5}	1.0×10^3	10
	8.50×10^{-5}	3.0×10^3	10
	9.02×10^{-5}	1.0×10^3	5
	6.94×10^{-5}	1.0×10^4	5
Linear P3HT	4.64×10^{-2}	7.26×10^5	20
	4.57×10^{-2}	7.08×10^5	20
	5.64×10^{-2}	3.02×10^5	10
	4.67×10^{-2}	1.63×10^5	10
PS-g-P3HT	4.47×10^{-2}	5.69×10^4	20
	3.86×10^{-2}	5.41×10^4	20
	3.87×10^{-2}	6.20×10^4	20
	3.91×10^{-2}	6.33×10^4	20
	5.87×10^{-2}	1.60×10^5	10
	5.95×10^{-2}	2.09×10^5	10
	5.80×10^{-2}	2.18×10^5	10
	5.87×10^{-2}	3.36×10^5	10

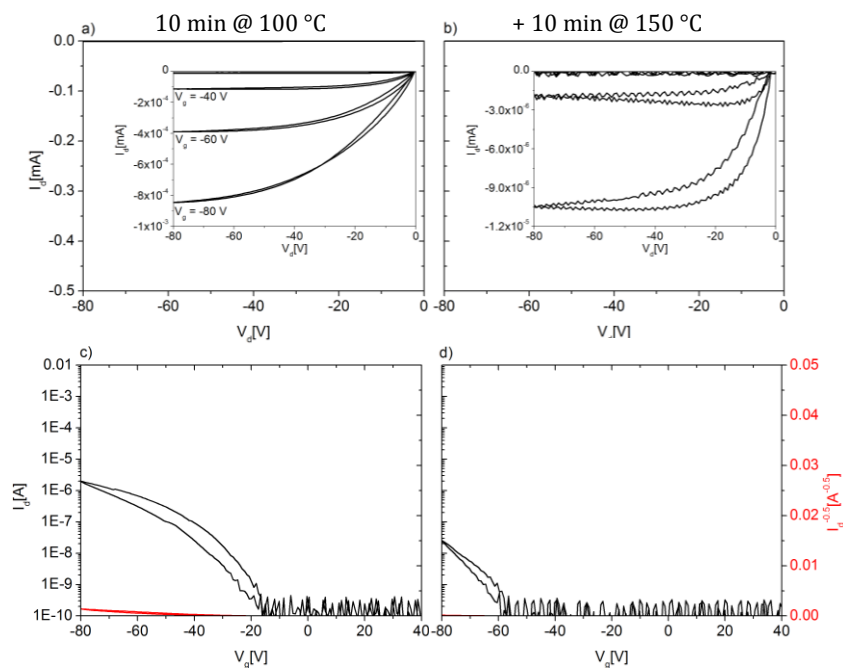


Fig. S 2 Representative OFET I-V-curves of the monolayer dried from chloroform annealed at 100 ° C for 10 min (left) and after additional annealing of the same device at 150°C for 10 min (right). The p-output characteristics are shown at the top (a-b) and the transfer characteristics in saturation regime ($V_d = -80V$) are the bottom (c-d). The channel length was 20 μm in all cases.

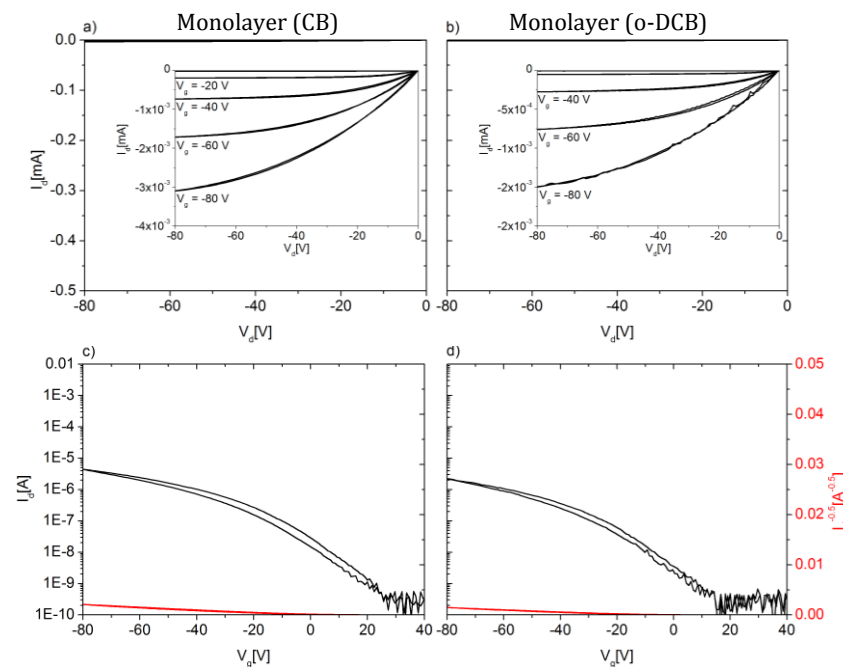


Fig. S 3 Representative OFET I-V-curves of the monolayer dried from chlorobenzene (CB) and o-dichlorobenzene (o-DCB). The p-output characteristics are shown at the top (a-b) and the transfer characteristics in saturation regime ($V_d = -80V$) are the bottom (c-d). The channel length was 20 μm in all cases.

Appendix:

Nanoscale Morphology from Donor–Acceptor Block Copolymers: Formation and Functions

David Heinrich^a, Martin Hufnagel^a, Chetan Raj Singh^a, Matthias Fischer^b, Shahidul Alam^c, Harald Hoppe^{c*}, Thomas Thurn-Albrecht^{b*}, and Mukundan Thelakkat^{a*}

^a Applied Functional Polymers, Macromolecular Chemistry I, University of Bayreuth, Universitätsstr. 30, 95440 Bayreuth, Germany

^b Institut für Physik, Martin-Luther-Universität, von-Danckelmann Platz 3, 06099 Halle, Germany

^c Center for Energy and Environmental Chemistry Jena (CEEC), Friedrich Schiller University Jena, Philosophenweg 7, 07743 Jena, Germany

*E-mail of corresponding authors:
herald.hoppe@uni-jena.de
thomas.thurn-albrecht@physik.uni-halle.de
mukundan.thelakkat@uni-bayreuth.de

Published in in: Leo K. (eds), *Elementary Processes in Organic Photovoltaics. Advances in Polymer Science*, 2017, 272, Springer, Cham.

Reproduced with Permission
Copyright 2017Springer Nature

Content

	Abstract
1	Introduction
2	Donor Building Block: P3HT
2.1	Controlled Synthesis as a Key for Structure Formation
2.2	Structure Elucidation in Bulk and Thin Films of P3HT
2.3	Structural Correlation with Charge Transport in Bulk and Thin Films
3	Acceptor Building Block: Poly(Perylene Bisimide Acrylate)/Poly(PBI)
3.1	Controlled Synthesis
3.2	Charge Carrier Transport in Polymeric
3.3	Effect of Polymer Architecture on the Structure of
4	Acceptor Building Block: Poly(fullerenes)/PPCBM
4.1	Controlled Synthesis
4.2	Structure Formation and Charge
5	Donor-Acceptor Block Copolymers: P3HT- <i>b</i> -PPerAcr
5.1	Synthesis of P3HT- <i>block</i> -PPerAcr
5.2	Structural Elucidation of P3HT- <i>b</i> -PPerAcr
5.3	Solar Cell Devices Based on P3HT- <i>b</i> -
6	Donor-Acceptor Block Copolymer: P3HT- <i>b</i> -PPCBM
6.1	Controlled Synthesis Without Cross Linking
6.2	Structure Formation
7	Conclusion and Outlook
	Acknowledgements
	References

Abstract

General design principles of donor–acceptor block copolymers are reviewed and specific results arising from block copolymers consisting of semicrystalline poly(3-hexylthiophene-2,5-diyl) (P3HT) blocks of appreciably high molecular weight and acceptor blocks carrying pendant perylene bisimides or fullerene derivatives are summarized. The chapter is structured according to the building blocks P3HT, poly(perylen bisimide acrylate), and a polystyrene copolymer grafted with phenyl-C₆₁-butyric acid methyl ester used for the synthesis of the corresponding block copolymers, and in each part the synthetic challenges, structure formation, and consequences for charge transport, and in some cases photovoltaic properties, are addressed.

Keywords Crystallization • Donor-acceptor block copolymers • Microphase separation • Poly(3-hexylthiophene-2,5-diyl) • Scattering techniques • Self-assembly

1 Introduction

Conjugated polymer–based organic solar cells have been successfully developed over the past 20 years,^{1–7} reaching current power conversion efficiencies (PCEs) over 10 %.^{8–15} One major requirement, which arises from the fact that organic semiconductors generally exhibit strong exciton binding energies one order of magnitude above the thermal energy (k_{BT}) and only small exciton diffusion lengths (a few nanometers), constitutes the existence of a so-called donor–acceptor (D–A) interface to facilitate exciton dissociation and thus charge generation at this heterojunction interface. Thus, only an intimate blend of donor and acceptor phases enables efficient charge generation throughout the bulk of the photoactive layer. Here the acceptor can be distinguished from the donor simply by having a larger electron affinity, thus forming a type II heterojunction. In other words, both the lowest unoccupied molecular orbital (LUMO) as well as the highest occupied molecular orbital (HOMO) of the acceptor need to have lower energy than the donor. In addition to

charge generation, their efficient extraction at the two opposing selective electrodes displays a second requirement for successful photovoltaic operation. Hence, donor and acceptor phases need to form a bicontinuous interpenetrating network of a certain coarse-grained lateral extension, providing percolation paths for both types of charge carriers (i.e., holes and electrons). To minimize charge recombination events, these phases need to be well separated at a length scale roughly corresponding to the exciton diffusion length,¹⁶ and both the charge generation and extraction benefit from the existence of semicrystalline phases. This three-dimensional mixing of donor and acceptor phases on the nanoscale is called the bulk heterojunction morphology.^{17,18}

Commonly, the formation of such bulk heterojunctions is practically obtained from blending the two molecular or polymeric components in a common organic solvent and casting a film from it, resulting in a morphology governed by a kinetically locked nonequilibrium distribution of those two phases. The disadvantage of this approach lies in the fact that the scale of phase separation can be subject to coarsening processes with time, resulting in an increase of domain sizes as a result of phase separation^{19,20} or unfavorable phase segregation toward an electrode,²¹⁻²³ reducing the amount of charge generation and extraction over time. These processes are generally termed *morphological degradation* and need to be prevented to ensure long-term efficient device operation. Hence several approaches have been developed to lock the scale of phase separation within the bulk heterojunction, among which (1) cross linking of single phases by, for example, epoxy-based agents,^{19,24} (2) increasing the glass transition temperature of the blend,^{22,25-28} (3) compatibilization of the donor and acceptor phases via bifunctional surfactants,^{29,30} and finally, (4) the use of microphase-separated D-A diblock copolymers as a single component with microstructures at thermodynamic equilibrium^{31,32} have been pursued. In the last approach, in addition to the viability of stable morphology, the scale of phase separation can be finely adjusted via precise control of the individual donor and acceptor blocks lengths to meet the restrictions of the exciton diffusion lengths. Furthermore, by definition of the respective volume fraction via the individual block lengths, certain phase distributions can be readily obtained, as predicted by the phase diagram of block copolymers. As an

illustration, **Fig. 1** summarizes various resulting phase distributions dependent on the relative volume fractions of phases A and B.

In this chapter, this approach toward creating microstructures in D–A block copolymers is reviewed. So far, polymer physics has described mostly the phase behavior of coil-coil (amorphous or liquid-like) block copolymers, that is, where both blocks exhibit a rather small persistence length (or Kuhn segment length), making them rather flexible. However, as already pointed out above, semicrystalline phases inhere the advantage of improved charge-transport and -generation capabilities, which triggered many authors to choose the so-called semicrystalline block copolymers (often referred to as rod-coil or rod-rod) to aim for well-defined phase separation in conjunction with crystallinity within the individual hole- and/or electron-transporting domains. With that approach, the goal of the majority of the studies was to obtain a controlled self-assembly of the donor and acceptor phases via molecular design of the functional blocks, yielding nanostructures suitable for photovoltaics and enabling efficient charge generation and transport over the whole lateral area of photovoltaic devices (compare with **Fig. 2**).

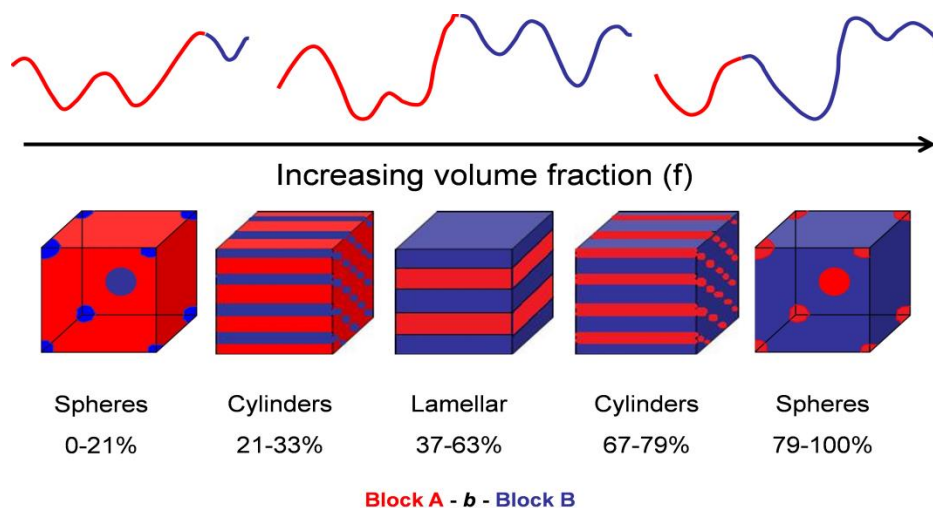


Fig. 1 Schematic representation of most commonly observed morphologies of coil-coil block copolymers dictated by relative volume fractions. Typical range of percent volume fractions for the morphologies is also shown. Left to right: spherical, cylindrical, lamellar, inverse-cylindrical, inverse spherical phases. The red phase represents polymer block A and the blue phase represents polymer block B. (Reproduced with permission from 33)

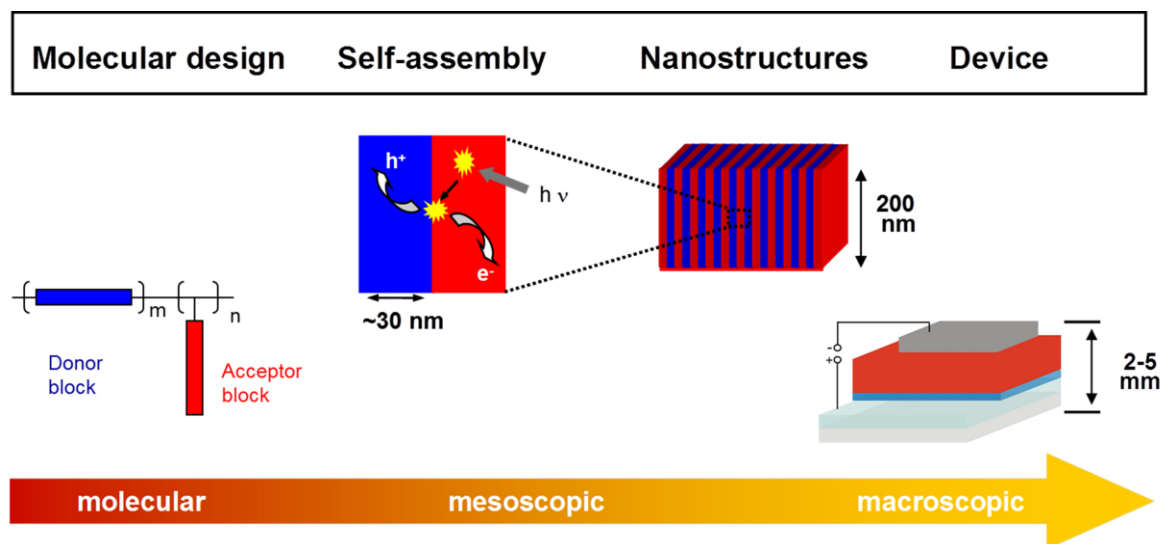


Fig. 2 The schematic shows the goal pursued: via control of molecular structure by design leading to morphological control through self-assembly of nanostructures, yielding functional control in devices spanning all length scales from molecular (nanoscopic) over mesoscopic nanostructures to macroscopic device levels.

Several attempts for reaching this goal were followed and have been described in the literature so far, from realizing first functional block copolymers with a dual function of electron- and hole-transporting phases,^{34–43} to using oligomers with a rather small scale of phase separation,⁴⁴ up to the current rather successful approaches based on diblock copolymers exhibiting a poly(3-hexylthiophene-2,5-diyl) (P3HT)-based donor block combined with a fullerene-based acceptor block.^{45,46} Because of the large diversity of chemical structures and the huge number of publications in this field, we limit our discussions to P3HT systems in which the acceptor block carries either perylene bisimides (PBIs) or fullerene derivatives (C₆₀, C₇₀) as pendant groups (see **Fig. 3**). For reviews of different kinds of semiconductor block copolymers, we draw attention to published work by Mori *et al.*,⁴³ Horowitz *et al.*,³⁴ Thelakkat *et al.*,^{39,40} and Scherf *et al.*⁴⁷ The chemical structures of some of the reported D–A block architectures are given in **Fig. 4**. Hashimoto *et al.*⁴⁸ developed the most successful P3HTb-poly(C₆₀) systems in which the fullerenes were grafted to a P3HT copolymer backbone, delivering PCEs of 2.46% in single-layer devices using polymer 4 (**Fig. 4**).

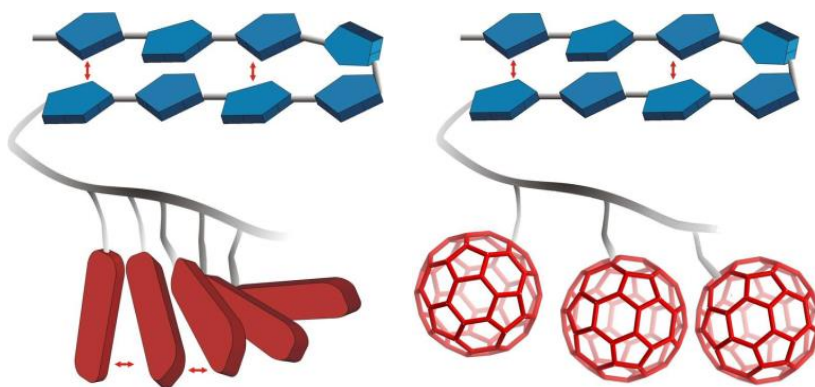


Fig. 3 Schematics of P3HT containing block copolymers carrying either perylene bisimides (PBI) or fullerene derivatives as pendant groups in the acceptor block. The double-headed red arrows indicate the $\pi-\pi$ interaction of the thiophene units leading to crystallinity and improved charge transport in these systems.

The best-performing device so far was indeed obtained using a non-fullerene-based acceptor block using a poly(9,9-dioctylfluorene)-co-(4,7-di-2-thienyl-2,1,3-benzothiadiazole) copolymer approaching 3% PCE.⁵¹ This success was largely the result of a considerably high open-circuit voltage of more than 1.2 V.

In this chapter, studies are reviewed which focus on an improved understanding of the self-assembling process by bringing the block copolymers first into the melt, accompanied by the formation of a microphase separation, and followed by a controlled crystallization upon slow cooling. A major challenge that still remains to be solved consists of obtaining the desired vertical phase orientation within the photoactive layer.

To understand and control the D-A nanostructure in block copolymer systems as introduced above, it is important to identify the driving forces responsible for structure formation. The classical microphase separation refers to systems with two amorphous blocks and is driven by their incompatibility, quantified by the product $N\chi$ (N is the degree of polymerization, and χ is the Flory-Huggins interaction parameter). In addition, the phase diagram depends on the volume fraction; cf. **Fig. 1**. The situation becomes more complex if additional ordering processes take place within the individual blocks, which can also lead to a separation of the components. Crystallization is such an ordering process, but the formation of liquid-crystalline phases can also influence microphase separation.⁵³ The complexity of microphase separation in crystalline-amorphous systems as well as in double-crystalline block copolymers has, been studied

in detail by, for instance, Register *et al.* using polyethylene as a model block.^{54,55} In general, it is useful to first study the individual components of such a complex block copolymer system by themselves before studying structure formation in the fully functionalized block copolymers. As P3HT can crystallize and as most D-A block copolymers synthesized until now contain P3HT as the donor block, the case of crystallization is most important. Schematically, this situation is illustrated in **Fig. 5**.

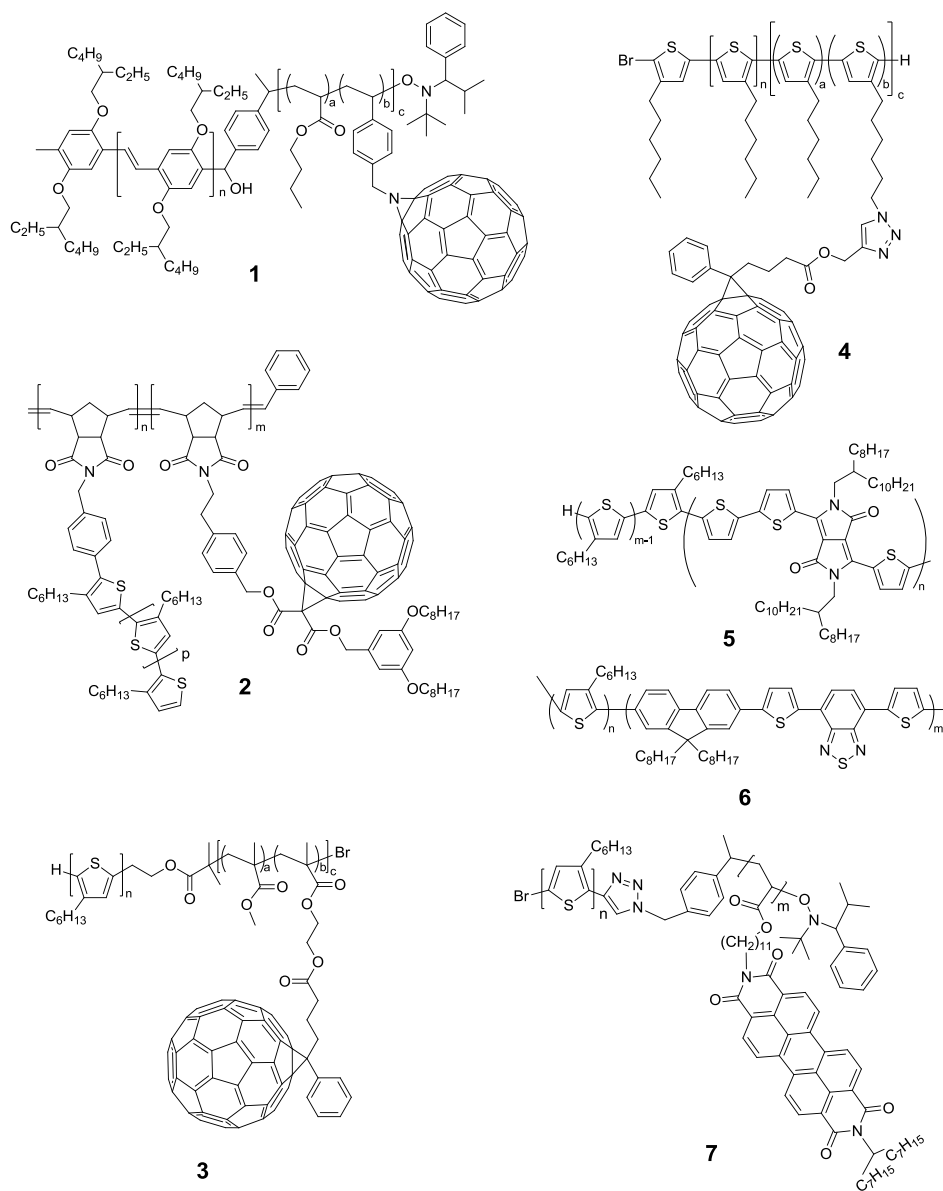


Fig. 4 Chemical structures of some of the selected P3HT-*b*-Poly(C₆₀) systems (polymers 1-4),^{28,48-50} all conjugated polymers (polymers 5,6),^{51,52} and a P3HT-*b*-PPerAcr system 7,⁴⁰ which were tested in polymer solar cells.

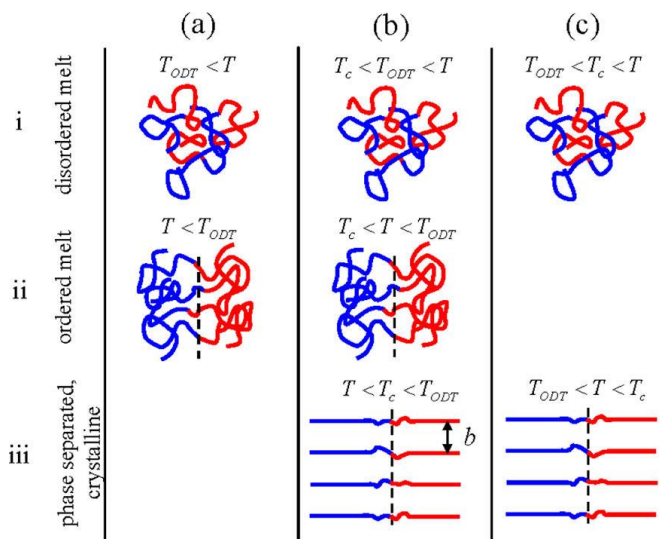


Fig. 5 Schematic illustration of possible ordering scenarios for block copolymers upon cooling (top to bottom): (a) A block copolymer with two noncrystallizable blocks forms a disordered melt at temperatures above the order–disorder temperature T_{ODT} (i), while for $T < T_{ODT}$ (ii) in the ordered melt the well-known microphase separated morphologies develop. For block copolymers with one or two crystallizable blocks, the crystallization of the individual blocks either occurs from an ordered melt (b) or directly from the disordered melt (c) depending on the relative locations of T_{ODT} and T_c . Here, for simplicity, only one melting/crystallization temperature T_c was assumed. For case (b) very often crystallization overrides the existing microphase structure leading to a nanostructure consisting of lamellar crystals as in case (c). The case where for (b) the microphase structure stays intact upon crystallization, is called confined crystallization. (Reproduced with permission from 56)

An additional aspect to be taken into account when considering structure formation in D–A block copolymers is the dependence on processing pathways. Drying from solution and cooling from the melt might not necessarily lead to the same nanostructure. Nevertheless it makes sense to first attempt to determine the equilibrium structure and to study deviations from it in a second step. To get information about phase diagrams, temperature-dependent in situ techniques are necessary, such as scattering techniques, complemented by imaging techniques used mostly at room temperature. To understand the structure formation in D–A block copolymers, in the following we first detail the controlled synthesis leading to structure formation in individual blocks.

2 Donor Building Block: P3HT

2.1 Controlled Synthesis as a Key for Structure Formation

Polythiophene, one of the most commonly used and most studied conjugated polymers, was earlier synthesized as an unsubstituted and insoluble derivative.^{57,58} Later irregular alkyl-substituted polythiophene⁵⁹ and in recent years regioregular poly(3-hexylthiophene-2,5-diyl), P3HT was prepared by Ni-catalyzed syntheses.^{60,61} A further development was the synthesis of the active Grignard monomer species through a Grignard metathesis reaction.⁶² This route, which starts from 2,5-dibromo-3-hexylthiophene, will be referred to as the McCullough route, whereas the Yokozawa route uses 2-bromo-3-hexyl-5-iodothiophene as the starting component (**Fig. 6**). Yokozawa *et al.*^{64,66} and McCullough *et al.*^{65,67} were able to show that the Ni-catalyzed polymerization of **2a** follows a chain growth mechanism and gives increased control over the properties of the targeted polymer.

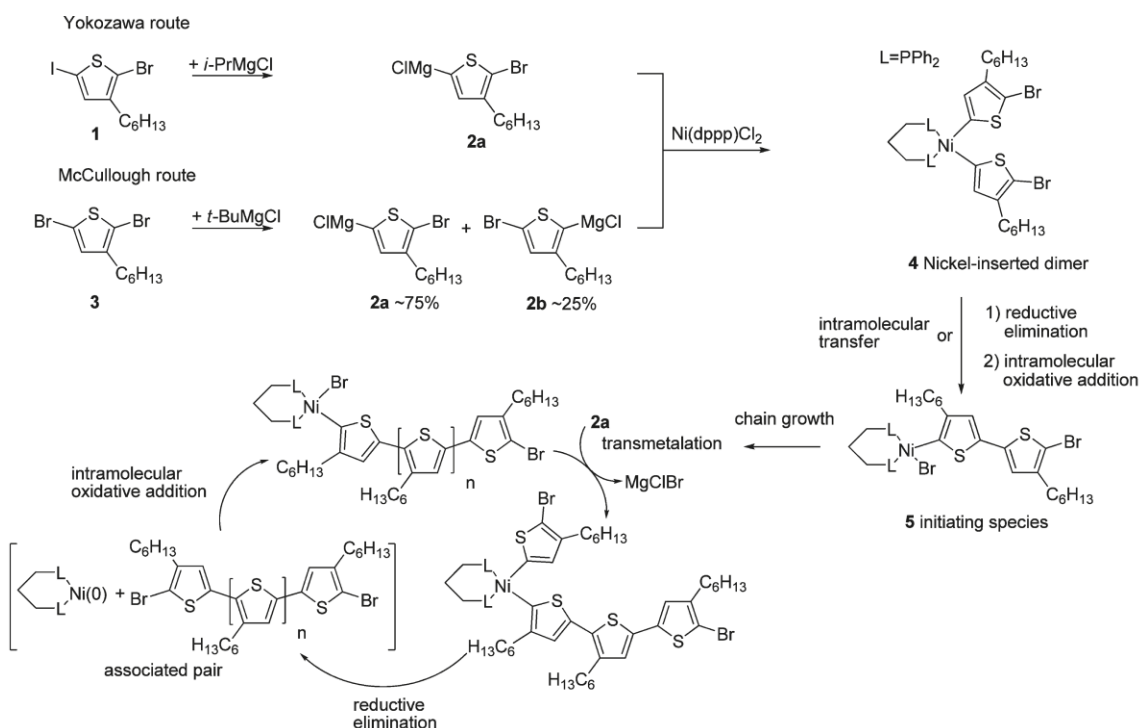


Fig. 6 Formation of the active Grignard monomer **2a** by Yokozawa and McCullough route, and chain growth mechanism of the Kumada catalyst transfer polymerization. (Reproduced with permission from 63)

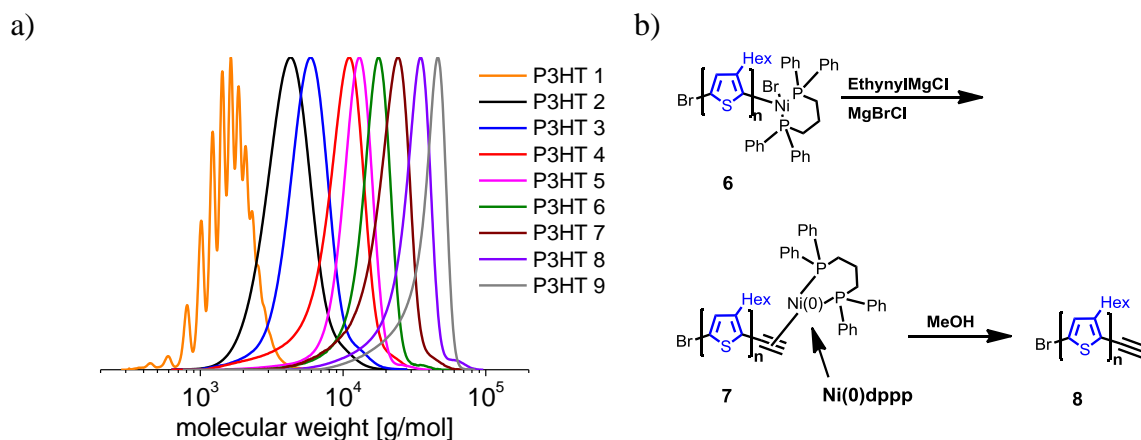


Fig. 7 a) Size exclusion chromatography (SEC) curves of a series of P3HTs with different molecular weights and narrow distributions. The SEC was calibrated against polystyrene standards. b) Formation of P3HT-Alkyne via endcapping with ethynyl magnesium chloride and quenching in methanol.

With this method it was possible to synthesize regioregular P3HT with narrow distributions and predictable molecular weights, which can be seen from the size exclusion chromatography (SEC) curves of a series of P3HTs with different molecular weights (**Fig. 7a**). The method is generally termed Kumada catalyst transfer polymerization (KCTP). Upon addition of the nickel catalyst, the active species **2a** forms the nickel inserted dimer **4**; species **2b** does not take part in the polymerization because of the sterical hindrance of the hexyl chain. One regio defect is always generated at the initial step from the inserted dimer **4** to the initiating species **5**. In the additional chain growth step, only head-to-tail couplings occur. After the monomer is consumed, the living chain remains active until the reaction is quenched with a suitable reagent. If P3HT is intended to be used in block copolymer systems or other, more complex architectures, it is important to control the end groups of the obtained polymers. Lohwasser *et al.*⁶³ showed that a detailed understanding of the mechanism involved makes it possible to perfectly control the end groups of P3HT. It has been shown that the quenching agent has a great effect on the final product.⁶⁸ Methanol as quenching agent was shown to lead to chain-chain coupling via disproportionation, which has a detrimental effect that cannot be observed after quenching the polymerization in dilute HCl. It has also been shown that a complete Grignard monomer formation was crucial to achieve almost 100% H/Br end groups. When LiCl was used as an additive, the complete consumption of t-BuMgCl and the complete formation of the

active species could be assured.⁶⁹ LiCl accelerates the active monomer formation and increases the molecular weight of the final polymer by also incorporating the second sterically disfavored monomer species **2b**. Wu *et al.*⁷⁰ found that the detrimental effect of the incorporation of the second monomer on the regioregularity is minimal. This is because of the lower reactivity of the sterically hindered monomer **2b**, which is only incorporated into the polymer chain once most of the majority species **2a** is consumed. A simple way to obtain functional end groups is highly advantageous when P3HT is intended to be part of a block copolymer or more complex polymer architectures. Jeffries *et al.*⁷¹ reported a straightforward method to obtain a series of end groups simply by adding a functional Grignard reagent in order to end cap the polymer. While this method proved to be highly versatile and efficient, it did lead only to monocapped products for a variety of end-capping agents. Only end groups like vinyl or alkyne, which form stable π -complexes with the nickel catalyst, did not lead to dicapped products. The formation of dicapped products in cases where the catalyst was not bound to the end group can be explained by the effect of a random catalyst walking along the polymer chain, which was observed by Tkachov *et al.*⁷²

The authors were able to show that the catalyst is not bound to one chain end but can move along the chain and initiate the polymerization at the other end of the polymer. This process, aside from having possibly negative effects on end capping, also leads to a change of position of regiodefects, which will not stay at one chain end but may rather be in the middle of the chain at the end of the polymerization. Especially alkyne-functionalized P3HT can be an interesting starting material for the synthesis of block copolymers containing P3HT. To obtain such polymers in high yield, it is again crucial to quench the polymerization in the appropriate media. Lohwasser *et al.*⁷³ showed that, in the case of alkyne functionalization, dilute HCl leads to a hydration and hydrohalogenation of the end group. Methanol, on the other hand, appeared to be a good choice in this particular case. The nickel is now in the Ni(0) state and no disproportionation reaction with the methanol is therefore possible (see **Fig. 7b**).

2.2 Structure Elucidation in Bulk and Thin Films of P3HT

2.2.1 Temperature-Dependent Phase Diagram

The structure of P3HT has been studied in detail by many authors, for instance.⁷⁴⁻⁷⁶ Depending on the conditions of sample preparation such as solvent, temperature, and molecular weight, it can exist in an amorphous phase with coiled chain conformations or in an aggregate phase containing planarized chains with a tendency to form semicrystalline domains. It has also now been well established that P3HT can adopt different morphologies.⁷⁶ Using selected samples of P3HT with well-defined molecular weight and high regioregularity from the series of materials mentioned above, Wu *et al.*⁷⁷ performed temperature-dependent in situ small- and wide-angle X-ray scattering experiments complemented by differential scanning calorimetry (DSC) and atomic force microscopy (AFM) experiments. **Fig. 8** shows the results of DSC measurements on a series of P3HTs with varying molecular weights.

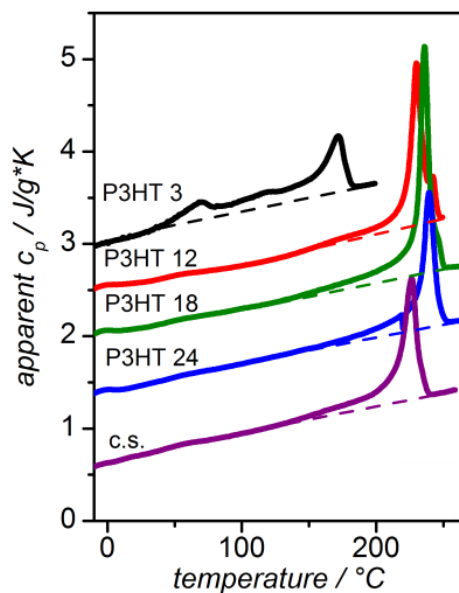


Fig. 8 Differential scanning calorimetry thermograms of samples of P3HT with a well-defined molecular weight. The sample names indicate the molecular weight M_n as obtained by matrix assisted laser desorption/ionization time-of-flight mass spectrometry; polydispersities are about 1.15. C.S. is a commercial sample with a broader molecular weight distribution. All data were obtained during a second heating run with a rate of 20 K/min. Other than with P3HT 24, all curves are shifted vertically for clarity. *Straight lines* below the melting peaks are used as a background signal subtracted for integrations to determine the melting enthalpy ΔH_m . Note the transition around 60 °C for P3HT 3 caused by side chain melting. (Reproduced with permission from 78)

Excluding the sample with the lowest molecular weight, all samples melt in a similar temperature range around 220 °C. P3HT 3 shows an additional peak around 60 °C, whose structural origin becomes clear when considering the temperature-dependent wide-angle X-ray scattering (WAXS) patterns shown in **Fig. 9** together with a sketch of the microstructure of P3HT. As described in the figure caption, the reflections indicating order in the crystal across the layers separated by side chains disappear around 60 °C, in line with the observed transition in the DSC. The samples with higher molecular weight do not show this transition, most likely because the corresponding ordering process at low temperatures is kinetically suppressed. This interpretation of the phase transition was later confirmed by nuclear magnetic resonance (NMR) experiments in which a structural disordering process of the alkyl side chains, not affecting the rigidity and conformation of the backbones, could also be observed.⁷⁹

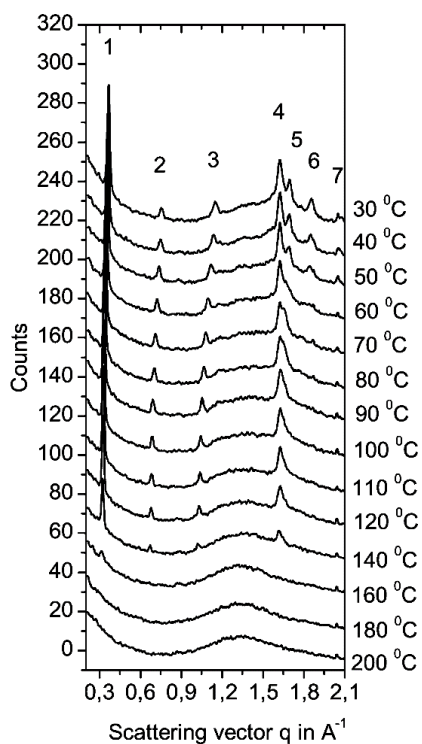
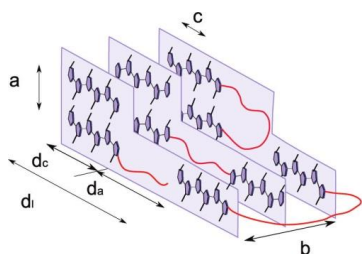


Fig. 9 *Top*: temperature-dependent wide-angle X ray powder scattering diagrams of P3HT 3 reflecting the crystal structure. All data were taken during heating. Bragg reflections are numbered from low to high scattering vector. Peaks 1–3 are caused by alternating layers of main and side chains in the a-direction, while peak 4 reflects the stacking. Peaks 5 and 6 carry mixed indices (hk0) and can only exist if crystal packing in different layers of main chains is in register. This kind of order is lost at the phase transition at 60 °C, which can therefore be attributed to side chain disordering. Peak 7 contains a contribution from the substrate and remains therefore visible up to the highest temperatures.



Bottom: scheme of the typical microstructure of regioregular P3HT. a, b, c, crystal lattice parameters; d_c , thickness of lamellar crystals; d_a , thickness of amorphous layers, d_l , long period (scheme not to scale: the long period is about one order of magnitude larger than the lattice parameters a, b, c). (Reproduced with permission from 77)

2.2.2 Semicrystalline Morphology of P3HT

That P3HT is semicrystalline is confirmed by the observation of a diffuse scattering signal in the X-ray diffraction pattern appearing underneath the Bragg reflections reflecting the crystalline fraction of the sample (**Fig. 9**). The corresponding morphology can be visualized by AFM. In the lower row of **Fig. 10**, a well-developed semicrystalline morphology, consisting of lamellar or fibrous crystals separated by amorphous domains on a scale of some 10 nm, is visible. These samples were crystallized by cooling from the melt. Directly after spin coating, crystallization is largely suppressed, as the images in the upper row show. A more quantitative analysis of the semicrystalline morphology is possible with SAXS, which allows a measurement of the long period of the semicrystalline structure. The result is shown in **Fig. 11** together with the contour length of the corresponding molecular weight. The results show that for low molecular weight the polymer crystallizes as extended chain crystals but starts to form folded chain crystals around a molecular weight of 12 kg/mol [matrix assisted laser desorption/ionization time-of-flight mass spectrometry (MALDI-TOF MS)].

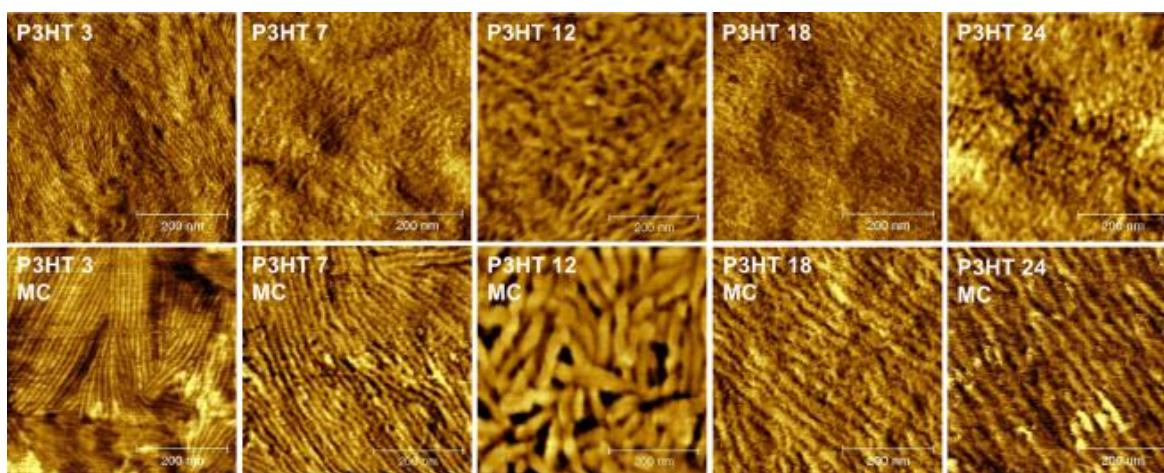


Fig. 10 Atomic force microscopy phase images of spin-cast (top) and melt-crystallized (bottom) films of P3HT with different molecular weights. The scan area for each sample is 500 x 500 nm². (Reproduced with permission from 80)

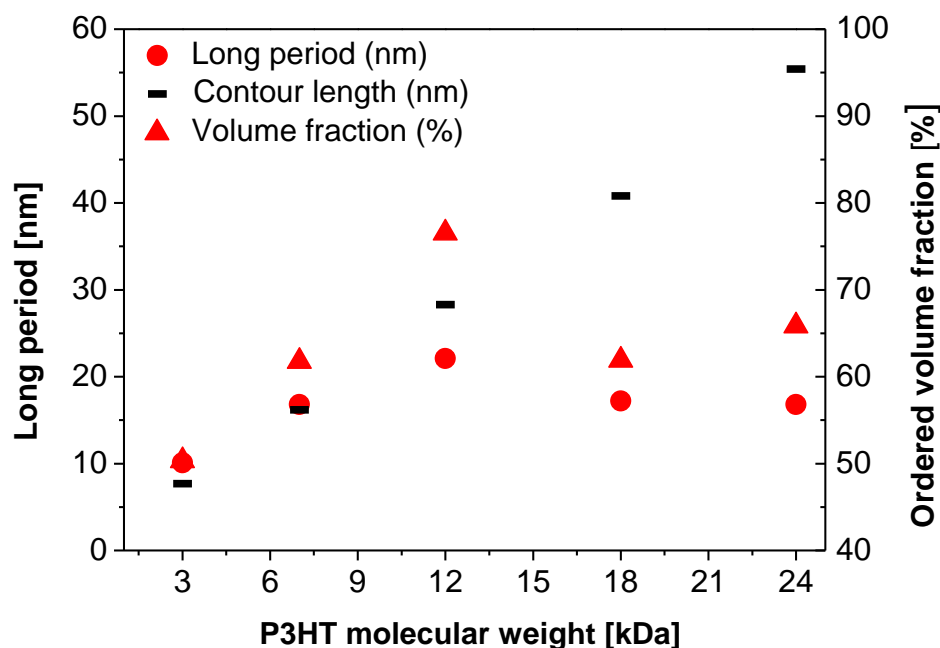


Fig. 11 Left axis: long period (circles) as measured by small-angle X-ray scattering in bulk samples and calculated contour lengths (black bars) vs. molecular weight of P3HT (matrix assisted laser desorption/ionization time-of-flight mass spectrometry). Right axis: volume fraction (triangle) of more ordered P3HT domains in melt-crystallized films determined by analysis of ellipsometric data. (Reproduced with permission from 80)

2.2.3 Quantitative Determination of Crystallinity

A common method to determine the crystallinity of a semicrystalline polymer is based on comparing the melting enthalpy as determined by DSC to the melting enthalpy of a 100 % crystalline sample. The latter value has to be determined independently by an absolute method such as X-ray diffraction or NMR. We therefore attempted a quantitative determination of the crystallinity based on temperature-dependent SAXS/WAXS measurements on the above-mentioned series of P3HT with different molecular weights. The analysis is based on the evaluation of the scattered intensity from the amorphous regions as shown in **Fig. 12**, providing an easy and fast method to determine the crystallinity in the class of side chain-substituted polymers. The resulting values for the crystallinity of our P3HTs are in the range of 68-80 % at room temperature depending on the molecular weight. Based on these values, an extrapolated reference melting enthalpy of a 100 % crystalline material was

determined ($\Delta H_{m,\infty} = \pm 33.3$ J/g) for use in DSC measurements. This value is consistent with a previous estimation based on NMR measurements⁷⁹ and includes a substantial correction to previously used values.⁸¹ For higher molecular weights a decrease of the crystallinity was observed that can be explained by the onset of chain folding as deduced from the analysis of the SAXS patterns. An in-depth analysis of the scattering patterns indicated that the crystalline regions of P3HT exhibit a large amount of internal disorder, considerably larger than typically found in other synthetic polymers. The results are described in detail in.⁷⁸

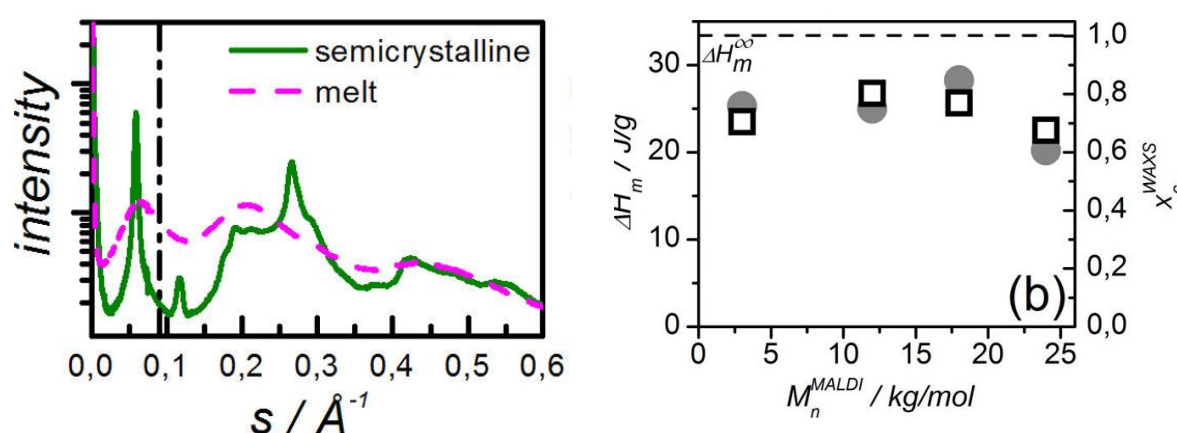


Fig. 12 Left: X-ray diffraction pattern of P3HT 18 in the semicrystalline state at 40 °C (solid line) after cooling from the melt and in the melt (dashed line). The vertical dot-dashed line indicates the range in which the intensities were compared to determine the crystallinity. Right: crystallinities determined by wide-angle X-ray scattering (squares) and differential scanning calorimetry melting enthalpies (gray circles) of P3HT showing the same trend with molecular weight. The broken horizontal line indicates the extrapolated melting enthalpy of a 100% crystalline sample. (Reproduced with permission from 78)

2.3 Structural Correlation with Charge Transport in Bulk and Thin Films

Based on the results described above, the effect of crystallinity and molecular weight on the hole mobility in P3HT was investigated in single-carrier devices using the space charge limited current (SCLC) method.⁸⁰ To vary the crystallinity in otherwise identical materials, we prepared two samples; one remained in the disordered state after spin coating, while the other was crystallized from the melt. As **Fig. 10** shows and as confirmed by X-ray scattering, crystallization is largely suppressed after spin coating because of the fast drying process. The results of the charge-transport investigation in **Fig. 13** show that there is a strong increase of up to one order of magnitude in hole

mobility upon crystallization. Even stronger was the effect of molecular weight, displaying a strong rise over nearly three orders of magnitude from the lowest to intermediate molecular weights. Beyond 12 kg/mol, the hole mobility decreased again and leveled off for highest molecular weights. This reduction thus occurred at a molecular weight, where chain folding sets in, resulting in a decrease in the overall crystallinity and an increase in the amorphous volume fraction. This result is in good agreement with the general model of chain organization, leading to predicted changes in certain material properties according to Vikar *et al.*⁸² In this case, however, the dependency is exponential, whereas the crystallinity itself displays the same behavior on a linear scale (compare with **Fig. 11**). It should be noted that the charge carrier mobility obtained for the melt-crystallized P3HT sample with MD12 kg/mol is one of the highest reported values for bulk charge transport through a film, thus reflecting the extraordinary quality of the material synthesized as described above. Based on these charge carrier mobility studies, the intermediate molecular weight sample could be identified as an ideal building block for the donor within block copolymers.

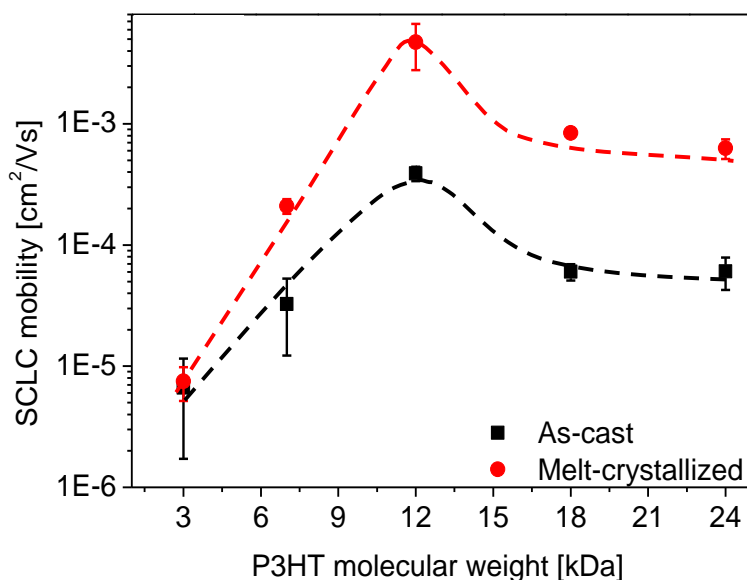


Fig. 13 Space charge limited current charge carrier mobility of holes in as-cast (*square*) and melt-crystallized (*circle*) P3HT films of different molecular weights (matrix assisted laser desorption/ionization time-of-flight mass spectrometry). Each data point represents the average of three to four sets of devices produced for varying film thicknesses in the range of 250–350 nm. Dashed lines are shown as a visual guide for the observed trend of charge carrier mobility. (Reproduced with permission from 80)

3 Acceptor Building Block:

Poly(Perylene Bisimide Acrylate) /Poly(PBI)

3.1 Controlled Synthesis

Polymers with pendant perylene bisimide side chains (PPBI) were first reported by Lindner *et al.*⁸³ in 2004. The authors synthesized an asymmetrical PBI monomer with a solubilizing swallow-tail substituent and an acrylate group for polymerization. This acrylate monomer was polymerized with nitroxide-mediated radical polymerization (NMRP).⁸⁴ It was possible to obtain moderate molecular weights by this method, and even block copolymers were obtained via sequential polymerization.⁴⁰ The homo-polymerization of this high-molecular-weight PBI monomer is not optimal. Narrow distributions, which are characteristic for controlled radical polymerizations, could not be obtained. In addition, the polymerization has to be performed at high monomer concentrations and the resulting polymer shows a limited solubility. This makes it difficult to achieve high molecular weights and also limits the choice of side chains that can be introduced. These synthetic restrictions were overcome by introducing the Copper-catalyzed azide-alkyne cycloaddition (CuAAC) “click” chemistry concept⁸⁵ and combining it with controlled radical polymerization. The first attempt to obtain PPBI polymer using this concept was reported by Tao *et al.*⁸⁶ in 2009.

Lang *et al.*⁸⁷ investigated this concept in detail and compared it to the conventional synthesis approach. The polymer backbone is synthesized independently and afterward decorated with the PBI moieties. The authors synthesized poly(propargyloxystyrene) via NMRP with alkyne functionality at each monomer unit and also PBIs with azide functionality. Alkynes can undergo a very efficient reaction at room temperature with azides in the presence of a Cu(I) catalyst and form stable 1,4-substituted triazoles.⁸⁶ It was reported that the polymer backbone can be almost quantitatively decorated with the PBI moieties as proven by Fourier transform infrared and proton NMR spectroscopy. These polymers had very narrow distributions as good as 1.16 and molecular weights of up to 15.000 g/mol.

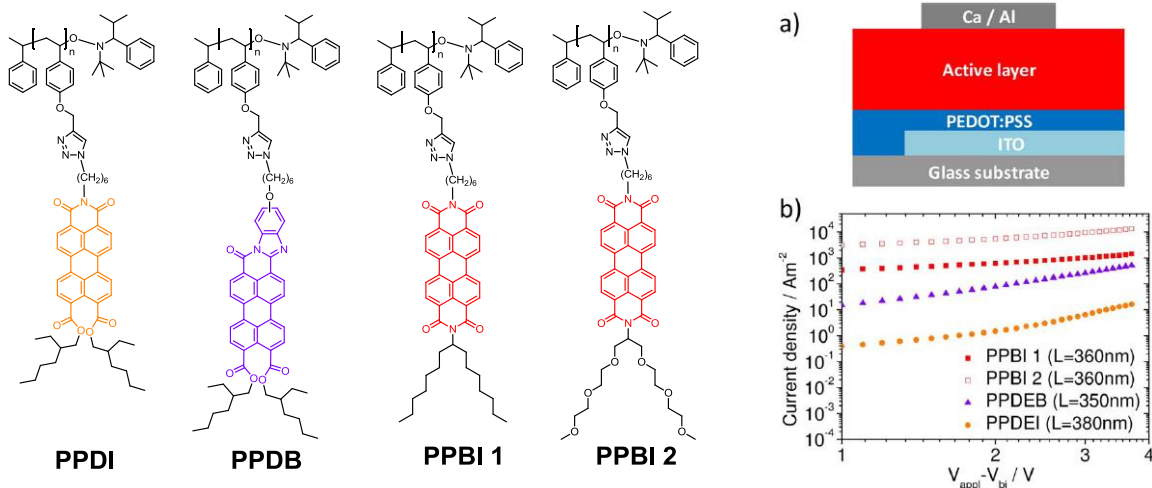


Fig. 14 Left: Pendant perylene side chains synthesized via “click chemistry” and right: a) Schematic of an electron-only device and (b) J - V characteristics for electron-only devices of compounds PPBI 1, PPBI 2, PPDB, and PPDI with active layer thickness L . (Reproduced with permission from 89)

The “clicked” polymers were compared with poly(PBI acrylates) (synthesized directly via NMRP) with different alkyl spacers. The comparison of the phase behavior showed a strong dependence on spacer lengths. In a further study, Lang *et al.*⁸⁸ investigated the effect of the spacer length and different phase behavior of PPBI polymers with hydrophilic side chains. Two sets of polymers were synthesized as shown in **Fig. 14**: **PPBI 1** - polymers with PPBIs with hydrophobic alky swallow tails; and **PPBI 2** - a set with hydrophilic oligo ethylene glycol swallow tails. In both cases three polymers were synthesized, using three different spacers [(CH₂)₆, (CH₂)₈, and (CH₂)₁₁]. Systematically investigating the influence of the PBI substitutions could be done because the approach of a polymer-analogous introduction of different pendant groups to a single precursor polymer made it possible to obtain a set of highly comparable polymers. All polymers had molecular weights up to 60.000 g/mol (SEC) and narrow distributions below 1.09. This also showed that this modular synthesis method is reliable even for higher molecular weights. A marked difference between hydrophilic PPBIs with OEG- and hydrophobic PPBIs with alkyl swallow tails was reported. The hydrophilic PPBIs were all found to be amorphous with the spacer length influencing the glass transition temperature, T_g , of the polymers. An increase in spacer length reduced T_g . A similar trend was observed for the T_g of the hydrophobic polymers with generally higher transition temperatures. If the spacer length did not exceed

(CH₂)₈, the polymers were not amorphous but liquid crystalline. The introduction of the new hydrophilic side chains claimed to increase the χ -parameter through a polar-apolar driving force and could be interesting for a supposed block copolymer implementation. Two other new perylene derivatives were introduced utilizing this reliable concept.⁸⁹ In this case, the electronically active perylene core was modified itself, tuning the absorption properties of the polymers. A poly(peryene diester benzimidazole) (**PPDB**) and poly(peryene diesterimide) (**PPDI**) with a blue - respectively, redshifted - absorption with respect to PBIs were successfully synthesized (see **Fig. 14**).

3.2 Charge Carrier Transport in Polymeric PBIs

As the same parent scaffold polymer was used for “clicking” the different perylene derivatives, the influence on charge-transport properties by modifying the pendant perylene core and the substituents on PBI could be well compared.⁸⁹ In organic field-effect transistor (OFET) devices, poor performance with high threshold voltages, hysteresis, and low on/off ratios were reported for each material. Electron mobility values of the OFET measurements are summarized in Table 1. Since the charge transport in OFET geometry is determined by a thin channel of charge at the gate-dielectric interface, the results can be heavily influenced by the interface effects, wetting/dewetting issues, and unfavorable alignment of the polymers within the channel. Thus, the SCLC method is better suited to compare the bulk charge transport properties of these polymers. The SCLC electron mobilities are usually determined by fitting measured J - V characteristics using the Mott-Gurney equation in electron-only SCLC devices.⁹⁰ The mobility values obtained from the SCLC devices are also mentioned in **Table 1**.

Table 1 Organic field-effect transistor (OFET) and space charge limited current (SCLC) (obtained from single-carrier devices with an active layer thickness of ca. 350 nm) mobility values for PDEB, PDEI, PPBI 1, and PPBI 2.^{80,90}

Polymer	OFET electron mobility (μ_e) (cm ² /Vs)	SCLC electron mobility (μ_e)(cm ² /Vs)
PPDB	-	6×10^{-4}
PPDI	-	5×10^{-6}
PPBI 1	2×10^{-6}	1×10^{-3}
PPBI 2	1×10^{-6}	1×10^{-2}

The typical J - V curves of electron-only devices for the four polymers mentioned above are depicted in **Fig. 14** together with a schematic of an electron only device. A comparison of the mobilities shows that except for PPDI, all other polymers are good electron-transport materials. The electron mobility in PPDI, $5 \times 10^{-6} \text{ cm}^2/\text{Vs}$, was two orders of magnitude lower than that of in PPDB, $6 \times 10^{-4} \text{ cm}^2/\text{Vs}$. Nevertheless, in comparison to PPDB, better electron transport was reported for both PPBI polymers, that is, PPBI 1 and PPBI 2. A direct comparison of PPBI 1 and PPBI 2 showed that not only the core of the π -conjugation system, but also the substituent have an impact on the charge-transport properties of the material. PPBIs with hydrophilic OEG, PPBI 2, showed a major increase of one order of magnitude in electron mobility over PPBI 1 with hydrophobic alky tails. The reported electron mobility in PPBI 2 was $1 \times 10^{-2} \text{ cm}^2/\text{Vs}$, which is among the highest bulk electron mobility values ever reported for polymers.^{91,92} However, the X-ray diffraction data suggested a liquid crystalline S_{mc} structure for PPBI 1, whereas it suggested an amorphous phase for PPBI 2.^{88,89} Thus, the less-ordered PPBI 2 was surprisingly superior in terms of electron mobility.

3.3 Effect of Polymer Architecture on the Structure of PBIs

From the different types of acceptor polymers introduced above, one, namely an acrylate with PPBIs with hydrophobic alkyl swallow tails, was selected for detailed structural investigations. This type of polymer was used later in the D-A block copolymers. To study the effect of the polymer architecture on structure, we included a low-molecular-weight model compound, PBI, as a reference material (cf. **Fig. 15**).⁹³ The results of polarized light microscopy had already suggested that there are structural differences between the low-molecular-weight model compound PBI and the corresponding polymer poly(perylene bisimide acrylate) (PPerAcr) (cf. **Fig. 15**, right). Through a combination of DSC, optical microscopy, and temperature dependent SAXS/WAXS, it was shown that both compounds display a lamello-columnar packing. While the PBI crystallizes, the PPerAcr suppresses order, leading to only a 2D lamello-columnar liquid-crystalline phase as schematically shown in **Fig. 15**. Most likely the reduced order in the polymeric compound is because of the quenched chemical disorder in the atactic polymer.

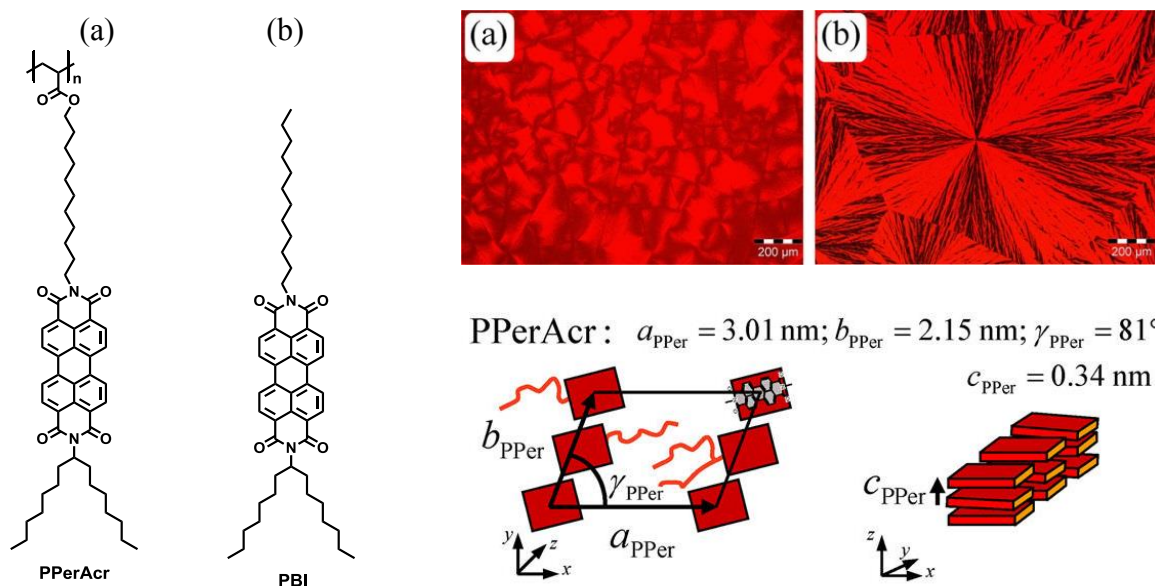


Fig.15 *left*: Chemical structures of the investigated materials: (a) Perylenebisimide side-chain polymer with polyacrylate backbone (PPerAcr); (b) asymmetrically substituted low molecular weight perylenebisimide (PBI); *right top*: Polarized light optical microscopy: PPerAcr (a) and PBI (b) at room temperature after cooling from the melt. Scale bar represents 200 μm in both cases; *right bottom*: Proposed lamella-columnar liquid crystalline structure for the polymer PPerAcr at $T = 20^\circ\text{C}$. Packing in the a - b -plane is not correlated with stacking in c -direction. (Reproduced with permission from 94)

In thin films, the a -axis is oriented perpendicularly to the substrate. Similarly as for P3HT, the ordering is suppressed directly after spin coating and a higher order is beneficial for charge transport, here electron transport.

4 Acceptor Building Block: Poly(fullerenes)/PPCBM

4.1 Controlled Synthesis

Basically, the preparation of pendant fullerene polymers can be achieved either by polymer-analogous modification of a preformed polymer^{46,94–98} or directly by polymerization of fullerene-derivatized monomers using organometallic catalysis.^{100–103} While many polymer-analogous approaches involve C_{60} as reagent, which often leads to polymer cross linking and multiaddition, we applied a well-controlled fullerene-grafting method using Steglich esterification.⁵⁰ A series of well-soluble fullerene-grafted

copolymer PPCBMs with high contents of pendant phenyl- C_{61} -butyric acid methyl ester (PCBM) between 30–64 wt% were synthesized (**Fig. 16**).¹⁰⁴ The tailor-made precursor copolymers poly(4-methoxystyrene-*stat*-4-*tert*-butoxystyrene) obtained here by reversible addition fragmentation chain transfer (RAFT) polymerization were functionalized via an efficient polymer-analogous esterification. Both the grafting density and the PCBM content could easily be tuned by the monomer ratio in the precursor copolymers. The resulting PCBM-grafted copolymers exhibit low-molecular-weight dispersity and no cross linking as a result of the controlled monofunctional grafting reaction, that is, Steglich esterification⁵⁰ of phenyl- C_{61} -butyric acid with the hydroxyl moieties of the precursor copolymer. The synthesized acceptor copolymers retain the optical and electrochemical properties of the incorporated PCBM independent of their fullerene weight fraction.

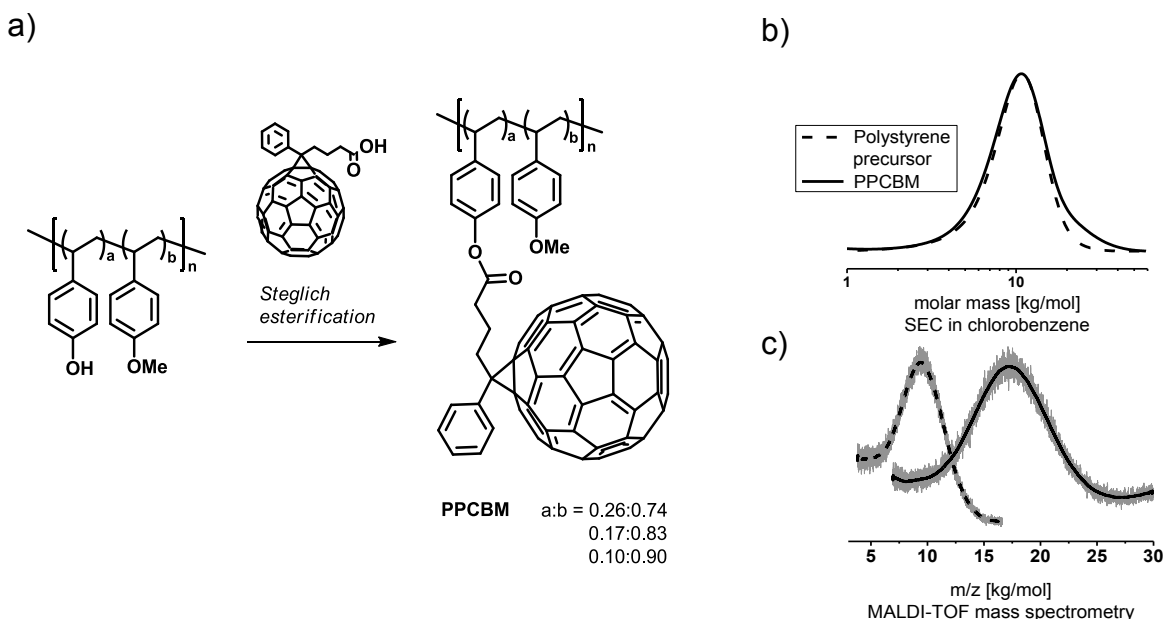


Fig. 16 (a) Synthesis route towards PPCBM acceptor polymers starting from a poly(4-*tert*-butoxystyrene-*stat*-4-methoxystyrene) copolymer with subsequent *tert*-butylether deprotection. The hydroxyl-functionalized precursor copolymer is grafted with phenyl- C_{61} -butyric acid (PC₆₁BA) using an optimized Steglich esterification protocol. (b) Characteristic size-exclusion chromatography (SEC) traces in chlorobenzene at 50 °C of a PPCBM polymer (*solid line*) with a monomer ratio of a:b=0.23:0.77 and 46 wt% PCBM in comparison to the corresponding precursor copolymer (*dashed line*). (c) Matrix assisted laser desorption/ionization time-of-flight mass spectrometry (MALDI-TOF) mass spectra confirming the molar mass growth after successful grafting of the precursor (*dashed line*) with PC₆₁BA moieties yielding PPCBM (*solid line*).

4.2 Structure Formation and Charge Transport

Earlier studies on side chain polymers carrying pendant C_{60} have shown a correlation of increasing electron mobility with increasing C_{60} content.¹⁰⁵ In these systems, for a C_{60} content of 23–60 wt%, a rather low electron mobility of 10^{-9} to $10^{-7} \text{cm}^2/\text{Vs}$ was determined by the SCLC method.^{14,106} Further, these fullerene polymers exhibit a C_{60} aggregation starting at a threshold of 12–13 vol% of incorporated C_{60} . The improved charge transport reported by Fang *et al.*¹⁰³ of pendant C_{60} polynorbornenes in OFET was attributed to the confined organization of fullerenes along the polymer chain. The potential for the application of pendant fullerene polymers as a suitable acceptor material in polymer solar cells was successfully demonstrated by Eo *et al.*¹⁰² Our structural studies using AFM, transmission electron microscopy, and X-ray diffraction reveal a homogeneous and amorphous morphology of the PPCBMs both in thin films and in bulk phase. In contrast to pristine PCBM or blends of polystyrene and PCBM, the strong tendency for nanocrystal formation of PCBM is fully suppressed in the PCBM-grafted copolymers. Additionally, the absence of nanocrystal formation in PPCBM was maintained even after prolonged thermal annealing (**Fig. 17**).

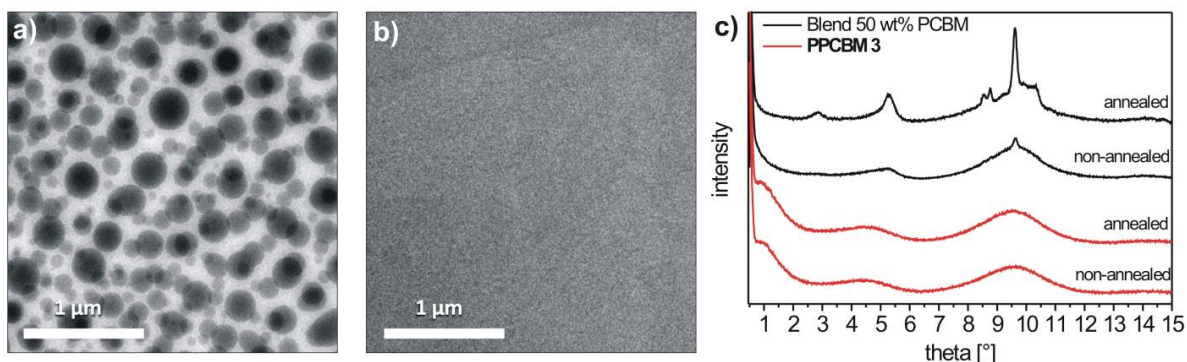


Fig. 17 Transmission electron microscopy images representing thin films made of (a) a blend consisting of 50 wt% PCBM content and 50 wt% polystyrene precursor and (b) a PPCBM acceptor polymer with 51 wt% of incorporated $PC_{61}BM$. By the covalent attachment of the $PC_{61}BM$ moieties to the polymer backbone, the demixing of the fullerenes and polymer is fully restrained leading to a homogenous morphology. (c) Powder X-ray diffractograms of the blend sample and PPCBM before and after annealing at 140 °C for 3 hours indicating a suppression of nanocrystal formation in the PPCBM acceptor polymer. (Reproduce with permission from 104)

The electron-transport properties were studied using the SCLC method. The maximum electron mobility μ_e of $1 \times 10^{-4} \text{ cm}^2/\text{Vs}$ was achieved for 37 wt% of incorporated phenyl-C₆₁-butyric methyl ester (PC₆₁BM). Despite the dilution of the electronically active fullerene moieties with the insulating polymer backbone, the PC₆₁BM-grafted copolymers exhibited exceptionally high charge transport compared to blend systems between polystyrene copolymers and PC₆₁BM. For 30 wt% PC₆₁BM content, the grafted copolymer exhibited three orders of magnitude better mobility than the corresponding blend. Thus, an efficient charge carrier percolation is facilitated by the homogeneous distribution of PC₆₁BM in the copolymer. Charge transport in the blends relies on nanocrystal formation and is improved by increasing the PC₆₁BM content. On the other hand, the PC₆₁BM-grafted copolymers exhibit excellent mobility and no nanocrystal formation even after thermal annealing. This can be of great advantage if issues of long-term stability in devices have to be addressed using fullerene materials. The modular synthetic approach presented here can also be transferred to other fullerene derivatives.

5 Donor–Acceptor Block Copolymers: P3HT-*b*-PPerAcr

5.1 Synthesis of P3HT-*b*-PPerAcr

P3HT-*b*-PPerAcr copolymers constitute one of the fully functionalized block copolymers carrying both donor and acceptor moieties obtained by controlled synthesis of the individual blocks, maintaining appreciable solubility in common solvents.^{37,86,107,108} The synthetic strategy of this system can be taken as a general criterion for the design of D–A block copolymer systems. P3HT-*b*-PPerAcr polymers were first synthesized by Sommer *et al.*¹⁰⁷ from a P3HT macroinitiator. For this, P3HT with a molecular weight of 8900 g/mol (SEC) and a narrow PDI was first synthesized by a modified version of the aforementioned Yokozawa route and in situ functionalized to obtain a macroinitiator suitable for NMRP. This macroinitiator was then used to polymerize a PBI acrylate. A set of block copolymers with small polydispersities and different PBI contents was obtained. The low degree of polymerization of these block

copolymers prevented them from phase separating into well-defined and ordered structures in the melt. By a modified synthetic strategy, Lohwasser *et al.*⁵⁶ obtained higher molecular weights, which led to a sufficient increase of the χ_N -parameter. P3HT with a high molecular weight (19.7 kg/mol in SEC, equivalent to a MALDI-TOF MS molecular weight of 12.4 kg/mol) and an alkyne end group was synthesized and converted into a macroinitiator suitable for NMRP via CuACC “click” chemistry. This macroinitiator was then used to polymerize the PBI acrylate monomer. This new method also prevented the formation of triblocks, which can occur when the macroinitiator is synthesized in situ as reported before. In this way, the synthesis of a series of D-A block copolymers P3HT-*b*-PPerAc with sufficient purity, a narrow distribution (PDI < 1.20), and a high molecular weights was realized (see **Fig. 18**). The structure formation and microphase separation in two selected block copolymers with 47 and 64 wt% of PPerAc are discussed in detail in the following.

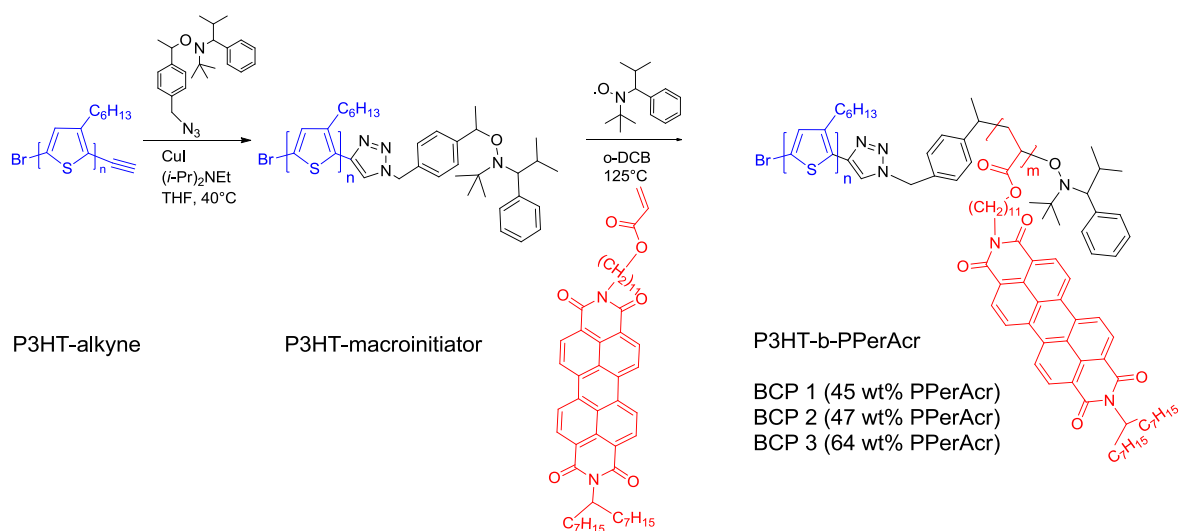


Fig. 18 Synthetic scheme for P3HT-*b*-PPerAc block copolymers starting from P3HT-alkyne and its conversion to a macroinitiator suitable for nitroxide-mediated radical polymerization NMRP of PerAc monomer. The listed samples BCP 1-3 are used for further investigations described ahead.

5.2 Structural Elucidation of P3HT-*b*-PPerAcr

Transmission electron microscopy images of two exemplary block copolymers of the type introduced above are shown in **Fig. 19**. The patterns are very similar to classical microphase structures as they had not been observed before on D-A block copolymers. Combined SAXS/WAXS measurements showed that indeed these samples microphase separate at elevated temperatures, where both components are in the molten state. The data in **Fig. 20** demonstrate that subsequent cooling leads to crystallization but leaves the microphase structure intact, as it becomes obvious from the unchanged position of the peak in the SAXS pattern reflecting the nanostructure. These results show that to achieve well-defined classical microphase structures, the key is high molecular weight leading to a large enough incompatibility χN , as it induces microphase separation at high temperatures with subsequent confined crystallization. The observed microstructures fitted the respective volume fractions well, and the crystalline packing within the individual blocks was analogous to those in the respective homopolymers. For the first time, typical lamellar or cylindrical phase-separated structures as known for amorphous coil-coil systems were realized for a crystalline-liquid crystalline, D-A block copolymer.⁵⁶ A similar block copolymer synthesized with the above-mentioned method exhibited only crystallization-induced microphase separation (cf. **Fig. 5**).

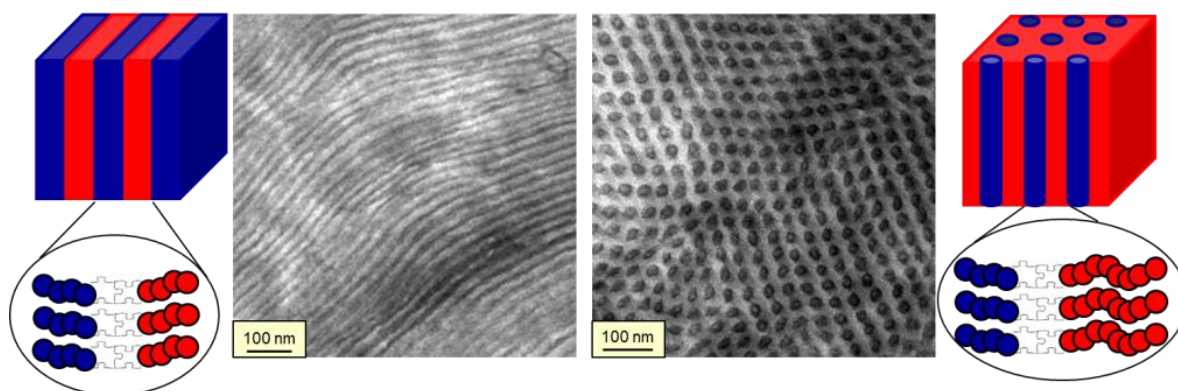


Fig. 19 Illustration of the microphase separation in donor-acceptor block copolymers, P3HT-*b*-PPerAcr with different volume fractions of PPerAcr and transmission electron micrographs of the two exemplary block copolymers exhibiting lamellar (BCP 2) and cylindrical (BCP 3) microphase structures.

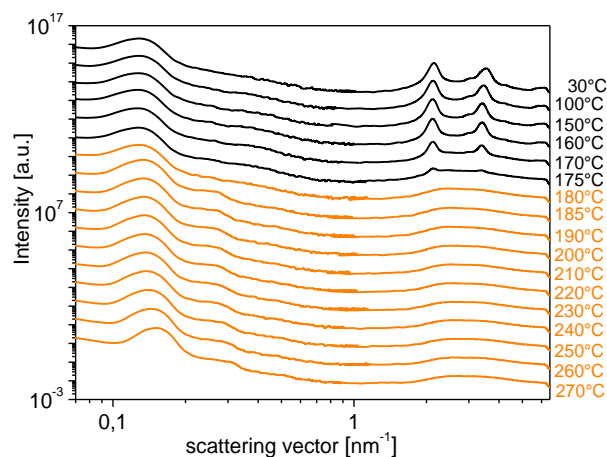


Fig. 20 Combined small-angle and wide-angle X-ray diffraction pattern of the asymmetric P3HT-*b*-PPerAcr (BCP 3) (cylindrical microstructures) recorded during cooling from the melt. Temperatures at which the block copolymer is in the molten state are marked in orange. Note that the position of the small angle peak reflecting the nanostructure remains unchanged upon crystallization (Bragg peaks at high scattering vector) indicating confined crystallization. (Reproduces with permission from 56)

Next, structural and electronic properties of thin films prepared from these block copolymers using a combination of X-ray scattering, AFM, and vertical charge transport measurements in diode devices were studied.¹⁰⁹ Exemplary results are shown in **Fig. 21**. Generally, the well-defined microphase structures found in bulk could also be prepared in thin films, but block copolymer self-assembly and crystallization of the individual components are interrelated, and well-developed microdomains form only after an annealing step above the melting temperature of both components. In addition, alignment parallel to the substrate induced by interfacial interactions was observed. The copolymers sustain ambipolar charge transport, but experiments on samples prepared with different thermal treatment show that the exact values of electron and hole mobilities depend strongly on orientation and connectivity of the microdomains as well as the molecular order within the domains. Generally, the measured mobilities were lower than in pure homopolymers, similarly as in blend morphologies, as they are used for organic solar cells. Apart from optimization of domain sizes, an important further step toward usage of the investigated materials in solar cell devices will be to achieve vertical alignment of the microphase structure.

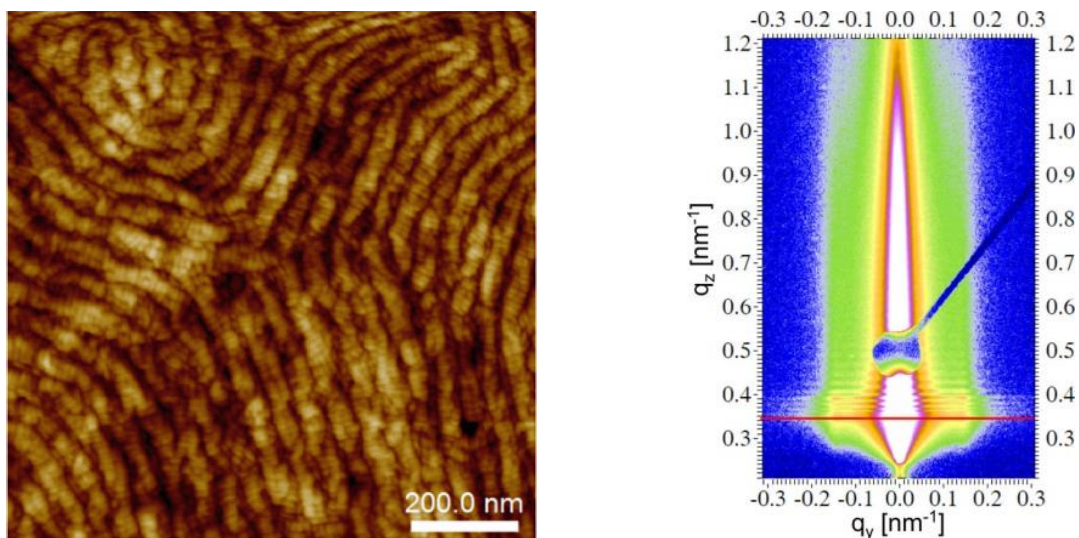


Fig. 21. a) Atomic force microscopy height image of an annealed film of the same P3HT-*b*-PPerAc with cylindrical microdomains (BCP 3) measured with a Bruker MultiMode 8 using PeakForce Taping™ mode (nanoscope 5 controller) and showing cylindrical microstructures lying flat on the substrate. We attribute the small-scale structure within the cylinders to P3TH crystals. b) Two dimensional grazing-incidence small-angle X-ray scattering image of a similarly prepared film. The specular reflection is masked by the beam stop. The *red line* indicates Yoneda's position. The two peaks around $q_y=0.14\text{nm}^{-1}$ reflect the lateral arrangement of cylindrical microdomains. (Reproduced with permission from 109)

5.3 Solar Cell Devices Based on P3HT-*b*-PPerAc

In general, the photovoltaic performance of the P3HT-*b*-PPerAc systems investigated up to now was weak for a variety of reasons, as discussed below. First, photovoltaic devices based on the P3HT-*b*-PPerAc diblock copolymers¹¹⁰ were realized with a PPerAc weight fraction of 55 wt% and two different block lengths of the P3HT block of 8.9 and 17.0 kg/mol. Here a strong dependence on the block length was found: Whereas the smaller-molecular-weight block copolymer yielded only about 3% maximum external quantum efficiency (EQE), the larger resulted in a maximum of 31% EQE and thus produced one order of magnitude larger photocurrent. However, overall device efficiencies remained low at 0.007 and 0.17% PCE as a result of the small open-circuit voltages and small fill factors. Nevertheless, an important lesson has been learned: For efficient charge transport, a certain scale of coarse graining in the donor and acceptor domains is required. The next step of improvement was reported about 2 years later with the same kind of block copolymer, exhibiting a PPerAc weight fraction of 45% and a higher total molecular weight of about 27 kg/mol.¹¹¹

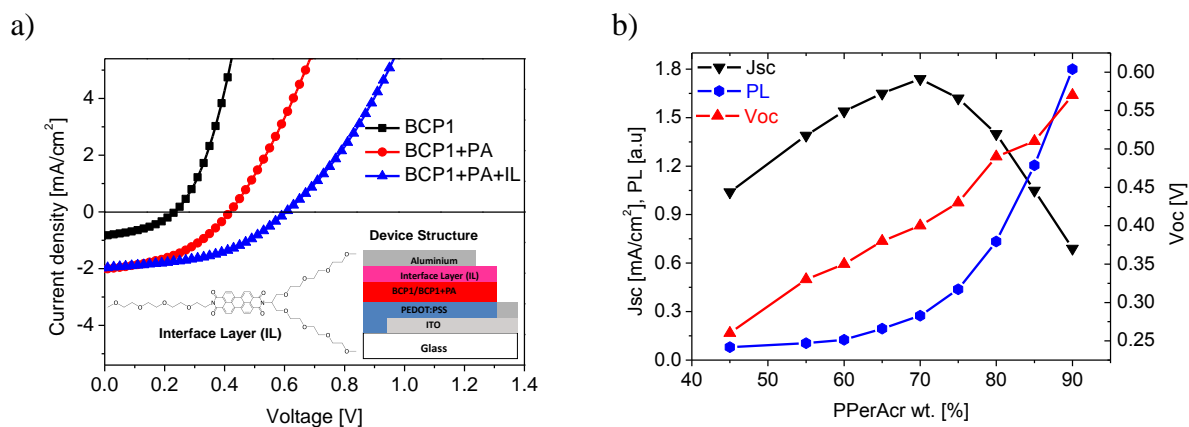


Fig. 22 a) Current-voltage characteristics of photovoltaic devices based on pristine P3HT-*b*-PPerAc (BCP1) (*black squares*), those with additional PPerAc (PA) homopolymers (*red circles*) and finally the device with an additional perylene bisimide (PBI) interface layer. b) Dependence of the short-circuit photocurrent, open circuit voltage, and photoluminescence intensity of P3HT-*b*-PPerAc:PPerAc block-copolymer:homopolymer blends. (Reproduced with permission from 111)

The corresponding results are shown in **Fig. 22**. While the pristine block copolymer delivered a PCE of 0.1% only, the addition of PPerAc homopolymer yielded a threefold improvement, yielding an overall PCE of about 0.34%. This improvement was largely based on doubling the photocurrent to 2 mA/cm² and a relative increase of the open-circuit voltage by another 60%. Using steady-state photoluminescence measurements, this increase could be partially assigned to a statistically increased PPerAc domain size, as the strong rise in the corresponding luminescence signal shows. A surprising result was the steady increase of the open-circuit voltage with increasing PPerAc fraction, reaching a maximum of 575 mV for the largest weight fraction (90 wt%) investigated. The key for understanding the rise in the open-circuit voltage was provided by X-ray photoelectron spectroscopy measurements on identically processed films, by which it was found that the PPerAc surface fraction was increasing over-stoichiometrically compared to the bulk fraction. Since the electron-extracting electrode of the photovoltaic devices was situated at this interface with the photoactive layer, an enrichment of the electron-transporting PPerAc phase could be related to the formation of a hole-blocking layer, thus preventing charge recombination at the electron-extracting electrode and improving the open-circuit voltage by a higher maintained quasi-Fermi level of the electrons.

Table 2 Summary of the photovoltaic parameters obtained for the P3HT-*b*-PPerAcr system (BCP 1), upon domain coarsening via homopolymer blending and blocking layer insertion using the PBI interlayer.¹¹¹

Active layer	J_{sc} (mA/cm ²)	V_{oc} (V)	FF (%)	H (%)	R_s (Ω)	R_{SH} (Ω)
BCP 1	0.84	0.23	41	0.08	12.1	1277
BCP 1+PA	2.00	0.41	45	0.34	18.5	1851
BCP 1+PA+IL	1.96	0.61	47	0.56	26.7	3002

To prove this hypothesis, an alcohol-soluble perylene derivative, PBI, was deposited as an extra layer to function as a hole-blocking electron-transporting layer on top of the photoactive layer. At the optimum blend ratio yielding the maximum photocurrent, the application of this PBI interlayer resulted in an increase of the open-circuit voltage yielding reasonable 610mV and a PCE of 0.56 %.¹¹¹ **Table 2** collects the device parameters from these experiments.

The block copolymers BCP 2 (lamellar morphology, 47 wt% PPerAcr) and BCP 3 (cylindrical morphology, 64 wt% PPerAcr) were used to undertake a first study of the interrelation between morphology and solar cell performance. Different thermal treatments were applied to vary the morphology: In the film obtained after spin coating, microphase separation as well as crystallization of the components are largely suppressed by the fast drying process. One film was annealed above the melting temperature of PPerAcr but below the melting temperature of P3HT. In this film both components crystallize, but there is no time for the development of a well-defined and ordered microphase structure because of the fast crystallization of the P3HT component. A third film was first annealed at a high temperature where both components are molten, leading to the development of a well-defined microphase structure with subsequent crystallization during cooling. Of course, this latter treatment also leads to an orientation of the microdomains parallel to the substrate, preventing a good charge transport to the electrodes; a high-performance photovoltaic device is not yet produced in this way. As an example, the results of the photovoltaic characterization of BCP 3, for which the structural analysis is shown above, are shown in **Fig. 23**. Clearly, the increase in crystallinity induced by the thermal treatment at the intermediate temperature led to a considerable increase in the photocurrent, whereas the unfavorable orientation of the microdomains induced by annealing in the melt state

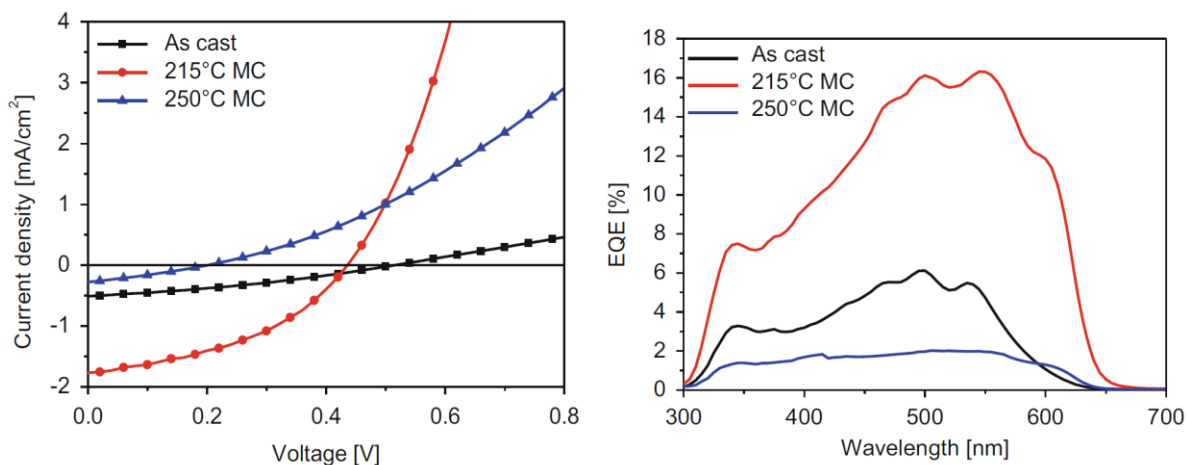


Fig. 23 Current-voltage characteristics (*I-V*, left) and external quantum efficiency (EQE, right) obtained from BCP 3 prepared in the following way: (i) as-cast (*black squares*), (ii) annealing at an intermediate temperature (215 °C) leading to crystallisation without well-ordered microphase separation (*red circles*), and (iii) annealing at high temperatures (250 °C) leading to the formation of well-defined microdomains oriented parallel to the substrate (*blue triangles*). Clearly, the unfavorable orientation of the lying cylinders results in the worst photovoltaic performance of all cases. (Reproduced with permission from 33)

again suppressed charge transport, leading to a very low short-circuit current and an even worse photovoltaic performance than in the “as-cast” case. These results demonstrate the combined influence of crystallinity and block copolymer morphology upon photovoltaic parameters.

As an outlook for further studies, therefore either a more favorable vertical microphase orientation or a bicontinuous phase like the gyroid structure may be most beneficial for obtaining high-performance organic photovoltaic devices based on self-assembling single-component block copolymers.

6 Donor–Acceptor Block Copolymer: P3HT-*b*-PPCBM

6.1 Controlled Synthesis Without Cross Linking

The very first reports on block copolymers carrying a poly(*p*-phenylene vinylene) conjugated block and a fullerene pendant block are related to the work of Hadziioannou *et al.*⁹⁴ Then the development of controlled P3HT polymerization and the capability of specific end functionalization of P3HT opened new perspectives for the synthesis of D–

A block copolymers comprising fullerene-grafted acceptor blocks. A variety of C₆₀-decorated block copolymers was reported.^{31,35,38,97,112} However, an elegant method for a controlled fullerene attachment without multiaddition or cross linking was first shown by Russel *et al.* using Steglich esterification⁵⁰ and Hashimoto *et al.* using alkyne-azide click chemistry.⁴⁸

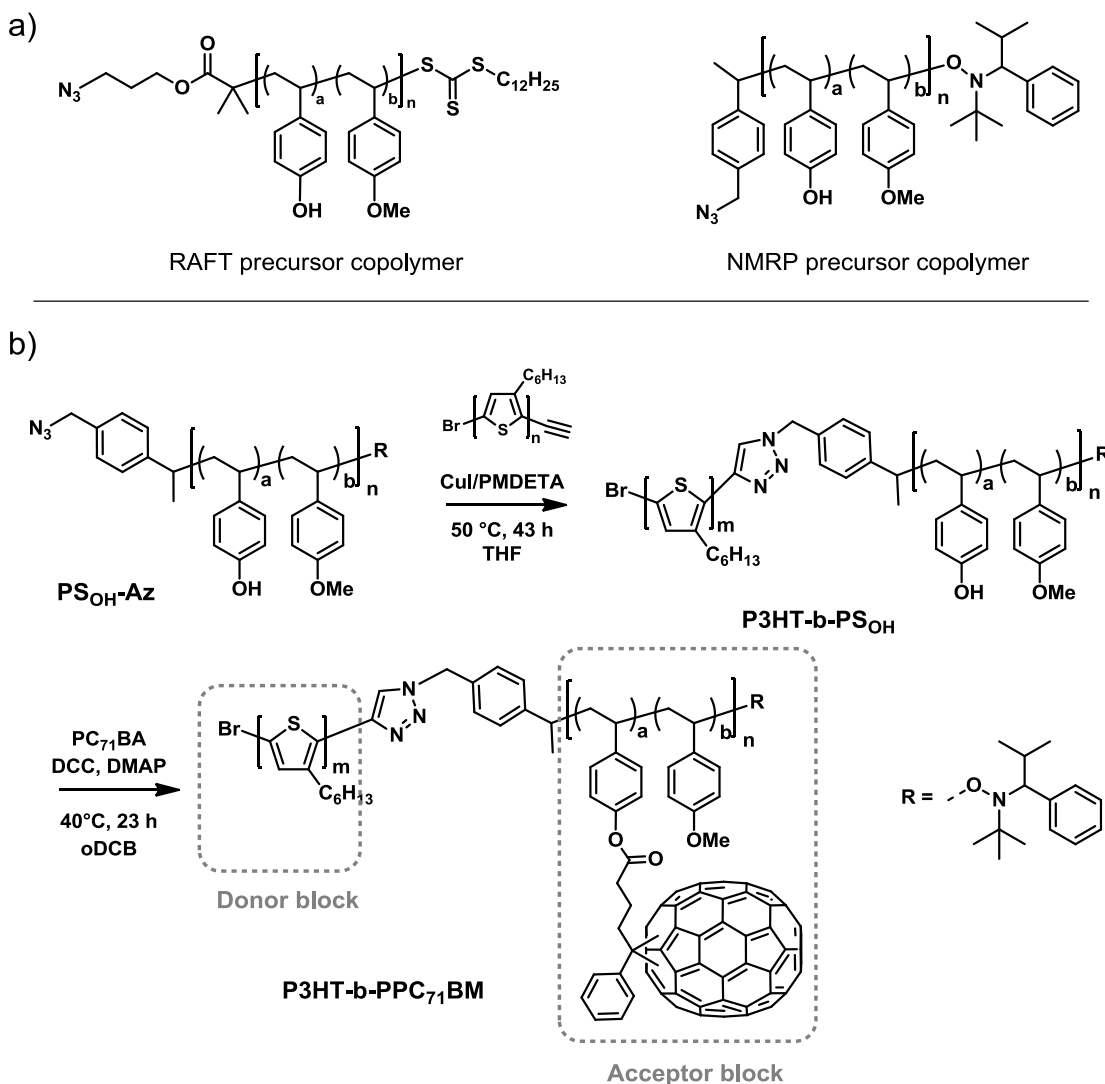


Fig. 24 a) Azide-terminated poly(4-hydroxystyrene-*stat*-4-methoxystyrene) copolymers obtained either by reversible addition-fragmentation chain transfer polymerization (RAFT) or nitroxide-mediated radical polymerization (NMRP) of 4-methoxystyrene and 4-*tert*-butoxystyrene with subsequent polymer-analogous deprotection of the *tert*-butyl ether group. b) Synthesis route of the donor-acceptor block copolymer P3HT-*b*-PPC₇₁BM via copper(I)-catalyzed alkyne-azide cycloaddition and Steglich esterification with PC₇₁BA.

We present a straightforward method for the preparation of novel D–A block copolymers based on an acceptor block with pendant PC₆₁BM or its C₇₀ analogue [6,6]-phenyl-C₇₁-butyric acid methyl ester (PC₇₁BM) and a regioregular P3HT as donor.⁴¹ Our strategy is based on a modular combination of azide-terminated polystyrene copolymers with alkyne-terminated P3HT using CuAAC to form the block copolymer. The polystyrene precursor poly(4-*tert*-butoxystyrene-*stat*-4-methoxystyrene) can be tailored precisely using controlled radical polymerization methods such as RAFT polymerization or NMRP. Subsequent acidic hydrolysis was used to deprotect the *tert*-butylether group, yielding a hydroxyl-functionalized copolymer. Polymer coupling with ethynyl-terminated regioregular P3HT⁷³ using CuAAC proceeds equally well for both RAFT and NMRP precursor copolymers.

Because of the modularity of the P3HT-*b*-PSOH block copolymer synthesis, a wide range of individual polymer designs can be realized in terms of the block lengths, grafting density with fullerene moieties, and the final D–A composition after PCBM grafting. Lastly, the fullerene acceptors are covalently attached to the preformed block copolymer to give the P3HT-*b*-PPCBM D–A block copolymers. To enhance the optical properties of the block copolymers, PC₇₁BM as the state-of-the-art acceptor in organic photovoltaics was introduced to these polymer systems. The esterification reaction of phenyl-C₇₁-butyric acid (PC₇₁BA) to the hydroxyl groups of the polystyrene precursor was first optimized in homopolymers and yielded near-quantitative conversion. An analogous grafting reaction with P3HT-*b*-PSOH yielded the fully functionalized D–A block copolymer P3HT-*b*-PPC₇₁BM (**Fig. 24**). As a result of incorporating C₇₀, the D–A block copolymer exhibits enhanced absorption in the whole visible range of 300–600 nm.

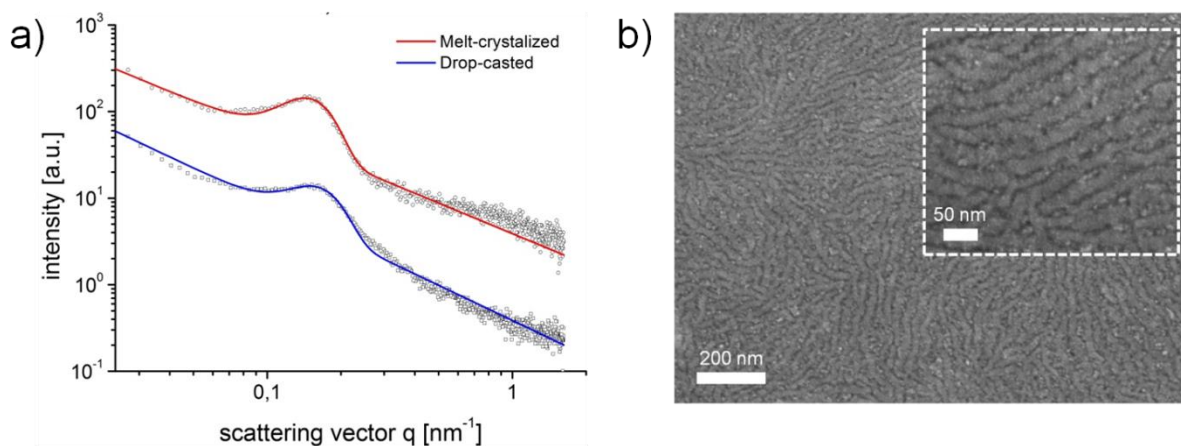


Fig. 25 a) GISAXS data of P3HT-*b*-PPC₇₁BM showing horizontal intensity profiles around Yoneda's position at room temperature of films prepared by drop-casting and spin-coating with subsequent annealing in the melt at 240 °C. The peaks indicate a periodic nanostructure which is consistent with bulk data from small-angle X-ray scattering measurements. b) Scanning electron microscope image of P3HT-*b*-PPC₇₁BM prepared by drop-casting of a 2 wt% dichlorobenzene solution. The inset shows a magnified section of the film. (Reproduced with permission from 41)

6.2 Structure Formation

Even though different synthetic approaches to realize fullerene-containing block copolymers have been reported, no microphase separation with ordered D–A domains was observed for C₆₀-grafted D–A block copolymers up to now. Structural investigations on these block copolymers are rare and show either a loss of nanoscale structure because of fullerene aggregation⁴⁹ or a disordered phase-separated morphology.^{48,50} In contrast, our structural analysis of the P3HT-*b*-PPC₇₁BM block copolymer based on SAXS in transmission and in grazing-incidence geometry (GISAXS) as well as scanning electron microscopy (SEM) gave clear evidence for the formation of a periodic nanostructure of 37 nm in bulk and in thin films (**Fig. 25**). Temperature dependent SAXS measurements both in the melt at 240 °C and in solid state at room temperature show the same periodic nanostructure. The fact that the SAXS peak is almost unchanged after cooling to room temperature, that is, after crystallization of the P3HT component, suggests that the nanostructure is already caused by a liquid–liquid phase separation in the melt.⁵⁶ Compared to the block copolymers described above, the high T_g in the acceptor block here seems to be a hurdle for the formation of equally well-developed microdomains on cooling from melt. Remarkably, the observed nanoscale morphology is nearly independent of the processing method, that is, from solution or by melt

crystallization above the melting point of P3HT at 240 °C. SAXS and GISAXS structural analysis correlates with the domain size observed in SEM.

Conclusion and Outlook

The biggest challenges in designing and synthesizing block copolymers carrying semicrystalline P3HT segments of appreciably high molecular weight and acceptor blocks carrying PPBIs or fullerene derivatives have been successfully accomplished. Some of the initial problems such as end-group fidelity of the first block are no longer issues, and the problems of subsequent polymerization using P3HT macroinitiator have been resolved by making use of the modular approach provided by click chemistry. This has led to well-defined P3HT-*b*-PPerAcr block polymers with required volume fractions and low polydispersity. One of the biggest tasks in the synthesis of pendant fullerene polymers is the attainment of sufficient fullerene content without compromising on solubility. Additionally, the multivalent attachment of fullerene to polymer backbone leading to cross linking and insoluble materials reported earlier could be avoided by adopting a polymer-analogous esterification. Thus, a combination of all these synthetic techniques involving NMRP, KCTP, and click chemistry has facilitated the tailored synthesis of such complex D–A structures exhibiting microphase separation and thus suitable for structure–property correlation studies. Note that using two P3HT-*b*-PPerAcr block copolymers of sufficient molecular weight and either 47 or 64 wt% PPerAcr in the acceptor block allows one to obtain microphase separation and subsequent confined crystallization via cooling from the melt, yielding lamellar in the former case and cylindrical microdomains in the latter case. In the synthesis, further efforts are needed to obtain controlled lengths of novel low-bandgap donor segments with low polydispersity and to integrate them into block copolymers.

In terms of the microscopic structure, the basic result of our investigations is that the crystalline–liquid crystalline D–A block copolymers, P3HT-*b*-PPerAcr, under study are in fact very complex systems, but the driving forces and principles underlying the structure formation are very similar to more conventional materials. There is generally a competition between liquid–liquid microphase separation and the formation of order

on a molecular scale via crystallization or the formation of a liquid-crystalline phase. P3HT shows the typical features of semicrystalline polymers, and PPerAcr forms a side chain liquid crystal. The morphology of block copolymers from such materials depends on the relative values of the different transition temperatures and on the mobility of the materials involved. In addition, there is not necessarily one well-defined equilibrium structure; the structure may depend on the processing conditions (thermal history, melt, or solvent processing). Also, the effect of the thin-film geometry on self-assembly is rather similar to simpler systems studied in the past. Because of interfacial interactions, microdomains tend to align parallel to the plane of the film. Moreover, crystallization under the constraints set by the microphase structure can lead to orientation of the crystals. It is important to note that for the systems studied, the crystallization of the individual components did not destroy the microdomains; that is, the crystallization was confined.

With respect to the application of diblock copolymers in photovoltaic devices, substantial progress in understanding the underlying principles has been made. At first, a certain scale of phase separation appeared to be required in order to allow efficient charge extraction. This has been shown by comparing D-A block copolymers bearing different molecular weights and via blending in a PPerAcr homopolymer, where the original block composition included only 45 wt% of PPerAcr before and 70 wt% after homopolymer addition. With microphase-separated block copolymers, the preferential alignment of the microdomains parallel to the electrode surface unfortunately constitutes a major hindrance for efficient charge extraction. However, as desired, the block copolymers exhibit ambipolar charge transport, but as the transport and structure are coupled, further optimization is necessary and probably also possible. An important further step toward the materials investigated here being used in solar cell devices will be to achieve vertical alignment of the microphase structure. This task is not trivial, as the two most established methods to orient thin-film block copolymers cannot be applied without difficulty. Electric field induced alignment is not efficient most likely because of the residual conductivity of the materials, and solvent annealing is difficult in crystalline systems, as it requires compatibilization of the components as well as dissolution of the crystals. Nevertheless, at this point it has already become clear

that the block copolymer architecture allows the preparation of well-defined and stable D–A nanostructures with the shape and size of the domains determined by the architecture and molecular weight of the polymer.

Acknowledgments

We acknowledge financial support from the German Research Foundation (DFG) within the priority program SPP1355, projects HO 3981/6, Th 807/3, and TH 1281/1. Part of the results was obtained from experiments on beamlines ID10 and Dubble at the European Synchrotron Radiation Facility (ESRF), Grenoble, France.

References

- 1 Sariciftci NS, Smilowitz L, Heeger A J, Wudl F (1992) *Science* 258:1476
- 2 Sariciftci NS, Braun D, Zhang C, Srdanov VI, Heeger AJ, Stucky G, Wudl F (1993) *Appl Phys Lett* 62:585
- 3 Yu G, Gao J, Hummelen JC, Wudl F, Heeger AJ (1995) *Science* 270:789
- 4 Yu G, Heeger AJ (1995) *J Appl Phys* 78:4510
- 5 Halls JJM, Walsh CA, Greenham NC, Marseglia EA, Friend RH, Moratti SC, Holmes AB (1995) *Nature* 376:498
- 6 Hoppe H, Sariciftci NS (2004) *J Mater Res* 19:1924
- 7 Hoppe H, Sariciftci NS (2008) *Photoresponsive Polymers II* 214:1
- 8 Chen JD, Cui CH, Li YQ, Zhou L, Ou QD, Li C, Li YF, Tang JX (2015) *Adv Mater* 27:1035
- 9 Liu C, Yi C, Wang K, Yang YL, Bhatta RS, Tsige M, Xiao SY, Gong X (2015) *ACS Appl Mater Interfaces* 7:4928
- 10 Huang F (2015) *Sci China Chem* 58:190
- 11 Liu YH, Zhao JB, Li ZK, Mu C, Ma W, Hu HW, Jiang K, Lin HR, Ade H, Yan H (2014) *Nat Commun* 5
- 12 Zhang SQ, Ye L, Zhao WC, Yang B, Wang Q, Hou JH (2015) *Sci China Chem* 58:248
- 13 Wu HB (2015) *Sci China Chem* 58:189
- 14 Li YF (2015) *Sci China Chem* 58:188
- 15 Etxebarria I, Ajuria J, Pacios R (2015) *Org Electron* 19:34
- 16 Kimber RGE, Walker AB, Schröder-Turk GE, Cleaver DJ (2010) *Phys Chem Chem Phys* 12:844

- 17 Hoppe H, Sariciftci NS (2006) *J Mater Chem* 16:45
- 18 Hoppe H, Glatzel T, Niggemann M, Schwinger W, Schaeffler F, Hinsch A, Lux-Steiner MC, Sariciftci NS (2006) *Thin Solid Films* 511:587
- 19 Drees M, Hoppe H, Winder C, Neugebauer H, Sariciftci NS, Schwinger W, Schaffler F, Topf C, Scharber MC, Zhu ZG, Gaudiana R (2005) *J Mater Chem* 15:5158
- 20 Nguyen LH, Hoppe H, Erb T, Gunes S, Gobsch G, Sariciftci NS (2007) *Adv Funct Mater* 17:1071
- 21 van Bavel SS, Barenklau M, de With G, Hoppe H, Loos J (2010) *Adv Funct Mater* 20:1458
- 22 Synooka O, Eberhardt KR, Singh CR, Hermann F, Ecke G, Ecker B, von Hauff E, Gobsch G, Hoppe H (2014) *Adv Energy Mater* 4:10
- 23 Sachs-Quintana IT, Heumuller T, Mateker WR, Orozco DE, Cheacharoen R, Sweetnam S, Brabec CJ, McGehee MD (2014) *Adv Funct Mater* 24:3978
- 24 Wantz G, Derue L, Dautel O, Rivaton A, Hudhomme P, Dagron-Lartigau C (2014) *Polym Int* 63:1346
- 25 Vandenberghe J, Conings B, Bertho S, Kesters J, Spoltore D, Esiner S, Zhao J, Van Assche G, Wienk MM, Maes W, Lutsen L, Van Mele B, Janssen RAJ, Manca J, Vanderzande DJM (2011) *Macromolecules* 44:8470
- 26 Cardinaletti I, Kesters J, Bertho S, Conings B, Piersimoni F, D'Haen J, Lutsen L, Nesladek M, Van Mele B, Van Assche G, Vandewal K, Salleo A, Vanderzande D, Maes W, Manca JV (2014) *J Photonics Energy* 4:1–12. Article Number 040997
- 27 Derue L, Dautel O, Tournebize A, Drees M, Pan HL, Berthumeyrie S, Pavageau B, Cloutet E, Chambon S, Hirsch L, Rivaton A, Hudhomme P, Facchetti A, Wantz G (2014) *Adv Mater* 26:5831
- 28 Khiev S, Derue L, Ayenew G, Medlej H, Brown R, Rubatat L, Hiorns RC, Wantz G, Dagron-Lartigau C (2013) *Polym Chem* 4:4145
- 29 Sivula K, Ball ZT, Watanabe N, Frechet JMJ (2006) *Adv Mater* 18:206
- 30 Biccocchi E, Haeussler M, Rizzardo E, Scully AD, Ghiggino KP (2015) *J Polym Sci, Polym Chem Ed* 53:888
- 31 Heuken M, Komber H, Erdmann T, Senkovskyy V, Kiriy A, Voit B (2012) *Macromolecules* 45:4101
- 32 Johnson K, Huang YS, Huettner S, Sommer M, Brinkmann M, Mulherin R, Niedzialek D, Beljonne D, Clark J, Huck WTS, Friend RH (2013) *J Am Chem Soc* 135:5074
- 33 Singh CR (2013) Dissertation, TU Ilmenau, Germany
- 34 Yassar A, Miozzo L, Gironda R, Horowitz G (2013) *Prog Polym Sci* 38:791
- 35 de Boer B, Stalmach U, van Hutten PF, Melzer C, Krasnikov VV, Hadziioannou G (2001) *Polymer* 42:9097
- 36 de Boer B, Stalmach U, Melzer C, Hadziioannou G (2001) *Synth Met* 121:1541
- 37 Zhang QL, Cirpan A, Russell TP, Emrick T (2009) *Macromolecules* 42:1079

- 38 van der Veen MH, de Boer B, Stalmach U, van de wetering KI, Hadziioannou G (2004) *Macromolecules* 37:3673
- 39 Sommer M, Huettner S, Thelakkat M (2010) *Complex Macromol Syst II* 228:123
- 40 Sommer M, Huettner S, Thelakkat M (2010) *J Mater Chem* 20:10788
- 41 Hufnagel M, Fischer M, Thurn-Albrecht T, Thelakkat M (2015) *Polym Chem* 6:813
- 42 Darling SB (2009) *Energy Environ Sci* 2:1266
- 43 Nakabayashi K, Mori H (2014) *Materials* 7:3274
- 44 Bu LJ, Guo XY, Yu B, Qu Y, Xie ZY, Yan DH, Geng YH, Wang FS (2009) *J Am Chem Soc* 131:13242
- 45 Sary N, Richard F, Brochon C, Leclerc N, Leveque P, Audinot JN, Berson S, Heiser T, Hadziioannou G, Mezzenga R (2010) *Adv Mater* 22:763
- 46 Miyanishi S, Zhang Y, Tajima K, Hashimoto K (2010) *Chem Commun* 46:6723
- 47 Scherf U, Gutacker A, Koenen N (2008) *Acc Chem Res* 41(9):1086
- 48 Miyanishi S, Zhang Y, Hashimoto K, Tajima K (2012) *Macromolecules* 45:6424
- 49 Barrau S, Heiser T, Richard F, Brochon C, Ngov C, van de Wetering K, Hadziioannou G, Anokhin DV, Ivanov DA (2008) *Macromolecules* 41:2701
- 50 Lee JU, Cirpan A, Emrick T, Russell P, Ho W, Russell TP, Jo WH (2009) *J Mater Chem* 19:1483
- 51 Guo CH, Lin YH, Witman MD, Smith KA, Wang C, Hexemer A, Strzalka J, Gomez ED, Verduzco R (2013) *Nano Lett* 13:2957
- 52 Ku S-Y, Brady MA, Treat ND, Cochran JE, Robb MJ, Kramer EJ, Chabiny ML, Hawker CJ (2012) *J Am Chem Soc* 134:16040
- 53 Olsen BD, Segalman RA (2008) *Mater Sci Eng R Rep* 62:37
- 54 Loo YL, Register RA, Ryan AJ (2002) *Macromolecules* 35:2365
- 55 Li S, Myers SB, Register RA (2011) *Macromolecules* 44:8835
- 56 Lohwasser RH, Gupta G, Kohn P, Sommer M, Lang AS, Thurn-Albrecht T, Thelakkat M (2013) *Macromolecules* 46:4403
- 57 Yamamoto T, Sanechika K, Yamamoto AJ (1980) *Polym Sci Polym Lett Ed* 18:9
- 58 Lin JWP, Dudek LP (1980) *J Polym Sci, Polym Chem Ed* 18:2869
- 59 Jen K-Y, Miller GG, Elsenbaumer RL (1986) *J Chem Soc, Chem Commun* 17:1346
- 60 McCullough RD, Lowe RD (1992) *J Chem Soc, Chem Commun* 1:70
- 61 Chen T-A, Rieke RD (1992) *J Am Chem Soc* 114:10087
- 62 Loewe RS, Khersonsky SM, McCullough RD (1999) *Adv Mater* 11:250
- 63 Lohwasser RH, Thelakkat M (2011) *Macromolecules* 44:3388
- 64 Yokoyama A, Miyakoshi R, Yokozawa T (2004) *Macromolecules* 37:1169
- 65 Sheina EE, Liu J, Iovu MC, Laird DW, McCullough RD (2004) *Macromolecules* 37:3526
- 66 Miyakoshi R, Yokoyama A, Yokozawa T (2005) *J Am Chem Soc* 127:17542
- 67 Iovu MC, Sheina EE, Gil RR, McCullough RD (2005) *Macromolecules* 38:8649

- 68 Miyakoshi R, Yokoyama A, Yokozawa T (2004) *Macromol Rapid Commun* 25:1663
- 69 Krasovskiy A, Straub BF, Knochel P (2006) *Angew Chem Int Ed* 45:159
- 70 Wu S, Huang L, Tian H, Geng Y, Wang F (2011) *Macromolecules* 44:7558
- 71 Jeffries-El M, Sauve G, McCullough RD (2005) *Macromolecules* 38:10346
- 72 Tkachov R, Senkovskyy V, Komber H, Sommer J-U, Kiriy A (2010) *J Am Chem Soc* 132:7803
- 73 Lohwasser RH, Thelakkat M (2012) *Macromolecules* 45:3070
- 74 Prosa TJ, Winokur MJ, McCullough RD (1996) *Macromolecules* 29:3654
- 75 Kline RJ, DeLongchamp DM, Fischer DA, Lin EK, Richter LJ, Chabiny ML, Toney MF, Heeney M, McCulloch I (2007) *Macromolecules* 40:7960
- 76 Brinkmann M (2011) *J Polym Sci B: Polym Phys* 49:1218
- 77 Wu ZY, Petzold A, Henze T, Thurn-Albrecht T, Lohwasser RH, Sommer M, Thelakkat M (2010) *Macromolecules* 43:4646
- 78 Balko J, Lohwasser RH, Sommer M, Thelakkat M, Thurn-Albrecht T (2013) *Macromolecules* 46:9642
- 79 Pascui OF, Lohwasser RH, Sommer M, Thelakkat M, Thurn-Albrecht T, Saalwachter K (2010) *Macromolecules* 43:9401
- 80 Singh CR, Gupta G, Lohwasser RH, Engmann S, Balko J, Thelakkat M, Thurn-Albrecht T, Hoppe H (2013) *J Polym Sci B Polym Phys* 51:943
- 81 Malik S, Nandi AK (2002) *J Polym Sci B* 40:2073
- 82 Virkar AA, Mannsfeld S, Bao ZA, Stingelin N (2010) *Adv Mater* 22:3857
- 83 Lindner SM, Thelakkat M (2004) *Macromolecules* 37:8832
- 84 Hawker CJ, Bosman AW, Harth E (2001) *Chem Rev* 101:3661
- 85 Kolb HC, Finn MG, Sharpless KB (2001) *Angew Chem Int Ed* 40:2004
- 86 Tao Y, McCulloch B, Kim S, Segalman RA (2009) *Soft Matter* 5:4219
- 87 Lang AS, Neubig A, Sommer M, Thelakkat M (2010) *Macromolecules* 43:7001
- 88 Lang AS, Thelakkat M (2011) *Polym Chem* 2:2213
- 89 Lang AS, Muth M-A, Heinrich CD, Carassco-Orozco M, Thelakkat M (2013) *J Polym Sci B Polym Phys* 51:1480
- 90 Mott NF, Gurney RW (1940) *Electronic processes in ionic crystals*. The Clarendon Press, Oxford
- 91 Steyrlleuthner R, Schubert M, Jaiser F, Blakesley JC, Chen Z, Facchetti A, Neher D (2010) *Adv Mater* 22:2799
- 92 Mueller CJ, Singh CR, Fried M, Huettner S, Thelakkat M (2015) *Adv Funct Mater* 25:2725–2736
- 93 Kohn P, Ghazaryan L, Gupta G, Sommer M, Wicklein A, Thelakkat M, Thurn-Albrecht T (2012) *Macromolecules* 45:5676
- 94 Stalmach U, de Boer B, Videlot C, van Hutten PF, Hadziioannou GJ (2000) *Am Chem Soc* 122:5464–5472
- 95 Hawker CJ (1994) *Macromolecules* 27:4836–4837

- 96 Liu B, Bunker CE, Sun Y-P (1996) *Chem Commun* 1241
- 97 Yang C, Lee JK, Heeger AJ, Wudl FJ (2009) *Mater Chem* 19:5416–5423
- 98 Heuken M, Komber H, Voit B (2012) *Macromol Chem Phys* 213:97–107
- 99 Zhang N, Schrick S, Wudl F, Prato M (1995) *Chem Mater* 7:441–442
- 100 Kim J, Yun MH, Lee J, Kim JY, Wudl F, Yang C (2011) *Chem Commun* 47:3078–3080
- 101 Eo M, Lee S, Park MH, Lee MH, Yoo S, Do Y (2012) *Macromol Rapid Commun* 33:1119–1125
- 102 Fang L, Liu P, Sveinbjornsson BR, Atahan-Evrenk S, Vandewal K, Osuna S, Jiménez-Osés G, Shrestha S, Giri G, Wei P, Salleo A, Aspuru-Guzik A, Grubbs RH, Houk KN, Bao Z (2013) *J Mater Chem C* 1:5747
- 103 Hufnagel M, Muth M-A, Brendel JC, Thelakkat M (2014) *Macromolecules* 47:2324
- 104 Adamopoulos G, Heiser T, Giovanella U, Ouldsaad S, Vandewetering K, Brochon C, Zorba T, Paraskevopoulos K, Hadziioannou G (2006) *Thin Solid Films* 511:371–376
- 105 Perrin L, Nourdine A, Planes E, Carrot C, Alberola N, Flandin L (2013) *J Polym Sci B Polym Phys* 51:291–302
- 106 Sommer M, Lang AS, Thelakkat M (2008) *Angw Chem Int Ed* 47:7901
- 107 Rajaram S, Armstrong PB, Kim BJ, Fréchet JM (2009) *Chem Mater* 21:1775
- 108 Gupta G, Singh CR, Lohwasser RH, Himmerlich M, Krischok S, Müller-Buschbaum P, Thelakkat M, Hoppe H, Thurn-Albrecht T (2015) *ACS Appl Mater Interfaces*. doi:10.1021/am5049948
- 109 Sommer M, Hüttner S, Steiner U, Thelakkat M (2009) *Appl Phys Lett* 95:183308(1–3)
- 110 Singh CR, Sommer M, Himmerlich M, Wicklein A, Krischok S, Thelakkat M, Hoppe H (2011) *Phys Status Solidi RRL* 5:247
- 111 Gholamkhash B, Holdcroft S (2010) *Chem Mater* 22:5371–5376

- 1 A. S. Lang, M.-A. Muth, C. D. Heinrich, M. Carrasco-Orozco and M. Thelakkat: “*Pendant perylene polymers with high electron mobility*”, J. Polym. Sci. Part B: Polym. Phys., 2013, **51**, 1480.
- 2 C. D. Heinrich and M. Thelakkat: “*Poly(-3-hexylthiophene) bottlebrush copolymers with tailored side-chain lengths and high charge carrier mobilities*”, J. Mater. Chem. C, 2016, **4**, 5370.
- 3 C. D. Heinrich, M. Hufnagel, C. R. Singh, M. Fischer, S. Alam, H. Hoppe, T. Thurn-Albrecht and M. Thelakkat: “*Nanoscale Morphology from Donor–Acceptor Block Copolymers: Formation and Functions*”, Adv. Polym. Sci., 2017, **272**, 157.
- 4 C. D. Heinrich, S. Tuncel Kostakoğlu and M. Thelakkat: “*Densely Grafted Liquid Crystalline Copper Phthalocyanine Side Chain Polymer: Synthesis and Characterization*”, J. Mater. Chem. C, 2017, **5**, 6259-6268.
- 5 M. Fischer, C. D. Heinrich, M. Thelakkat and T. Thurn-Albrecht: “*Impact of Molecular Dynamics on Structure Formation of Donor-Acceptor Block Copolymers*”, intended for submission.
- 6 C. D. Heinrich, P. M. Reichstein and M. Thelakkat: “*Monolayer Brushes for Highly Efficient Polymeric SAMFETs*”, intended for submission.

Vielen Dank !

Allen, die auf irgendeine Weise zum Gelingen dieser Doktorarbeit beigetragen haben möchte ich an dieser Stelle herzlich danken.

Vielen herzlichen Dank meinem Doktorvater Prof. Mukundan Thelakkat. Für die Möglichkeit unter sehr großzügigen Bedingungen selbstständig zu forschen. Für den Ansporn sich weiterzuentwickeln und kritisch zu denken. Danke Muku!

Bei Prof. Thomas Thurn-Albrecht und Matthias Fischer bedanke ich mich für die erfolgreiche Zusammenarbeit bei der Strukturaufklärung der Blockcopolymere. Außerdem möchte ich mich bei Sinem Tuncel-Kostakoğlu für ihre Phthalocyanine bedanken, durch die meine Arbeit noch etwas bunter geworden ist.

Meinen Labor-Kollegen am Ende des Ganges: Anne N., Helga, Katha, Martina F., Paul, Philip und Jannik. Danke für das tolle Arbeitsklima, die fachlichen Diskussionen und den Geruch von Tosylat. Danke auch allen AFUPOs, insbesondere den B6-lern, für die Aufnahme in ihr Exil.

Der gesamten MC1 danke ich für die Unterstützung und freundliche Aufnahme. Christian Neuber für Hilfe bei fachlichen Fragen. Alexander Kern, Christina und Petra für schnelle Hilfe bei allen administrativen Dingen und natürlich Doris, Irene, Jutta und Sandra bei allen Fragen rund ums Labor.

Für den schnellen und unkomplizierten Zugang zu Analysemethoden an anderen Lehrstühlen möchte ich mich bei Carmen Kunert (TEM), Markus Hundt (AFM) und Dr. Martin Dulle (XRD) bedanken.

Besten Dank für hunderte GPC-Messungen an Katha und Paul. Für ein geringere Anzahl aber dafür umso aufwendigerer MALDI-ToF Messungen danke ich Hubertus, Martin

und Alexander Krimaloswski. Danke auch an Tina für ihr Geschick bei der Präparation von Proben für die Flash-DSC.

Ein großes Dankeschön an meine Praktikanten Anna Gräser, Marius Feldmann, Tobias Jurzek, Alexander Krimalowski, Svenja Marl und Zilin Wang sowie meine Bacheloranden Florian Meichsner und Philip Schmode.

Dem Hochschulsport und der Sportlergruppe danke ich für die beste Möglichkeit einen freien Kopf zu bekommen wenn der Laborgott einem gerade nicht gewogen war.

Der allerbesten Sofia der Welt, danke ich für die überragende Unterstützung (*summa cum laude!*) während der gesamten Doktorarbeit – besonders aber in unserem gemeinsamen Abgabejahr! Ab jetzt schaffen wir jedes Jahr wieder 1000 km!

Zuletzt danke ich herzlich meiner lieben Familie für die Unterstützung. Besonders meiner Mutter für viel Korrekturlesen während des Studiums und meinem Vater, der in mir überhaupt erst die Liebe zu Chemie geweckt hat.

(Eidesstattliche) Versicherungen und Erklärungen

(§ 8 S. 2 Nr. 6 PromO)

Hiermit erkläre ich mich damit einverstanden, dass die elektronische Fassung meiner Dissertation unter Wahrung meiner Urheberrechte und des Datenschutzes einer gesonderten Überprüfung hinsichtlich der eigenständigen Anfertigung der Dissertation unterzogen werden kann.

(§ 8 S. 2 Nr. 8 PromO)

Hiermit erkläre ich eidesstattlich, dass ich die Dissertation selbständig verfasst und keine anderen als die von mir angegebenen Quellen und Hilfsmittel benutzt habe.

(§ 8 S. 2 Nr. 9 PromO)

Ich habe die Dissertation nicht bereits zur Erlangung eines akademischen Grades anderweitig eingereicht und habe auch nicht bereits diese oder eine gleichartige Doktorprüfung endgültig nicht bestanden.

(§ 8 S. 2 Nr. 10 PromO)

Hiermit erkläre ich, dass ich keine Hilfe von gewerblichen Promotionsberatern bzw. -vermittlern in Anspruch genommen habe und auch künftig nicht nehmen werde.

Bayreuth den 27.02.2018,